NASA CR-166,604

A Reproduced Copy

OF

NASA CR-166,604

Flow-Field Measurements on an Airfoil with an Oscillating Trailing-Edge Flap Using Holographic Interferometry

W. D. Bachalo

CONTRACT NAS2-11080
July 1984

NASA

NASA CONTRACTOR REPORT 166604

Flow-Field Measurements on an Airfoil with an Oscillating Trailing-Edge Flap Using Holographic Interferometry

W. D. Bachalo
Complere Inc.
P.O. Box 1697
Palo Alto, CA 94302

Prepared for
Ames Research Center
under Contract NAS2-11080

National Aeronautics and
Space Administration

Ames Research Center
Moffett Field, California 94035

LIST OF FIGURES

NOMENCLATURE

c	chord length
C_p	pressure coefficient $(p-p_\infty)/(0.5\ \rho_\infty U_\infty^2)$
f	focal length of lens
K	Gladstone-Dale constant
L	span of the airfoil
$L\emptyset$	lens designation
M	Mach number
N	number of fringes from reference fringe
n	index of refraction
P	pressure
r	turbulent recovery factor
T	temperature
U	flow speed
α	airfoil angle of attack
δ	flap mean angle relative to wing chord plane
$\gamma = 1.4$	
λ	laser wavelength
ρ	density

Subscripts

ad	adiabatic wall
e	outer edge of the boundary layer
o	reference condition
t	total or stagnation conditions
w	wall or airfoil surface conditions
∞	free-stream conditions

FLOW-FIELD MEASUREMENTS ON AN AIRFOIL WITH AN OSCILLATING TRAILING-EDGE FLAP USING HOLOGRAPHIC INTERFEROMETRY

1.0 Introduction

Unsteady loads on aircraft wings resulting from gusts and maneuvering dictate the flutter margin and fatigue requirements of the aircraft components. The weight of the components affects aircraft operational costs and range. Active control technology has been used in an effort to control these unsteady forces and to improve the aircraft handling characteristics.

At transonic speeds, the unsteady flow field is complicated by the presence of mixed inviscid flow regimes, shocks, and shock-induced separation. The unsteady flows are further complicated by the strong coupling between the steady and the unsteady flow fields. Phase lags between the flap position and the embedded shock waves and the viscous flow response adds to the complexities involved in understanding and predicting these flows.

The prediction of these unsteady flows is of increased interest. However, flows with significant separation are difficult to predict even in the steady flow regimes. Thus, detailed experimental investigations are required to measure and document the inviscid flow, shock-wave behavior and the shock-wave boundary-layer interactions for oscillating airfoils. These data must be obtained in sufficient detail to guide the theoretical development of the prediction methods and provide a source of data for the evaluation of the computational efforts.

In this report, the data obtained using holographic interferometry are presented. Optical diagnostics have proven especially useful in transonic flow research because of the sensitivity of these flows to perturbations produced by material probes. As a result of the relatively continuous change of the flow-field density, these flows are mapped in detail with the use of interferometry.

In addition to the detailed visualization of the flow fields, the interferograms provide an instantaneous mapping of the density field, albeit spatially integrated over the span of the airfoil. If the flow can be assumed to be two-dimensional, the fringe patterns can be used with the isentropic flow assumption to obtain the instantaneous surface pressure distribution. Flow-speed profiles in the wake were also obtained for representative conditions.

The following section contains a description of the holographic interferometry method, a presentation of the results, and comments on application of the method in large-scale facilities.

2.0 Experimental Procedure

2.1 Description of the Model

The airfoil used in the investigation had a NACA 64A010 profile with a 50-cm chord and a span of 1.37 m. The airfoil had a movable graphite-epoxy flap fixed to the main airfoil section at 25% chord, figure 1. Hydraulic actuators were used to drive the flap at frequencies from 0 to 50 Hz. The airfoil was mounted between splitter plates that were affixed to the floor and ceiling at the NASA Ames 11-Foot Transonic Wind Tunnel.

Optical access was provided for by windows installed in the splitter plates as shown in figure 2. A pair of windows was used in each splitter plate with the windows mounted flush to the inside and outside walls of the splitter plates.

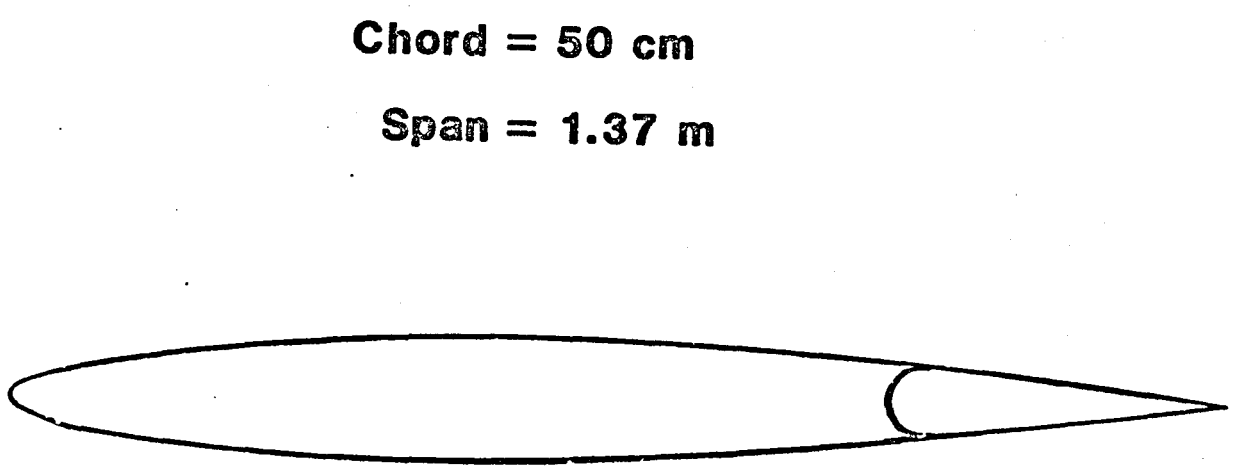

Figure 1.- 64A010 Airfoil With Oscillating Control Surface.

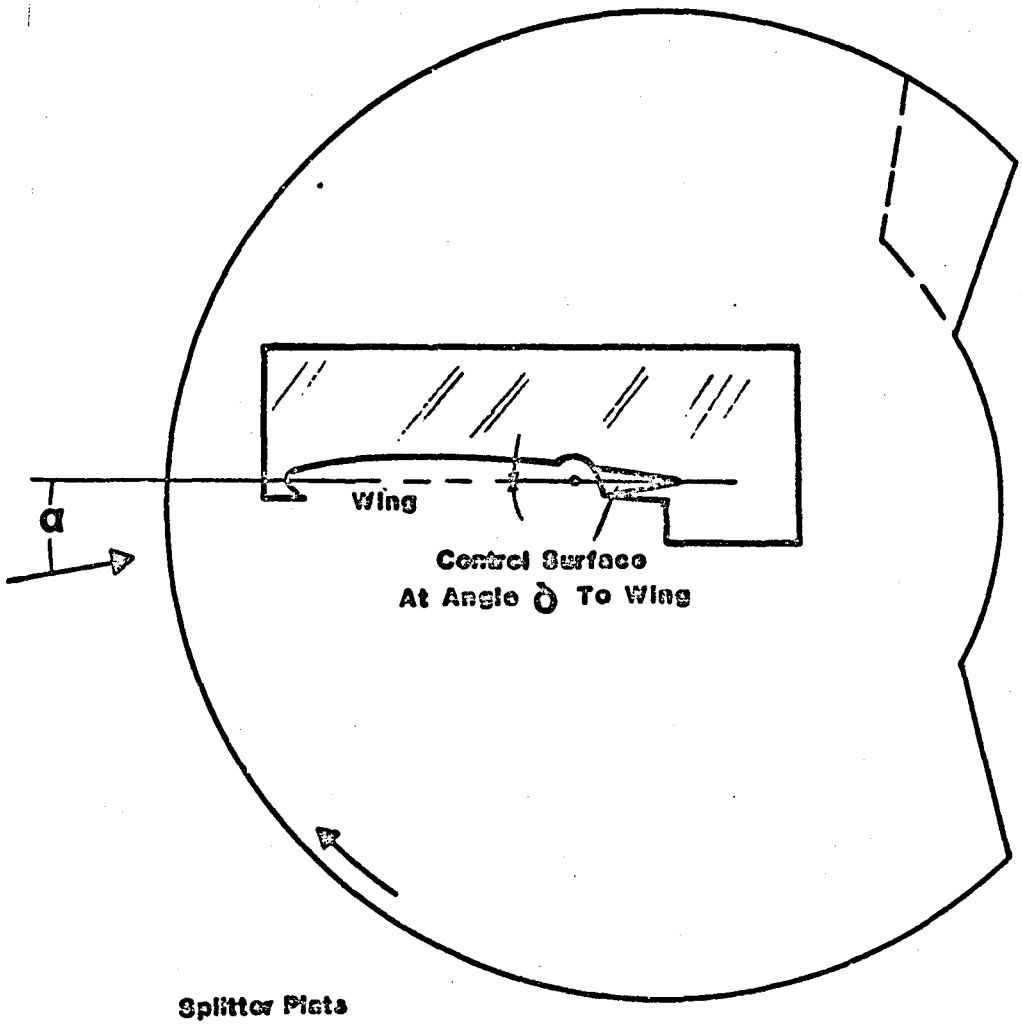

Figure 2.- Airfoil Mounting System Showing Optical Access

2.2 Holographic Interferometry

Interferometry which utilizes the mixing of two coherent waves for the purpose of measuring the distortion in one of the waves, has been used in small-scale wind tunnels and is well understood. The introduction of holography as an intermediary to store the light-wave information allows a great deal of versatility in the use of the technique and significantly extends the possible application.[1]

With holography, the amplitude and phase distribution of a light wave passing through the flow field at some instant of time can be stored and later reconstructed for comparison to waves formed at other conditions. This allows the storage of several test conditions for later comparison and analysis outside of the test facility. In addition to the interferometry techniques, the shadowgraph and Schlieren flow visualization techniques are also available. The ability to reconstruct the light field outside of the wind tunnel allows a much greater flexibility in spatial filtering and photographing the images.

Transonic flows are especially suitable to the application of interferometry since compressibility occurs but the density changes are not all stepwise through shocks as in supersonic flow.[2,3] In addition, the shocks present in the transonic flow fields are weak so that the entire flow field can be assumed to be isentropic. Thus, the interference fringes are at the same time a mapping of the constant density and the flow-speed contours. These data can be readily reduced, with the use of other wind-tunnel conditions, to the surface static pressure and viscous layer temperature profiles.

A Quanta Ray DCR-1 Nd:YAG laser is used in the Ames Portable Holographic Interferometer as the light source.[4] This laser is capable of producing pulse repetition rates between 2/sec and 20/sec at up to 80 mJ of energy in the green line (0.532 μm). Because of the high rep rate capability, a separate HeNe laser is not required for aligning the optics as in the case of a pulsed ruby laser system.

The hologram recording system is composed of a transmitting and receiving components (figs. 3, 4, and 5), connected by two optical paths for the object and reference beams. The Quanta Ray DCR-1 pulsed Nd:YAG laser used in the system produces a beam that has a so-called "donut" intensity distribution due to the laser's unstable resonator configuration. Thus, the first elements in the system consisting of lens L1 and a spatial filter of 150-μm aperture is used to produce a smooth beam intensity distribution. The beam is then divided into two paths with a beam splitter (B.S.), shown in figure 4.

The object beam is transmitted through the beam splitter and expanded with lens L3 to overfill the Schlieren mirror. Because the foci of L3 and the Schlieren mirror coincide, a collimated beam is formed and transmitted through the test section. The object beam is approximately 1 meter in diameter and is received and refocused to the receiver stage. Lens L6 is used to collimate the object beam to an appropriate size for recording at the holographic plate (fig. 5).

The reference beam is directed through the beam splitter and over the wind tunnel. Lens L2 is used to control the size of the reference beam at the receiver stage. Lenses L4 and L5 are used to expand and collimate the reference beam to 90 mm in diameter which then also falls on the holographic plate.

A 4-in. by 5-in. film holder is used to hold the high-resolution holographic film plates for recording the information. When using the dual plate interferometry technique, holograms are recorded with no flow in the tunnel (reference condition) and subsequent plates are recorded at the test conditions.

After processing the exposed film, the reconstruction system is used for viewing and photographing the aerodynamic information. The dual plate holder is used to position the reference and test plates to produce interference between the two reconstructed object waves. A lens is used to image the test section onto the film plane of a 4-in. by 5-in. camera and produces a beam diameter of suitable size for recording on 4 by 5 sheet film.

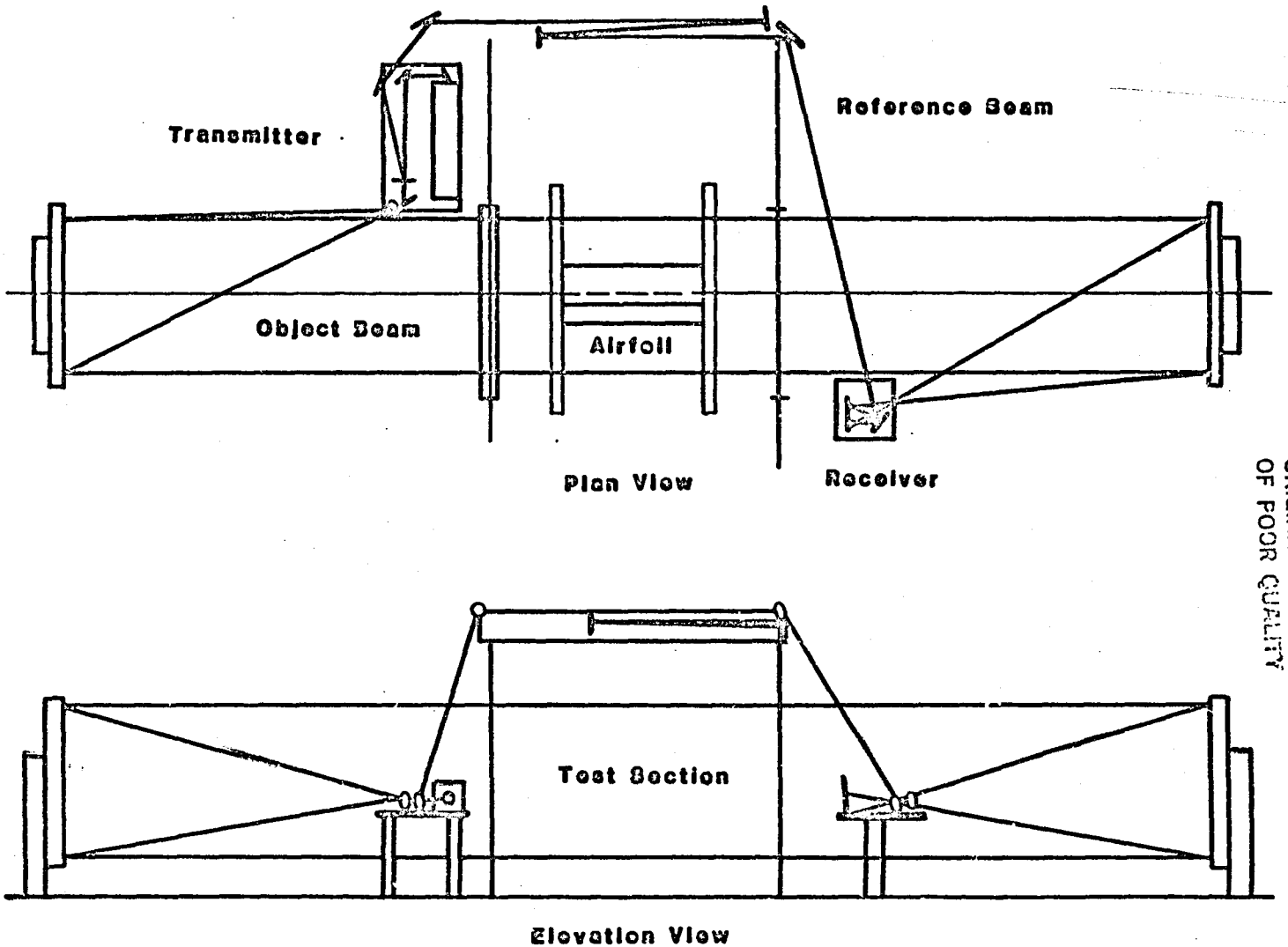

Figure 3.- 11-foot Holographic Interferometer

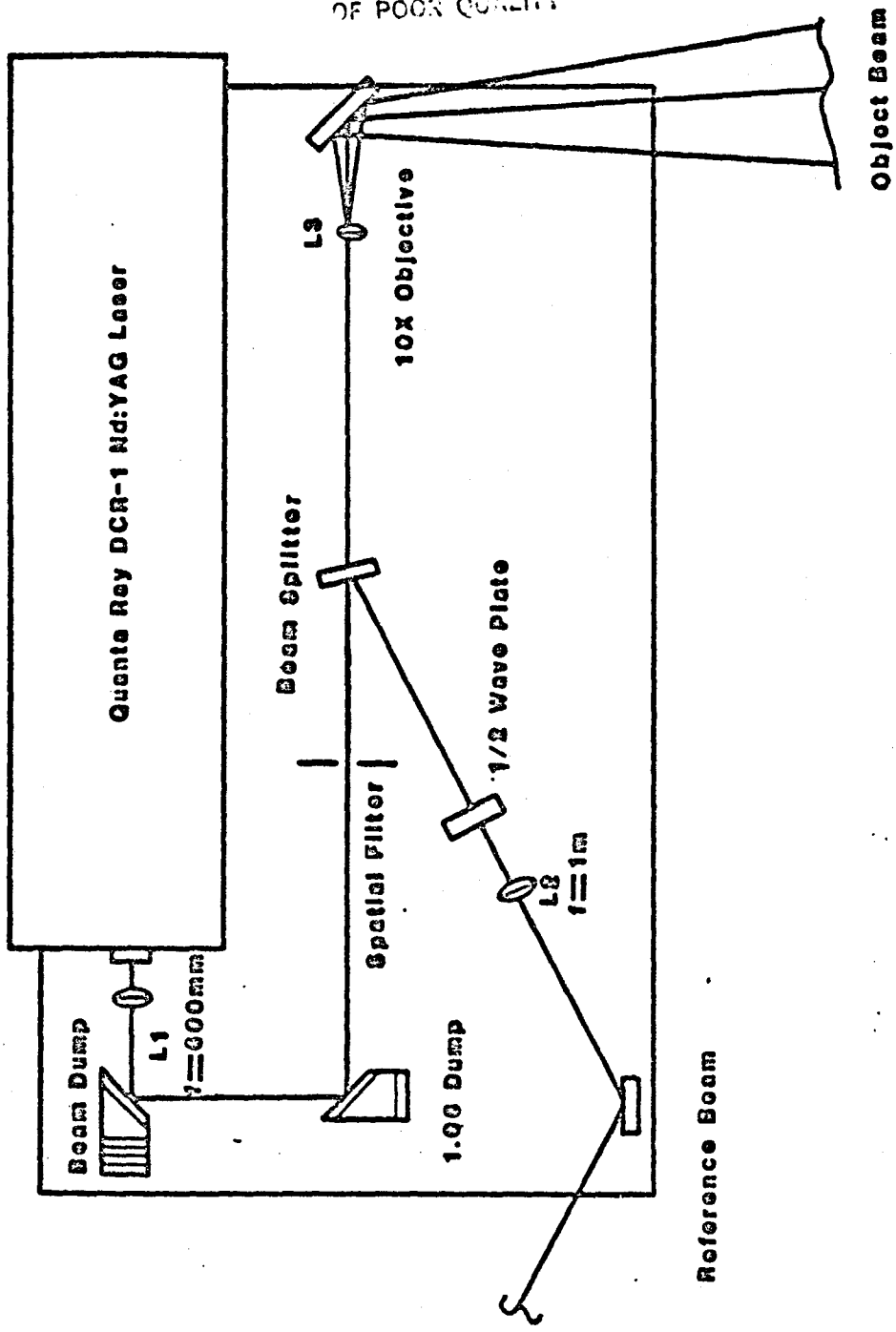

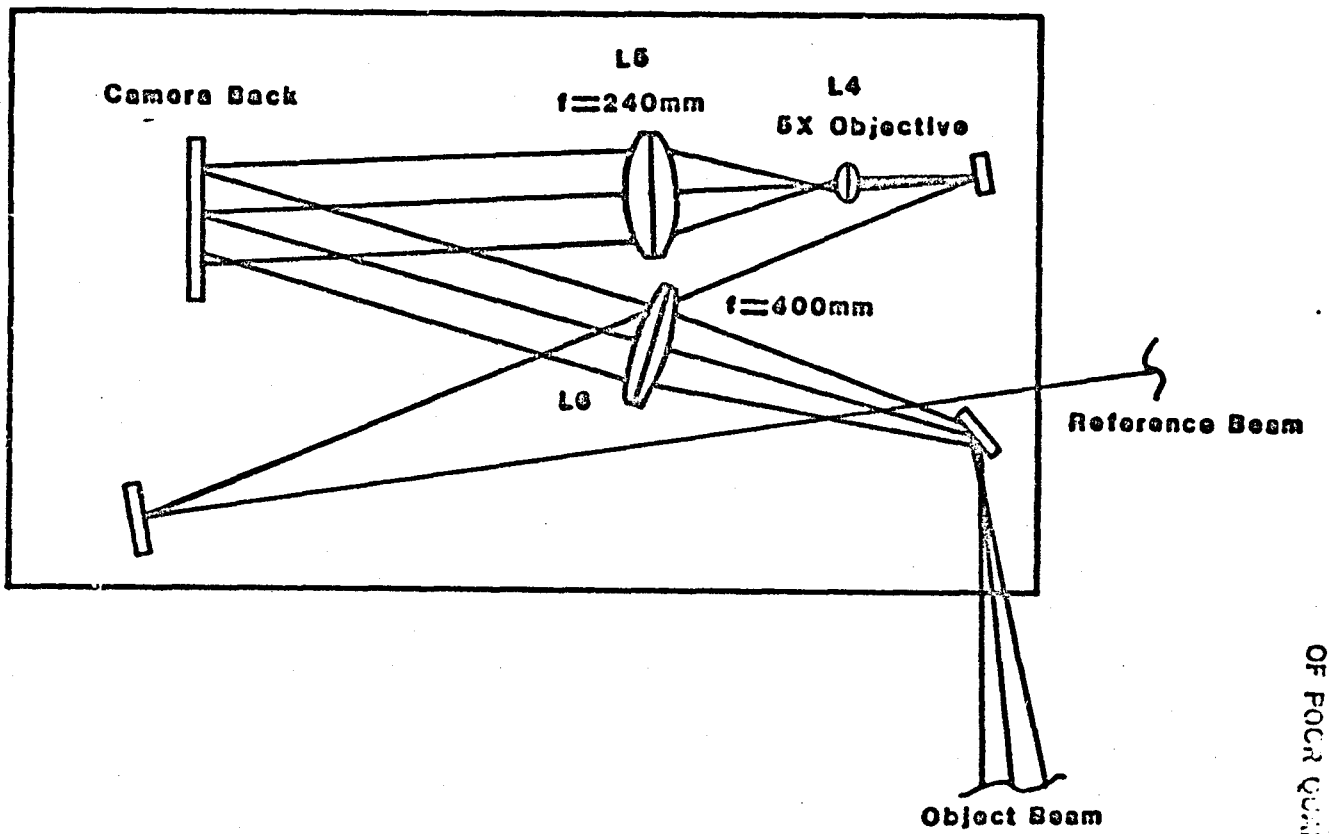

Figure 5.- Ames Portable Holographic System Receiver

One major difficulty when utilizing the dual plate technique arises when the density of the entire flow field is disturbed. In this case, it is difficult if not impossible to ascertain when the interferometer is aligned to the infinite fringe condition, that is, to the case wherein fringes only occur as a result of changes in the flow density. This condition occurs in most airfoil tests. Fortunately, a knowledge of the transonic flow characteristics and other alignment criteria has led to reconstructed interferograms producing good agreement with other measured data.

2.3 Data Reduction

Obtaining quantitative results from the interferograms is straightforward for two-dimensional flows. The pathlength through the wind tunnel in the present case was 1.37 meters so the density changes at the test flow Mach numbers was sufficient to produce an optimum number of interference fringes in the infinite fringe mode. Using the infinite fringe mode has the advantage of the fringes producing a direct mapping of the constant density contours which in turn, map the Mach contours.

Evaluation of the density change per fringe can be determined using the following relationships. In an inhomogeneous density test field the phase shift of the light wave is

$$\left(\frac{\Delta\phi}{2\pi}\right) = \frac{1}{\lambda}\int_{\zeta}^{\zeta_1} [n(x,y) - n_o]dz$$

where λ is the laser wavelength and n is the index of refraction. When the interferometer is aligned in the infinite fringe mode, the equation of the fringes is

$$\int_{\zeta}^{\zeta_1} [n(x,y) - n_o]dz = N\lambda$$

where N is an integer. Applying the Gladstone-Dale Constant relating phase variation to density, the integrated relationship is

$$\rho(x,y) = \rho_o + \frac{N\lambda}{KL}$$

The constant values in the present case are:

$$L = 1.37 \text{ m}$$

$$\lambda = 0.532 \text{ } \mu\text{m}$$

$$K = 0.226 \text{ } (\text{gm/cm}^3)^{-1}$$

$$\frac{\lambda}{KL} = \frac{0.532 \times 10^{-3} \text{ mm}}{0.226 \text{ } (\text{gm/cm}^3)^{-1} \text{ } 1370 \text{ mm}}$$

Combining the constants and adjusting for the wall boundary layers result in:

$$\rho_1 - \rho_0 = 1.08 \times 10^{-4} \frac{\text{lbm/ft}^3}{\text{fringe}}$$

It remains to identify a particular fringe to be used as the reference with its corresponding density. This can be done in several ways. If there is a region of undisturbed flow in the field of view, the wind-tunnel conditions can be used. Unfortunately, this is not generally the case. Instead, a surface pressure measurement can be converted to density by using the total temperature, T_o, and the total pressure, P_o. Another independent reference can be obtained from the inviscid flow velocity measured with the laser velocimeter.

Manual counting of the fringe allows an estimated resolution of about 0.3 of a fringe width and a spatial resolution of ±0.10 mm using a metric scale and a loupe.

The viscous flow speeds can be derived using the Crocco relationship given by

$$\frac{T}{T_e} = 1 + r\frac{\gamma - 1}{2} M_e^2 \left[1 - \left(\frac{U}{U_e}\right)^2\right] + \frac{T_w - T_{ad}}{T_e}\left(1 - \frac{U}{U_e}\right)$$

and the perfect gas law. The turbulent recovery factor r, was taken equal to 0.88, the model surface is assumed to be adiabatic so $T_w = T_{ad}$, and T_e is the temperature at the outer edge of the boundary layer.

The wake coordinates were referenced to the trailing edge of the airfoil, x/c=1.0 at the trailing edge and y/c=0. At the downstream stations, y/c=0 was taken parallel to the lower window from the trailing edge.

2.4 Real-Time Shadowgraph and Schlieren Flow Visualization

A great deal of information on flow-field behavior, particularly the dynamic characteristics, can be obtained from simple flow visualization techniques. The Nd:YAG laser used in these experiments was capable of producing light pulses of approximately 20-nanoseconds duration at a repetition rate of 10 pps. The flap was oscillated at 30 Hz. Thus, the laser was fired at every third cycle of the flap. In order to produce the illusion of a continuous oscillatory motion, the laser was fired at a frequency slightly different from 10 Hz which produced a continuous change in the phase shift between the laser pulse and flap.

Both shadowgraph and Schlieren techniques were used to visualize the flow. Various orientations of the Schlieren knife edge were used to observe the inviscid and viscous flow phenomena. Because of the short duration exposures used, the spatially averaged features of the flow were recorded at all possible phase angles of the oscillation.

A movie camera was interfaced to the laser such that the camera framing rate which could be adjusted also triggered the laser. The system was configured to allow the simultaneous recording and viewing of the results.

2.5 Laser Trigger Operation

An electronics circuit was designed to enable the firing of the laser at preselected phase angles of the airfoil oscillation. The primary constraint on the system was the need to fire the laser flash lamp at the design condition of 10 Hz. In addition, the count to the data acquisition computer was limited at 40 per revolution. Thus, a clock frequency was used that was controlled by the trigger logic circuit to provide a fixed number of counts per cycle of the flap driver. The clock was then divided using a digit switch control to produce the desired number of counts per cycle of the flap. For example, 360 counts per cycle was used. This number was further divided by 9 to provide the 40 counts per revolution to the data acquisition computer. A frame count digit switch was used to divide the 360 counts per cycle down to produce the approximately 10 pulses per second required by the laser. The division used here depended upon the flap oscillation frequency. Flap frequencies that were an integer multiple of 10 were maintained to simplify the operation of the system.

A phase delay digit switch was also provided to enable the firing of the laser at any phase angle of the flap. When the primary counter was set to produce 360 counts per cycle of the flap, the phase delay selector could be set directly to the angle in degrees after the once-per-rev signal from the flap.

The signal from the triggering circuit was connected to a pulse amplifier that produced the required 12-volt signal level to fire the laser flash lamp. There is a delay of ~250 μsec between the firing of the flash lamp and laser Q-switch. At an oscillation frequency of 30 Hz this delay represented a phase error of

$$\frac{250\times10^{-6}\ \text{sec}}{0.033\ \text{sec/revolution}} \times 360^\circ = 2.7^\circ$$

or less than 1% error in the phase angle. Thus, a correction for the Q-switch delay was not made.

3.0 Results and Discussion

The results represent the first quantitative interferometric data obtained in any facility as large as the 11-foot transonic tunnel. Because of the optical path lengths involved and the structural supports that resonate when the tunnel is running, the acquisition of holographic interferometry data can be difficult. A problem associated with the large-scale facilities is the length of the optical path through the highly turbulent compressible flow. Light waves passing through such flow fields are distorted and energy is deflected from the otherwise collimated beam. This resulted in a minimal light intensity at the holographic film plane.

In the present investigation, the number of windows involved also contributed to the loss in the transmitted energy. There were eight (8) windows in the optical path. Although these windows were of optical quality, the surfaces were contaminated with a thin film of oil and other material which further reduced their transmission of light.

Because of an error in manufacturing, the apertures used in transforming the laser beam to the correct profile also contributed to the loss in available laser power.

Inadequate laser power proved to be the primary difficulty during the tests. The quality of the interferograms reflects the need for eliminating this problem. Because of the low light exposures large development times were required. This caused background fog to occur on the holographic plates which produced poor reconstructions with low signal-to-noise. Because the sources of the problems have been identified, many of the problems can be eliminated from future tests.

Results were obtained at a freestream Mach number of $M = 0.8$, flap frequency of $f = 30$ Hz and chord Reynolds numbers of 6.6×10^6 and 12.3×10^6 corresponding to $P_t \approx 2100$ and 4200 psf; $\alpha = 0°$ and $P_t = 2100$ unless otherwise specified. Interferometric data were obtained at airfoil angles of attack $\alpha = 0°$ and $4°$ and mean flap angles, $\delta = 0°$ and $-4°$. Data were recorded at several phase angles of the flap.

Figures 6 through 9 are the interferograms for the full field of view. These figures represent infinite fringe interferograms so each fringe is a constant density line (isopycnic). As discussed earlier, the long optical path lengths (11 feet) through the flow around the splitter plates and the turbulent flow field over the airfoil produced strong optical distortions. Thus, the quality of the interferograms are not as good as those obtained in smaller facilities. However, the interferograms do portray the flow features with reasonable reliability. Flap angles and other pertinent information are given in the figures with the pressure data.

Figures 10 through 13 are the surface pressures obtained from the static pressure orifices and from the interferometric results. The interferometric pressures were obtained under the assumption of isentropic flow and the following expressions:

$$\frac{P}{P_t} = \left(\frac{\rho}{\rho_t}\right)^{\gamma}$$

$$C_p = \frac{2}{\gamma M_\infty^2}\left[\left(\frac{P}{P_t}\right)\left(\frac{P_t}{P_\infty}\right) - 1\right]$$

where M_∞ is the freestream Mach number, $\gamma = 1.4$ and P_t and ρ_t are the pressure and density at the stagnation conditions. A reference pressure was obtained from a surface pressure tap near the forward section of the field of view. When the shock extended out of the field of view, a second reference pressure was used downstream of the shock.

The constant density contours were used with the following relationship to identify the Mach contours.

$$M = \left[\frac{2}{\gamma-1}\left(\frac{\rho^{(1-\gamma)}}{\rho_t} - 1\right)\right]^{\frac{1}{2}}$$

Figures 14 through 17 are the traces of the Mach contours for the run parameters tested. The scale for the figures can be obtained from the width of the window shown on the first figures of each series.

Enlarged views of the trailing edge are presented in figures 18 through 21. These results primarily show the behavior of the viscous flow under the imposed parametric flow conditions. Although the interferograms are of low quality, the general characteristics of the turbulent boundary layers and wakes including the thickness and the occurrence of flow separation are visible. These results were used with the Crocco relationship to obtain estimates of the flow-speed profiles in the wakes shown in figures 22 to 24. The level of confidence in the thickness of the profiles is good. However, the velocity deficit was not as large as anticipated or expected. This may have been caused by the three-dimensionality in the flow including the sidewall boundary-layer interaction and a slight curvature of the wake in the spanwise direction. The effect of such spanwise nonuniformity would be most pronounced at the low-speed regions of the wake.

Representative strips of the real-time Schlieren flow visualization movie are presented in figures 25 - 27. Each sequence of photos covers one cycle of oscillation. Although the Schlieren technique does not produce the detail available with the interferometry technique, the information on the dynamic behavior of the flow will be useful for the qualitative comparisons to the flow prediction methods. During these tests, a strip of tape was applied to the leading edge of the model to protect it from erosion by particulate in the flow. At flow conditions wherein the shock was upstream of the flap juncture, the shock showed significant oscillation even at the steady flow conditions. Under flapping conditions, the shock motion and dynamic flow separation were clearly visible. At larger angles of attack, bursting of surface-generated vorticity away from the airfoil could be seen. The high levels of turbulence produced by the dynamic stall generated observable pressure disturbances in the otherwise inviscid flow downstream of the shock.

4.0 Summary

Holography interferometry was used to obtain flow visualization and quantitative results from a flow field generated by a NACA 64A010 airfoil with an oscillating control surface. The interferometric results complement the data obtained with dynamic pressure instrumentation, hot-wire anemometry, and laser Doppler velocimetry. Comparisons of the surface pressure data with the interferometric results showed good agreement at low angles of attack but differences occurred at the larger angles of attack. These differences yield information on the relative two-dimensionality of the flow field at increasing flap angles and airfoil angle of attack.

Enlargements of the trailing-edge region show the details of the boundary layer and wakes under dynamic flow conditions. The wake profiles obtained from the interferometric data did not produce the expected velocity deficits. The discrepancy was assumed to be a result of the spanwise curvature of the wake and sidewall effects.

Real-time shadowgraph and Schlieren flow visualization movies showed the dynamic behavior of the flow field.

In general, the tests demonstrated the feasibility of applying advanced flow visualization and interferometry techniques to large-scale wind-tunnel testing. With further refinements to the methodology, the optical techniques can provide an efficient means for obtaining detailed flow-field results.

References

1. W. D. Bachalo and D. H. Johnson, "Laser Velocimetry and Holographic Interferometry measurements in Transonic Flows," Laser Velocimetry and Particle Sizing, Hemisphere Publishing Corp., 1979, edited by H. Doyle Thompson and Warren H. Stevenson.

2. F. W. Spaid and W. D. Bachalo, "Experiments on the Flow about a Supercritical Airfoil Including Holographic Interferometry," AIAA Journal, Vol. 18, No. 4, April 1981.

3. D. A. Johnson and W. D. Bachalo, "Transonic Flow Past a Symmetrical Airfoil-Inviscid and Turbulent Flow Properties," AIAA Journal, Vol. 18, No. 1, January 1980.

4. J. E. Craig, C. Lee, W. D. Bachalo, "Nd:YAG Holographic Interferometer for Aerodynamic Research," SPIE Proceedings, Vol. 353, August 1982.

6(a) Phase Angle = 0°

Figure 6.- Interferograms of the NACA 64A010 Airfoil with Oscillating Flap, Mean Flap Angle at 0°

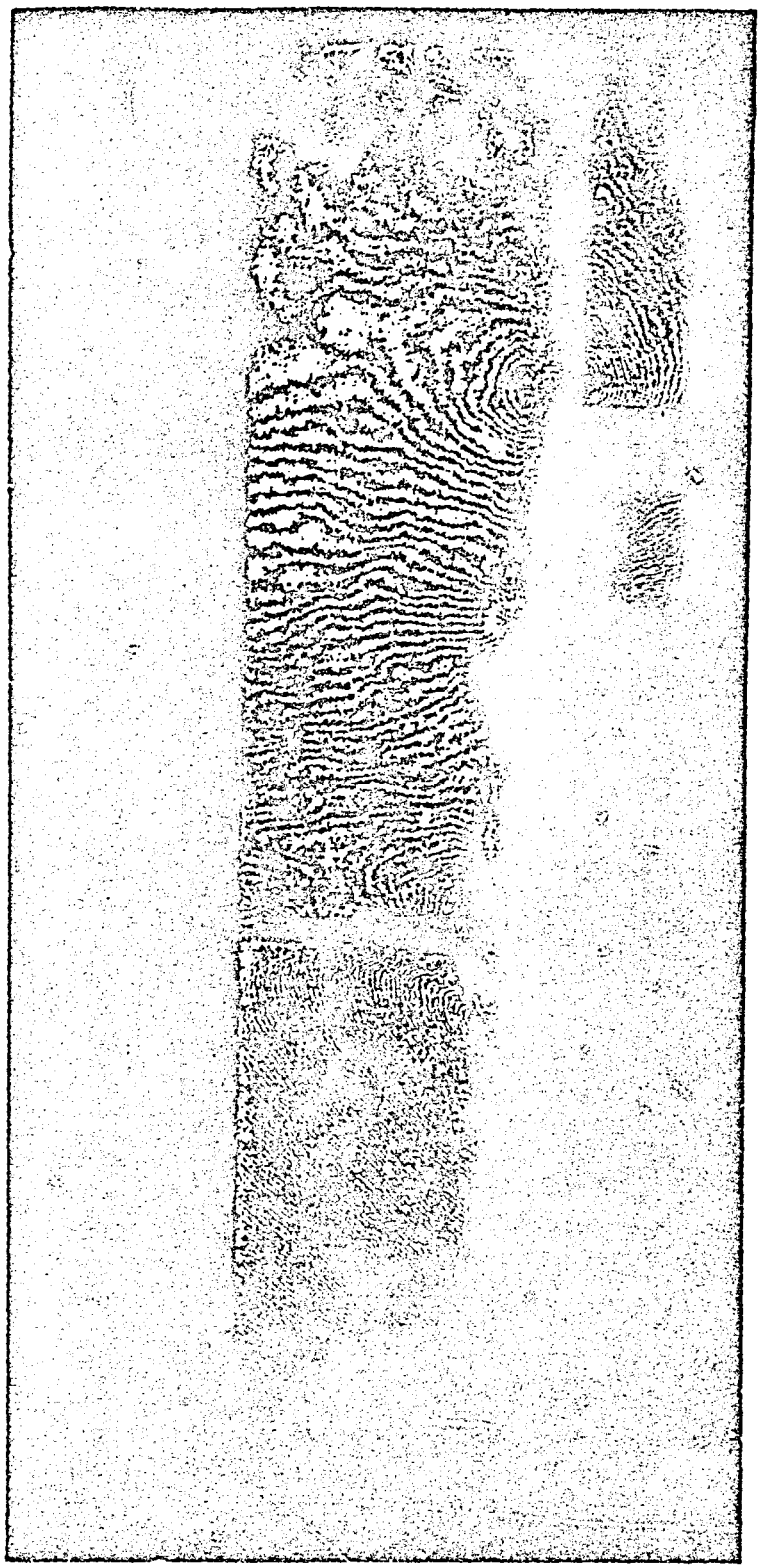

6(b) Phase Angle = 36°

6(c) Phase Angle - 54°

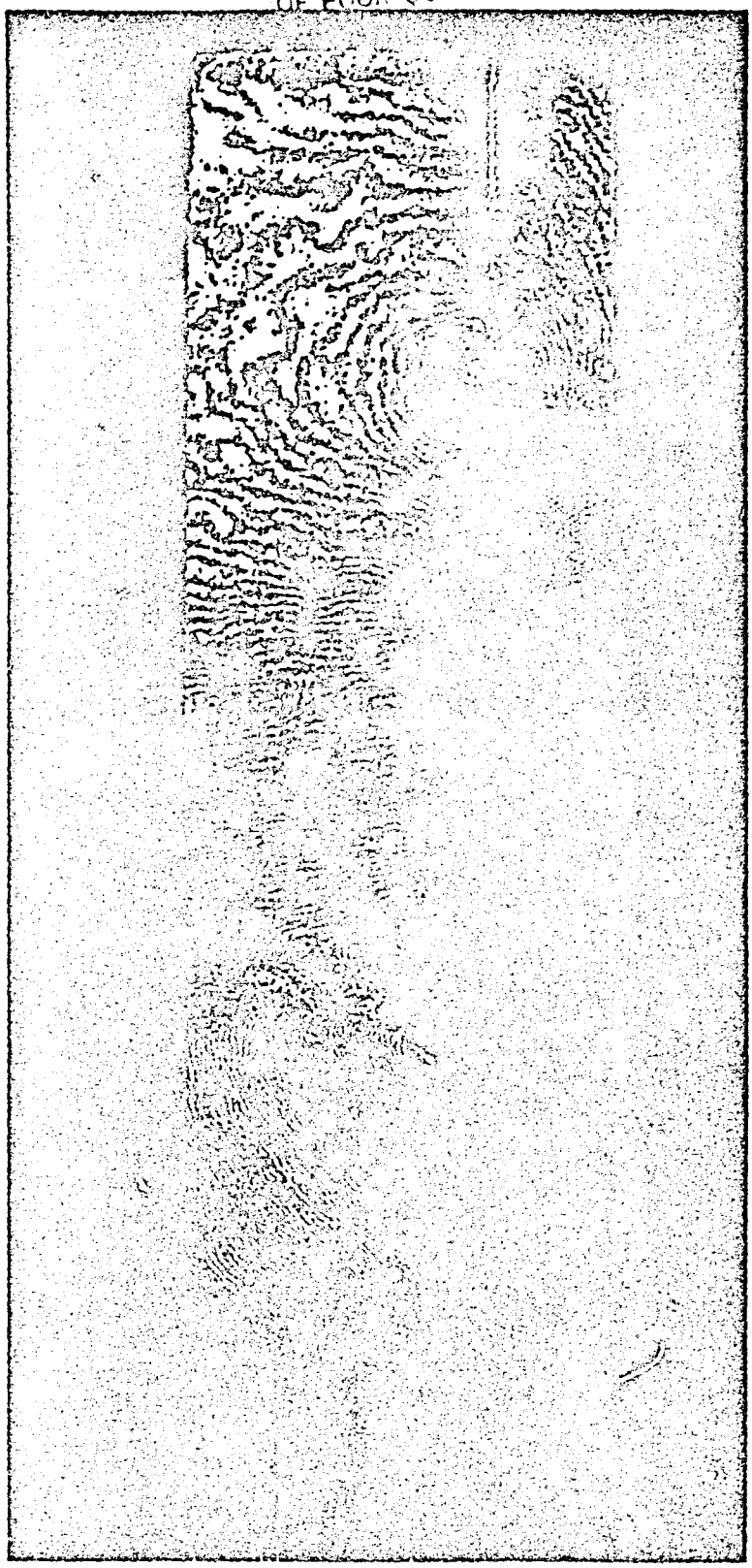

6(d) Phase Angle = 72

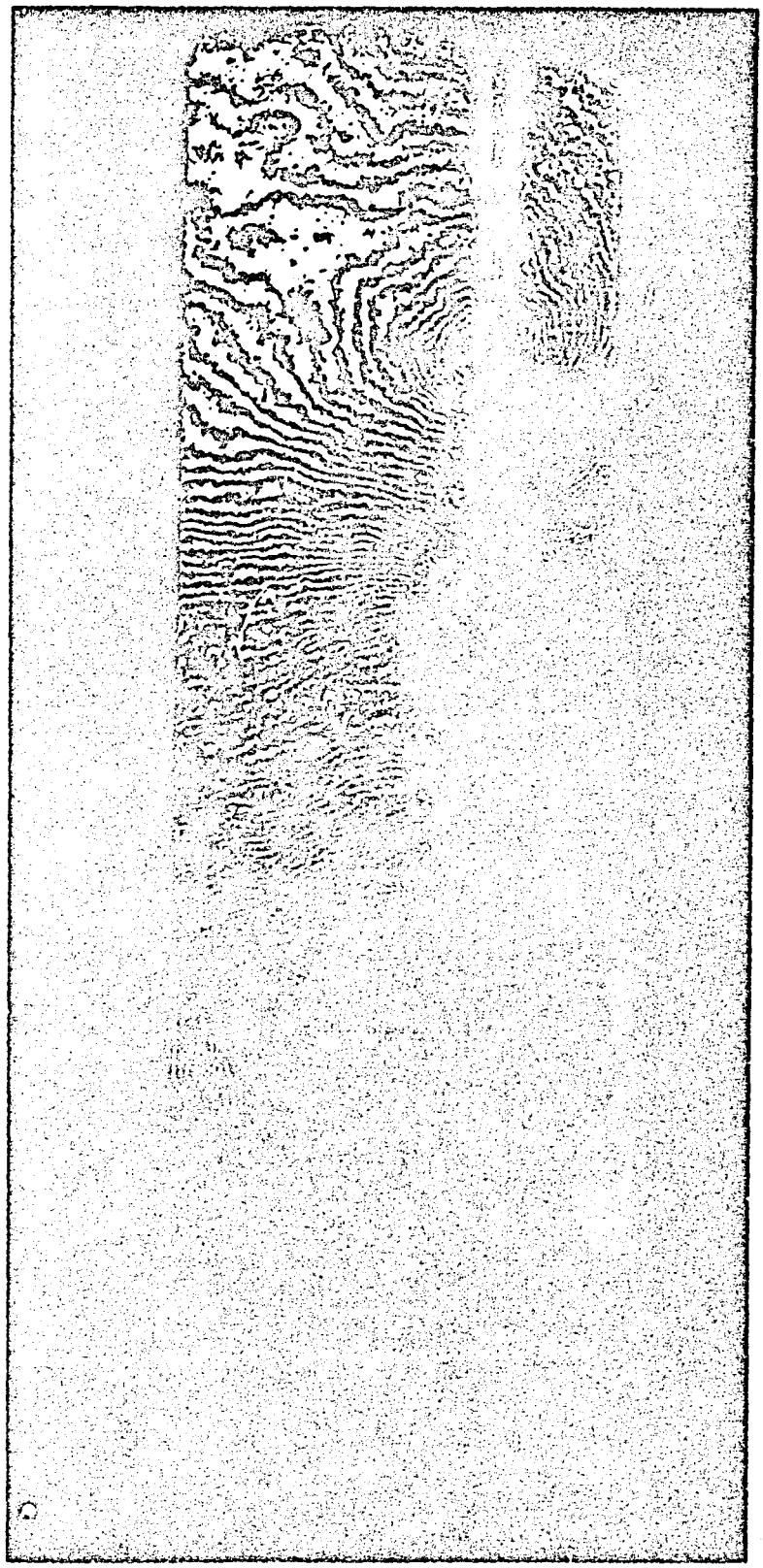

6(c) Phase Angle = 108

6(f) Phase Angle = 180

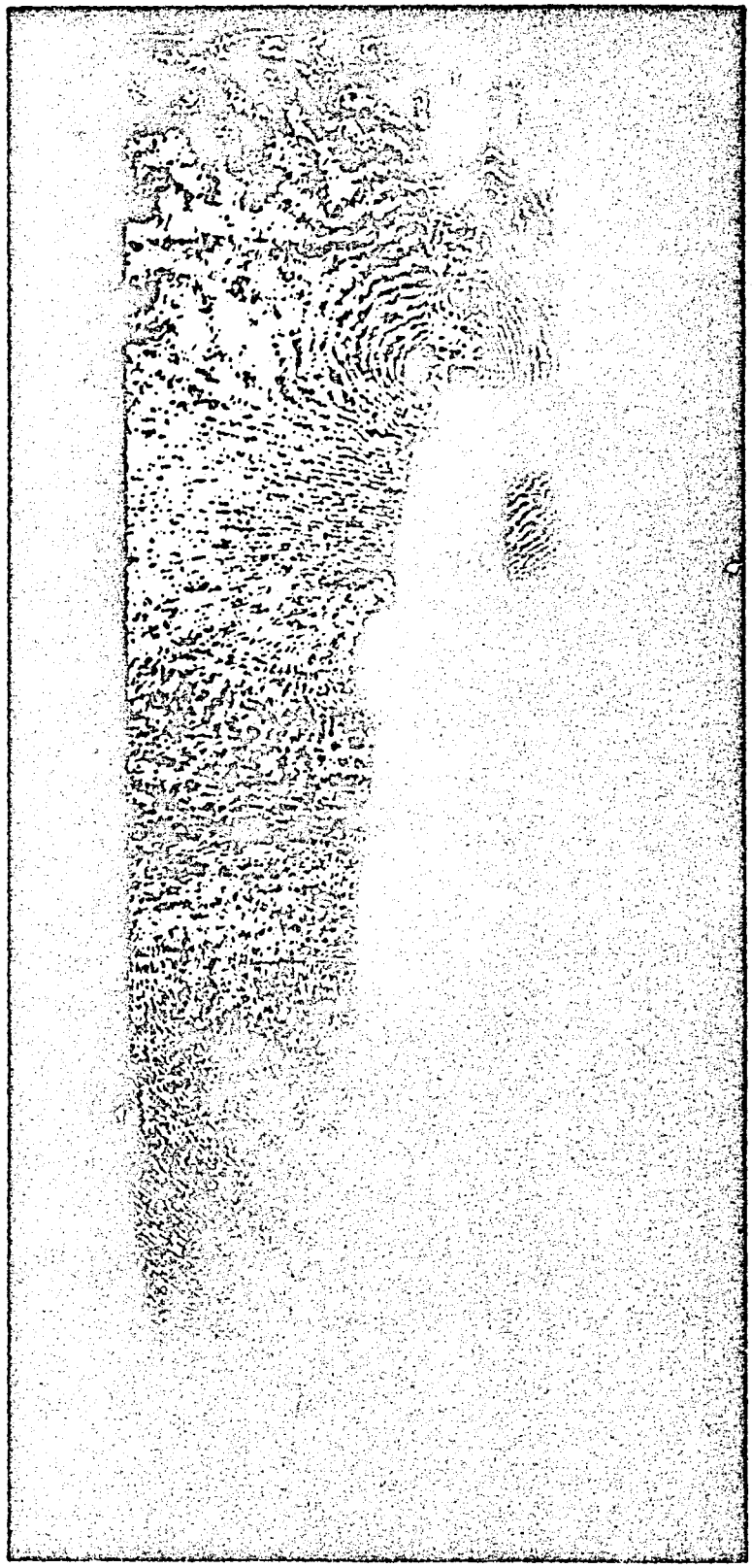

6(g) Phase Angle = 216

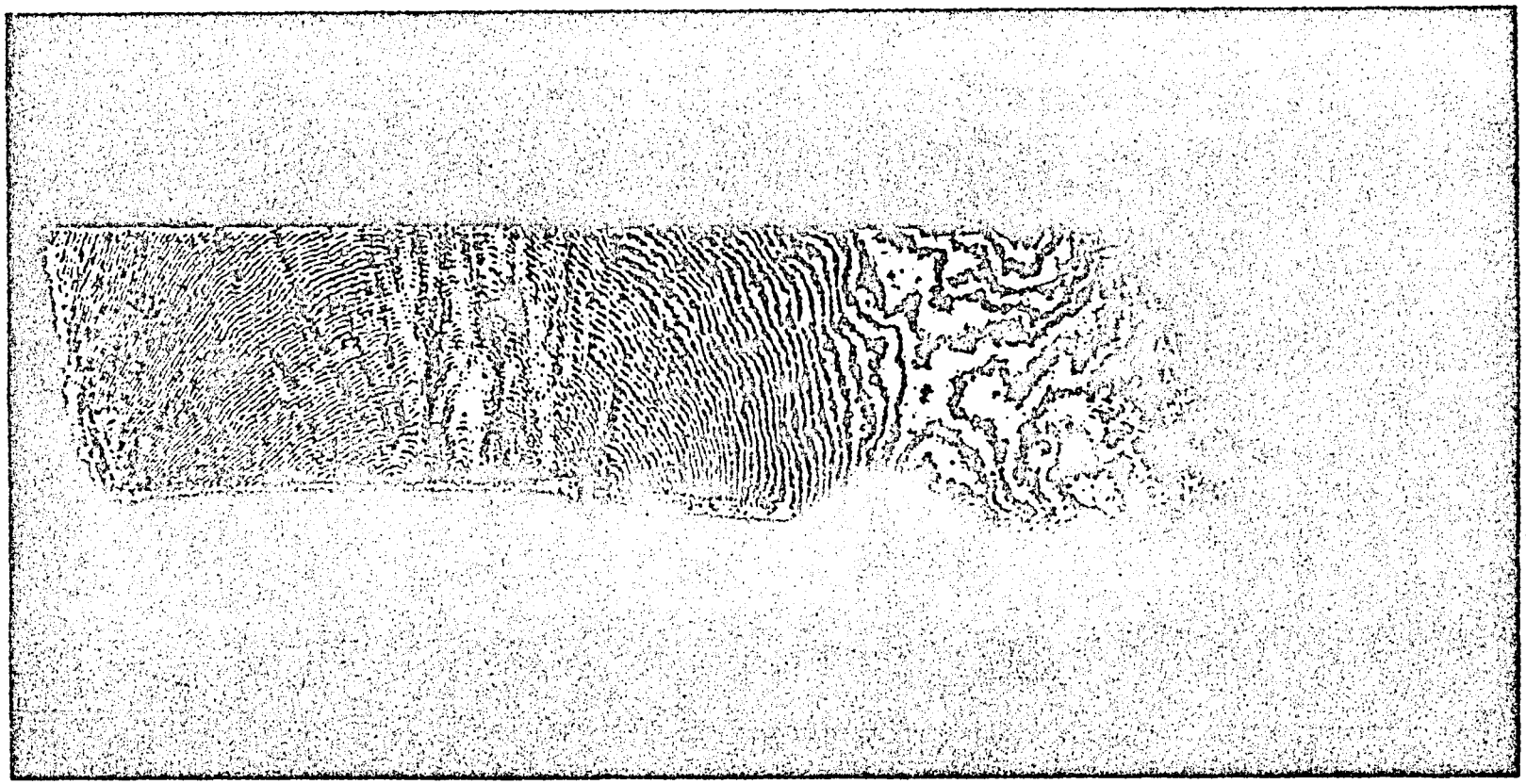

7(a) Phase Angle = 18°

Figure 7.- Interferograms of the NACA 64A010 Airfoil with Oscillating Flap, Mean Flap Angle at -4°

7(b) Phase Angle = 54°

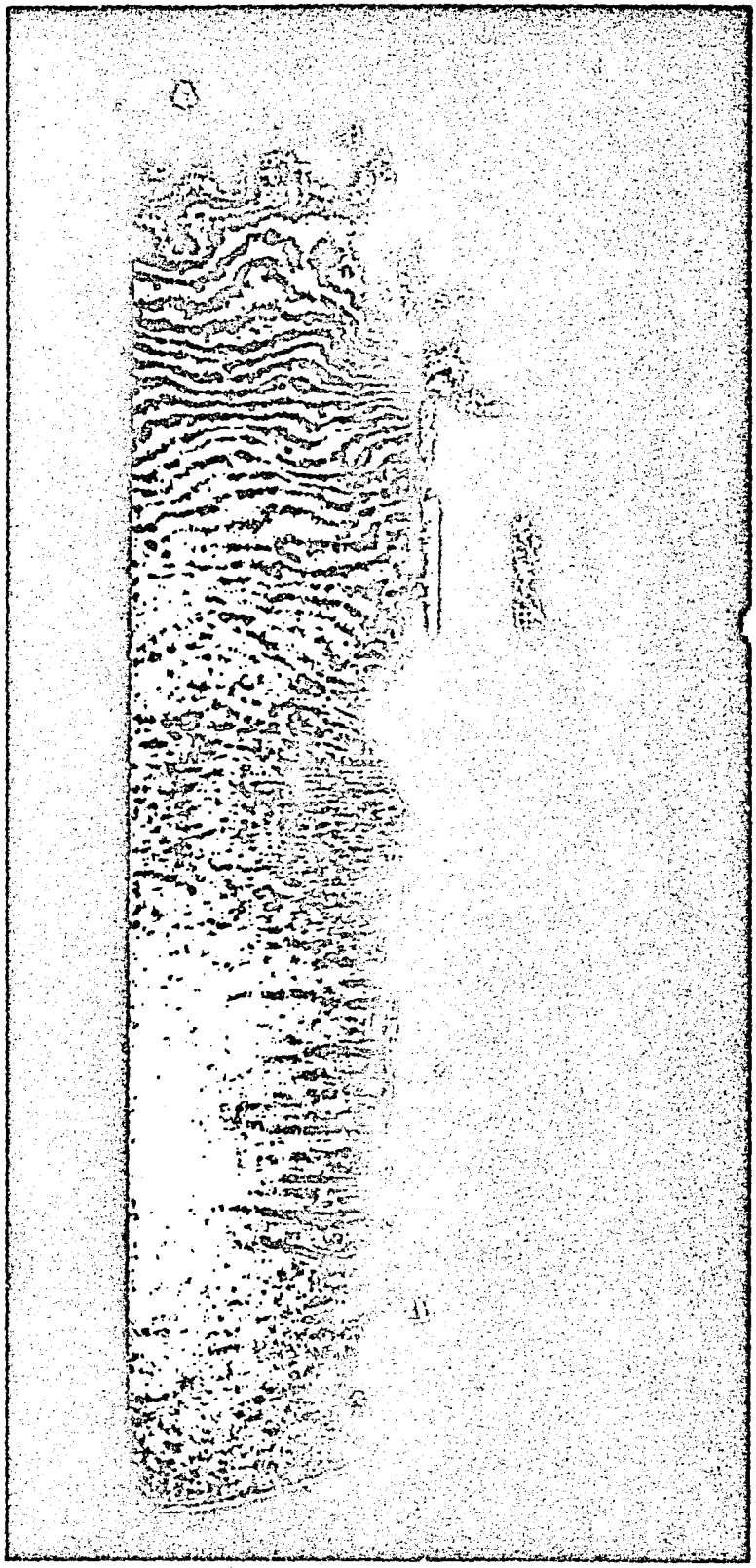

7(c) Phase Angle = 126°

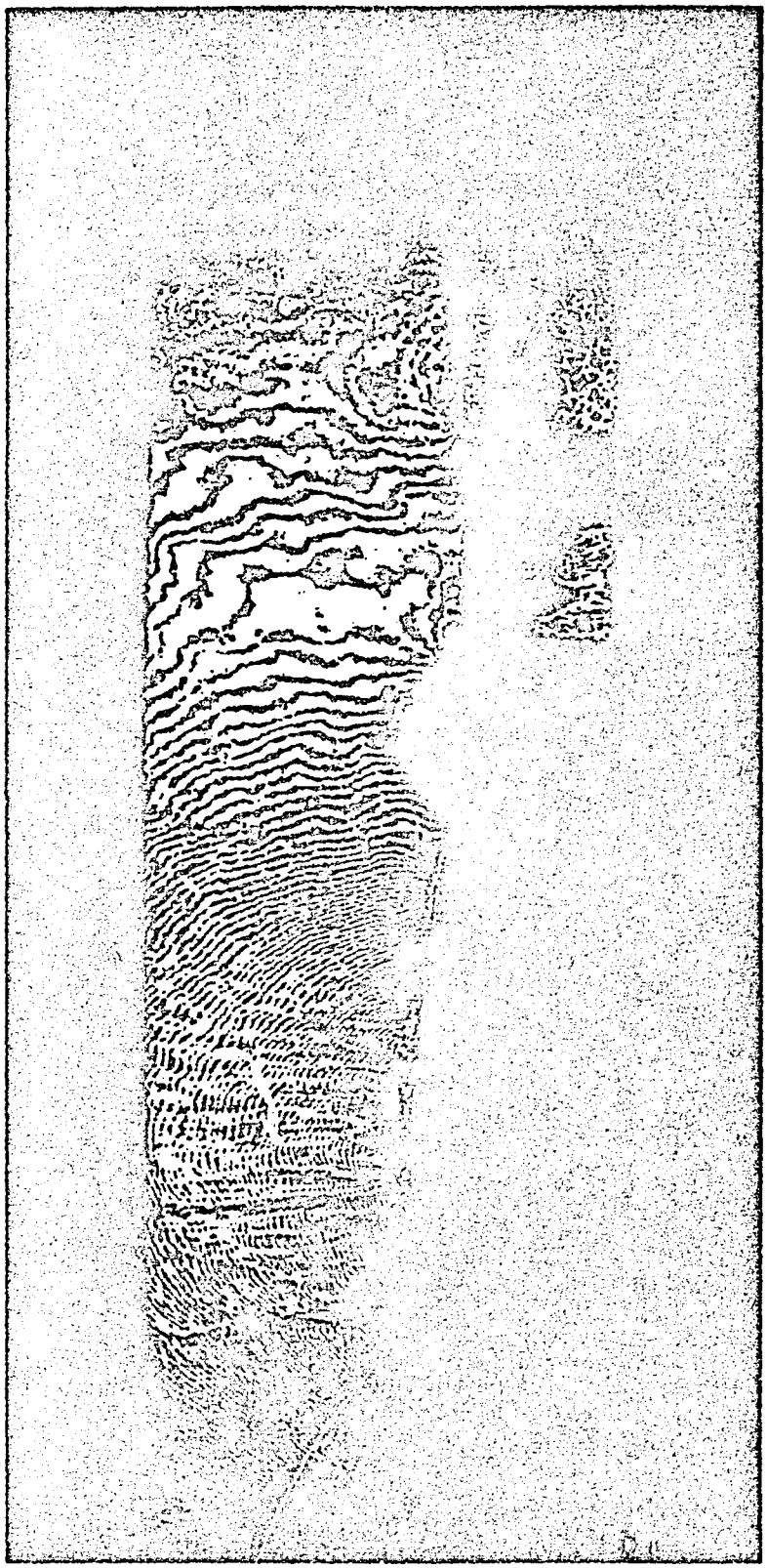

Y(a) Phase Angle = 162°

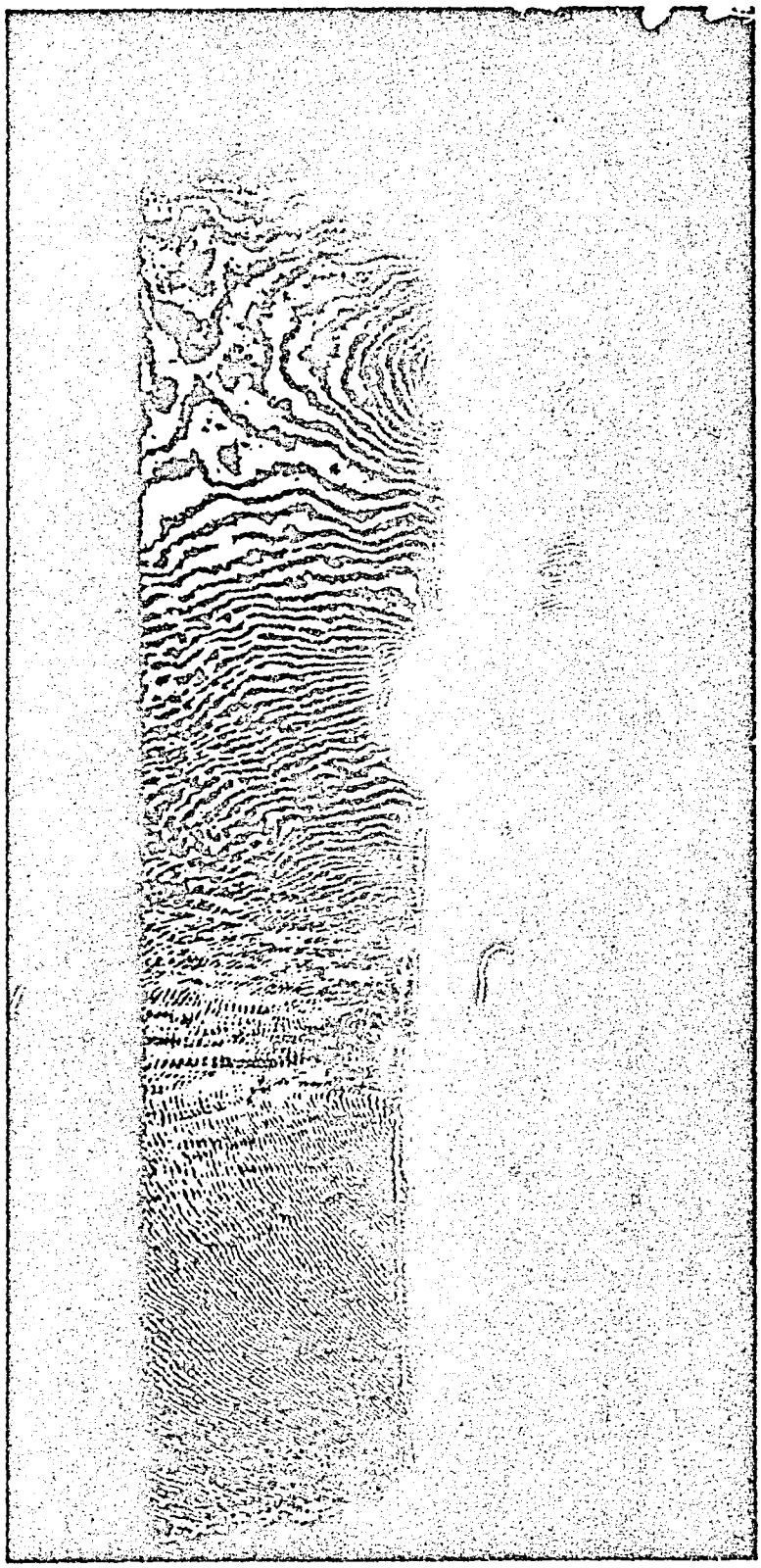

7(e) Phase Angle = 234°

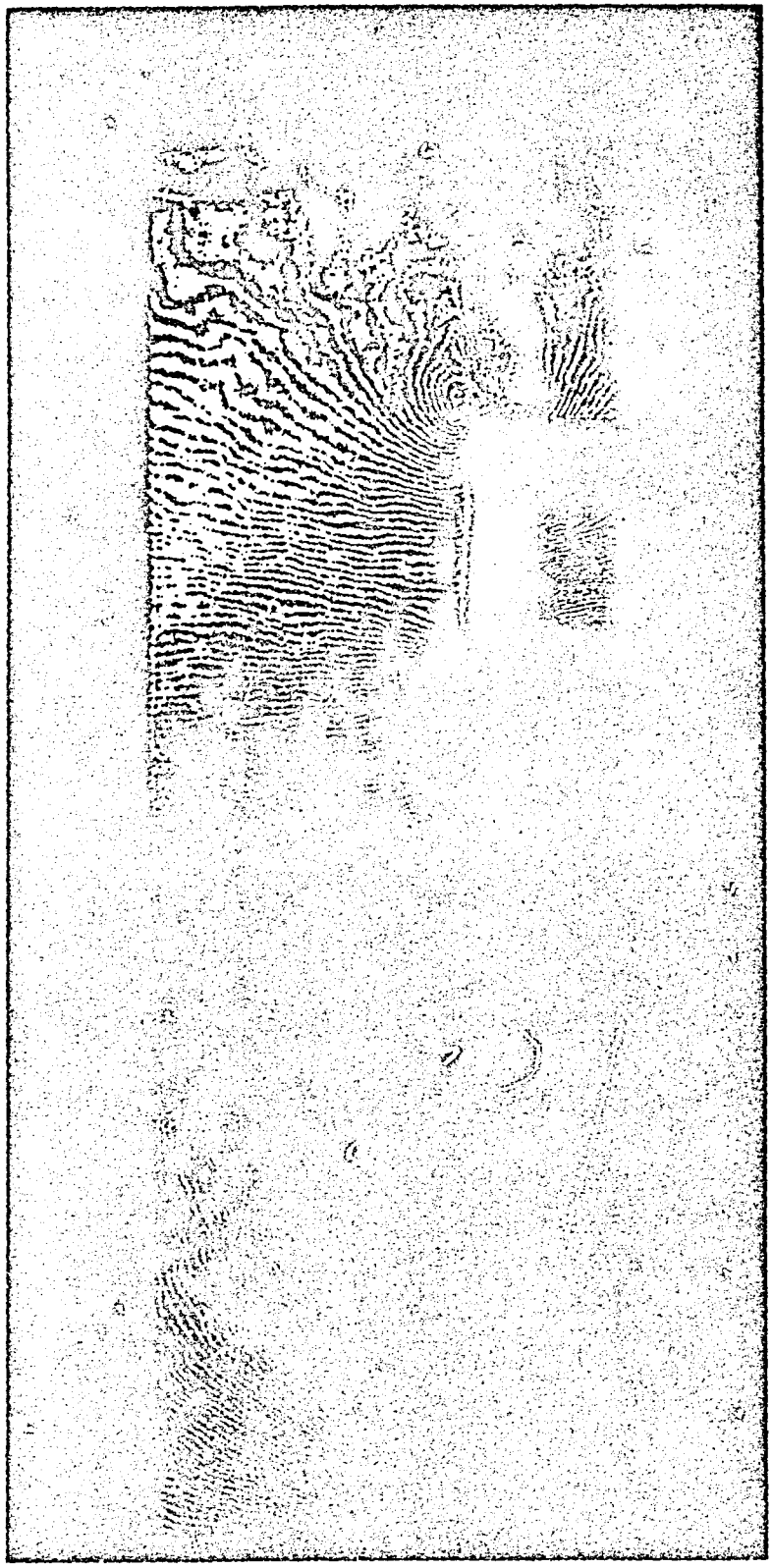

7(f) Phase Angle = 270°

7(g) Phase Angle = 306°

7(h) Phase Angle = 342°

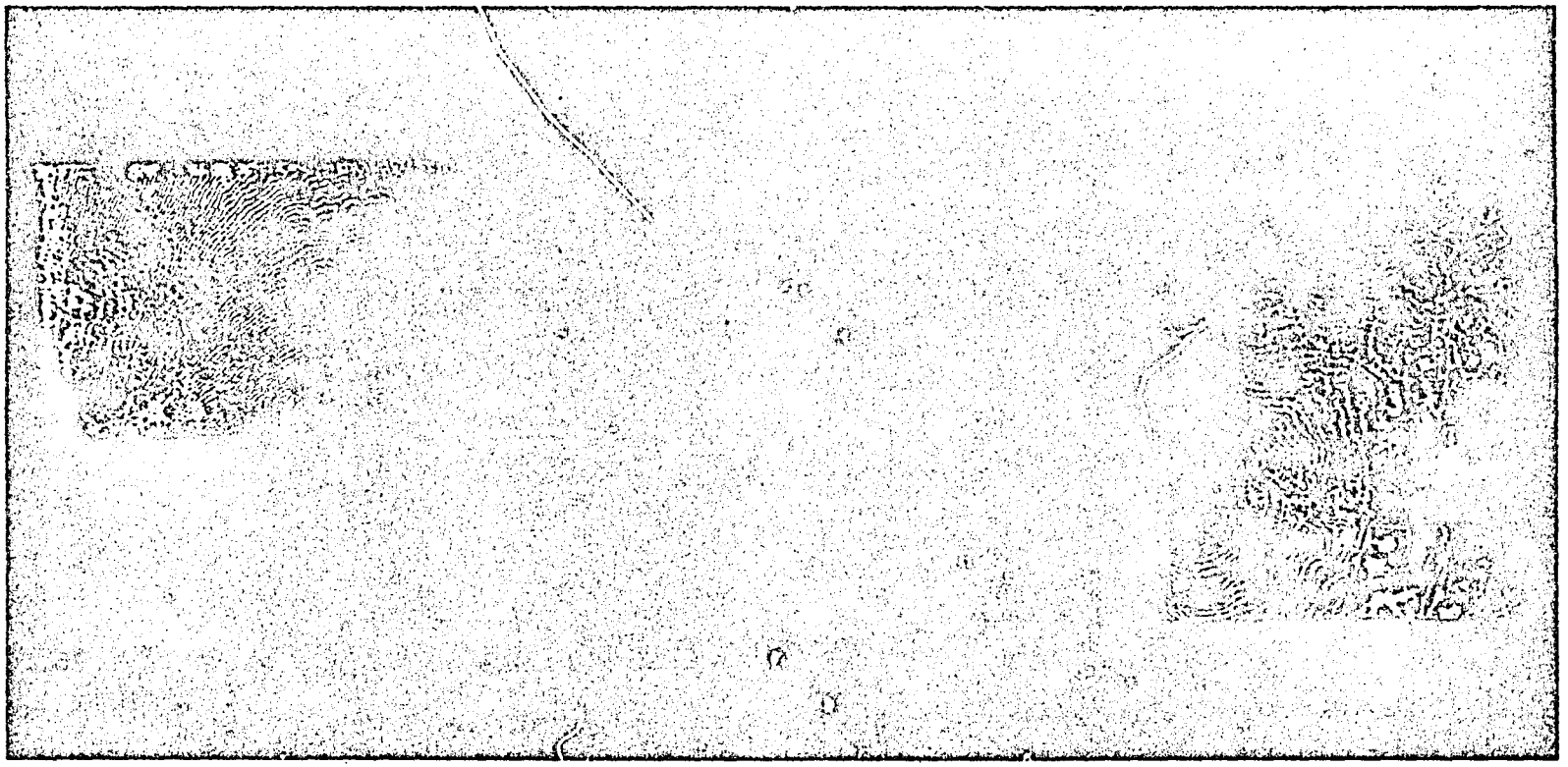

8(a) Phase Angle = 126°

Figure 8.- Interferograms of the NACA 64A010 Airfoil with Oscillating Flap, Mean Flap Angle at 0°, P_T = 4238 psf

8(b) Phase Angle = 198°

8(c) Phase Angle = 270°

9(a) Phase Angle = 0°

Figure 9.- Interferograms of the NACA 64A010 Airfoil with Oscillating Flap, Mean Flap Angle at -4°, Airfoil Angle of Attack at +4°

9(b) Phase Angle = 90°

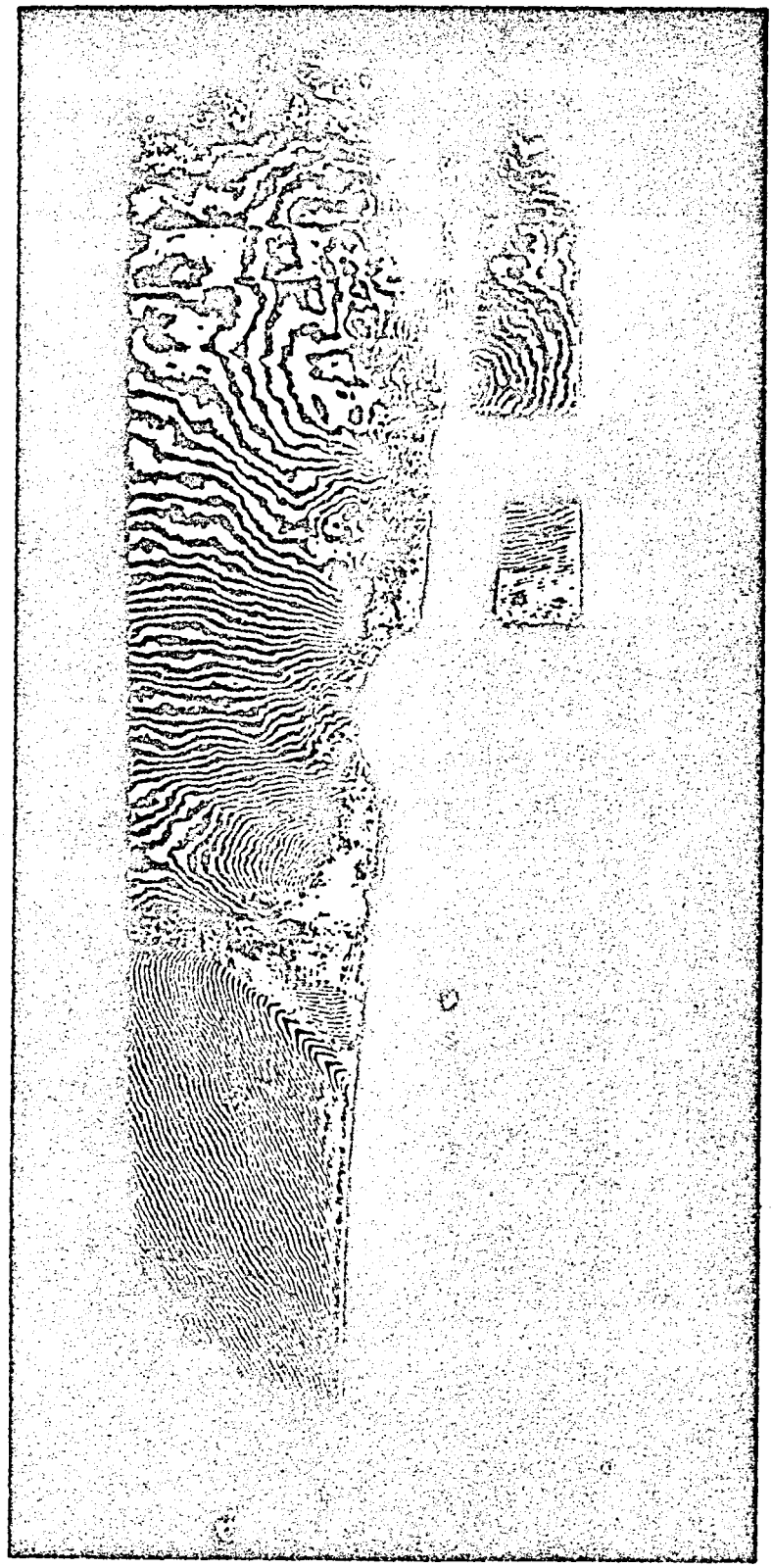

9(c) Phase Angle = 180°

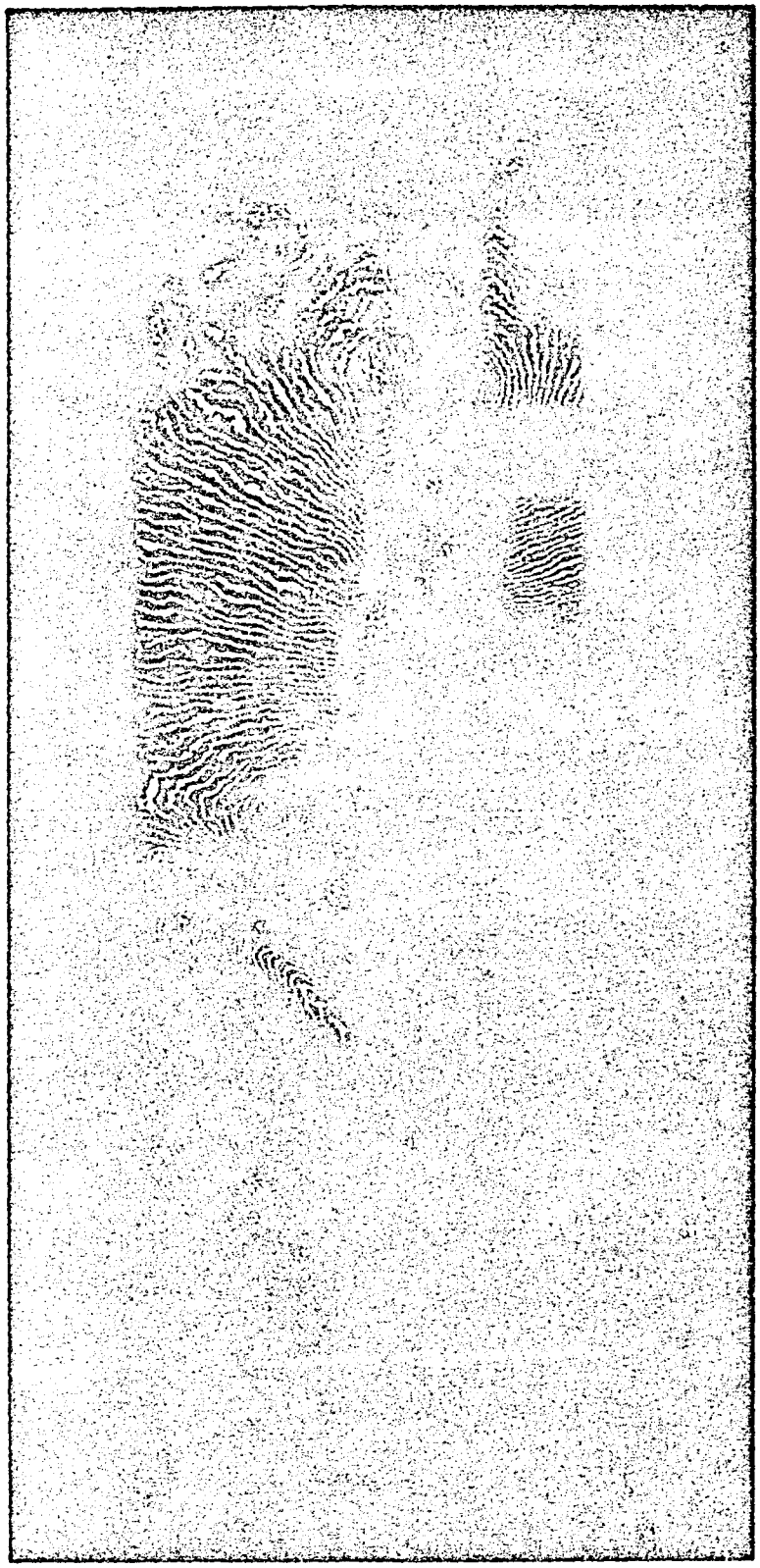

9(d) Phase Angle = 225°

9(e) Phase Angle = 270°

HOLOGRAPHIC DATA - 11 foot - Oscillating Flap
0117

RUN: 117	SEQ: 3	
FLAP MEAN: 0	AMPL: 2	FREQ: 30
PHASE NO.: 1	ANGLE: 0	DELTA:-.04
MACH: .8	ALPHA: 0	PRINT NO.: 1
Ptot: 2089.3 psf	Pinf: .1373 psf	Ttot: 549.3 Rankine

UPPER SURFACE:	x/c	N	Cp	LOWER SURFACE:	x/c	N	Cp
	.25	7	-.55				
	.3	0	-.591				
	.35	-8	-.639				
	.4	-21	-.715				
	.45	-36	-.802				
	.5	-45	-.853				
	.75	-8	-.063				
	.8	0	-.011				
	.85	10	.054				
	.9	15	.086				
	.95	22	.132				
	1	31	.192				
	1.05	27	.112				
	1.1	20	.066				
	1.15	17	.047				
	1.2	12	.014				

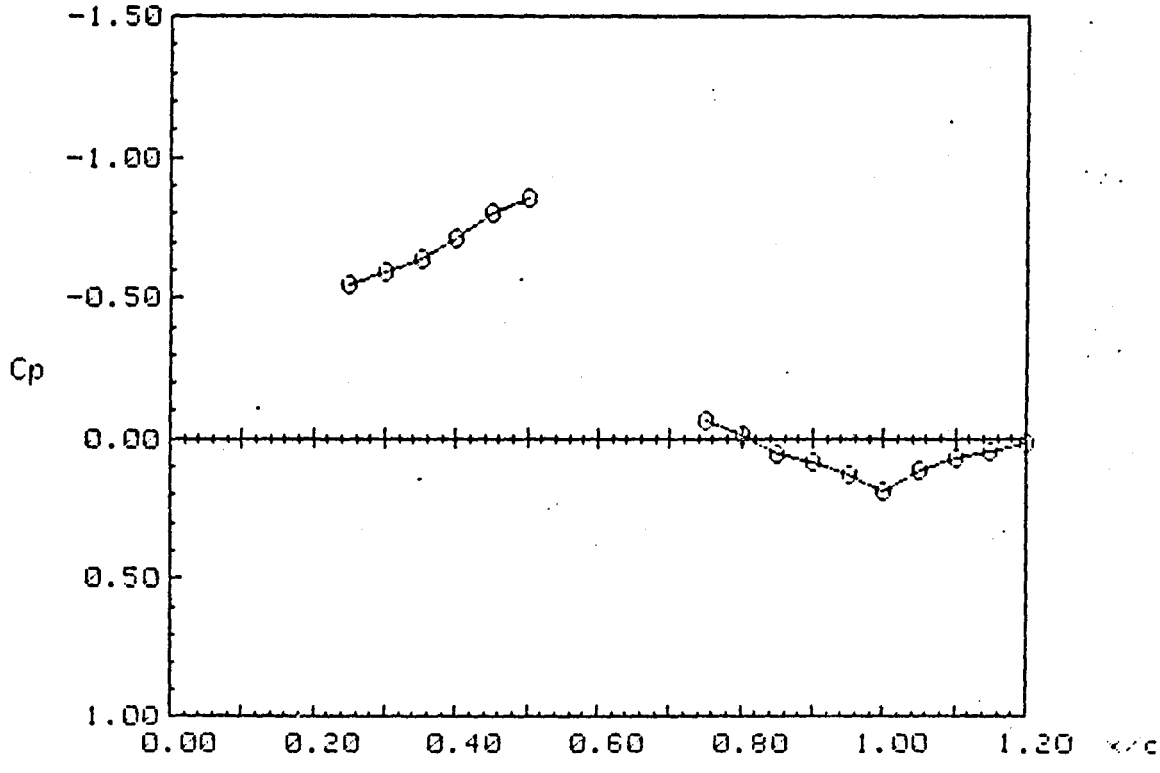

Figure 10.- Comparisons of the Pressures Obtained From the Surface Pressure Taps and the Interferometric Results. $\delta = 0° \pm 2°$, $\alpha = 0°$

PRESSURE DATA - 11 foot - Oscillating Flap

RUN: 117 SEQ: 3
FLAP MEAN: 0 AMPL.: 2 FREQ.: 30
PHASE NO.: 1 ANGLE: 0 DELTA:-.04
MACH: .8 ALPHA: 0
Ptot: 2089.3 psf Pinf: 1373 psf Ttot: 549.3 Rankine

UPPER SURFACE:	x/c	Cp
	0	1.174
	.05	-.217
	.1	-.347
	.15	-.429
	.2	-.488
	.25	-.531
	.3	-.591
	.35	-.655
	.4	-.741
	.45	-.811
	.5	-.84
	.55	-.852
	.6	-.276
	.643	-.118
	.705	-.07
	.797	-.011
	.849	.076
	.95	.15

LOWER SURFACE:	x/c	Cp
	.05	-.162
	.1	-.257
	.15	-.339
	.2	-.393
	.25	-.433
	.3	-.489
	.35	-.494
	.4	-.604
	.45	-.665
	.5	-.468
	.55	-.337
	.6	-.284
	.643	-.218
	.762	-.169
	.793	-.077
	.824	-.029
	.849	-.001
	.895	.053
	.946	.125

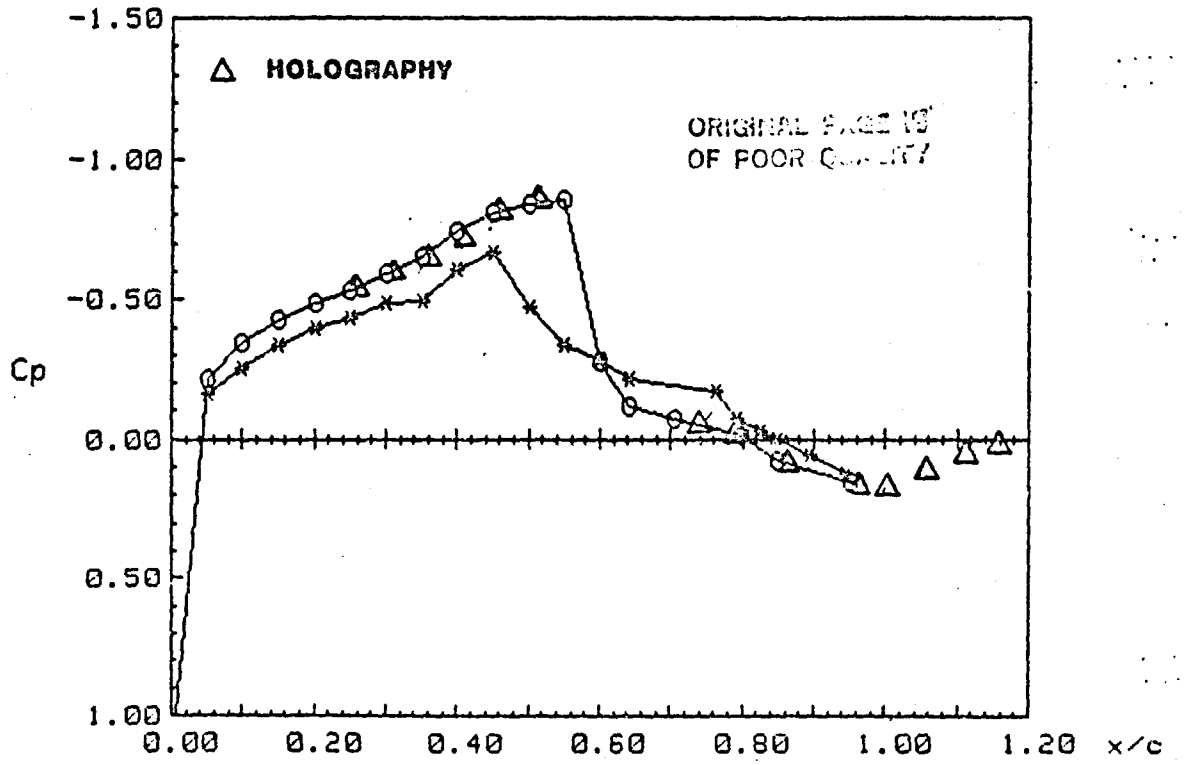

HOLOGRAPHIC DATA - 11 foot - Oscillating Flap
36117

RUN: 117	SEQ: 3	
FLAP MEAN: 0	AMPL: 2	FREQ: 30
PHASE NO.: 5	ANGLE: 36	DELTA:-1.18
MACH: .8	ALPHA: 0	PRINT NO.: 1
Ptot: 2089.3 psf	Pinf: 1373 psf	Ttot: 549.3 Rankine

UPPER SURFACE:	x/c	N	Cp	LOWER SURFACE:	x/c	N	Cp
	.15	44	-.396				
	.2	31	-.475				
	.25	21	-.536				
	.3	11	-.595				
	.35	0	-.66				
	.4	-11	-.725				
	.45	-25	-.805				
	.5	-30	-.834				
	.6	-40	-.152				
	.65	-29	-.082				
	.7	-25	-.056				
	.75	-21	-.03				
	.8	-14	.015				
	.85	-7	.061				
	.9	0	.107				
	.95	6	.146				
	1	15	.206				
	1.05	9	.166				
	1.1	4	.133				
	1.15	0	.107				
	1.2	-3	.087				

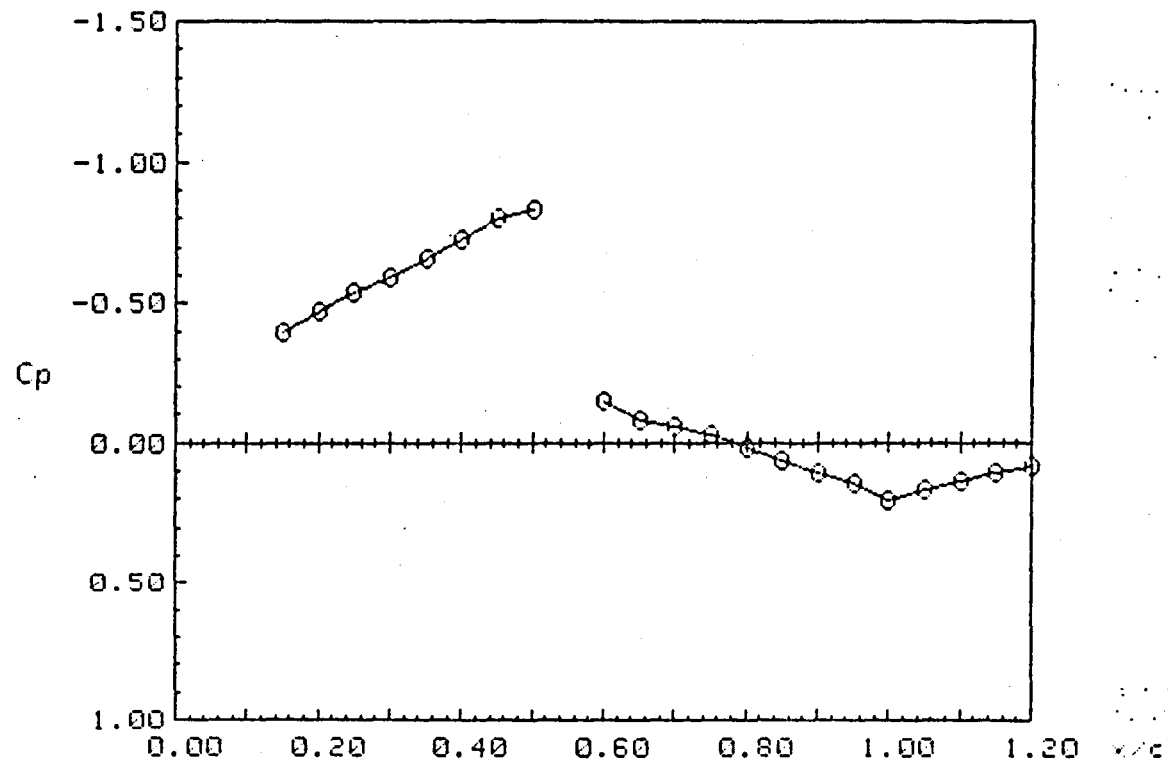

PPESSURE DATA - 11 foot - Oscillating Flap

RUN: 117 SEQ: 3
FLAP MEAN: 0 AMPL.: 2 FREQ.: 30
PHASE NO.: 5 ANGLE: 36 DELTA:-1.12
MACH: .8 ALPHA: 0
Ptot: 2089.3 psf Pinf: 1373 psf Ttot: 549.3 Rankine

UPPER SURFACE: x/c	Cp	LOWER SURFACE: x/c	Cp
0	1.174	.05	-.148
.05	-.233	.1	-.246
.1	-.36	.15	-.33
.15	-.439	.2	-.389
.2	-.496	.25	-.433
.25	-.547	.3	-.489
.3	-.599	.35	-.523
.35	-.661	.4	-.633
.4	-.745	.45	-.704
.45	-.813	.5	-.74
.5	-.841	.55	-.387
.55	-.441	.6	-.299
.6	-.138	.643	-.243
.643	-.046	.762	-.23
.705	-.029	.793	-.127
.797	.024	.824	-.058
.849	.092	.849	-.02
.95	.149	.895	.044
		.946	.123

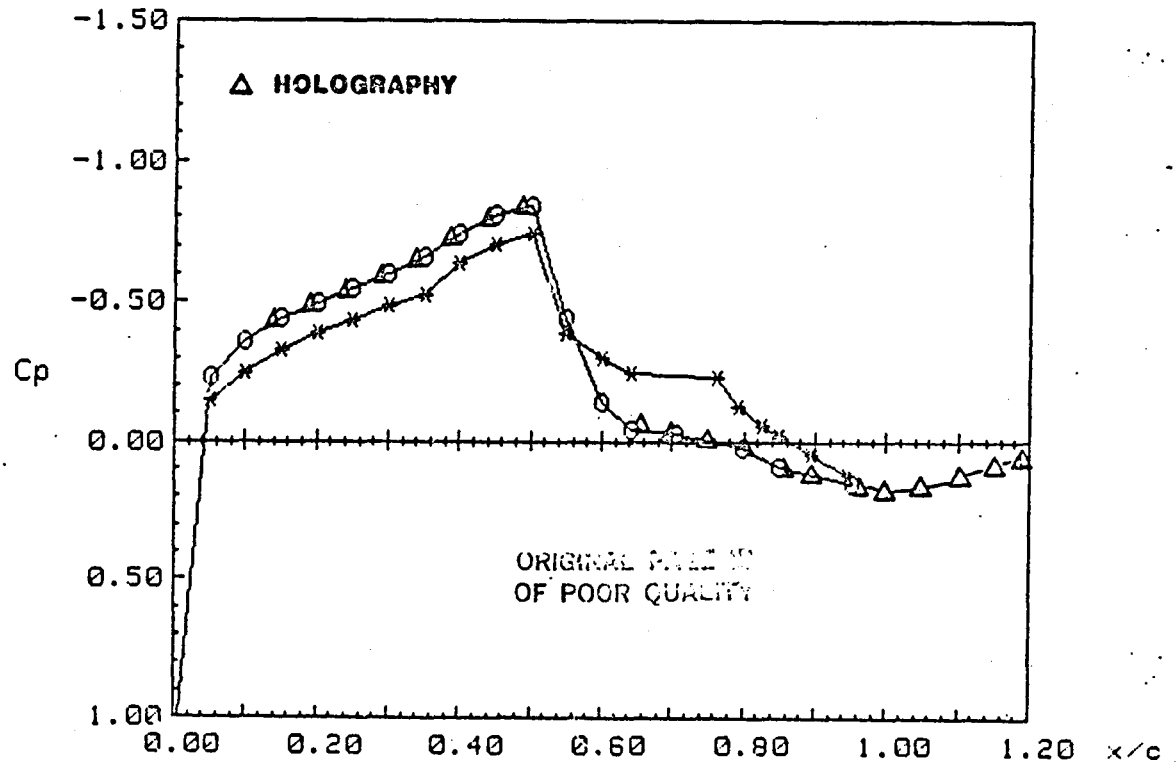

HOLOGRAPHIC DATA - 11 foot - Oscillating Flap
54328
RUN: 128 SEQ: 11
FLAP MEAN: 0 AMPL: 2 FREQ: 33
PHASE NO.: 7 ANGLE: 54 DELTA:-1.62
MACH: .8 ALPHA: 0 PRINT NO.: 3
Ptot: 2087.9 psf Pinf: 1370 psf Ttot: 550.15 Rankine

UPPER SURFACE:	x/c	N	Cp
	.25	8	-.552
	.3	0	-.599
	.35	-9	-.653
	.4	-21	-.723
	.45	-33	-.792
	.6	-37	-.134
	.65	-30	-.089
	.7	-26	-.064
	.75	-20	-.025
	.8	-11	.033
	.85	-5	.073
	.9	0	.106
	.95	7	.152
	1	17	.218
	1.05	12	.185
	1.1	5	.138
	1.15	2	.119
	1.2	0	.106

LOWER SURFACE:	x/c	N	Cp

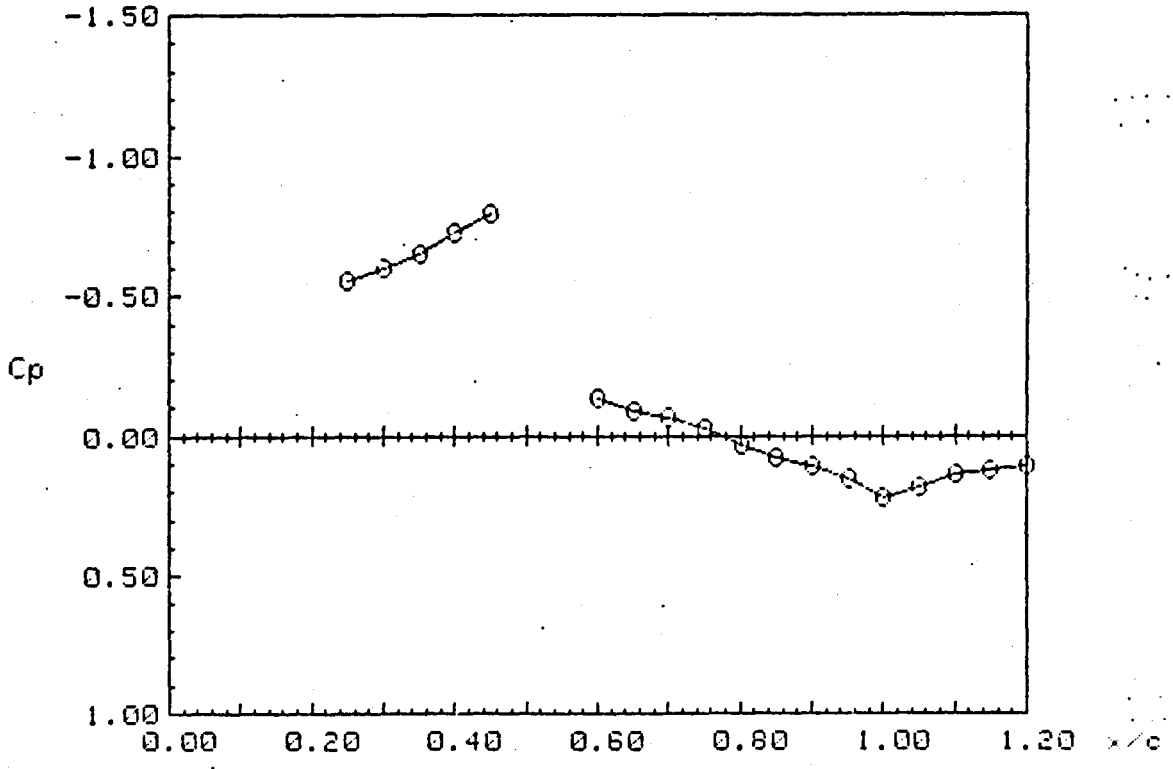

PRESSURE DATA - 11 foot - Oscillating Flap

RUN: 128 SEQ: 11
FLAP MEAN: 0 AMPL.: 2 FREQ.: 30
PHASE NO.: 7 ANGLE: 54 DELTA:-1.54
MACH: .8 ALPHA: 0
Ptot: 2087.9 psf Pinf: 1370 psf Ttot: 550.15 Rankine

UPPER SURFACE: x/c	Cp	LOWER SURFACE: x/c	Cp
0	1.178	.05	-.152
.05	-.234	.1	-.249
.1	-.362	.15	-.349
.15	-.44	.2	-.419
.2	-.496	.25	-.455
.25	-.561	.3	-.52
.3	-.608	.35	-.547
.35	-.668	.4	-.655
.4	-.75	.45	-.723
.45	-.812	.5	-.794
.5	-.851	.55	-.598
.55	-.241	.6	-.324
.6	-.113	.643	-.239
.643	.007	.762	-.243
.705	-.008	.793	-.134
.797	.027	.824	-.06
.849	.097	.849	-.018
.95	.148	.895	.046
		.946	.126

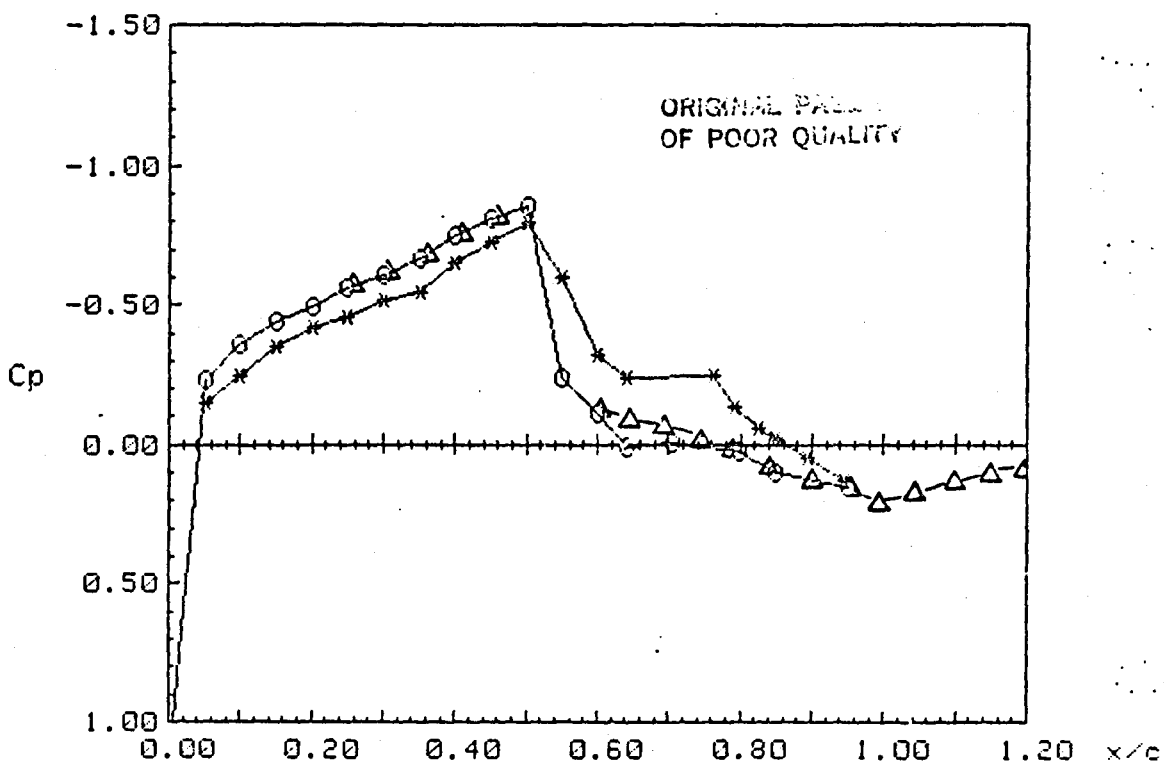

HOLOGRAPHIC DATA - 11 foot - Oscillating Flap
72117

RUN: 117	SEQ: 3	
FLAP MEAN: 0	AMPL: 2	FREQ: 30
PHASE NO.: 9	ANGLE: 72	DELTA:-1.88
MACH: .8	ALPHA: 0	PRINT NO.: 1
Ptot: 2089.3 psf	Pinf: 1373 psf	Ttot: 549.3 Rankine

UPPER SURFACE:	x/c	N	Cp	LOWER SURFACE:	x/c	N	Cp
	.15	10	-.437				
	.2	0	-.497				
	.25	-9	-.552				
	.3	-17	-.599				
	.35	-28	-.664				
	.4	-40	-.734				
	.45	-36	-.711				
	.55	-14	-.122				
	.6	-9	-.09				
	.65	0	-.032				
	.7	5	0				
	.75	10	.032				
	.8	19	.091				
	.85	28	.151				
	.9	32	.177				
	.95	37	.21				
	1	46	.27				
	1.05	40	.137				
	1.1	34	.098				
	1.15	32	.085				
	1.2	29	.065				

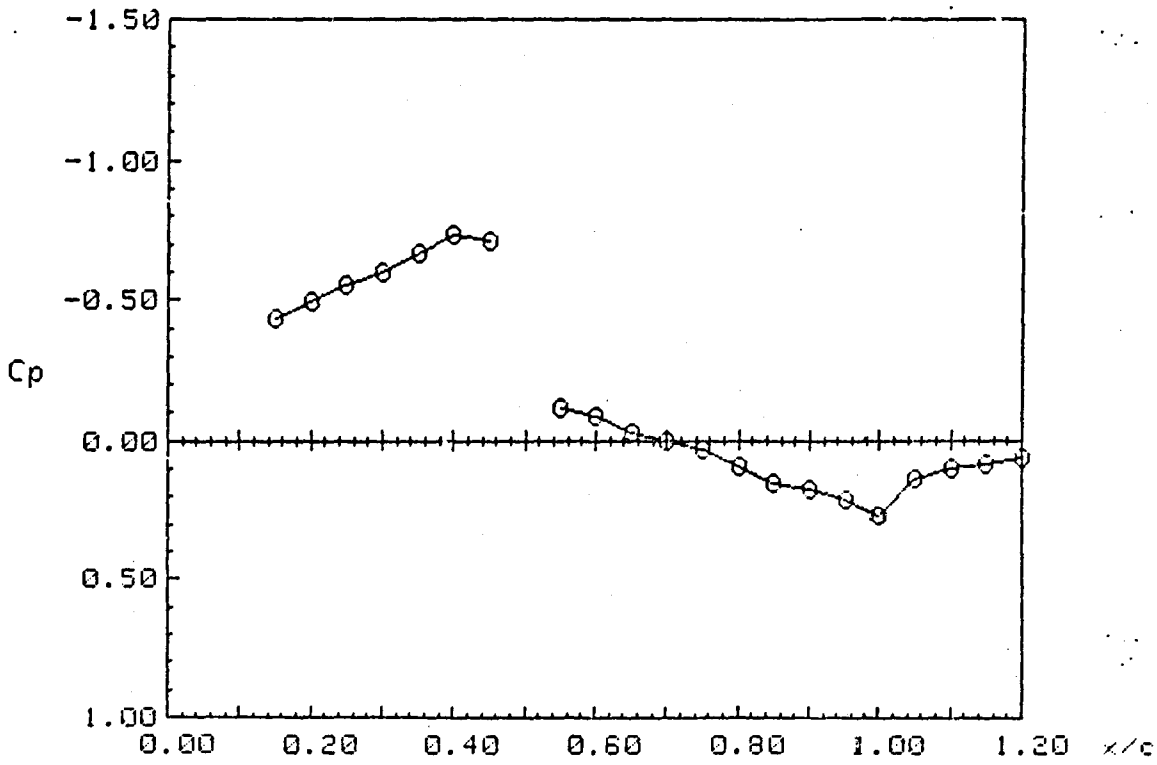

PRESSURE DATA - 11 foot - Oscillating Flap

RUN: 117 SEQ: 3
FLAP MEAN: 0 AMPL.: 2 FREQ.: 30
PHASE NO.: 9 ANGLE: 72 DELTA:-1.88
MACH: .8 ALPHA: 0
Ptot: 2089.3 psf Pinf: 1373 psf Ttot: 549.3 Rankine

UPPER SURFACE:	x/c	Cp	LOWER SURFACE:	x/c	Cp
	0	1.172		.05	-.152
	.05	-.236		.1	-.252
	.1	-.362		.15	-.34
	.15	-.441		.2	-.402
	.2	-.497		.25	-.452
	.25	-.546		.3	-.516
	.3	-.597		.35	-.545
	.35	-.658		.4	-.652
	.4	-.741		.45	-.729
	.45	-.806		.5	-.779
	.5	-.684		.55	-.73
	.55	-.166		.6	-.329
	.6	-.096		.643	-.266
	.643	-.032		.762	-.244
	.705	-.026		.793	-.14
	.797	.022		.824	-.069
	.849	.089		.849	-.024
	.95	.143		.895	.042
				.946	.122

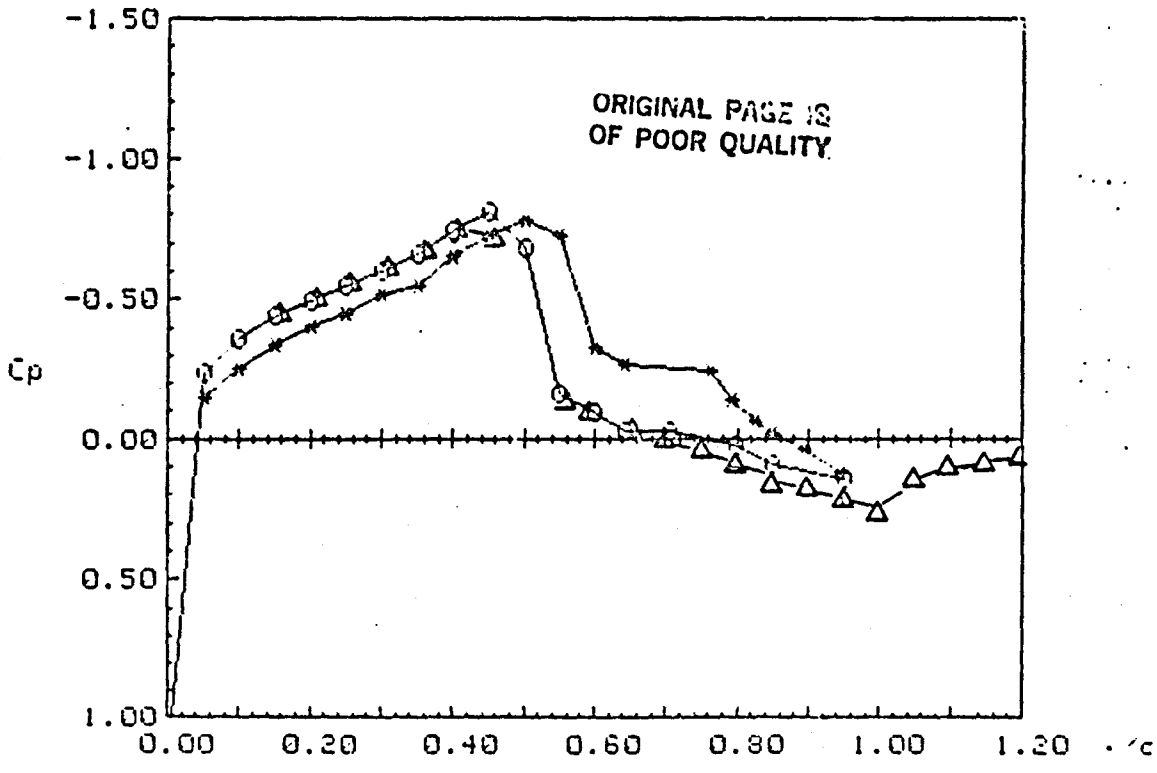

100117
RUN: 117 SEQ: 3
FLAP MEAN: 0 AMPL: 2 FREQ: 30
PHASE NO.: 13 ANGLE: 100 DELTA:-1.9
MACH: .8 ALPHA: 0 PRINT NO.: 1
Ptot: 2089.3 psf Pinf: 1373 psf Ttot: 549.3 Rankine

UPPER SURFACE:	x/c	N	Cp
	.15	0	-.427
	.2	-9	-.482
	.25	-17	-.531
	.3	-24	-.572
	.35	-28	-.596
	.4	-38	-.655
	.45	-33	-.626
	.55	0	-.186
	.6	7	-.142
	.65	15	-.091
	.7	19	-.065
	.75	23	-.039
	.8	30	.006
	.85	41	.078
	.9	47	.117
	.95	53	.157
	1	63	.223
	1.05	57	.183
	1.1	53	.157
	1.15	49	.13
	1.2	46	.111

LOWER SURFACE:	x/c	N	Cp

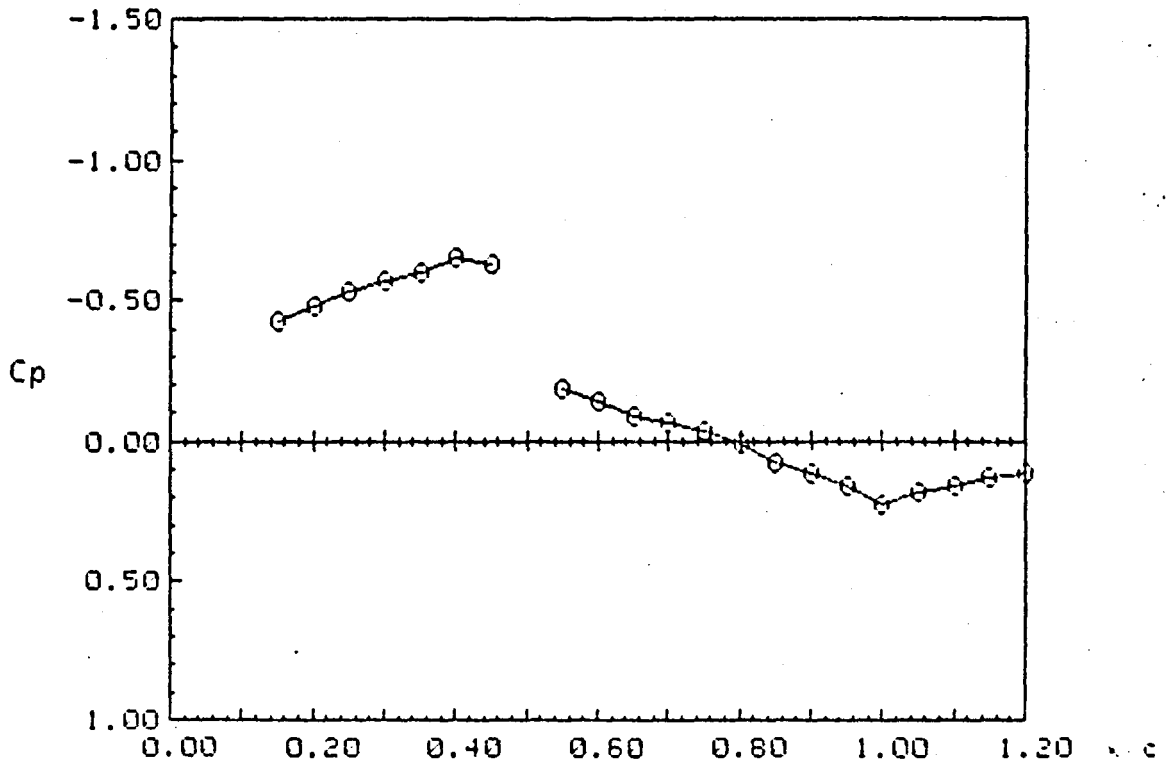

PRESSURE DATA - 11 foot - Oscillating Flap

RUN: 117 SEQ: 3
FLAP MEAN: 0 AMPL.: 2 FREQ.: 30
PHASE NO.: 13 ANGLE: 108 DELTA:-1.9
MACH: .8 ALPHA: 0
Ptot: 2089.3 psf Pinf: 1373 psf Ttot: 549.3 Rankine

UPPER SURFACE: x/c	Cp	LOWER SURFACE: x/c	Cp
0	1.171	.05	-.169
.05	-.223	.1	-.269
.1	-.349	.15	-.36
.15	-.427	.2	-.421
.2	-.482	.25	-.471
.25	-.527	.3	-.535
.3	-.577	.35	-.572
.35	-.634	.4	-.666
.4	-.71	.45	-.747
.45	-.75	.5	-.799
.5	-.273	.55	-.788
.55	-.186	.6	-.439
.6	-.14	.643	-.267
.643	-.067	.762	-.209
.705	-.064	.793	-.11
.797	-.007	.824	-.049
.849	.066	.849	-.006
.95	.135	.895	.051
		.946	.126

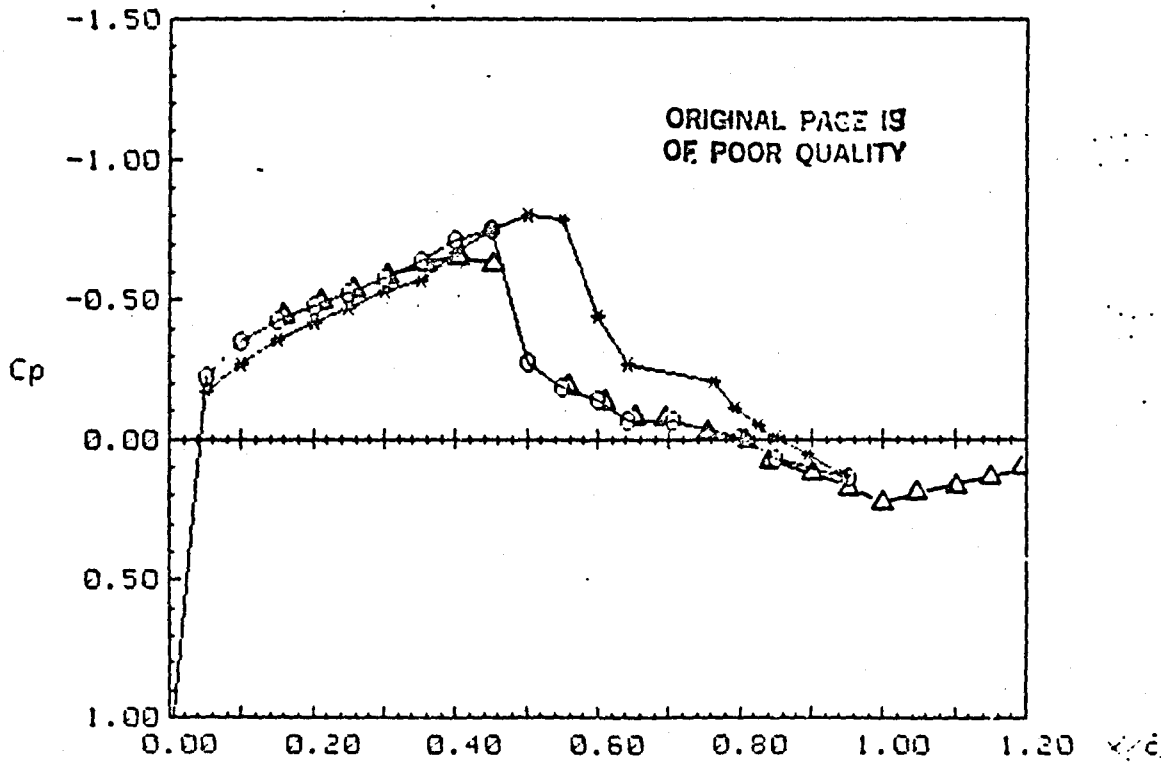

HOLOGRAPHIC DATA - 11 foot - Oscillating Flap
144217

RUN: 117	SEQ: 3	
FLAP MEAN: 0	AMPL: 2	FREQ: 30
PHASE NO.: 17	ANGLE: 144	DELTA:-1.22
MACH: .8	ALPHA: 0	PRINT NO.: 2
Ptot: 2089.3 psf	Pinf: 1373 psf	Ttot: 549.3 Rankine

UPPER SURFACE:	x/c	N	Cp	LOWER SURFACE:	x/c	N	Cp
	.15	0	-.401				
	.2	-8	-.45				
	.25	-17	-.505				
	.3	-24	-.547				
	.35	-31	-.589				
	.4	-39	-.636				
	.55	0	-.268				
	.6	6	-.231				
	.65	20	-.142				
	.7	24	-.117				
	.75	25	-.11				
	.8	37	-.033				
	.85	49	.045				
	.9	57	.097				
	.95	66	.157				
	1	79	.243				
	1.05	71	.19				
	1.1	64	.143				
	1.15	59	.11				
	1.2	55	.084				

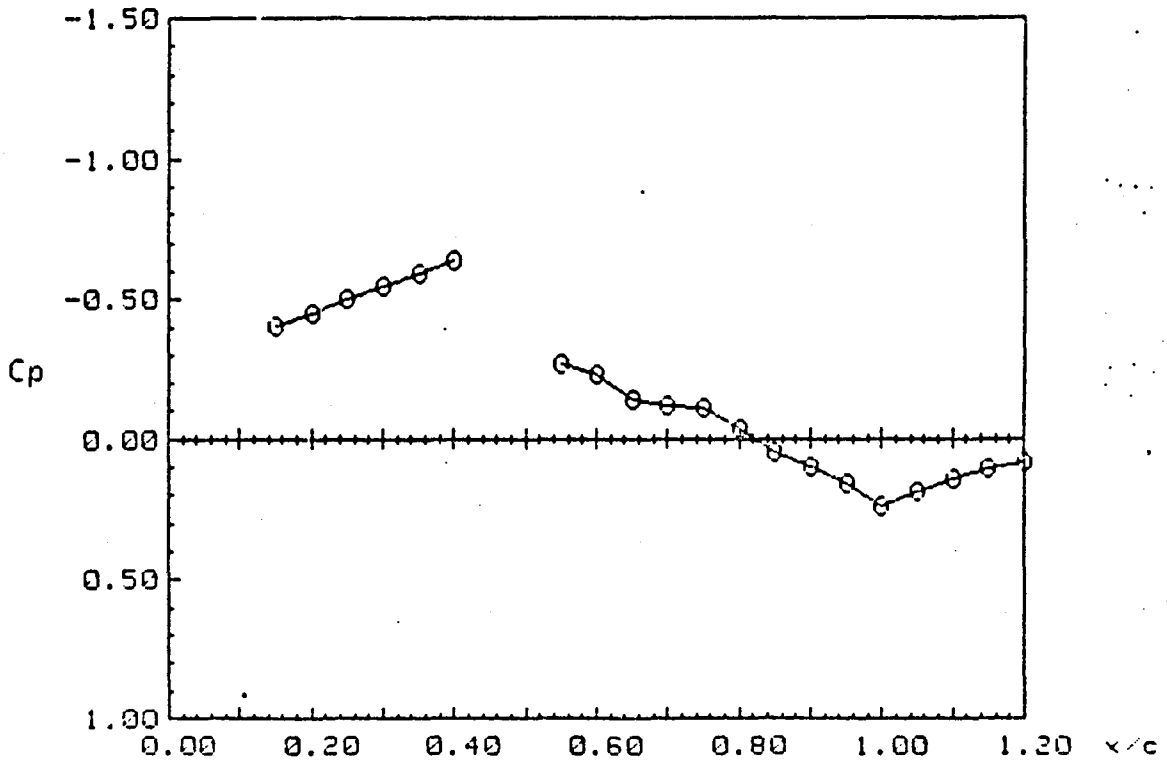

PRESSURE DATA - 11 foot - Oscillating Flap

RUN: 117 SEQ: 3
FLAP MEAN: 0 AMPL.: 2 FREQ.: 30
PHASE NO.: 17 ANGLE: 144 DELTA:-1.22
MACH: .8 ALPHA: 0
Ptot: 2089.3 psf Pinf: 1373 psf Ttot: 549.3 Rankine

UPPER SURFACE: x/c	Cp	LOWER SURFACE: x/c	Cp
0	1.171	.05	-.189
.05	-.198	.1	-.288
.1	-.325	.15	-.381
.15	-.401	.2	-.439
.2	-.456	.25	-.492
.25	-.502	.3	-.552
.3	-.539	.35	-.604
.35	-.589	.4	-.684
.4	-.656	.45	-.757
.45	-.524	.5	-.817
.5	-.359	.55	-.81
.55	-.268	.6	-.554
.6	-.202	.643	-.254
.643	-.12	.762	-.128
.705	-.127	.793	-.046
.797	-.065	.824	0
.849	.036	.849	.025
.95	.129	.895	.07
		.946	.133

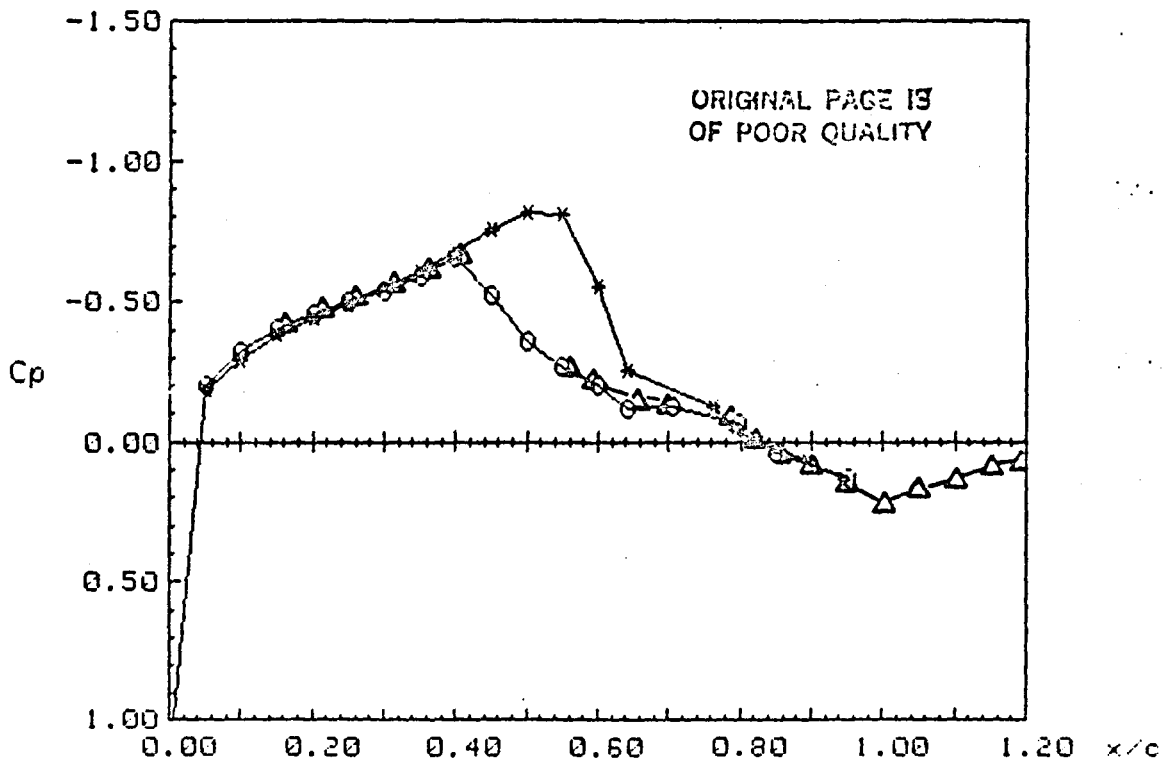

HOLOGRAPHIC DATA - 11 foot - Oscillating Flap
180217

RUN: 117	SEQ: 3	
FLAP MEAN: 0	AMPL: 2	FREQ: 30
PHASE NO.: 21	ANGLE: 180	DELTH: 0
MACH: .8	ALPHA: 0	PRINT NO.: 2
Ptot: 2089.3 psf	Pinf: 1373 psf	Ttot: 549.3 Rankine

UPPER SURFACE:	x/c	N	Cp	LOWER SURFACE:	x/c	N	Cp
	.15	14	-.346				
	.2	0	-.432				
	.25	-10	-.493				
	.3	-18	-.541				
	.35	-26	-.589				
	.4	-36	-.648				
	.45	-45	-.701				
	.6	-5	-.21				
	.65	0	-.178				
	.7	3	-.159				
	.75	4	-.153				
	.8	16	-.076				
	.85	29	.008				
	.9	37	.06				
	.95	47	.125				
	1	60	.212				
	1.05	51	.118				
	1.1	45	.079				
	1.15	41	.053				
	1.2	39	.04				

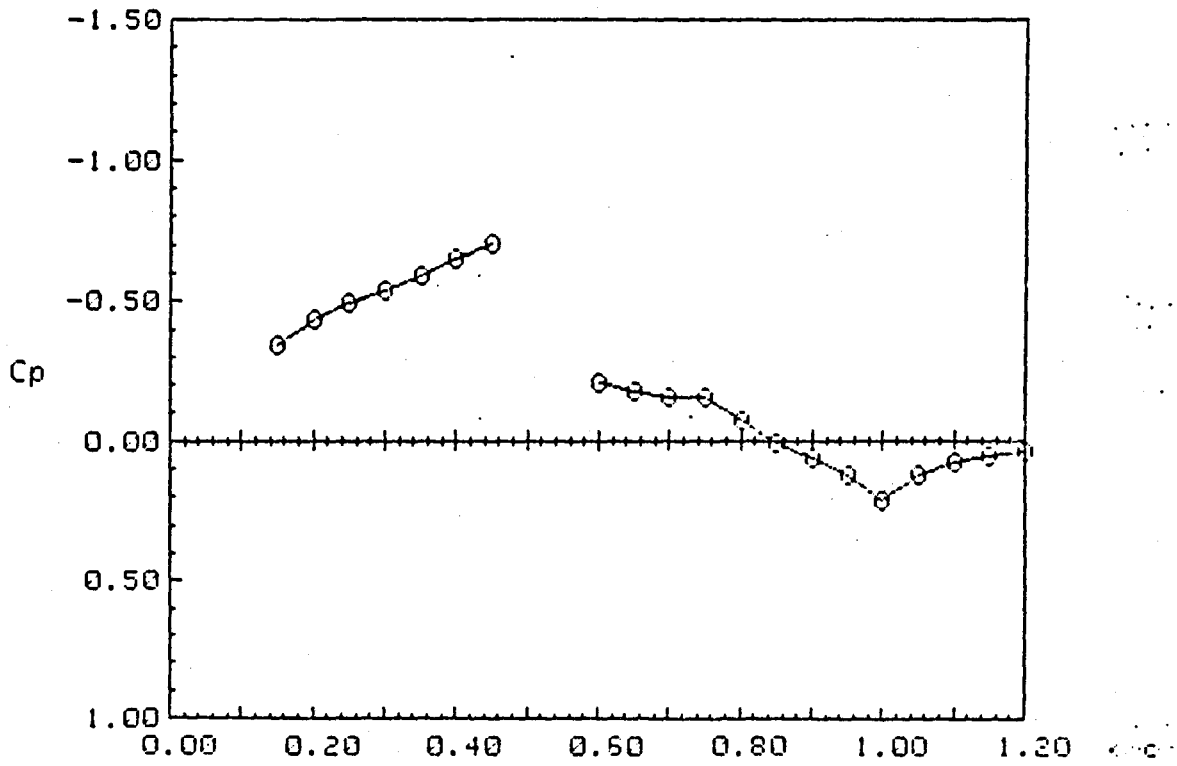

PRESSURE DATA - 11 foot - Oscillating Flap

RUN: 117 SEQ: 3
FLAP MEAN: 0 AMPL.: 2 FREQ.: 30
PHASE NO.: 21 ANGLE: 180 DELTA: 0
MACH: .8 ALPHA: 0
Ptot: 2089.3 psf Pinf: 1373 psf Ttot: 549.3 Rankine

UPPER SURFACE: x/c	Cp
0	1.171
.05	-.168
.1	-.299
.15	-.376
.2	-.432
.25	-.47
.3	-.508
.35	-.563
.4	-.639
.45	-.675
.5	-.484
.55	-.341
.6	-.263
.643	-.178
.705	-.201
.797	-.128
.849	.004
.95	.126

LOWER SURFACE: x/c	Cp
.05	-.213
.1	-.31
.15	-.405
.2	-.457
.25	-.513
.3	-.566
.35	-.623
.4	-.7
.45	-.765
.5	-.826
.55	-.819
.6	-.352
.643	-.185
.762	-.004
.793	.021
.824	.048
.849	.06
.895	.093
.946	.139

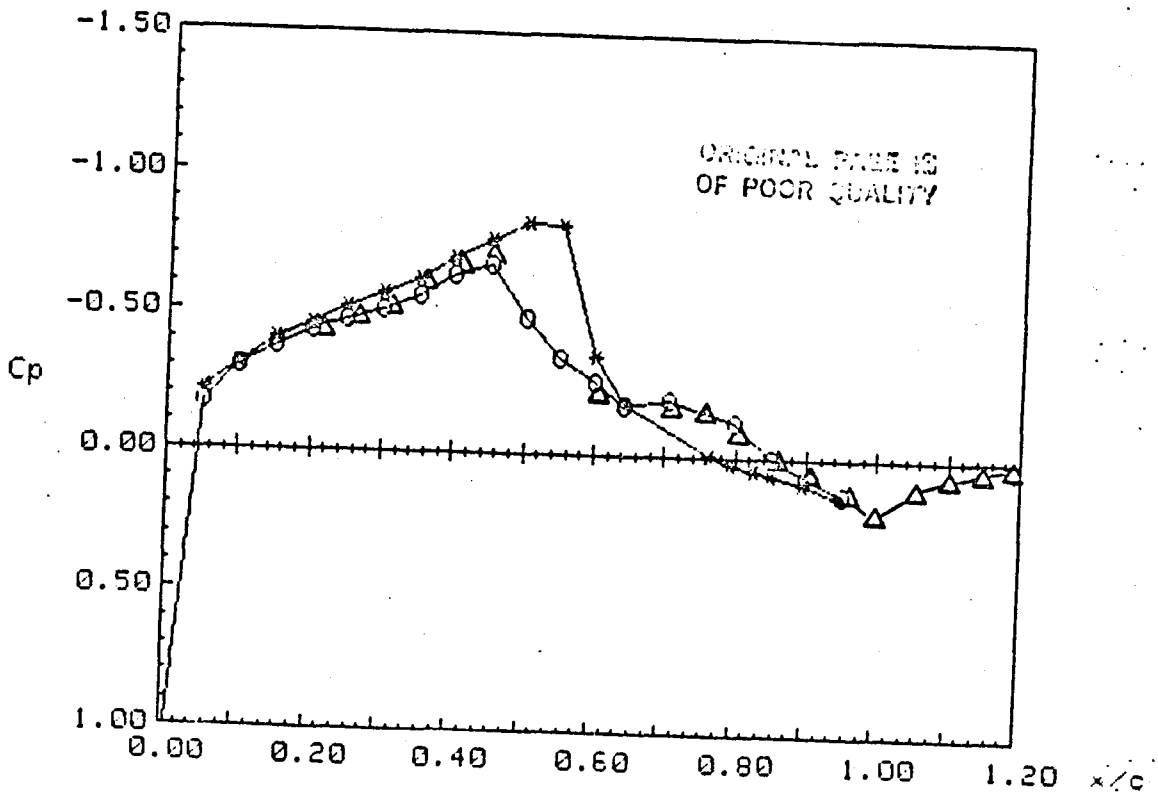

HOLOGRAPHIC DATA - 11 foot - Oscillating Flap
216217

RUN: 117 SEQ: 3
FLAP MEAN: 0 AMPL: 2 FREQ: 30
PHASE NO.: 25 ANGLE: 216 DELTA: 1.15
MACH: .8 ALPHA: 0 PRINT NO.: 2
Ptot: 2089.3 psf Pinf: 1373 psf Ttot: 549.3 Rankine

UPPER SURFACE:	x/c	N	Cp	LOWER SURFACE:	x/c	N	Cp
	.2	0	-.428				
	.25	-10	-.489				
	.3	-18	-.538				
	.35	-27	-.591				
	.4	-38	-.656				
	.45	-52	-.738				
	.5	-56	-.761				
	.55	-34	-.633				
	.7	0	-.246				
	.75	5	-.215				
	.8	19	-.126				
	.85	39	.003				
	.9	51	.081				
	.95	62	.153				
	1	76	.246				
	1.05	67	.186				
	1.1	62	.153				
	1.15	59	.134				
	1.2	56	.114				

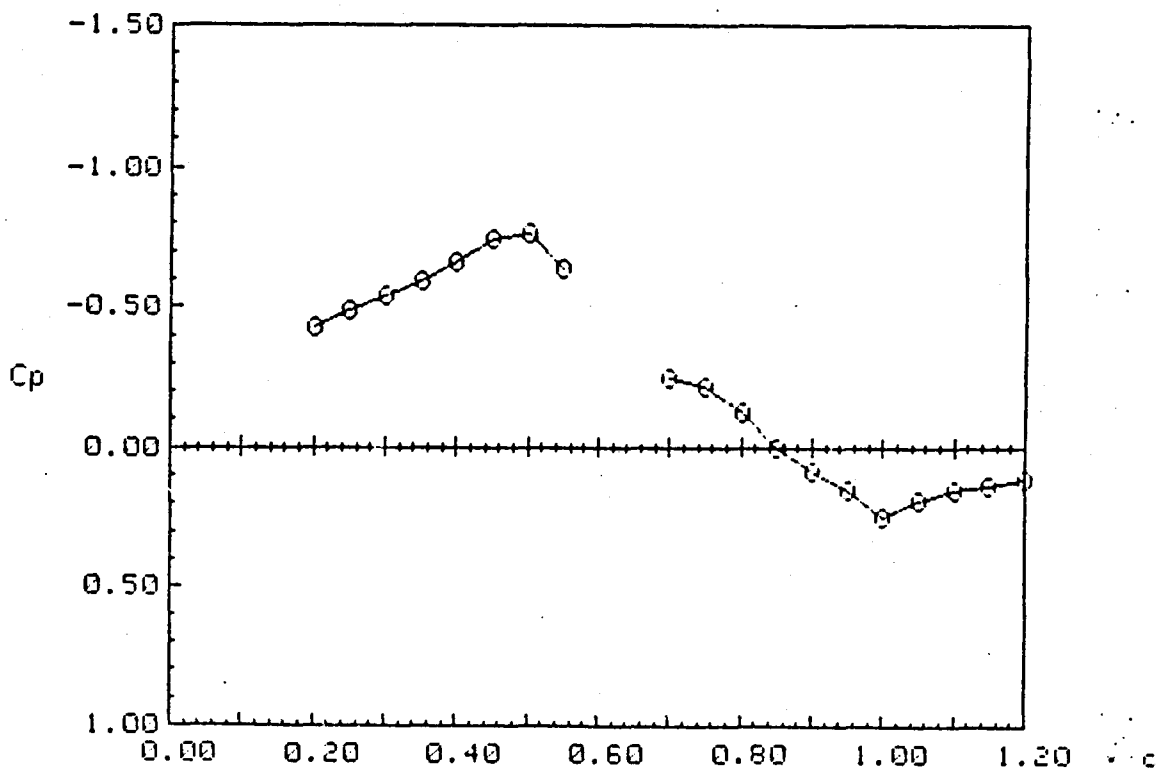

PRESSURE DATA - 11 foot - Oscillating Flap

RUN: 117 SEQ: 3
FLAP MEAN: 0 AMPL.: 2 FREQ.: 30
PHASE NO.: 25 ANGLE: 216 DELTA: 1.15
MACH: .8 ALPHA: 0
Ptot: 2089.3 psf Pinf: 1373 psf Ttot: 549.3 Rankine

UPPER SURFACE:	x/c	Cp	LOWER SURFACE:	x/c	Cp
	0	1.17		.05	-.229
	.05	-.153		.1	-.324
	.1	-.297		.15	-.421
	.15	-.368		.2	-.469
	.2	-.428		.25	-.529
	.25	-.471		.3	-.576
	.3	-.516		.35	-.631
	.35	-.579		.4	-.707
	.4	-.667		.45	-.784
	.45	-.732		.5	-.832
	.5	-.75		.55	-.627
	.55	-.421		.6	-.178
	.6	-.289		.643	-.111
	.643	-.207		.762	.078
	.705	-.246		.793	.067
	.797	-.171		.824	.083
	.849	-.019		.849	.085
	.95	.124		.895	.105
				.946	.144

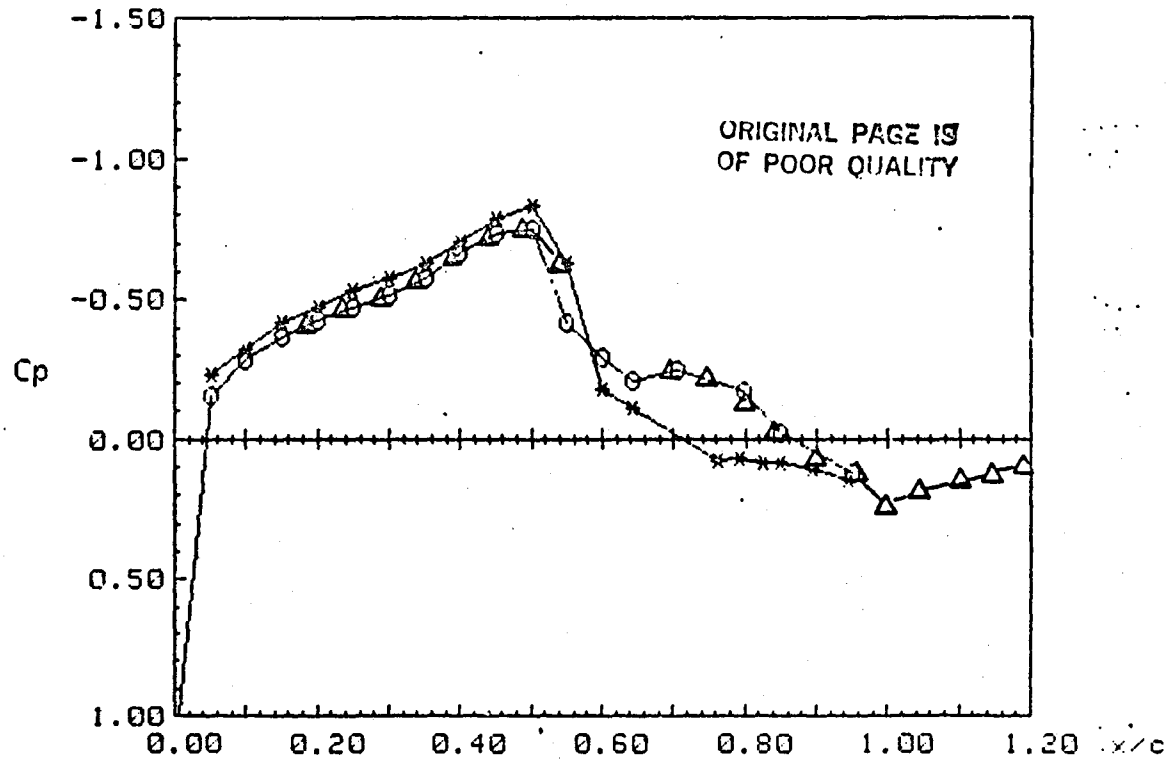

HOLOGRAPHIC DATA - 11 foot - Oscillating Flap
270128

RUN: 128	SEQ: 11	
FLAP MEAN: 0	AMPL: 2	FREQ: 30
PHASE NO.: 31	ANGLE: 270	DELTA: 2.02
MACH: .8	ALPHA: 0	PRINT NO.: 1
Ptot: 2087.9 psf	Pinf: 1370 psf	Ttot: 550.15 Rankine

UPPER SURFACE:	x/c	N	Cp	LOWER SURFACE:	x/c	N	Cp
	.2	0	-.449				
	.25	-11	-.516				
	.3	-19	-.564				
	.35	-29	-.624				
	.4	-40	-.688				
	.45	-57	-.787				
	.5	-69	-.855				
	.55	-64	-.827				
	.7	0	-.245				
	.75	-2	-.258				
	.8	12	-.17				
	.85	26	-.08				
	.9	39	.004				
	.95	53	.095				
	1	63	.161				
	1.05	55	.108				
	1.1	50	.075				
	1.15	47	.056				
	1.2	44	.036				

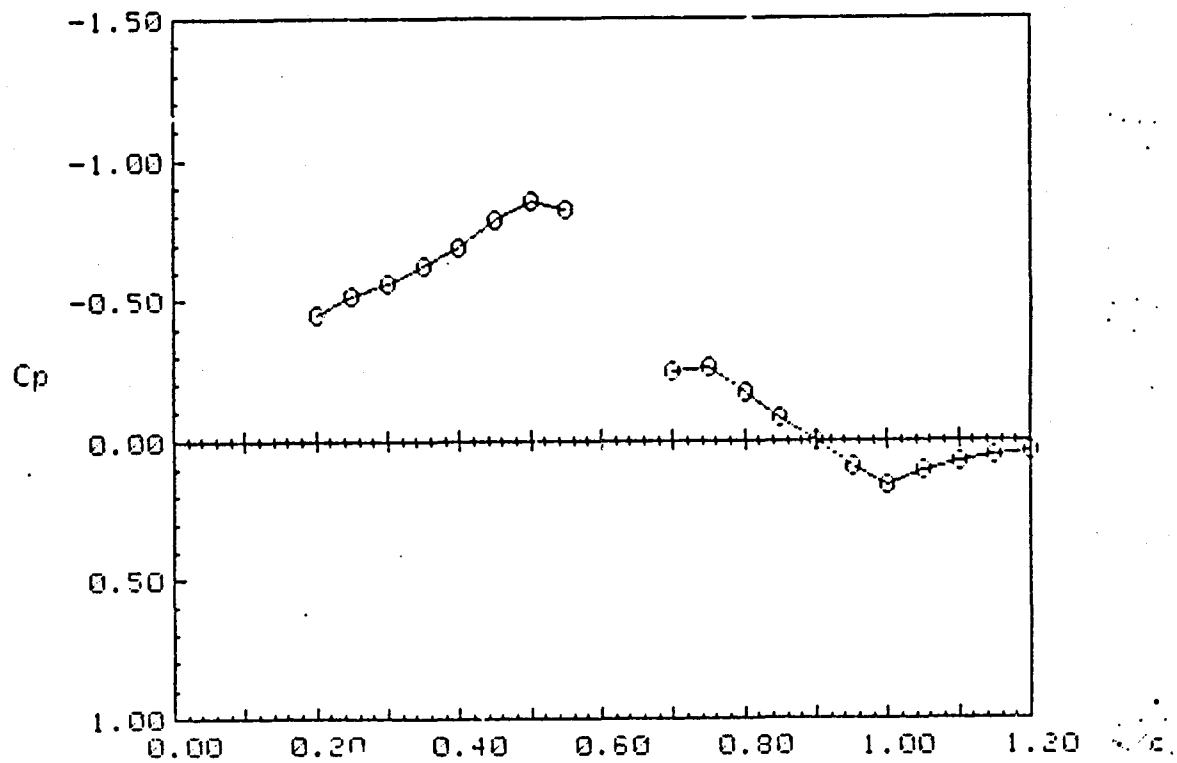

PRESSURE DATA - 11 foot - Oscillating Flap

RUN: 128 SEQ: 11
FLAP MEAN: 0 AMPL.: 2 FREQ.: 30
PHASE NO.: 31 ANGLE: 270 DELTA: 2.04
MACH: .8 ALPHA: 0
Ptot: 2087.9 psf Pinf: 1370 psf Ttot: 550.15 Rankine

UPPER SURFACE: x/c	Cp	LOWER SURFACE: x/c	Cp
0	1.174	.05	-.23
.05	-.163	.1	-.325
.1	-.302	.15	-.43
.15	-.385	.2	-.474
.2	-.449	.25	-.544
.25	-.511	.3	-.582
.3	-.557	.35	-.638
.35	-.621	.4	-.702
.4	-.708	.45	-.773
.45	-.775	.5	-.71
.5	-.816	.55	-.114
.55	-.8	.6	-.134
.6	-.437	.643	-.047
.643	-.193	.762	.088
.705	-.232	.793	.076
.797	-.165	.824	.087
.849	-.002	.849	.083
.95	.133	.895	.102
		.946	.145

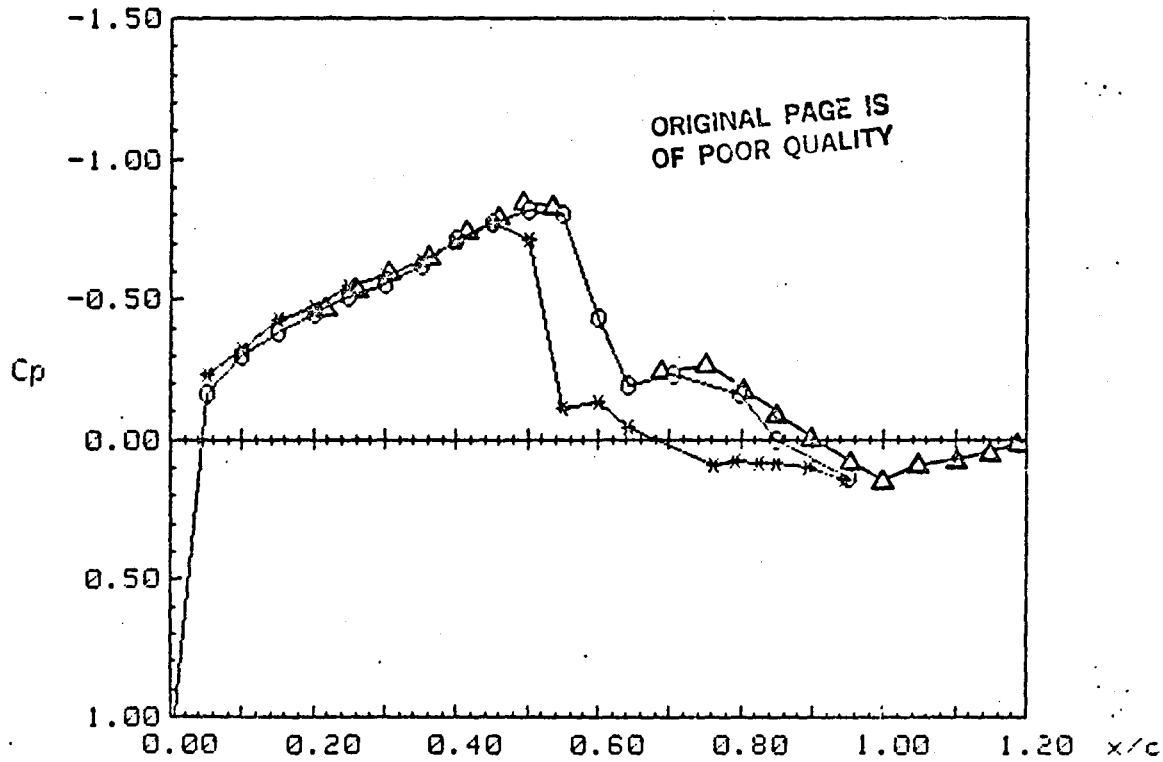

HOLOGRAPHIC DATA - 11 foot - Oscillating Flap
18241
RUN: 141 SEQ: 8
FLAP MEAN:-4 AMPL: 2 FREQ: 30
PHASE NO.: 3 ANGLE: 18 DELTA:-4.37
MACH: .8 ALPHA: 0 PRINT NO.: 2
Ptot: 2128.2 psf Pinf: 1395.2 psf Ttot: 550.34 Rankine

UPPER SURFACE:	x/c	N	Cp	LOWER SURFACE:	x/c	N	Cp
	.15	19	-.348				
	.2	8	-.415				
	.25	0	-.462				
	.3	-8	-.51				
	.35	-14	-.545				
	.5	0	-.238				
	.55	7	-.195				
	.6	19	-.121				
	.65	30	-.051				
	.7	37	-.007				
	.75	43	.031				
	.8	42	.025				
	.85	44	.037				
	.9	46	.05				
	.95	47	.057				
	1	50	.076				
	1.05	45	.044				
	1.1	39	.006				
	1.15	33	-.032				

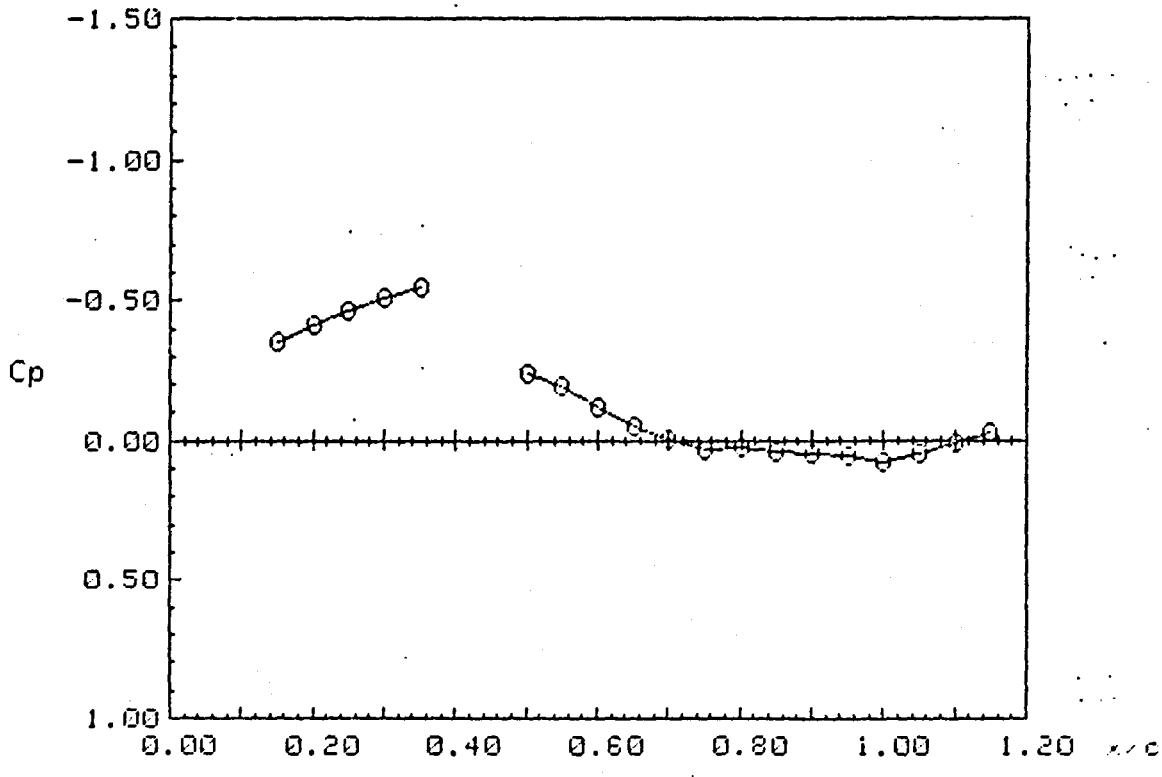

Figure 11.- Comparisons of the Pressures Obtained From the Surface Taps and the Interferometric Results. $\delta = -4°$, $\alpha = 0°$

PRESSURE DATA - 11 foot - Oscillating Flap

RUN: 141 SEQ: 8
FLAP MEAN:-4 AMPL.: 2 FREQ.: 30
PHASE NO.: 3 ANGLE: 18 DELTA:-4.57
MACH: .8 ALPHA: 0
Ptot: 2128.2 psf Pinf: 1395.2 psf Ttot: 550.34 Rankine

UPPER SURFACE: x/c	Cp	LOWER SURFACE: x/c	Cp
0	1.175	.05	-.268
.05	-.129	.1	-.35
.1	-.268	.15	-.447
.15	-.348	.2	-.503
.2	-.408	.25	-.562
.25	-.462	.3	-.614
.3	-.493	.35	-.659
.35	-.539	.4	-.748
.4	-.481	.45	-.821
.45	-.385	.5	-.882
.5	-.238	.55	-.909
.55	-.149	.6	-.933
.6	-.073	.643	-.774
.643	.048	.762	-.334
.705	.093	.793	-.27
.797	.147	.824	-.198
.849	.162	.849	-.152
.95	.151	.895	-.055
		.946	.048

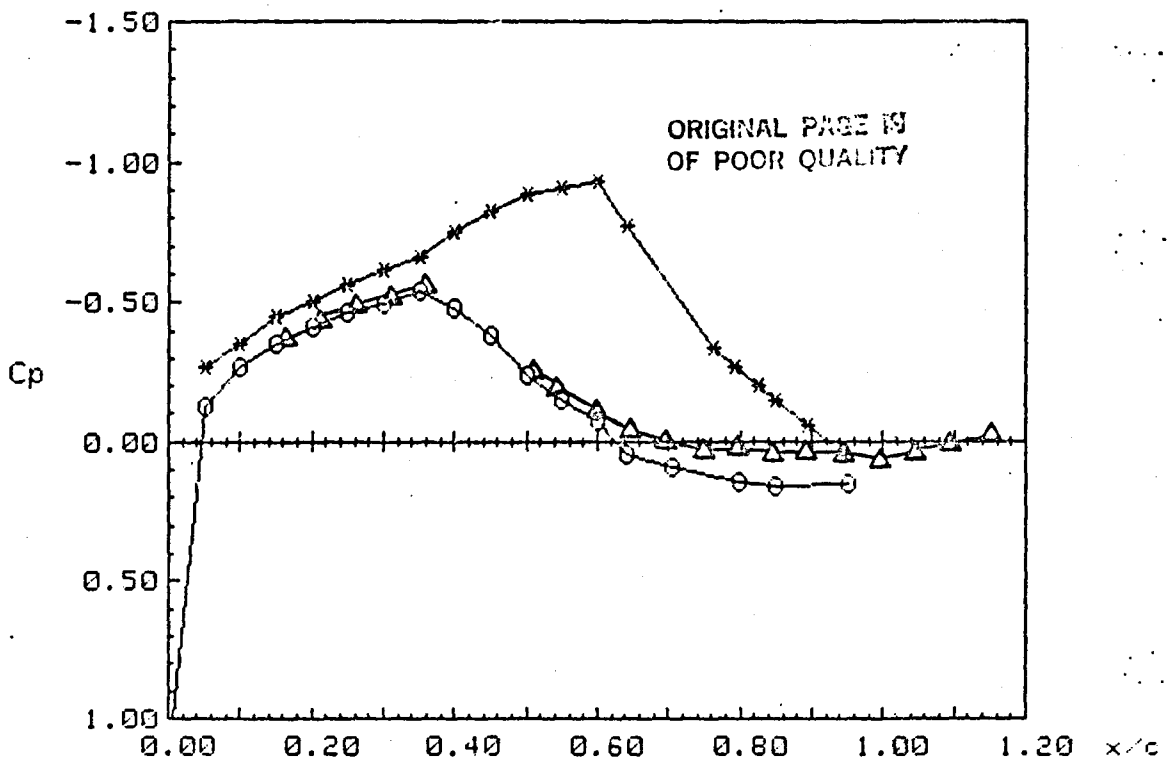

HOLOGRAPHIC DATA - 11 foot - Oscillating Flap
54240

RUN: 140	SEQ: 8	
FLAP MEAN:-4	AMPL: 2	FREQ: 30
PHASE NO.: 7	ANGLE: 54	DELTA:-5.65
MACH: .8	ALPHA: 0	PRINT NO.: 2
Ptot: 2128.2 psf	Pinf: 1397.2 psf	Ttot: 551.25 Rankine

UPPER SURFACE:	x/c	N	Cp	LOWER SURFACE:	x/c	N	Cp
	.2	0	-.371				
	.25	-2	-.384				
	.55	0	-.124				
	.6	16	-.023				
	.65	34	.092				
	.7	47	.176				
	.75	58	.248				
	.8	64	.288				
	.85	65	.295				
	.9	67	.308				
	.95	68	.315				
	1	73	.348				
	1.05	78	.381				
	1.1	75	.361				
	1.15	74	.354				
	1.2	73	.348				

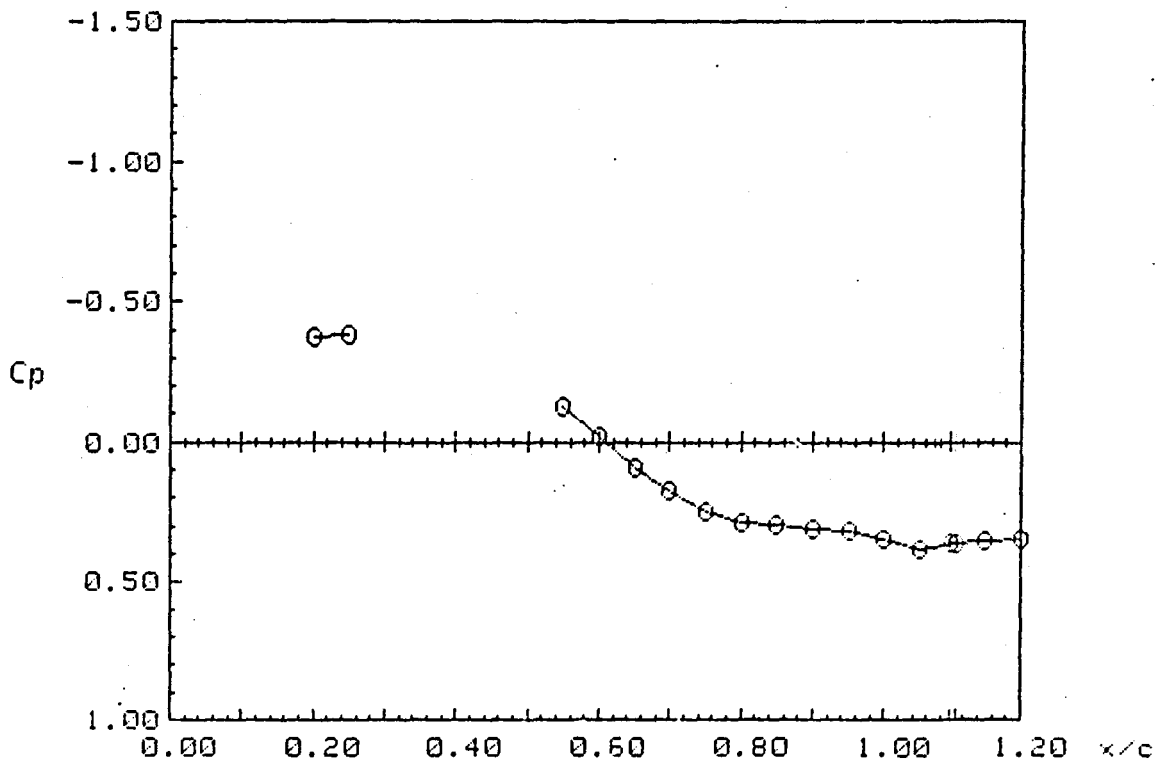

PRESSURE DATA - 11 foot - Oscillating Flap

RUN: 140 SEQ: 8
FLAP MEAN:-4 AMPL.: 2 FREQ.: 30
PHASE NO.: 7 ANGLE: 54 DELTA:-5.65
MACH: .8 ALPHA: 0
Ptot: 2128.2 psf Pinf: 1397.2 psf Ttot: 551.25 Rankine

UPPER SURFACE: x/c	Cp	LOWER SURFACE: x/c	Cp
0	1.176	.03	-.265
.05	-.12	.1	-.348
.1	-.253	.15	-.445
.15	-.322	.2	-.505
.2	-.371	.25	-.563
.25	-.401	.3	-.613
.3	-.372	.35	-.658
.35	-.399	.4	-.748
.4	-.393	.45	-.821
.45	-.328	.5	-.882
.5	-.217	.55	-.906
.55	-.124	.6	-.931
.6	-.044	.643	-.791
.643	.076	.762	-.297
.705	.125	.793	-.276
.797	.164	.824	-.258
.849	.161	.849	-.235
.95	.106	.893	-.171
		.946	-.102

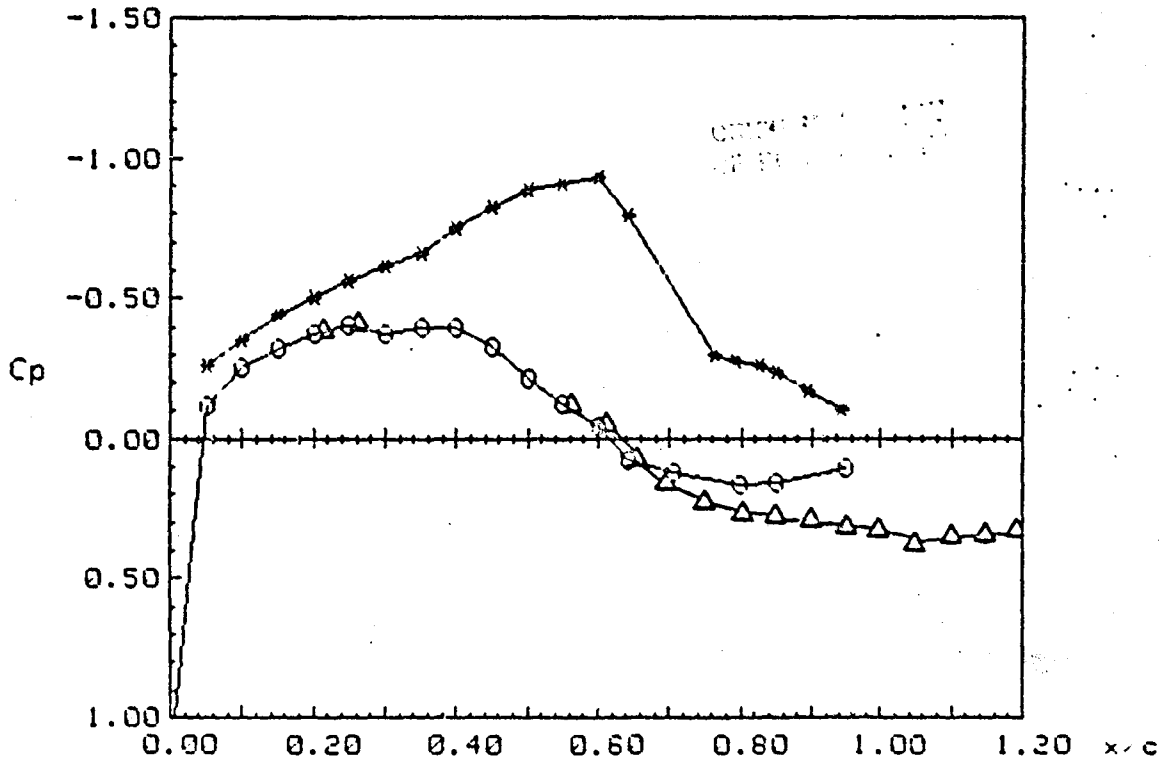

HOLOGRAPHIC DATA - 11 foot - Oscillating Flap
162241

RUN: 141	SEQ: 8	
FLAP MEAN:-4	AMPL: 2	FREQ: 30
PHASE NO.: 19	ANGLE: 162	DELTA:-4.74
MACH: .8	ALPHA: 0	PRINT NO.: 2
Ptot: 2128.2 psf	Pinf: 1395.2 psf	Ttot: 550.34 Rankine

UPPER SURFACE: x/c	N	Cp	LOWER SURFACE: x/c	N	Cp
.2	0	-.331			
.25	-10	-.392			
.3	-17	-.434			
.35	-24	-.476			
.4	-28	-.499			
.5	0	-.3			
.55	14	-.215			
.6	26	-.14			
.65	40	-.052			
.7	45	-.021			
.75	52	.024			
.8	57	.056			
.85	60	.075			
.9	60	.075			
.95	62	.088			
1	66	.114			
1.05	68	.127			
1.1	64	.101			
1.15	59	.069			

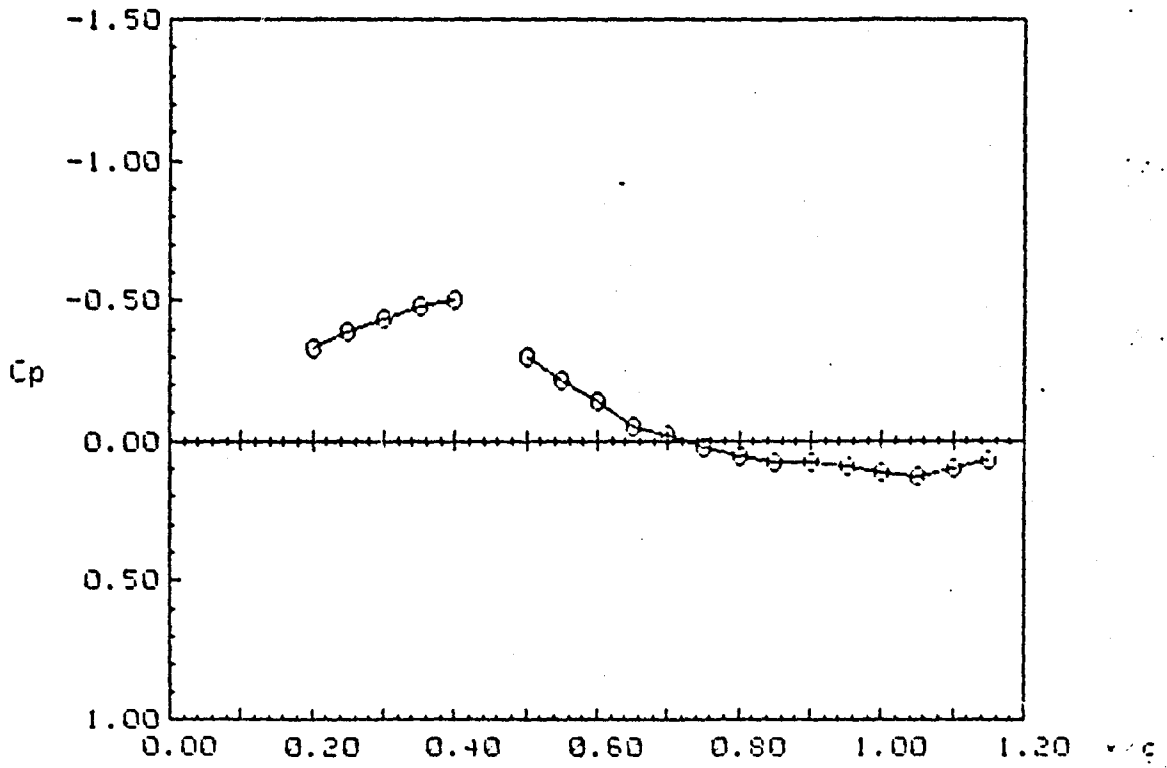

PRESSURE DATA - 11 foot - Oscillating Flap

RUN: 141 SEQ: 8
FLAP MEAN:-4 AMPL.: 2 FREQ.: 30
PHASE NO.: 19 ANGLE: 162 DELTA:-4.74
MACH: .8 ALPHA: 0
Ptot: 2128.2 psf Pinf: 1395.2 psf Ttot: 550.34 Rankine

UPPER SURFACE: x/c	Cp	LOWER SURFACE: x/c	Cp
0	1.176	.05	-.239
.05	-.061	.1	-.375
.1	-.198	.15	-.477
.15	-.275	.2	-.52
.2	-.331	.25	-.582
.25	-.374	.3	-.630
.3	-.407	.35	-.677
.35	-.446	.4	-.763
.4	-.469	.45	-.842
.45	-.419	.5	-.905
.5	-.3	.55	-.936
.55	-.205	.6	-.962
.6	-.133	.643	-.814
.643	-.018	.762	-.275
.705	.002	.793	-.274
.797	.039	.824	-.251
.849	.063	.849	-.239
.95	.034	.895	-.184
		.946	-.12

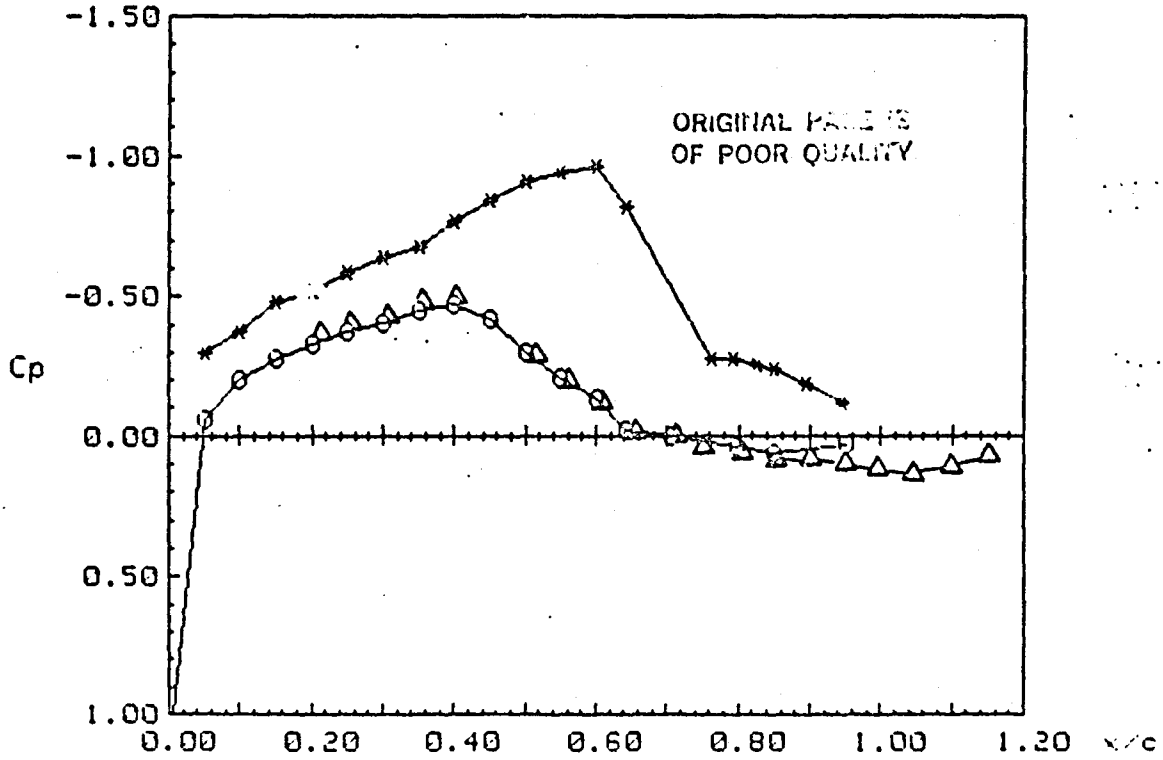

HOLOGRAPHIC DATA - 11 foot - Oscillating Flap
234241

RUN: 141 SEQ: 8
FLAP MEAN:-4 AMPL: 2 FREQ: 30
PHASE NO.: 27 ANGLE: 234 DELTA:-2.39
MACH: .8 ALPHA: 0 PRINT NO.: 2
Ptot: 2128.2 psf Pinf: 1395.2 psf Ttot: 550.34 Rankine

UPPER SURFACE:	x/c	N	Cp	LOWER SURFACE:	x/c	N	Cp
	.15	0	-.305				
	.2	-13	-.384				
	.25	-26	-.462				
	.3	-34	-.509				
	.35	-42	-.557				
	.4	-53	-.621				
	.45	-47	-.586				
	.6	0	-.191				
	.65	11	-.123				
	.7	15	-.098				
	.75	21	-.06				
	.8	30	-.003				
	.85	35	.029				
	.9	39	.054				
	.95	44	.086				
	1	54	.151				
	1.05	49	.118				
	1.1	45	.093				
	1.15	39	.054				
	1.2	37	.041				

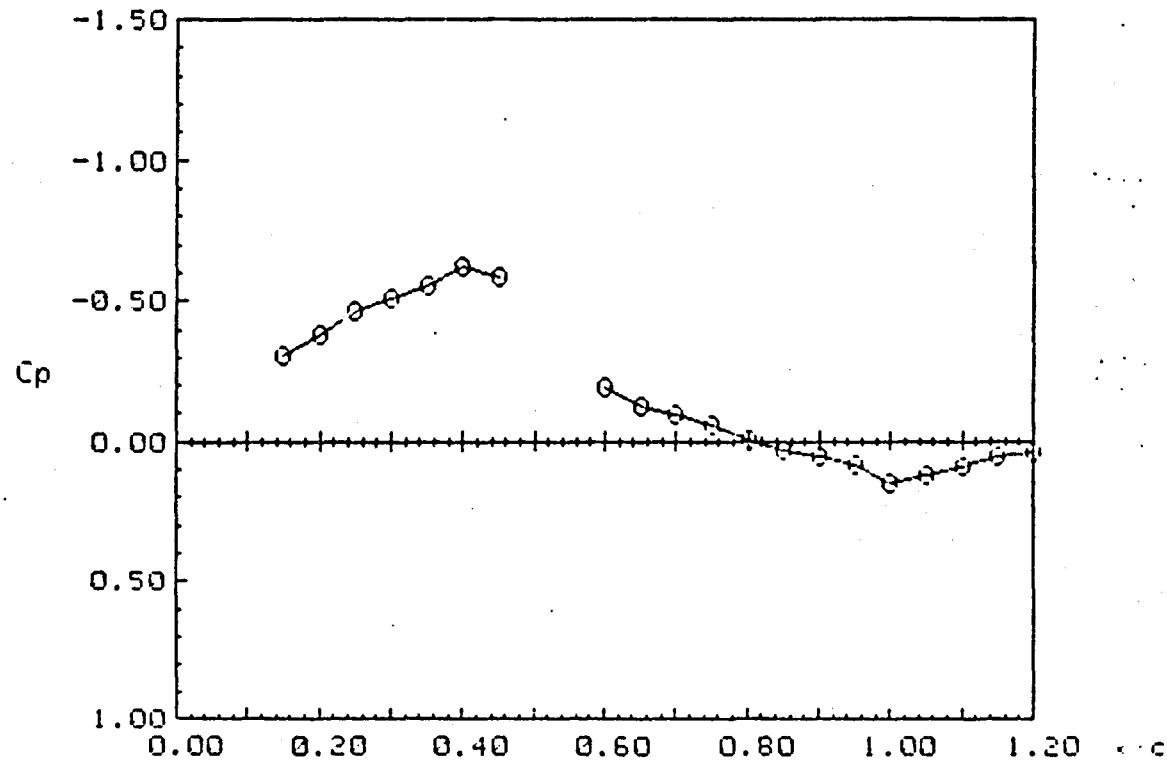

PRESSURE DATA - 11 foot - Oscillating Flap

RUN: 141 SEQ: 8
FLAP MEAN:-4 AMPL.: 2 FREQ.: 30
PHASE NO.: 27 ANGLE: 234 DELTA:-2.39
MACH: .8 ALPHA: 0
Ptot: 2128.2 psf Pinf: 1395.2 psf Ttot: 350.34 Rankine

UPPER SURFACE:	x/c	Cp	LOWER SURFACE:	x/c	Cp
	0	1.169		.05	-.31
	.05	-.08		.1	-.388
	.1	-.223		.15	-.495
	.15	-.305		.2	-.53
	.2	-.368		.25	-.597
	.25	-.421		.3	-.649
	.3	-.461		.35	-.695
	.35	-.519		.4	-.778
	.4	-.58		.45	-.855
	.45	-.494		.5	-.916
	.5	-.343		.55	-.953
	.55	-.262		.6	-.983
	.6	-.191		.643	-.836
	.643	-.077		.762	-.245
	.705	-.074		.793	-.191
	.797	-.004		.824	-.118
	.849	.064		.849	-.082
	.95	.121		.895	.016
				.946	.096

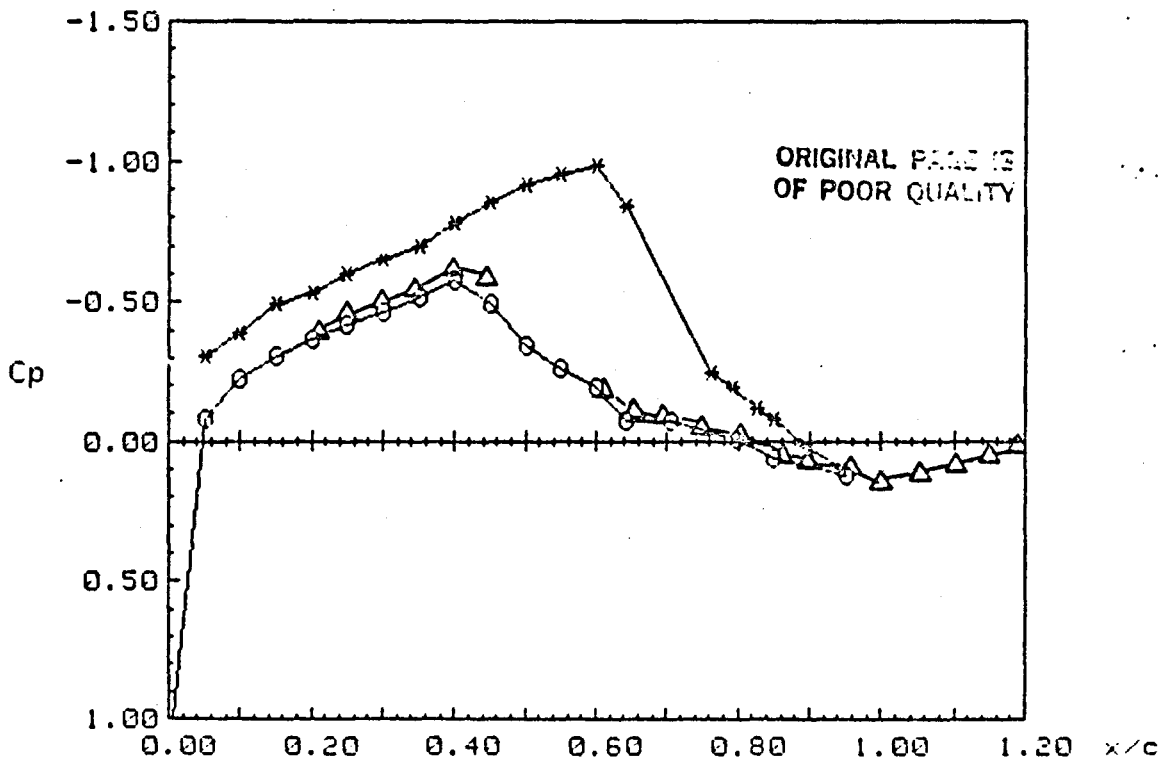

HOLOGRAPHIC DATA - 11 foot - Oscillating Flap
270140

RUN: 140	SEQ: 8	
FLAP MEAN:-4	AMPL: 2	FREQ: 30
PHASE NO.: 31	ANGLE: 270	DELTA:-2.07
MACH: .8	ALPHA: 0	PRINT NO.: 1
Ptot: 2128.2 psf	Pinf: 1397.2 psf	Ttot: 551.25 Rankine

UPPER SURFACE:	x/c	N	Cp	LOWER SURFACE:	x/c	N	Cp
	.2	0	-.382				
	.25	-6	-.419				
	.3	-9	-.437				
	.35	-16	-.479				
	.4	-25	-.532				
	.6	0	-.181				
	.65	14	-.094				
	.7	22	-.043				
	.75	32	.021				
	.8	43	.091				
	.85	52	.15				
	.9	59	.195				
	.95	69	.261				
	1	79	.327				
	1.05	76	.307				
	1.1	75	.301				
	1.15	73	.287				
	1.2	72	.281				

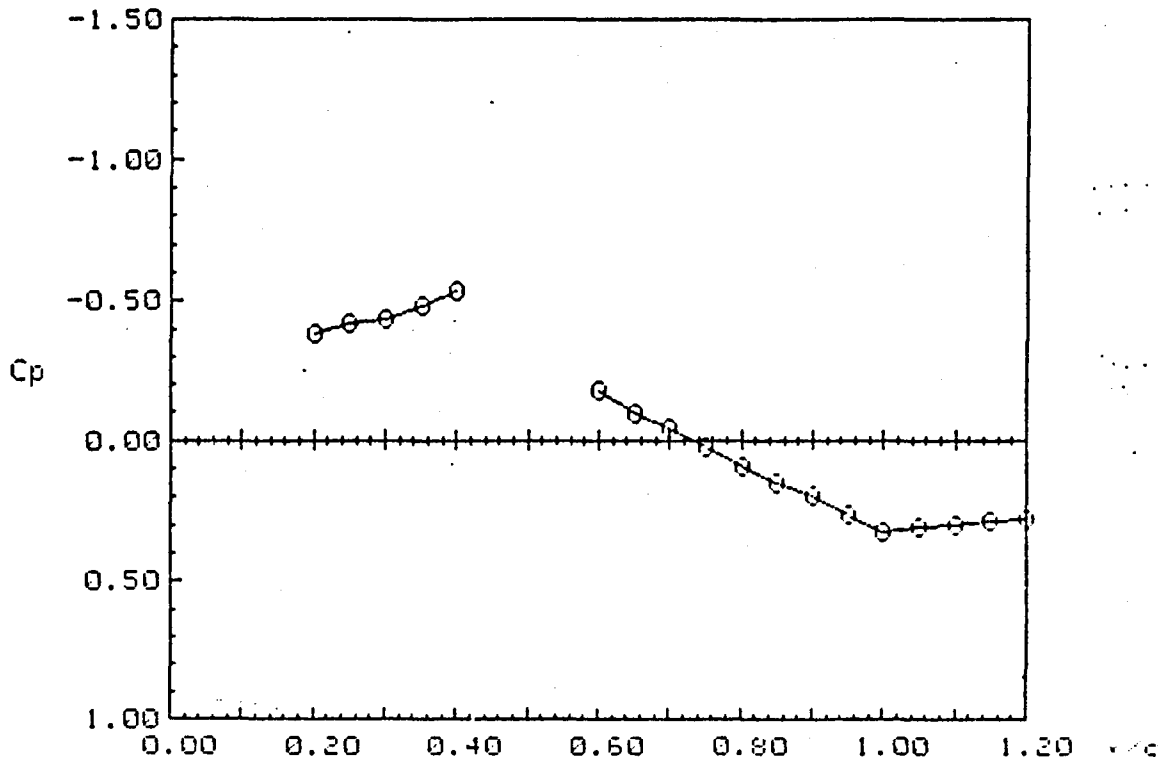

PRESSURE DATA - 11 foot - Oscillating Flap

RUN: 140 SEQ: 8
FLAP MEAN:-4 AMPL.: 2 FREQ.: 30
PHASE NO.: 31 ANGLE: 270 DELTA:-2.07
MACH: .8 ALPHA: 0
Ptot: 2128.2 psf Pinf: 1397.2 psf Ttot: 551.25 Rankine

UPPER SURFACE: x/c	Cp	LOWER SURFACE: x/c	Cp
0	1.166	.05	-.31
.05	-.099	.1	-.39
.1	-.242	.15	-.497
.15	-.32	.2	-.535
.2	-.382	.25	-.603
.25	-.438	.3	-.655
.3	-.472	.35	-.702
.35	-.531	.4	-.783
.4	-.604	.45	-.857
.45	-.581	.5	-.916
.5	-.359	.55	-.951
.55	-.26	.6	-.979
.6	-.181	.643	-.854
.643	-.064	.762	-.226
.705	-.055	.793	-.122
.797	.015	.824	-.048
.849	.082	.849	-.005
.95	.153	.895	.077
		.946	.147

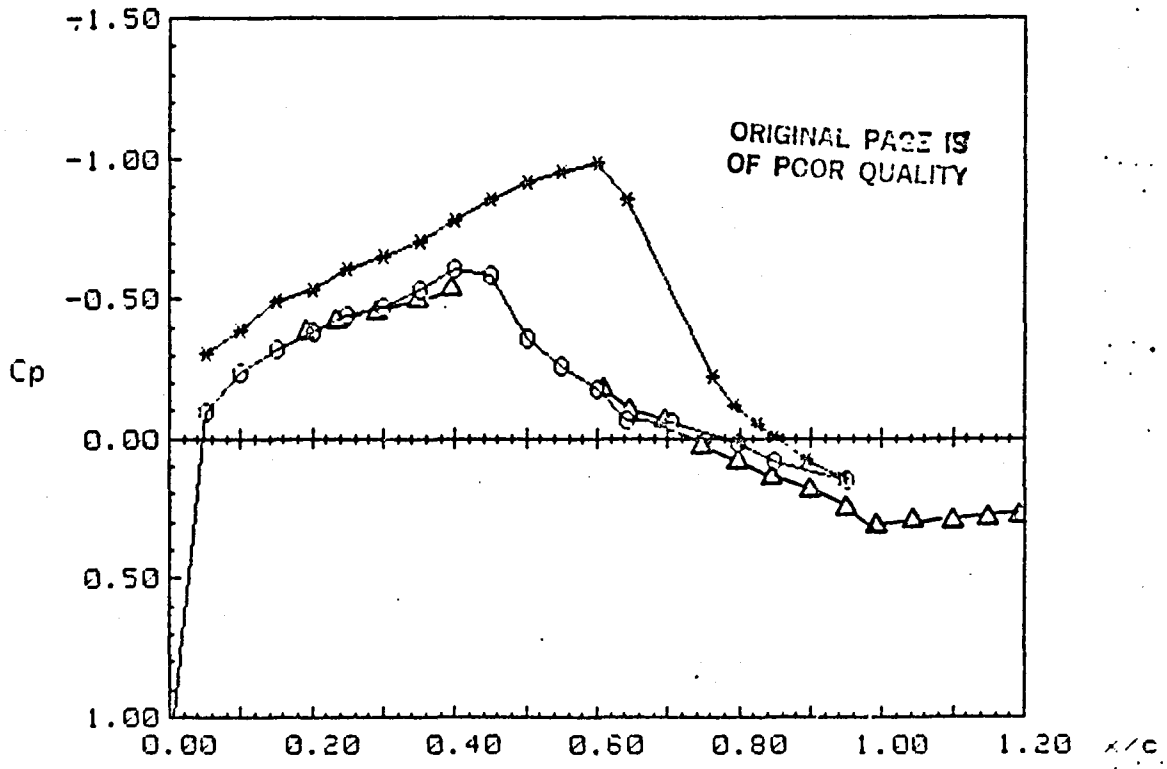

HOLOGRAPHIC DATA - 11 foot - Oscillating Flap
306341
RUN: 141 SEQ: 8
FLAP MEAN:-4 AMPL: 2 FREQ: 30
PHASE NO.: 35 ANGLE: 306 DELTA:-2.3
MACH: .8 ALPHA: 0 PRINT NO.: 3
Ptot: 2128.2 psf Pinf: 1395.2 psf Ttot: 550.34 Rankine

UPPER SURFACE:	x/c	N	Cp	LOWER SURFACE:	x/c	N	Cp
	.2	0	-.402				
	.25	-9	-.456				
	.3	-17	-.504				
	.35	-25	-.551				
	.4	-37	-.621				
	.55	0	-.229				
	.6	12	-.155				
	.65	26	-.067				
	.7	31	-.036				
	.75	36	-.004				
	.8	45	.053				
	.85	50	.085				
	.9	54	.111				
	.95	59	.143				
	1	65	.182				
	1.05	58	.137				
	1.1	53	.105				
	1.15	49	.079				
	1.2	46	.06				

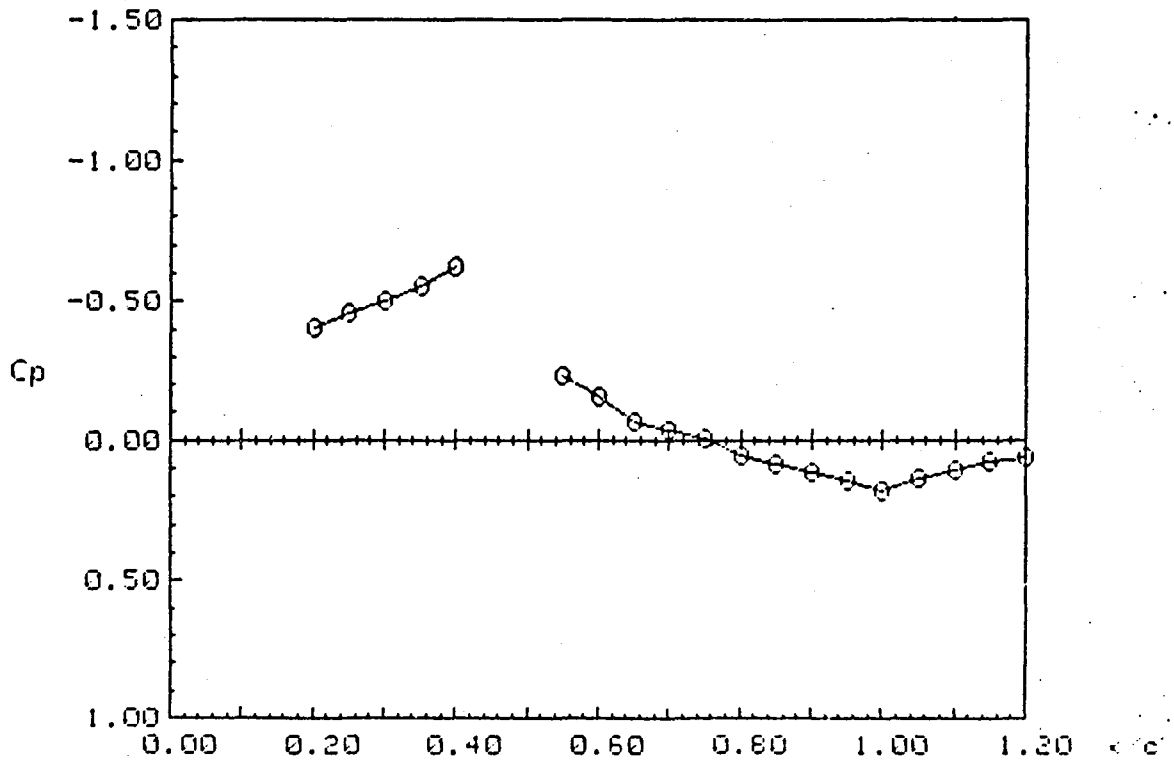

PRESSURE DATA - 11 foot - Oscillating Flap

RUN: 141 SEQ: 8
FLAP MEAN:-4 AMPL.: 2 FREQ.: 30
PHASE NO.: 35 ANGLE: 306 DELTA:-2.3
MACH: .8 ALPHA: 0
Ptot: 2128.2 psf Pinf: 1395.2 psf Ttot: 550.34 Rankine

UPPER SURFACE: x/c	Cp	LOWER SURFACE: x/c	Cp
0	1.171	.05	-.296
.05	-.11	.1	-.376
.1	-.253	.15	-.48
.15	-.337	.2	-.524
.2	-.402	.25	-.588
.25	-.461	.3	-.642
.3	-.501	.35	-.687
.35	-.555	.4	-.772
.4	-.594	.45	-.847
.45	-.514	.5	-.906
.5	-.322	.55	-.941
.55	-.229	.6	-.971
.6	-.155	.643	-.808
.643	-.089	.762	-.236
.705	-.022	.793	-.139
.797	.053	.824	-.073
.849	.11	.849	-.031
.95	.162	.895	.051
		.946	.126

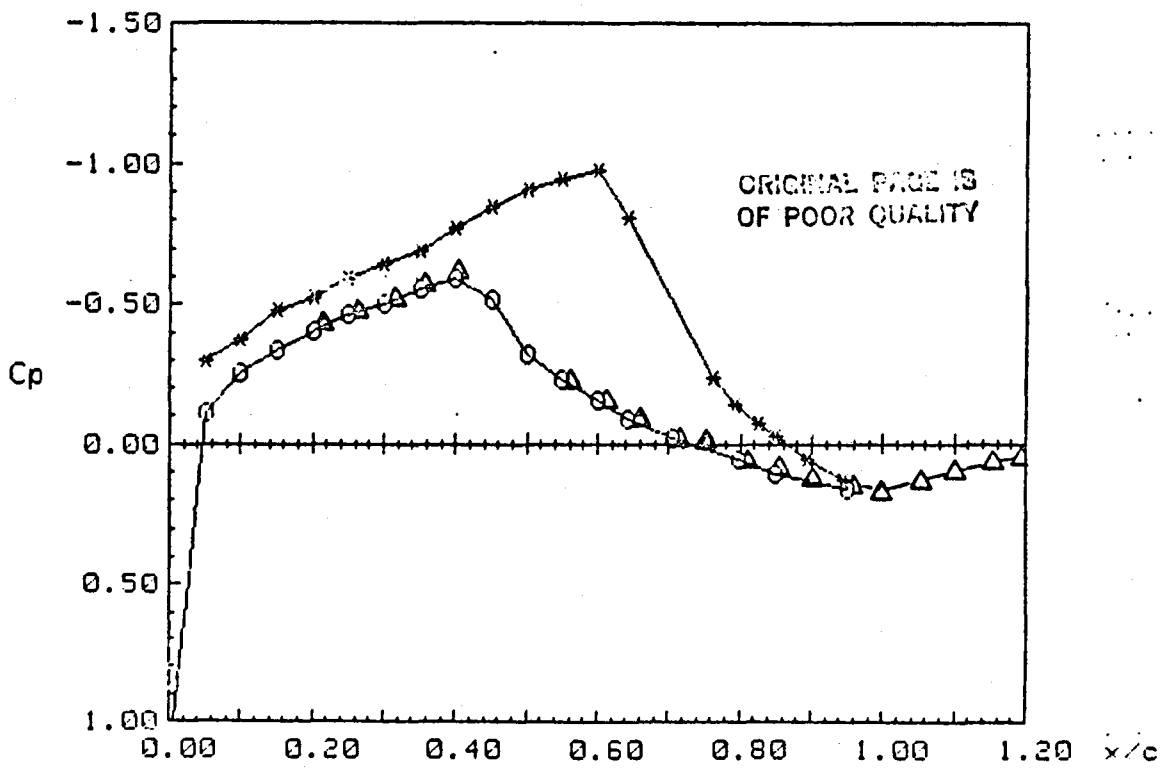

HOLOGRAPHIC DATA - 11 foot - Oscillating Flap
342140

RUN: 140 SEQ: 8
FLAP MEAN:-4 AMPL: 2 FREQ: 30
PHASE NO.: 39 ANGLE: 342 DELTA:-3.3
MACH: .8 ALPHA: 0 PRINT NO.: 1
Ptot: 2128.2 psf Pinf: 1397.2 psf Ttot: 551.25 Rankine

UPPER SURFACE:	x/c	N	Cp	LOWER SURFACE:	x/c	N	Cp
	.25	0	-.464				
	.3	-5	-.494				
	.35	-9	-.518				
	.4	-18	-.571				
	.55	0	-.187				
	.6	17	-.081				
	.65	33	.021				
	.7	42	.079				
	.75	53	.15				
	.8	64	.222				
	.85	69	.255				
	.9	74	.288				
	.95	80	.327				
	1	88	.381				
	1.05	84	.354				
	1.1	82	.341				
	1.15	80	.327				
	1.2	80	.327				

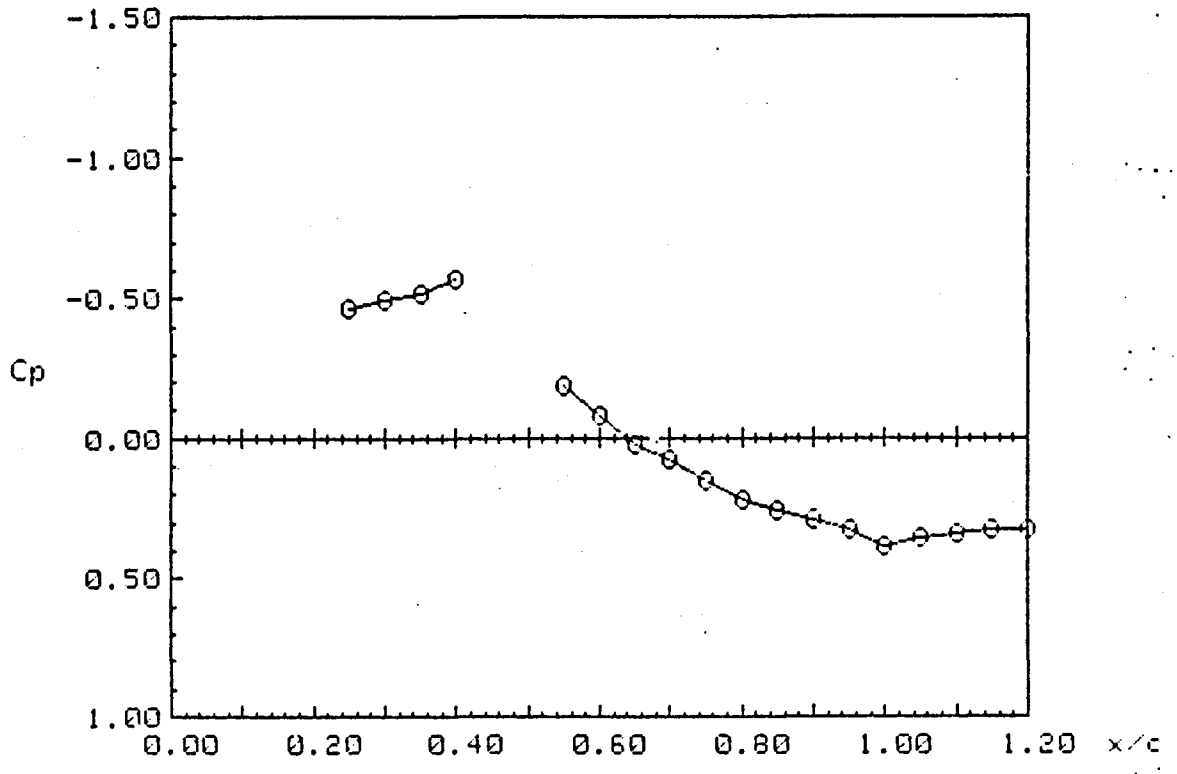

PRESSURE DATA - 11 foot - Oscillating Flap

RUN: 140 SEQ: 8
FLAP MEAN:-4 AMPL.: 2 FREQ.: 30
PHASE NO.: 39 ANGLE: 342 DELTA:-3.3
MACH: .8 ALPHA: 0
Ptot: 2128.2 psf Pinf: 1397.2 psf Ttot: 551.25 Rankine

UPPER SURFACE: x/c	Cp	LOWER SURFACE: x/c	Cp
0	1.168	.05	-.286
.05	-.127	.1	-.369
.1	-.268	.15	-.47
.15	-.346	.2	-.522
.2	-.407	.25	-.583
.25	-.464	.3	-.636
.3	-.495	.35	-.681
.35	-.551	.4	-.765
.4	-.618	.45	-.838
.45	-.399	.5	-.897
.5	-.266	.55	-.929
.55	-.187	.6	-.955
.6	-.109	.643	-.807
.643	.009	.762	-.309
.705	.044	.793	-.201
.797	.104	.824	-.129
.849	.142	.849	-.068
.95	.166	.895	.029
		.946	.121

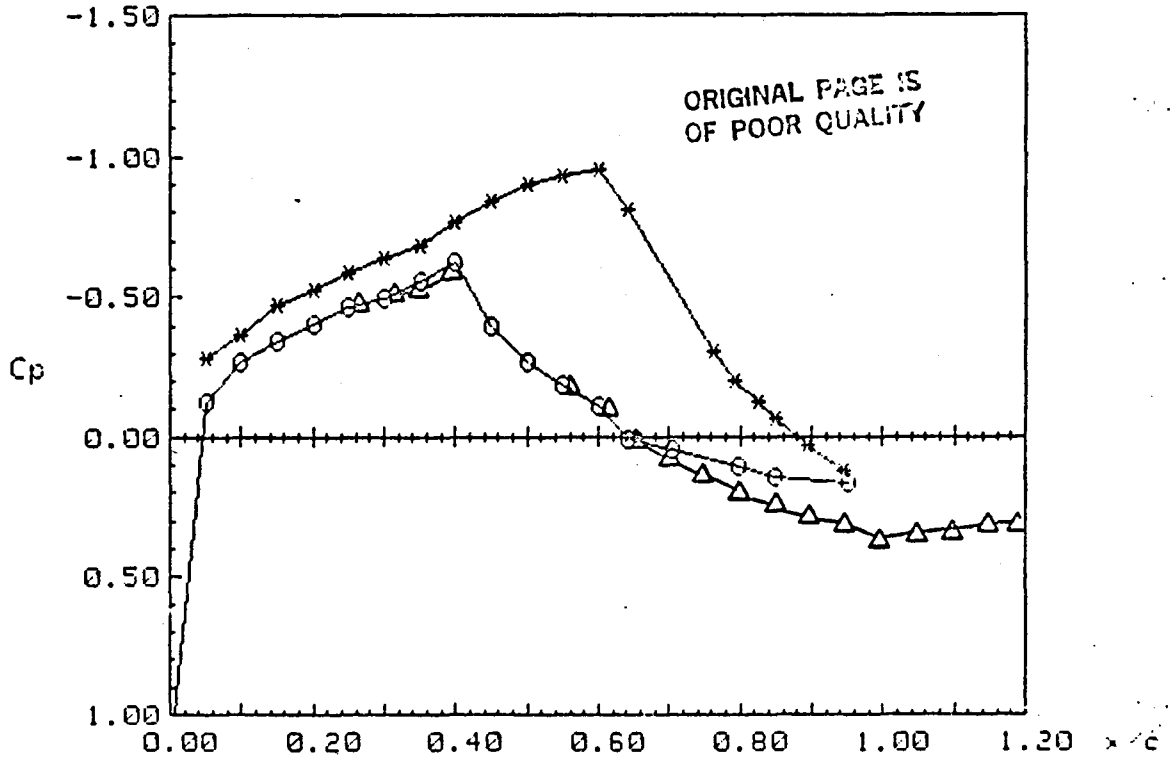

HOLOGRAPHIC DATA - 11 foot - Oscillating Flap
54144
RUN: 144 SEQ: 33
FLAP MEAN: 0 AMPL: 2 FREQ: 30
PHASE NO.: 7 ANGLE: 54 DELTA:-1.58
MACH: .8 ALPHA: 0 PRINT NO.: 1
Ptot: 4238 psf Pinf: 2788.8 psf Ttot: 580 Rankine

UPPER SURFACE:	x/c	N	Cp	LOWER SURFACE:	x/c	N	Cp
	.15	42	-.421				
	.2	22	-.484				
	.25	0	-.553				
	.3	-14	-.597				
	.35	-30	-.646				
	.4	-46	-.695				
	.45	-61	-.741				
	.6	0	-.127				
	.65	17	-.071				
	.7	29	-.03				
	.75	40	.007				
	.8	0	-.005				
	.85	17	.052				
	.9	27	.086				
	.95	42	.138				
	1	62	.207				
	1.05	53	.176				
	1.1	45	.148				
	1.15	38	.124				
	1.2	33	.107				

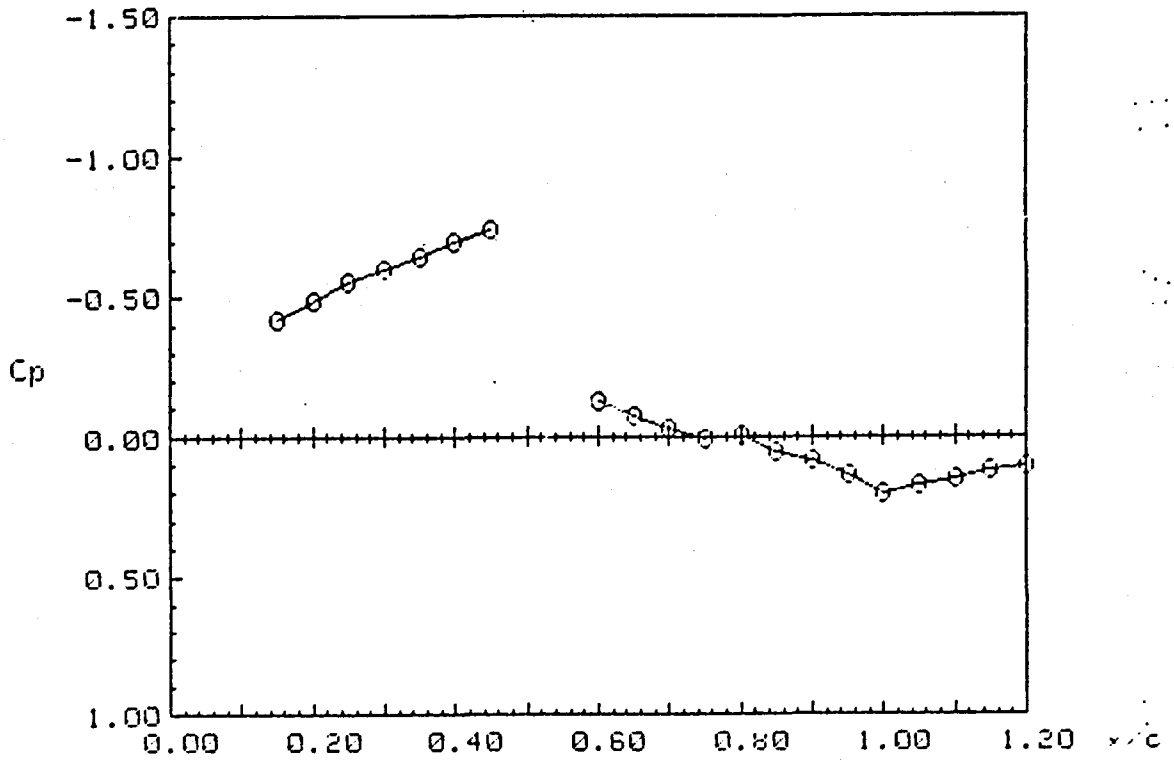

Figure 12.- Comparisons of the Pressures Obtained From the Surface Pressure Taps and the Interferometric Results. $\delta = 0°$, $\alpha = 0°$, $P_T = 4238$ psf

PRESSURE DATA - 11 foot - Oscillating Flap

RUN: 144 SEQ: 33
FLAP MEAN: 0 AMPL.: 2 FREQ.: 30
PHASE NO.: 7 ANGLE: 54 DELTA:-1.58
MACH: .8 ALPHA: 0
Ptot: 4238 psf Pinf: 2788.8 psf Ttot: 580 Rankine

UPPER SURFACE:	x/c	Cp	LOWER SURFACE:	x/c	Cp
	0	1.175		.05	-.134
	.05	-.243		.1	-.224
	.1	-.353		.15	-.316
	.15	-.429		.2	-.379
	.2	-.483		.25	-.429
	.25	-.553		.3	-.489
	.3	-.588		.35	-.524
	.35	-.647		.4	-.623
	.4	-.727		.45	-.697
	.45	-.765		.5	-.717
	.5	-.759		.55	-.35
	.55	-.16		.6	-.305
	.6	-.127		.643	-.236
	.643	-.053		.762	-.085
	.705	-.041		.793	-.129
	.797	-.005		.824	-.057
	.849	.087		.849	-.009
	.95	.146		.895	.053
				.946	.13

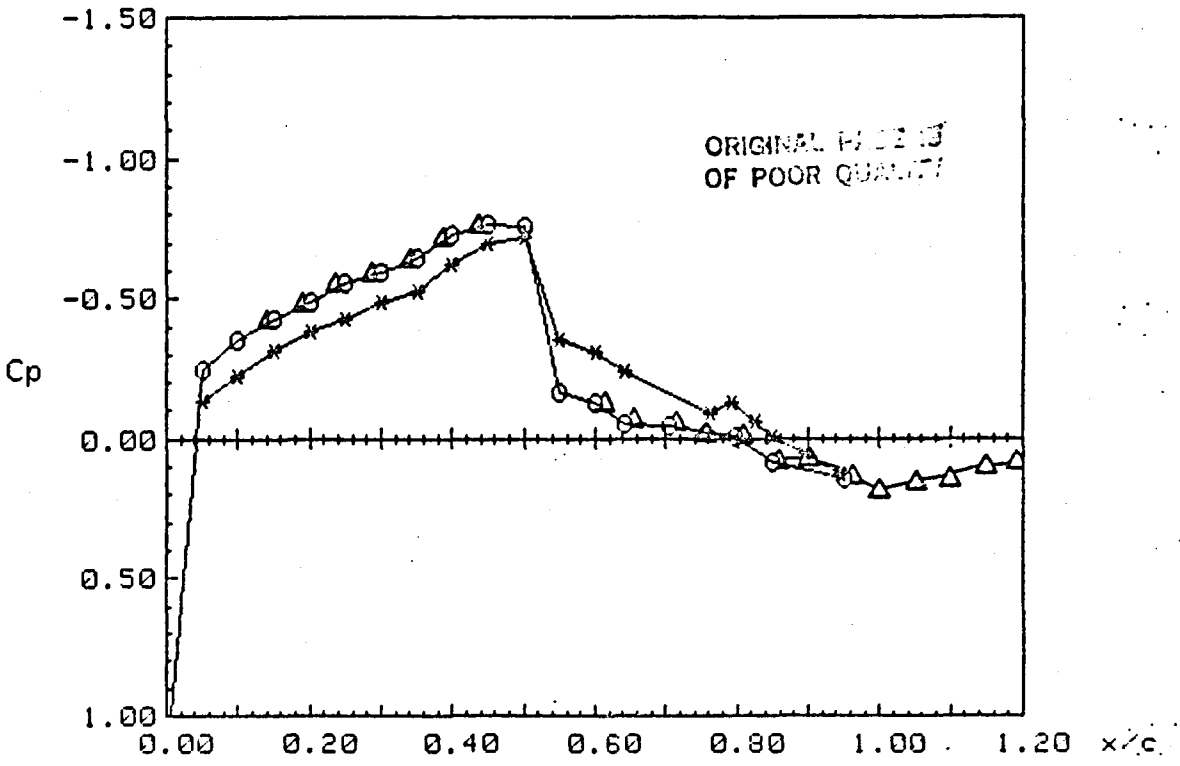

HOLOGRAPHIC DATA - 11 foot - Oscillating Flap
126144

RUN: 144	SEQ: 33	
FLAP MEAN: 0	AMPL: 2	FREQ: 30
PHASE NO.: 15	ANGLE: 126	DELTA:-1.7
MACH: .8	ALPHA: 0	PRINT NO.: 1
Ptot: 4238 psf	Pinf: 2788.8 psf	Ttot: 580 Rankine

UPPER SURFACE:	x/c	N	Cp	LOWER SURFACE:	x/c	N	Cp
	.15	36	-.404				
	.2	13	-.478				
	.25	0	-.518				
	.3	-9	-.547				
	.35	-20	-.581				
	.4	-31	-.615				
	.55	0	-.217				
	.6	19	-.155				
	.65	39	-.088				
	.7	47	-.061				
	.75	58	-.024				
	.8	76	.037				
	.85	97	.108				
	.9	105	.136				
	.95	124	.201				
	1	134	.236				
	1.05	126	.208				
	1.1	120	.187				
	1.15	114	.167				
	1.2	111	.156				

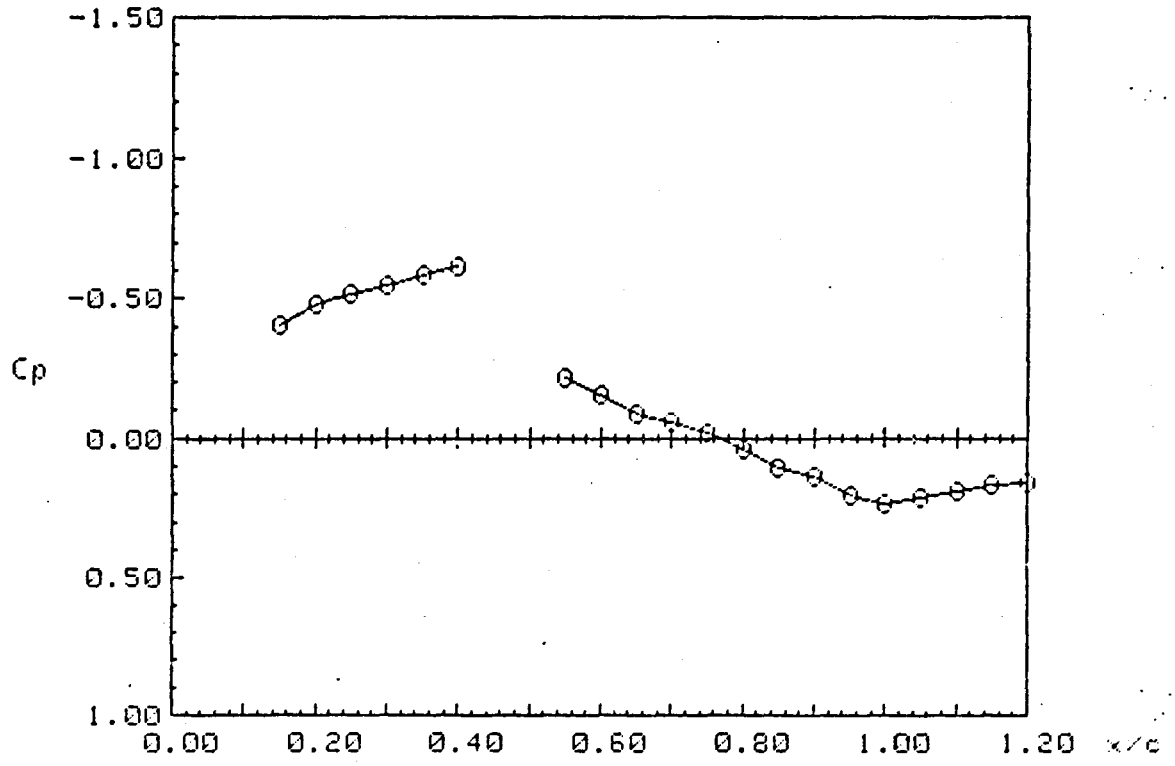

PRESSURE UNIT - 11 foot - Oscillating Flap

RUN: 144 SEQ: 33
FLAP MEAN: 0 AMPL.: 2 FREQ.: 30
PHASE NO.: 15 ANGLE: 126 DELTA:-1.7
MACH: .8 ALPHA: 0
Ptot: 4238 psf Pinf: 2788.8 psf Ttot: 580 Rankine

UPPER SURFACE: x/c	Cp	LOWER SURFACE: x/c	Cp
0	1.172	.05	-.167
.05	-.213	.1	-.257
.1	-.324	.15	-.352
.15	-.399	.2	-.413
.2	-.454	.25	-.464
.25	-.518	.3	-.528
.3	-.542	.35	-.559
.35	-.59	.4	-.654
.4	-.659	.45	-.736
.45	-.449	.5	-.77
.5	-.313	.55	-.737
.55	-.217	.6	-.324
.6	-.199	.643	-.227
.643	-.108	.762	-.084
.705	-.101	.793	-.075
.797	-.055	.824	-.018
.849	.047	.849	.016
.95	.132	.895	.067
		.946	.138

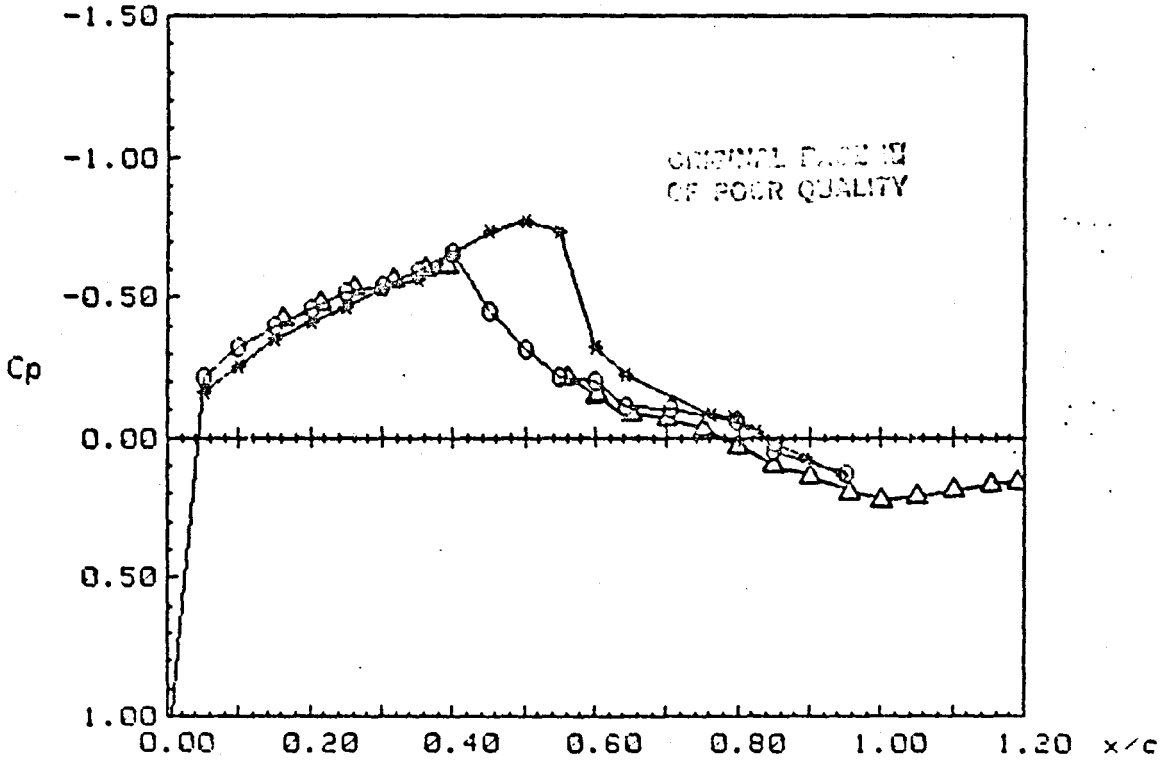

HOLOGRAPHIC DATA - 11 foot - Oscillating Flap
180249
RUN: 149 SEQ: 7
FLAP MEAN:-4 AMPL: 2 FREQ: 30
PHASE NO.: 21 ANGLE: 180 DELTA:-4.05
MACH: .8 ALPHA: 4 PRINT NO.: 2
Ptot: 2127.5 psf Pinf: 1394.9 psf Ttot: 547.34 Rankine

UPPER SURFACE:	x/c	N	Cp	LOWER SURFACE:	x/c	N	Cp
	.15	0	-.889				
	.2	-8	-.933				
	.25	-16	-.976				
	.3	-23	-1.014				
	.35	-29	-1.045				
	.4	-36	-1.082				
	.45	-45	-1.129				
	.65	-18	-.22				
	.7	-4	-.133				
	.75	0	-.108				
	.8	10	-.046				
	.85	22	.03				
	.9	23	.036				
	.95	30	.081				
	1	33	.1				
	1.05	32	.094				
	1.1	32	.094				
	1.15	30	.081				
	1.2	27	.062				

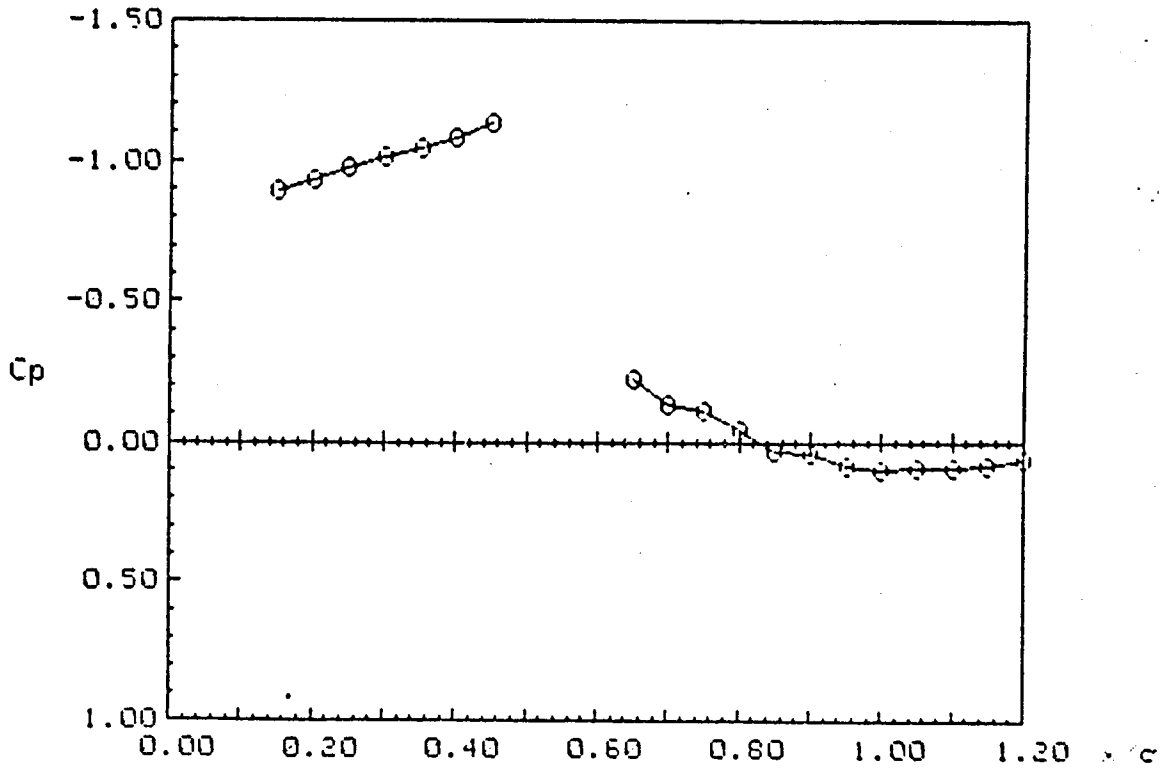

Figure 13.- Comparisons of the Pressures Obtained From the Surface Pressure Taps and the Interferometric Results. $\delta = -4°$, $\alpha = 4°$

PRESSURE DATA - 11 foot - Oscillating Flap

RUN: 149 SEQ: 7
FLAP MEAN:-4 AMPL.: 2 FREQ.: 30
PHASE NO.: 21 ANGLE: 180 DELTA:-4.05
MACH: .8 ALPHA: 4
Ptot: 2127.5 psf Pinf: 1394.9 psf Ttot: 547.34 Rankine

UPPER SURFACE: x/c	Cp	LOWER SURFACE: x/c	Cp
0	.988	.05	.242
.05	-.84	.1	.064
.1	-.846	.15	-.064
.15	-.389	.2	-.144
.2	-.915	.25	-.225
.25	-.95	.3	-.302
.3	-.977	.35	-.38
.35	-1.017	.4	-.492
.4	-1.075	.45	-.562
.45	-1.085	.5	-.584
.5	-.645	.55	-.437
.55	-.554	.6	-.341
.6	-.507	.643	-.285
.643	-.484	.762	-.409
.705	-.219	.793	-.206
.797	.002	.824	-.111
.849	.082	.849	-.063
.95	.146	.895	.015
		.946	.084

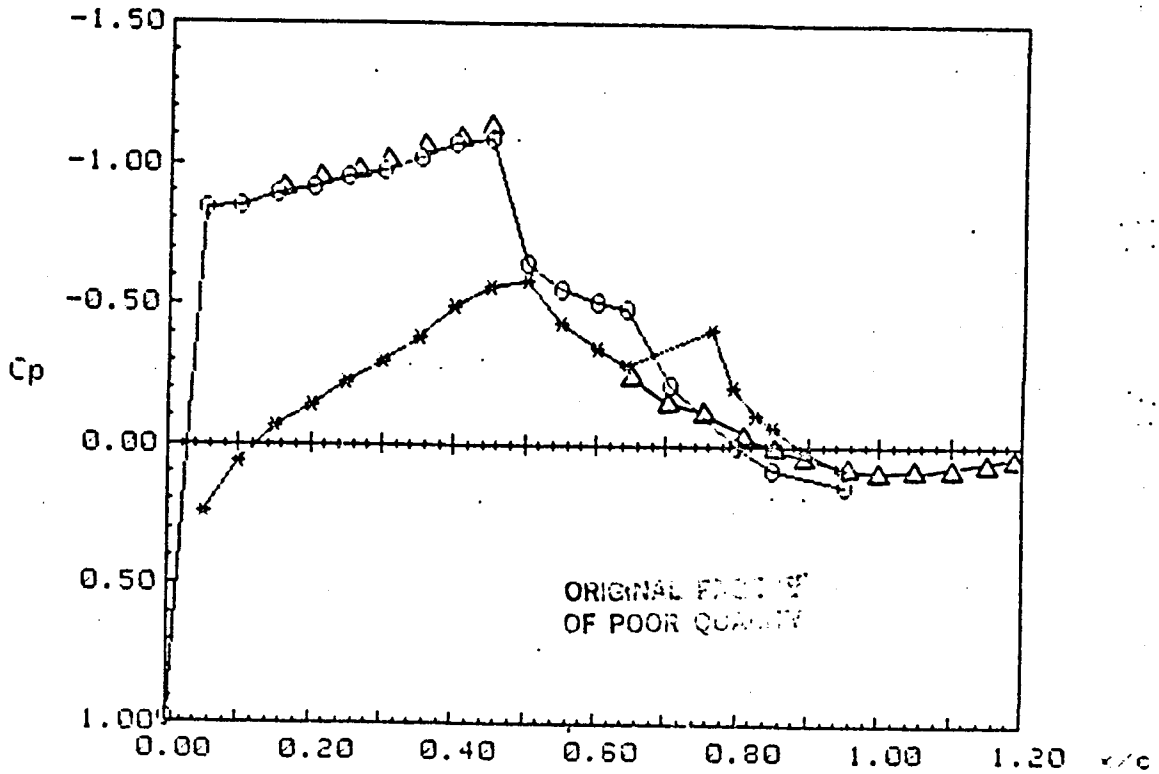

HOLOGRAPHIC DATA - 11 foot - Oscillating Flap
225449
RUN: 149 SEQ: 7
FLAP MEAN:-4 AMPL: 2 FREQ: 30
PHASE NO.: 26 ANGLE: 225 DELTA:-2.63
MACH: .8 ALPHA: 4 PRINT NO.: 4
Ptot: 2127.5 psf Pinf: 1394.9 psf Ttot: 547.34 Rankine

UPPER SURFACE:	x/c	N	Cp	LOWER SURFACE:	x/c	N	Cp
	.1	20	-.826				
	.15	11	-.876				
	.2	5	-.908				
	.25	0	-.935				
	.3	-5	-.962				
	.35	-11	-.995				
	.4	-20	-1.042				
	.45	-31	-1.1				
	.5	-32	-1.105				
	.65	-27	-.34				
	.7	-11	-.243				
	.75	0	-.175				
	.8	10	-.113				
	.85	18	-.063				
	.9	26	-.013				
	.95	33	.031				
	1	36	.05				
	1.05	36	.05				
	1.1	32	.025				
	1.15	29	.006				
	1.2	25	-.019				

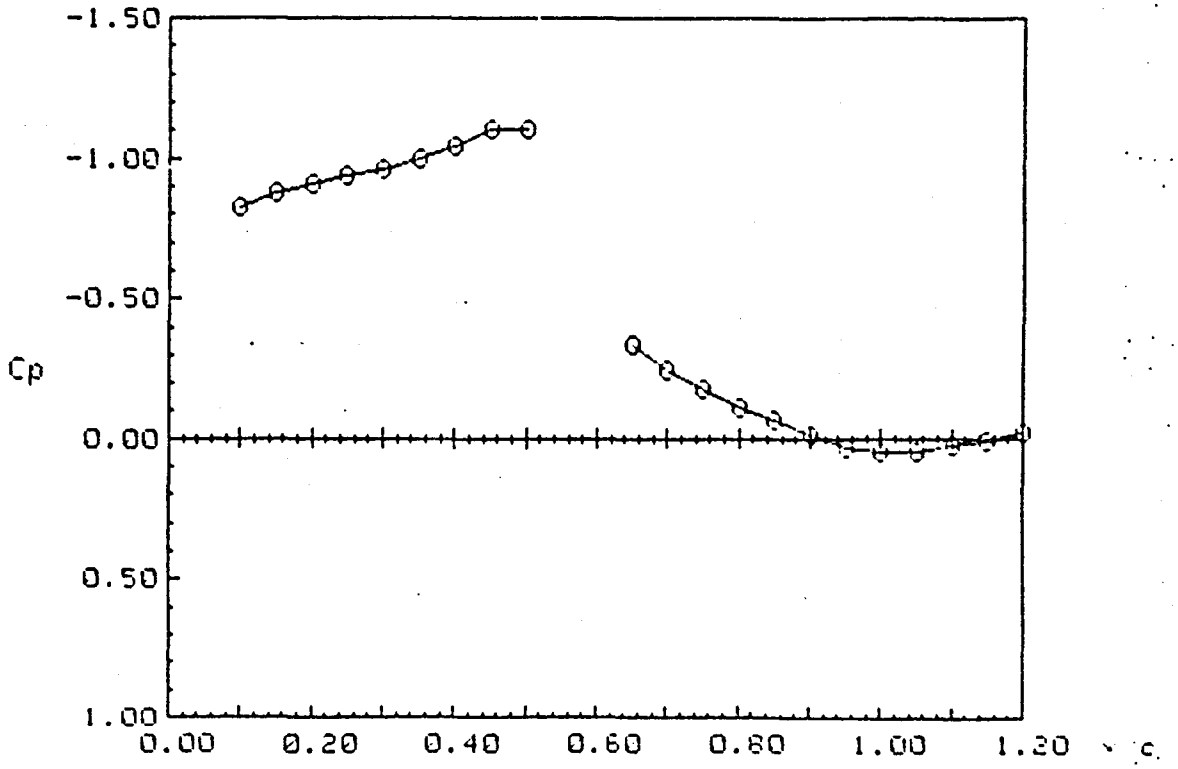

RUN: 149 SEQ: 7
FLAP MEAN:-4 AMPL.: 2 FREQ.: 30
PHASE NO.: 26 ANGLE: 225 DELTA:-2.63
MACH: .8 ALPHA: 4
Ptot: 2127.5 psf Pinf: 1394.9 psf Ttot: 547.34 Rankine

UPPER SURFACE:	x/c	Cp
	0	.992
	.05	-.821
	.1	-.829
	.15	-.874
	.2	-.9
	.25	-.935
	.3	-.963
	.35	-1.003
	.4	-1.062
	.45	-1.251
	.5	-.911
	.55	-.583
	.6	-.539
	.643	-.495
	.705	-.317
	.797	-.033
	.849	.068
	.95	.14

LOWER SURFACE:	x/c	Cp
	.05	.235
	.1	.059
	.15	-.07
	.2	-.146
	.25	-.226
	.3	-.302
	.35	-.377
	.4	-.484
	.45	-.553
	.5	-.438
	.55	-.321
	.6	-.271
	.643	-.228
	.762	-.291
	.793	-.105
	.824	-.05
	.849	-.024
	.895	.033
	.946	.091

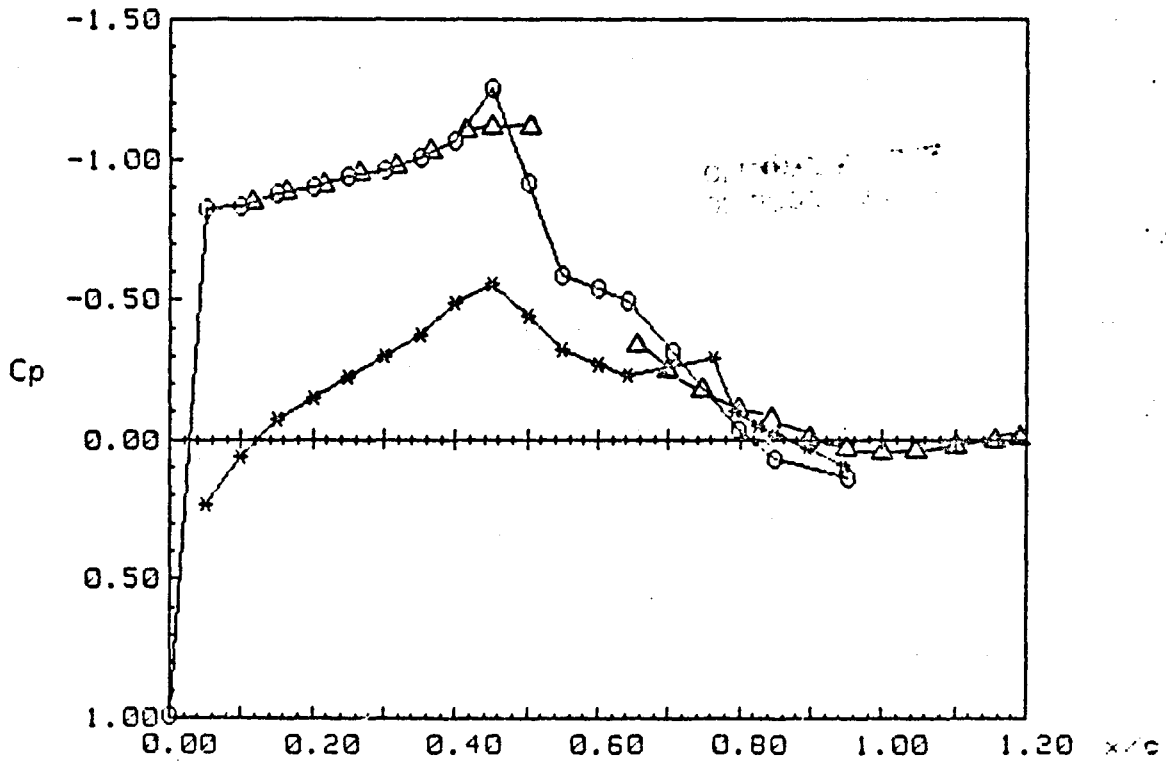

HOLOGRAPHIC DATA - 11 foot - Oscillating Flap
270149

RUN: 149 SEQ: 7
FLAP MEAN:-4 AMPL: 2 FREQ: 30
PHASE NO.: 31 ANGLE: 270 DELTA:-1.97
MACH: .8 ALPHA: 4 PRINT NO.: 1
Ptot: 2127.5 psf Pinf: 1394.9 psf Ttot: 547.34 Rankine

UPPER SURFACE:	x/c	N	Cp	LOWER SURFACE:	x/c	N	Cp
	.15	12	-.865				
	.2	5	-.903				
	.25	0	-.93				
	.3	-4	-.952				
	.35	-9	-.979				
	.4	-17	-1.022				
	.45	-28	-1.08				
	.5	-35	-1.116				
	.55	-25	-1.064				
	.7	-14	-.374				
	.75	0	-.289				
	.8	16	-.192				
	.85	23	-.148				
	.9	35	-.073				
	.95	43	-.023				
	1	48	.008				
	1.05	48	.008				
	1.1	43	-.023				
	1.15	39	-.048				
	1.2	38	-.055				

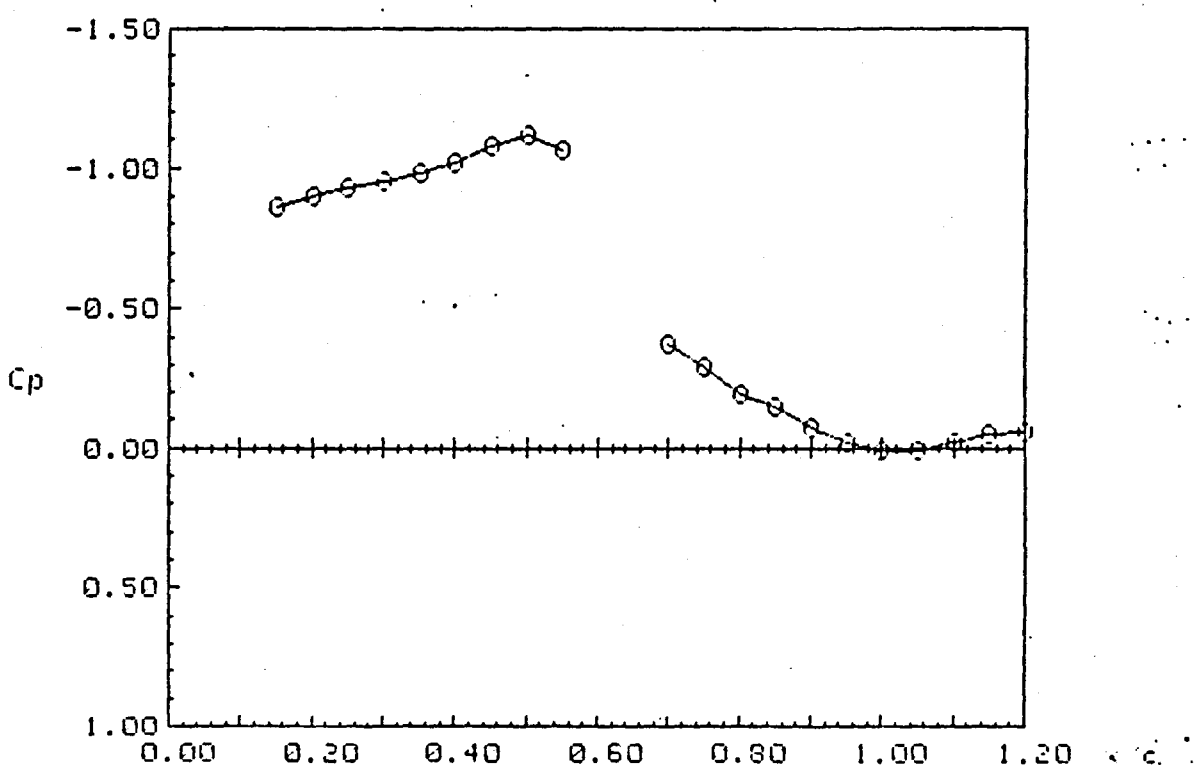

PRESSURE DATA - 11 foot - Oscillating Flap

RUN: 149 SEQ: 7
FLAP MEAN:-4 AMPL.: 2 FREQ.: 30
PHASE NO.: 31 ANGLE: 270 DELTA:-1.97
MACH: .8 ALPHA: 4
Ptot: 2127.5 psf Pinf: 1394.9 psf Ttot: 547.34 Rankine

UPPER SURFACE: x/c	Cp	LOWER SURFACE: x/c	Cp
0	.993	.05	.243
.05	-.817	.1	.07
.1	-.824	.15	-.059
.15	-.868	.2	-.13
.2	-.895	.25	-.203
.25	-.93	.3	-.275
.3	-.958	.35	-.343
.35	-.999	.4	-.397
.4	-1.058	.45	-.395
.45	-1.248	.5	-.34
.5	-1.182	.55	-.318
.55	-.608	.6	-.265
.6	-.549	.643	-.213
.643	-.522	.762	-.293
.705	-.428	.793	-.107
.797	-.151	.824	-.054
.849	.002	.849	-.031
.95	.141	.895	.029
		.946	.088

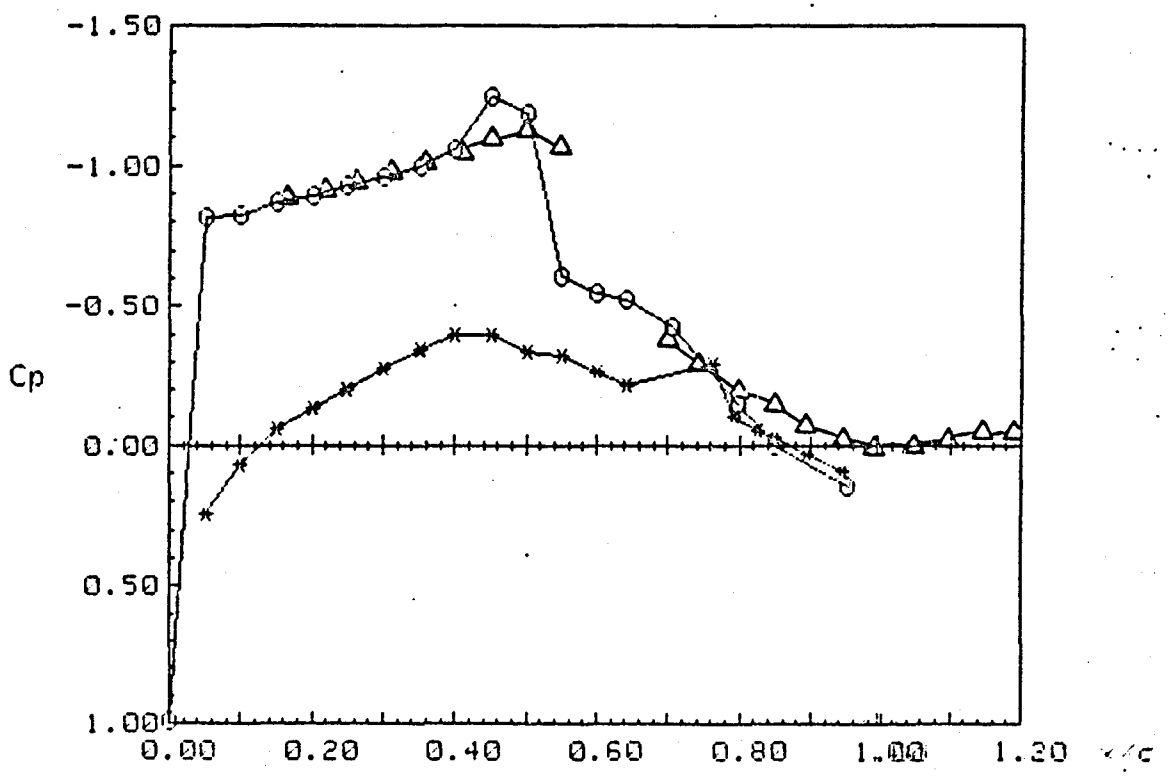

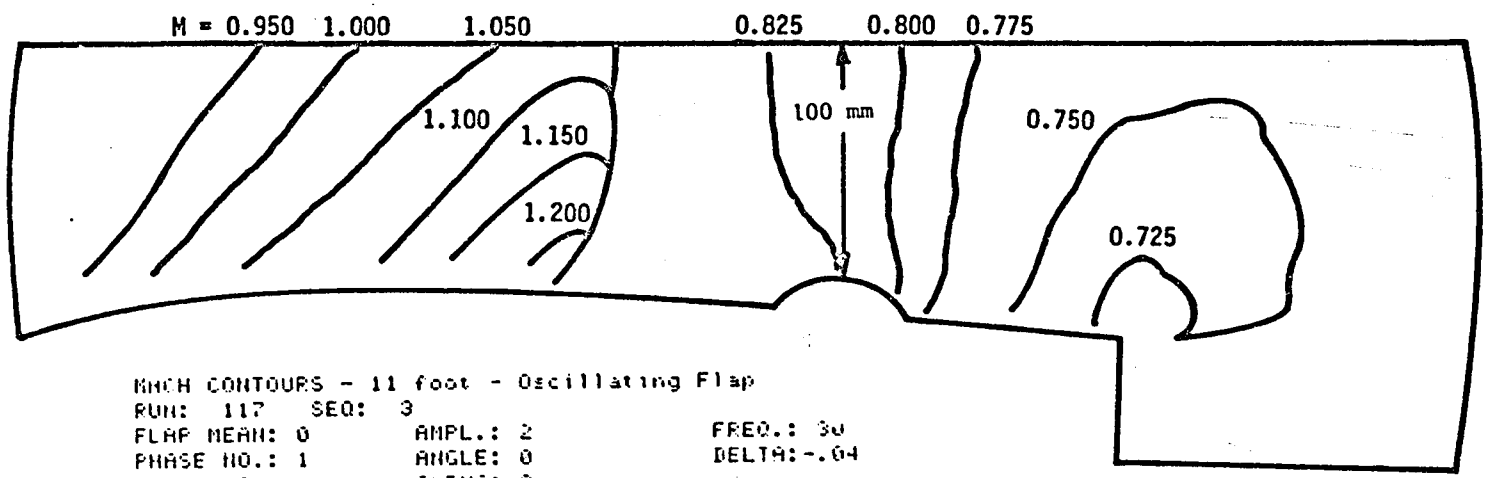

MACH CONTOURS - 11 foot - Oscillating Flap
RUN: 117 SEQ: 3
FLAP MEAN: 0 AMPL.: 2 FREQ.: 30
PHASE NO.: 1 ANGLE: 0 DELTA:-.04
MACH: .8 ALPHA: 0
Ptot: 2089.3 psf Pinf: 1373 psf Ttot: 549.3 Rankine

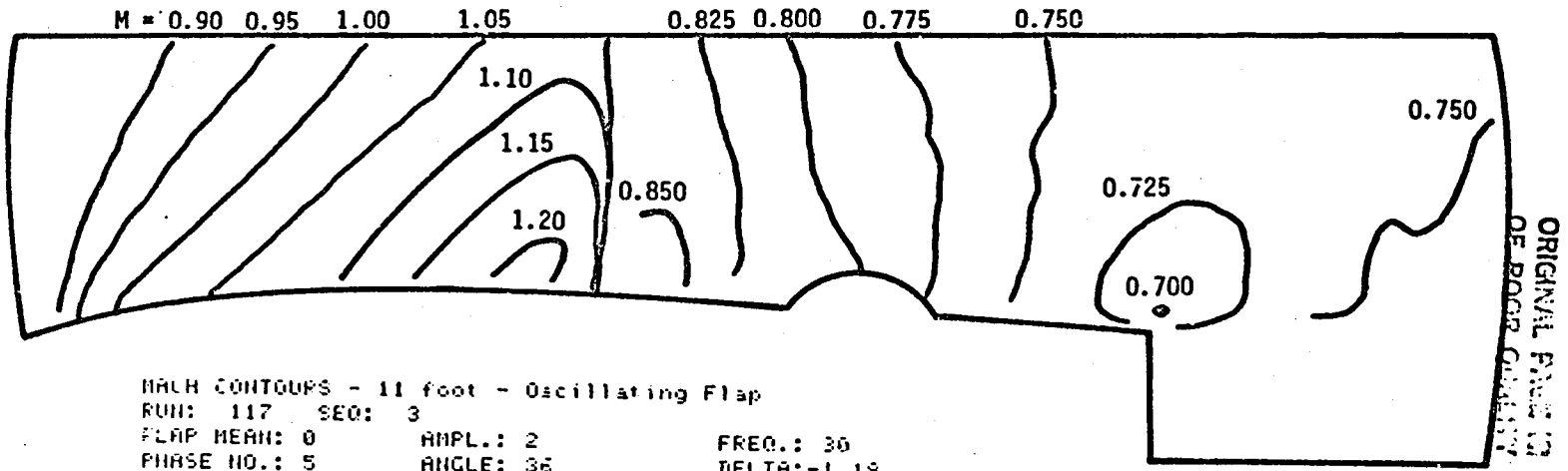

MACH CONTOURS - 11 foot - Oscillating Flap
RUN: 117 SEQ: 3
FLAP MEAN: 0 AMPL.: 2 FREQ.: 30
PHASE NO.: 5 ANGLE: 36 DELTA:-1.18
MACH: .8 ALPHA: 0
Ptot: 2089.3 psf Pinf: 1373 psf Ttot: 549.3 Rankine

Figure 14.- Mach Contours Obtained From the Interferograms. $\delta = 0°$, $\alpha = 0°$

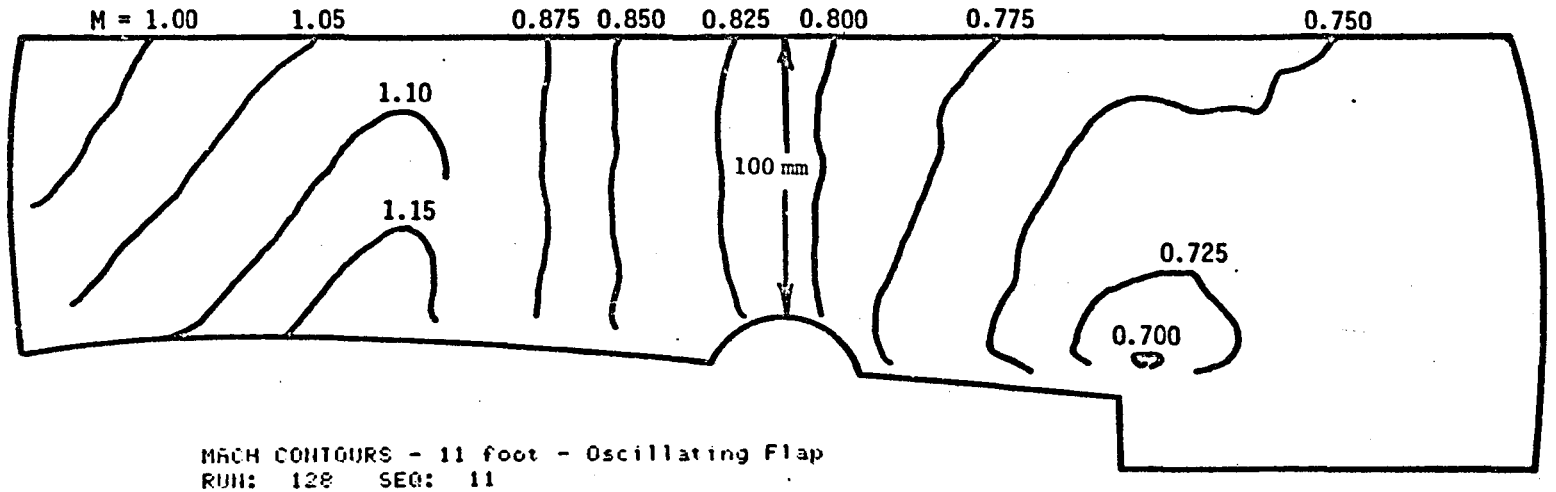

MACH CONTOURS - 11 foot - Oscillating Flap
RUN: 128 SEQ: 11
FLAP MEAN: 0 AMPL.: 2 FREQ.: 30
PHASE NO.: 7 ANGLE: 54 DELTA:-1.62
MACH: .8 ALPHA: 0
Ptot: 2087.9 psf Pinf: 1370 psf Ttot: 550.15 Rankine

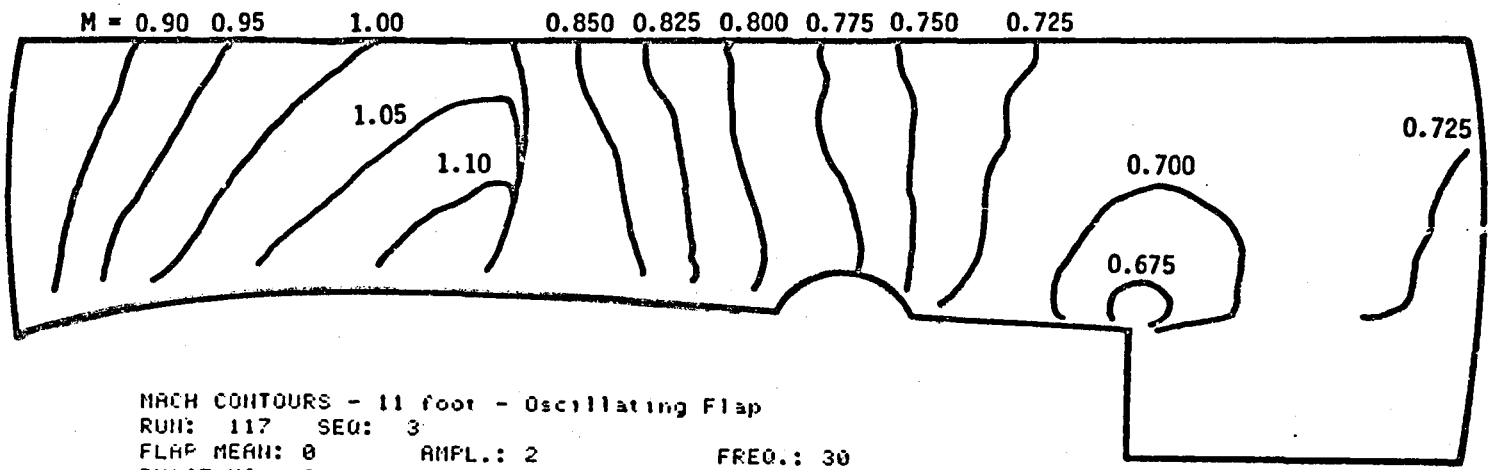

MACH CONTOURS - 11 foot - Oscillating Flap
RUN: 117 SEQ: 3
FLAP MEAN: 0 AMPL.: 2 FREQ.: 30
PHASE NO.: 9 ANGLE: 72 DELTA:-1.88
MACH: .8 ALPHA: 0
Ptot: 2089.3 psf Pinf: 1373 psf Ttot: 549.3 Rankine

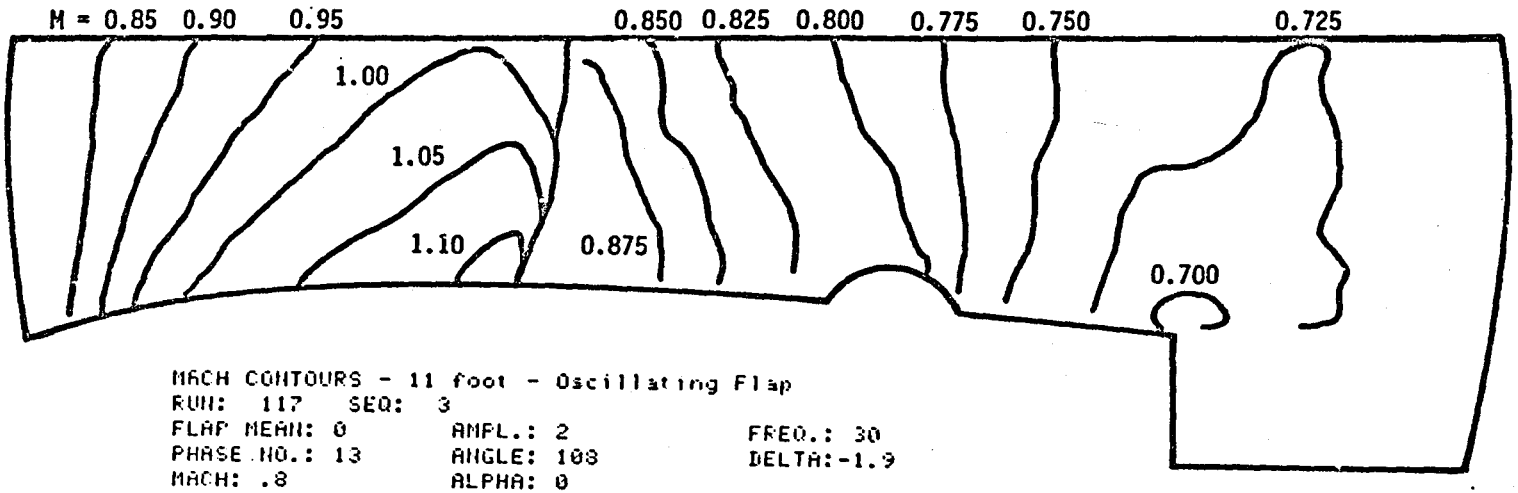

MACH CONTOURS - 11 foot - Oscillating Flap
RUN: 117 SEQ: 3
FLAP MEAN: 0 AMPL.: 2 FREQ.: 30
PHASE NO.: 13 ANGLE: 108 DELTA:-1.9
MACH: .8 ALPHA: 0
Ptot: 2089.3 psf Pinf: 1373 psf Ttot: 549.3 Rankine

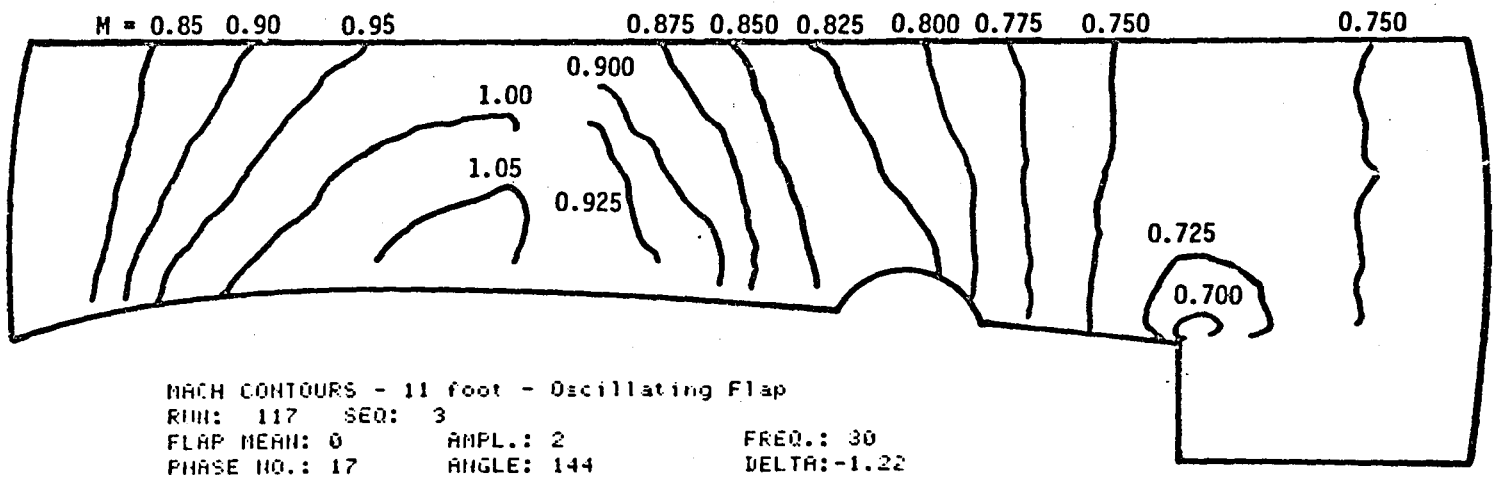

MACH CONTOURS - 11 foot - Oscillating Flap
RUN: 117 SEQ: 3
FLAP MEAN: 0 AMPL.: 2 FREQ.: 30
PHASE NO.: 17 ANGLE: 144 DELTA:-1.22
MACH: .8 ALPHA: 0
Ptot: 2089.3 psf Pinf: 1373 psf Ttot: 549.3 Rankine

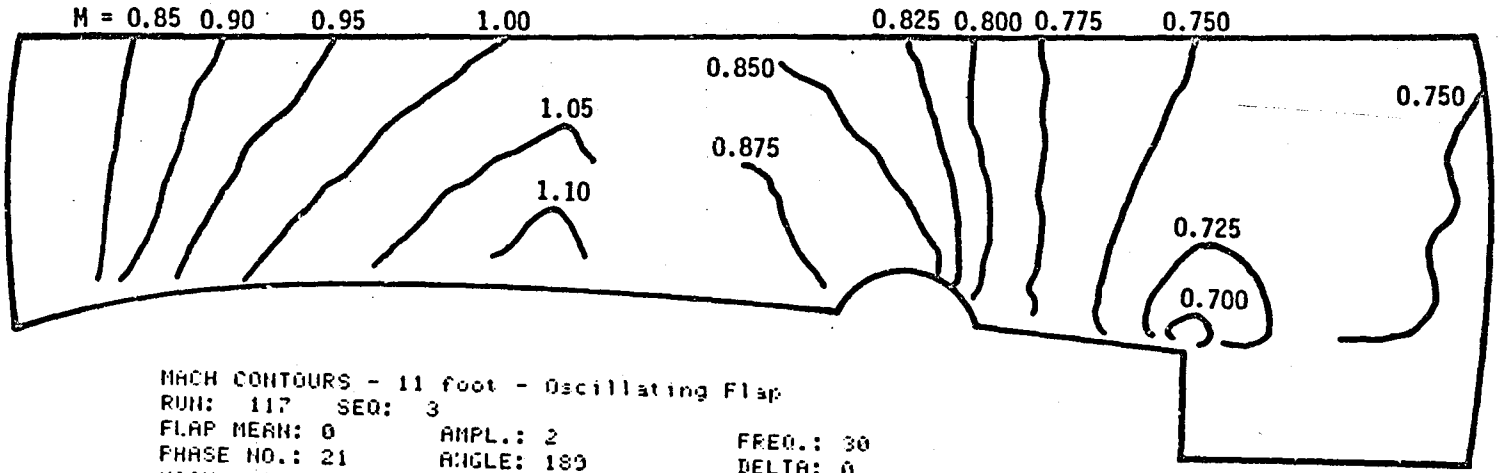

MACH CONTOURS - 11 foot - Oscillating Flap
RUN: 117 SEQ: 3
FLAP MEAN: 0 AMPL.: 2 FREQ.: 30
PHASE NO.: 21 ANGLE: 180 DELTA: 0
MACH: .8 ALPHA: 0
Ptot: 2089.3 psf Pinf: 1373 psf Ttot: 549.3 Rankine

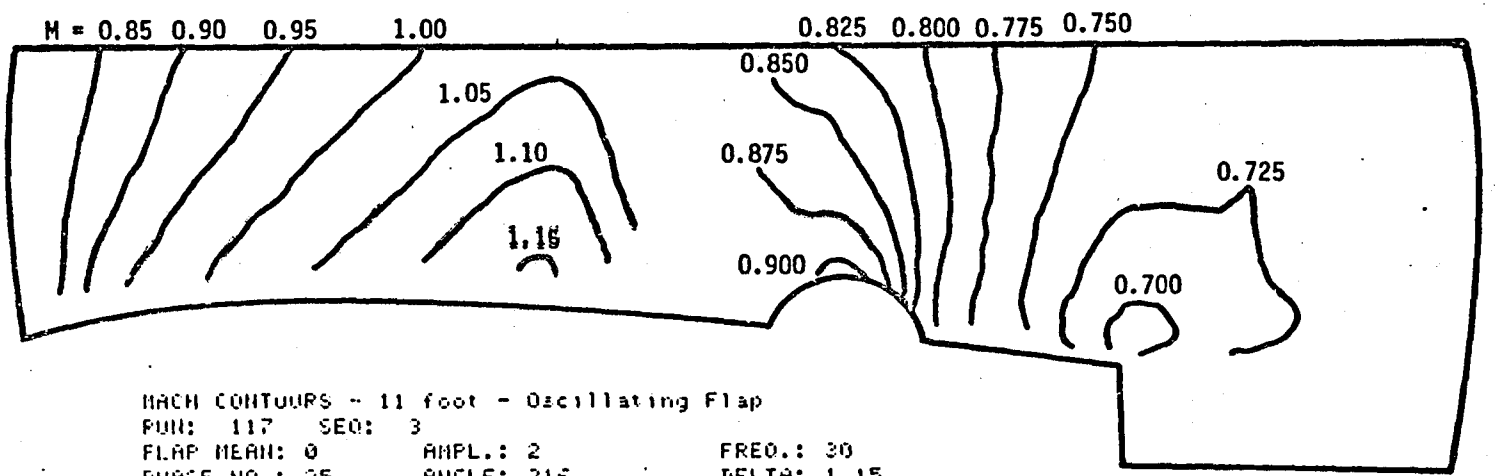

MACH CONTOURS - 11 foot - Oscillating Flap
RUN: 117 SEQ: 3
FLAP MEAN: 0 AMPL.: 2 FREQ.: 30
PHASE NO.: 25 ANGLE: 216 DELTA: 1.15
MACH: .8 ALPHA: 0
Ptot: 2089.3 psf Pinf: 1373 psf Ttot: 549.3 Rankine

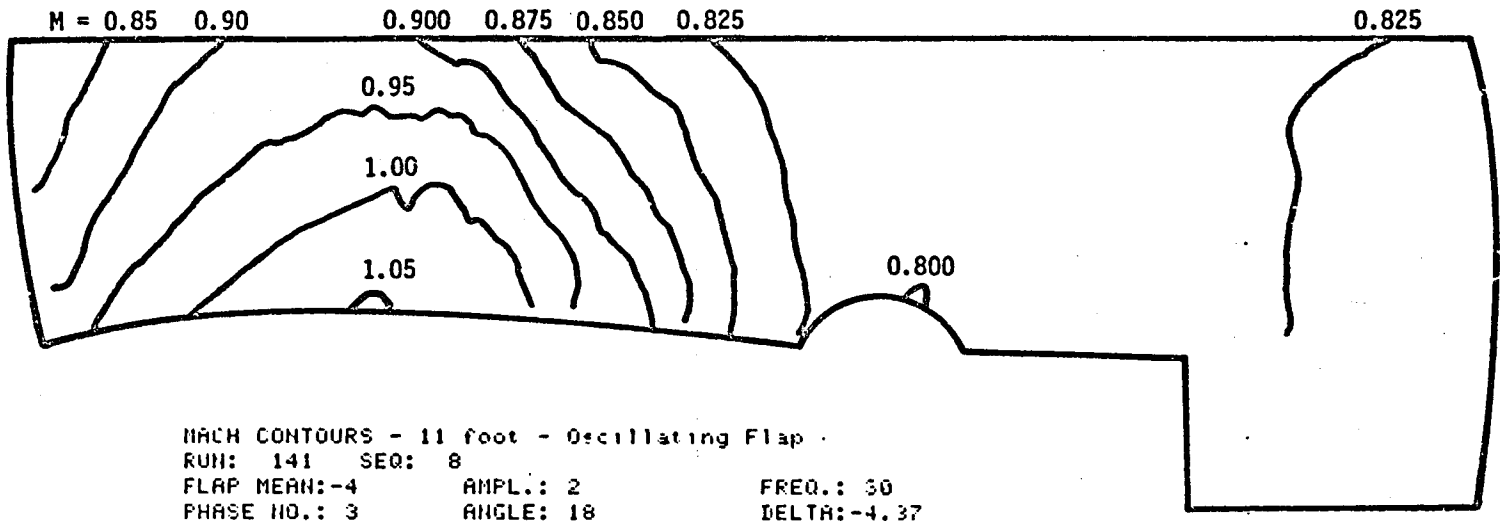

MACH CONTOURS - 11 foot - Oscillating Flap
RUN: 141 SEQ: 8
FLAP MEAN:-4 AMPL.: 2 FREQ.: 30
PHASE NO.: 3 ANGLE: 18 DELTA:-4.37
MACH: .8 ALPHA: 0
Ptot: 2128.2 psf Pinf: 1395.2 psf Ttot: 550.34 Rankine

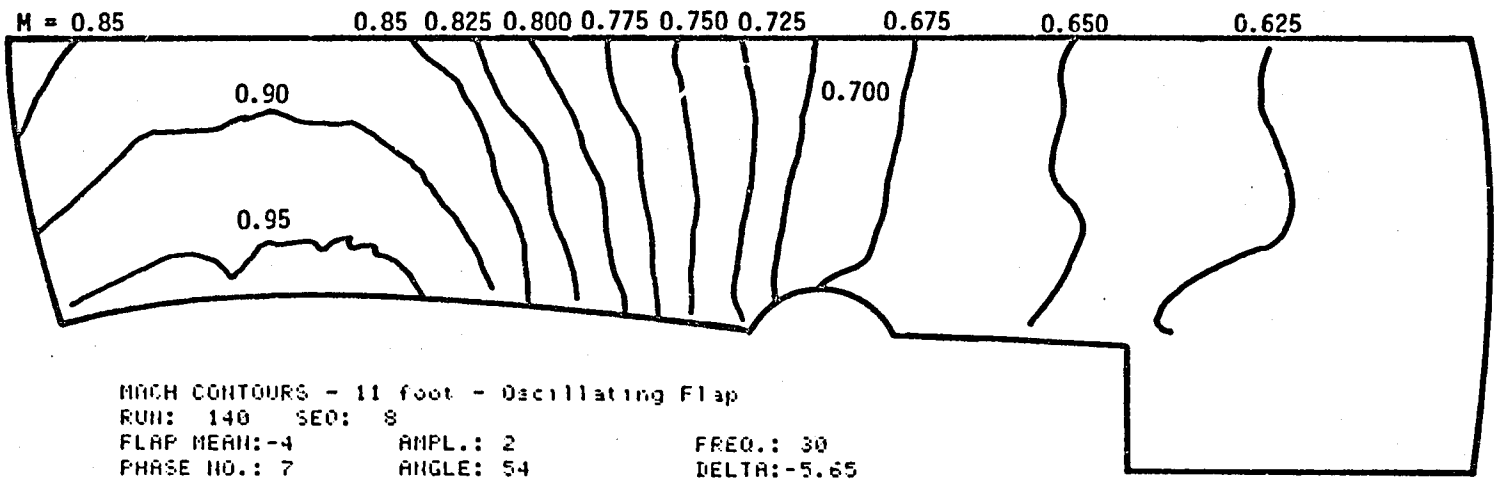

MACH CONTOURS - 11 foot - Oscillating Flap
RUN: 140 SEQ: 8
FLAP MEAN:-4 AMPL.: 2 FREQ.: 30
PHASE NO.: 7 ANGLE: 54 DELTA:-5.65
MACH: .8 ALPHA: 0
Ptot: 2128.2 psf Pinf: 1397.2 psf Ttot: 551.25 Rankine

Figure 15.- Mach Contours Obtained From the Interferograms. $\delta = -4°$, $\alpha = 0°$

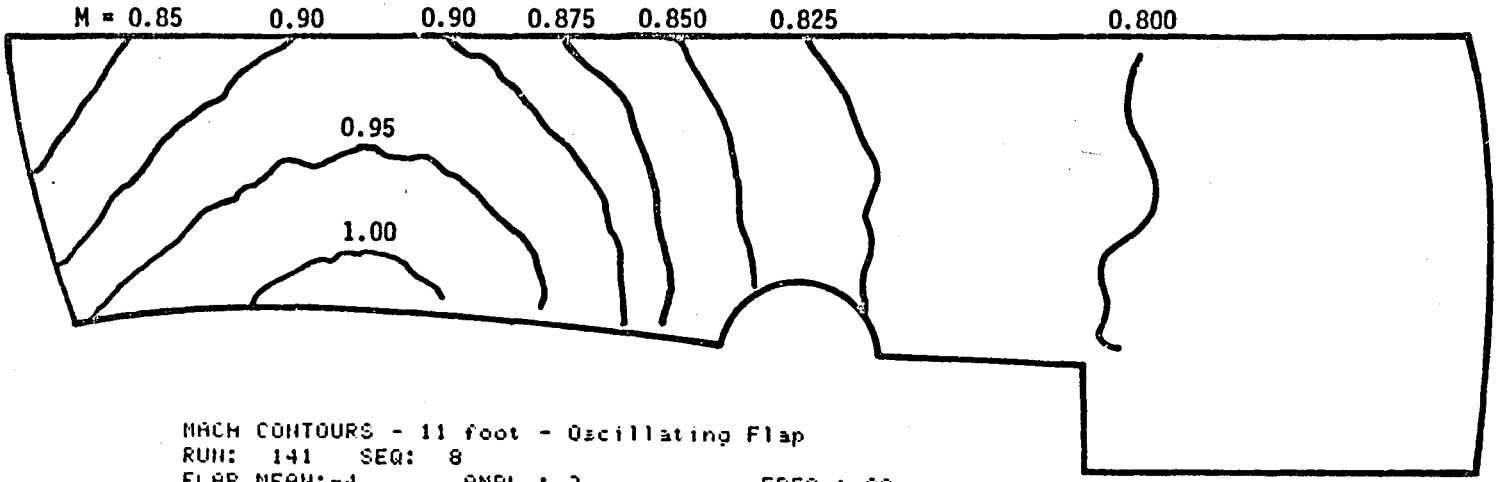

MACH CONTOURS - 11 foot - Oscillating Flap
RUN: 141 SEQ: 8
FLAP MEAN:-4 AMPL.: 2 FREQ.: 30
PHASE NO.: 19 ANGLE: 162 DELTA:-4.74
MACH: .8 ALPHA: 0
Ptot: 2128.2 psf Pinf: 1395.2 psf Ttot: 550.34 Rankine

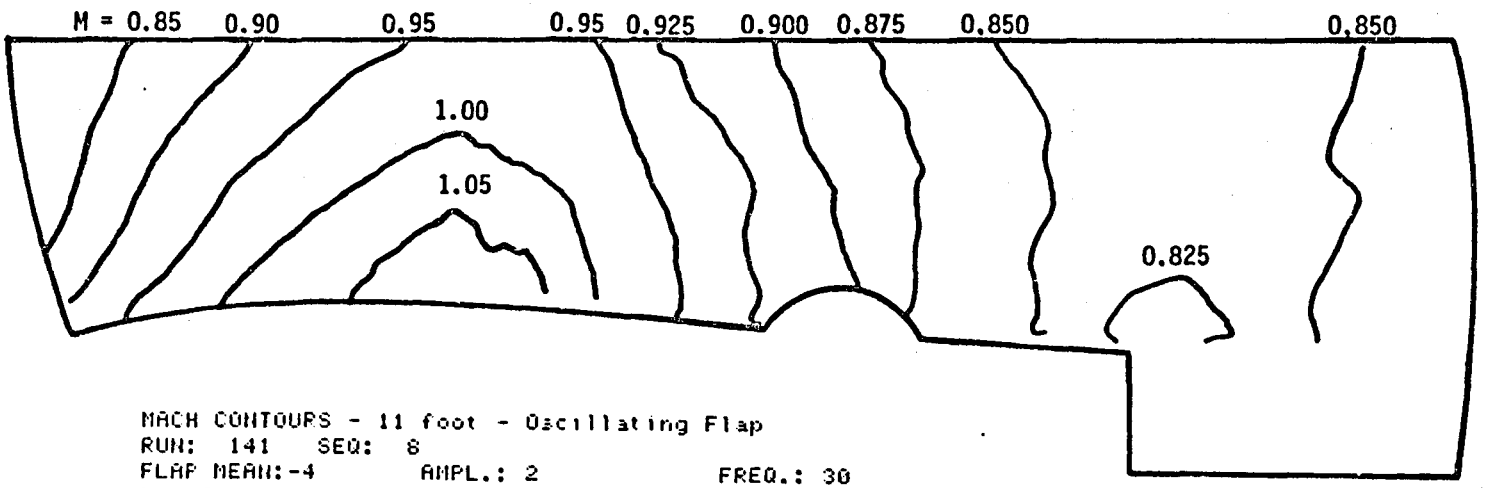

MACH CONTOURS - 11 foot - Oscillating Flap
RUN: 141 SEQ: 8
FLAP MEAN:-4 AMPL.: 2 FREQ.: 30
PHASE NO.: 27 ANGLE: 234 DELTA:-2.39
MACH: .8 ALPHA: 0
Ptot: 2128.2 psf Pinf: 1395.2 psf Ttot: 550.34 Rankine

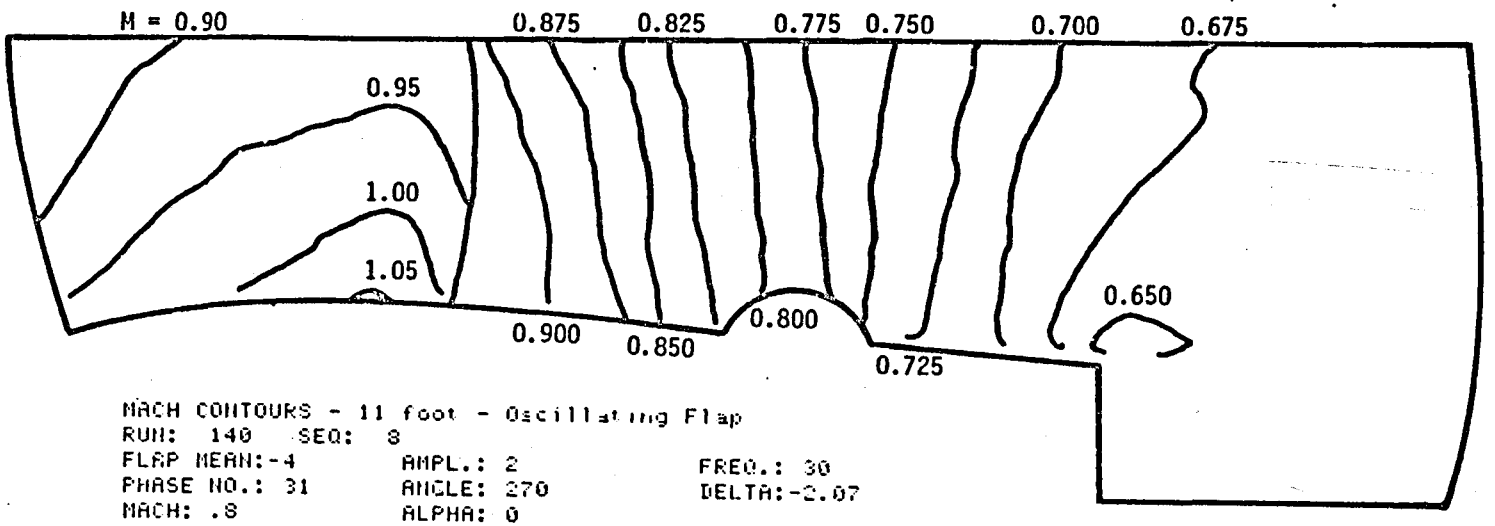

MACH CONTOURS - 11 foot - Oscillating Flap
RUN: 140 SEQ: 8
FLAP MEAN:-4 AMPL.: 2 FREQ.: 30
PHASE NO.: 31 ANGLE: 270 DELTA:-2.07
MACH: .8 ALPHA: 0
Ptot: 2128.2 psf Pinf: 1397.2 psf Ttot: 551.25 Rankine

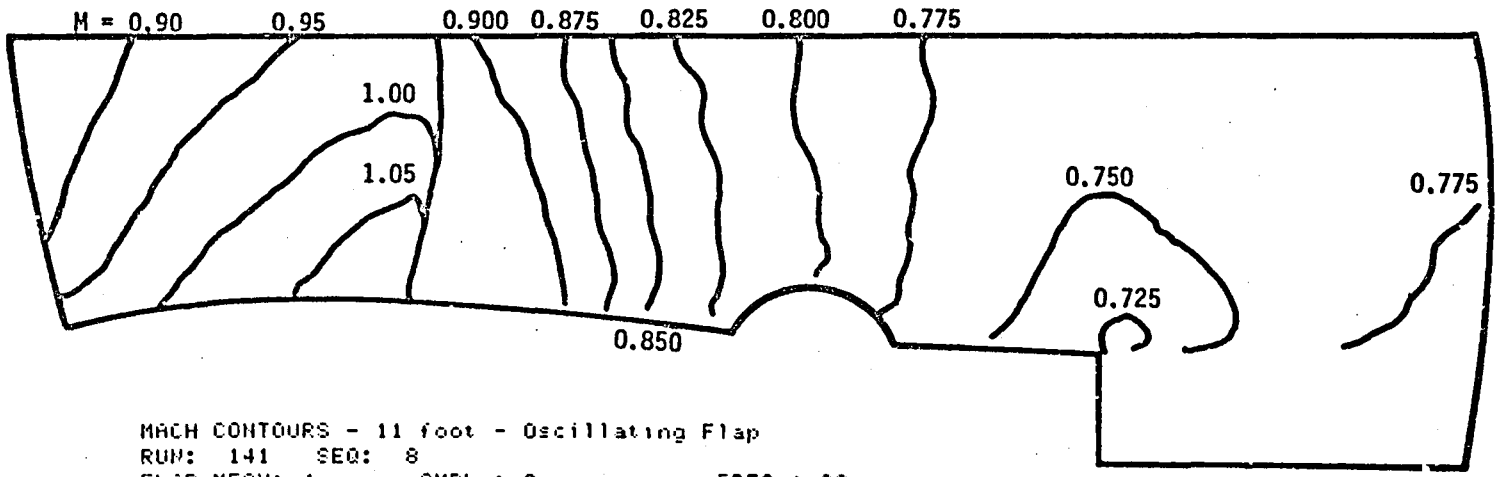

MACH CONTOURS - 11 foot - Oscillating Flap
RUN: 141 SEQ: 8
FLAP MEAN:-4 AMPL.: 2 FREQ.: 30
PHASE NO.: 35 ANGLE: 306 DELTA:-2.3
MACH: .8 ALPHA: 0
Ptot: 2128.2 psf Pinf: 1395.2 psf Ttot: 550.34 Rankine

MACH CONTOURS - 11 foot - Oscillating Flap
RUN: 140 SEQ: 8
FLAP MEAN:-4 AMPL.: 2 FREQ.: 30
PHASE NO.: 39 ANGLE: 342 DELTA:-3.3
MACH: .8 ALPHA: 0
Ptot: 2128.2 psf Pinf: 1597.2 psf Ttot: 551.25 Rankine

C-2

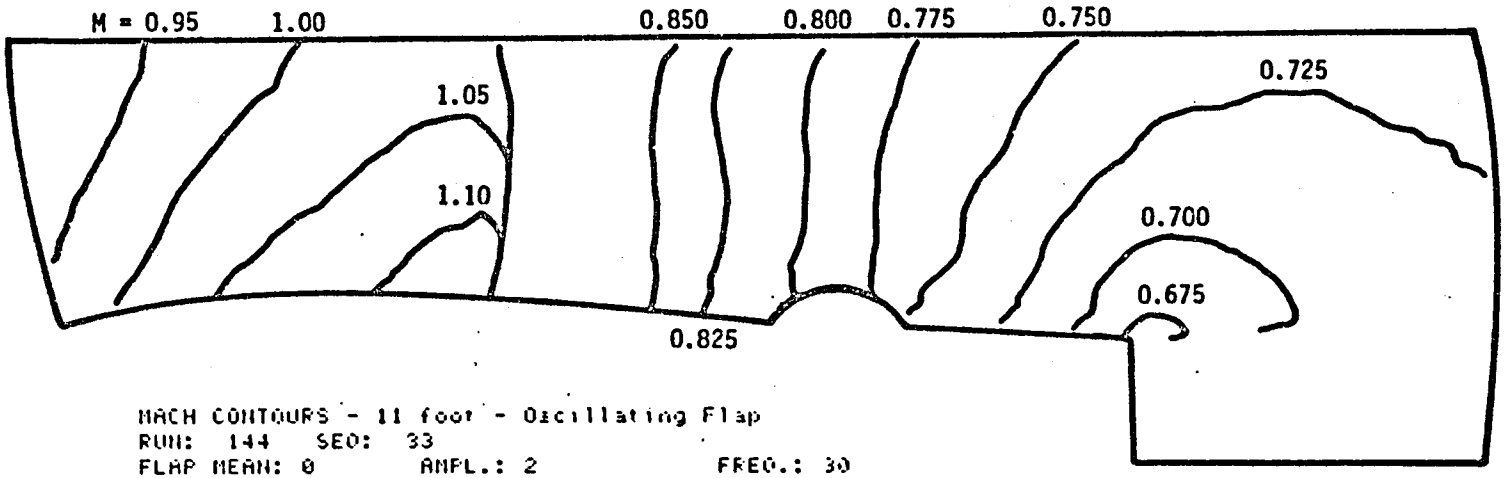

MACH CONTOURS - 11 foot - Oscillating Flap
RUN: 144 SEQ: 33
FLAP MEAN: 0 AMPL.: 2 FREQ.: 30
PHASE NO.: 7 ANGLE: 54 DELTA:-1.58
MACH: .8 ALPHA: 0
Ptot: 4238 psf Pinf: 2788.8 psf Ttot: 580 Rankine

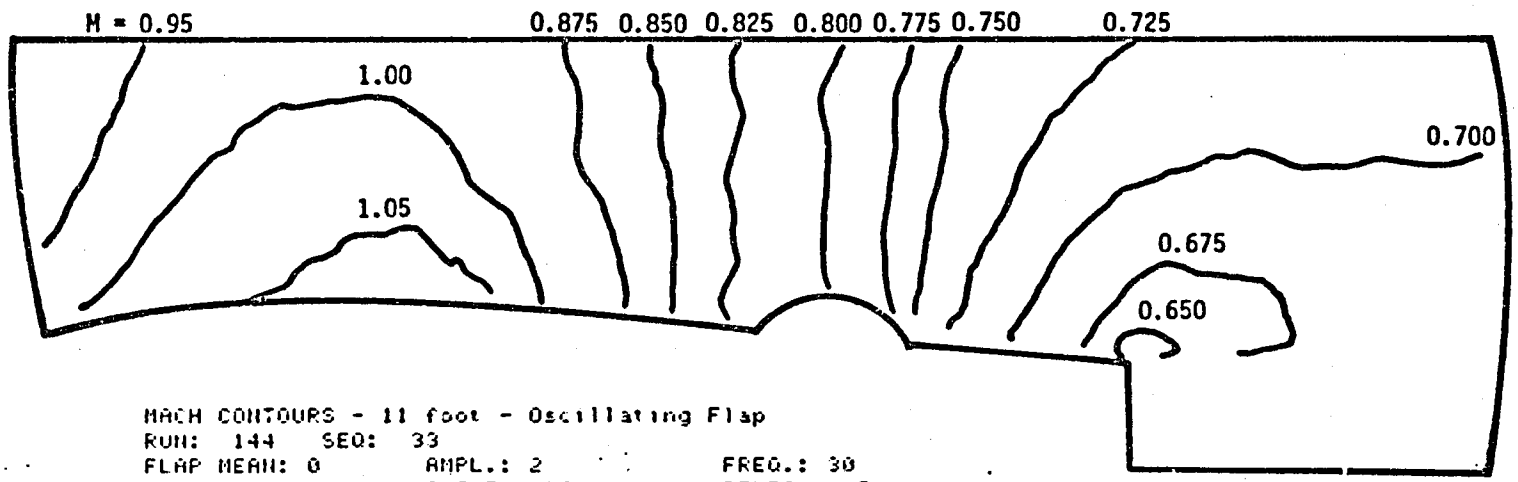

MACH CONTOURS - 11 foot - Oscillating Flap
RUN: 144 SEQ: 33
FLAP MEAN: 0 AMPL.: 2 FREQ.: 30
PHASE NO.: 15 ANGLE: 126 DELTA:-1.7
MACH: .8 ALPHA: 0
Ptot: 4238 psf Pinf: 2788.8 psf Ttot: 580 Rankine

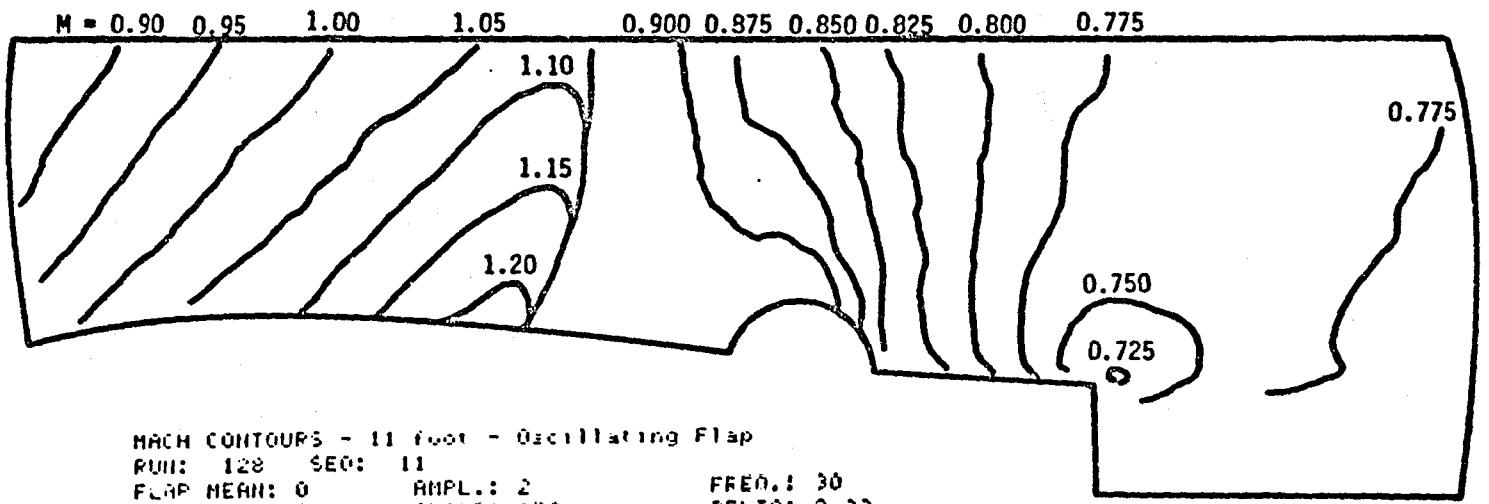

MACH CONTOURS - 11 foot - Oscillating Flap
RUN: 128 SEQ: 11
FLAP MEAN: 0 AMPL.: 2 FREQ.: 30
PHASE NO.: 31 ANGLE: 270 DELTA: 2.02
MACH: .8 ALPHA: 0
Ptot: 2087.9 psf Pinf: 1370 psf Ttot: 550.15 Rankine

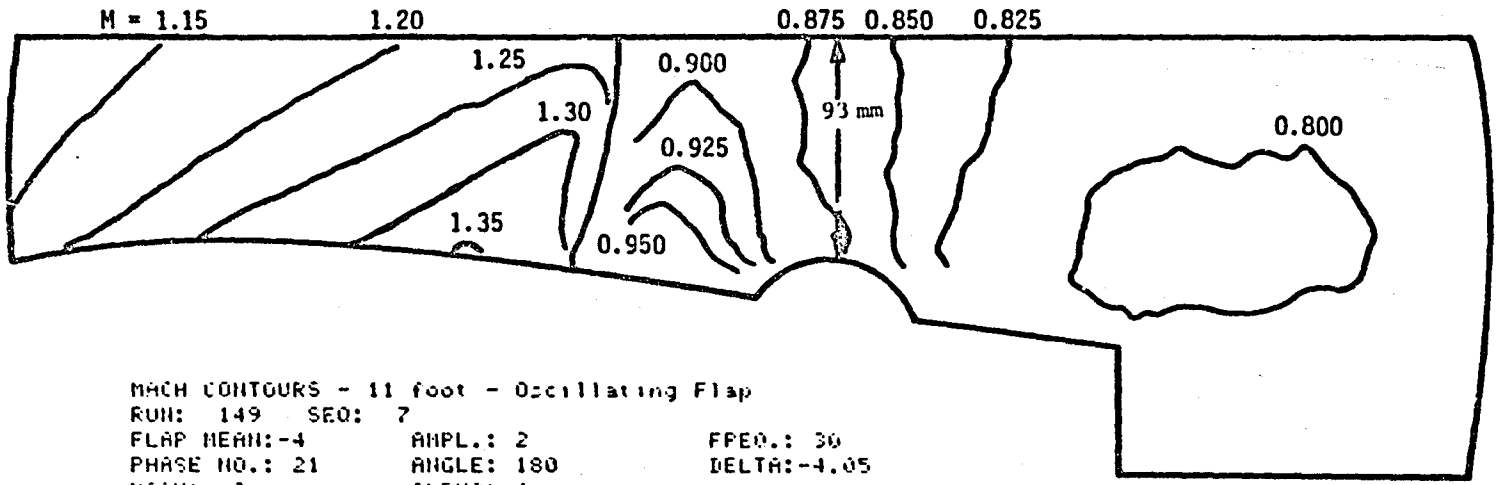

MACH CONTOURS - 11 foot - Oscillating Flap
RUN: 149 SEQ: 7
FLAP MEAN:-4 AMPL.: 2 FREQ.: 30
PHASE NO.: 21 ANGLE: 180 DELTA:-4.05
MACH: .8 ALPHA: 4
Ptot: 2127.5 psf Pinf: 1394.9 psf Ttot: 547.34 Rankine

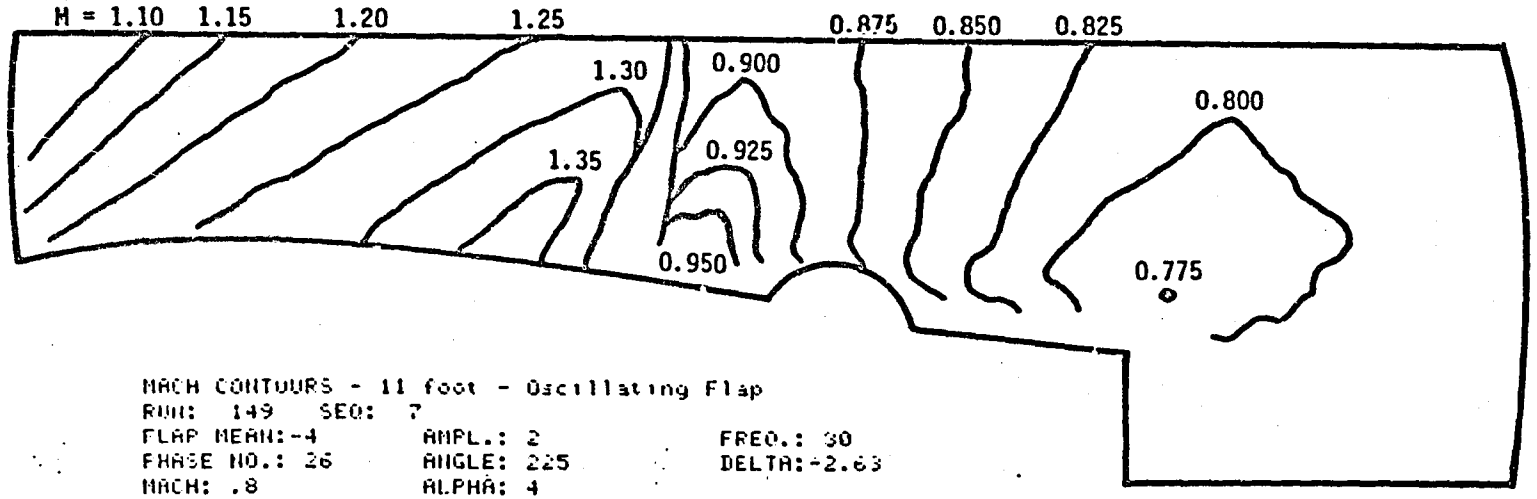

MACH CONTOURS - 11 foot - Oscillating Flap
RUN: 149 SEQ: 7
FLAP MEAN:-4 AMPL.: 2 FREQ.: 30
PHASE NO.: 26 ANGLE: 225 DELTA:-2.63
MACH: .8 ALPHA: 4
Ptot: 2127.5 psf Pinf: 1394.9 psf Ttot: 547.34 Rankine

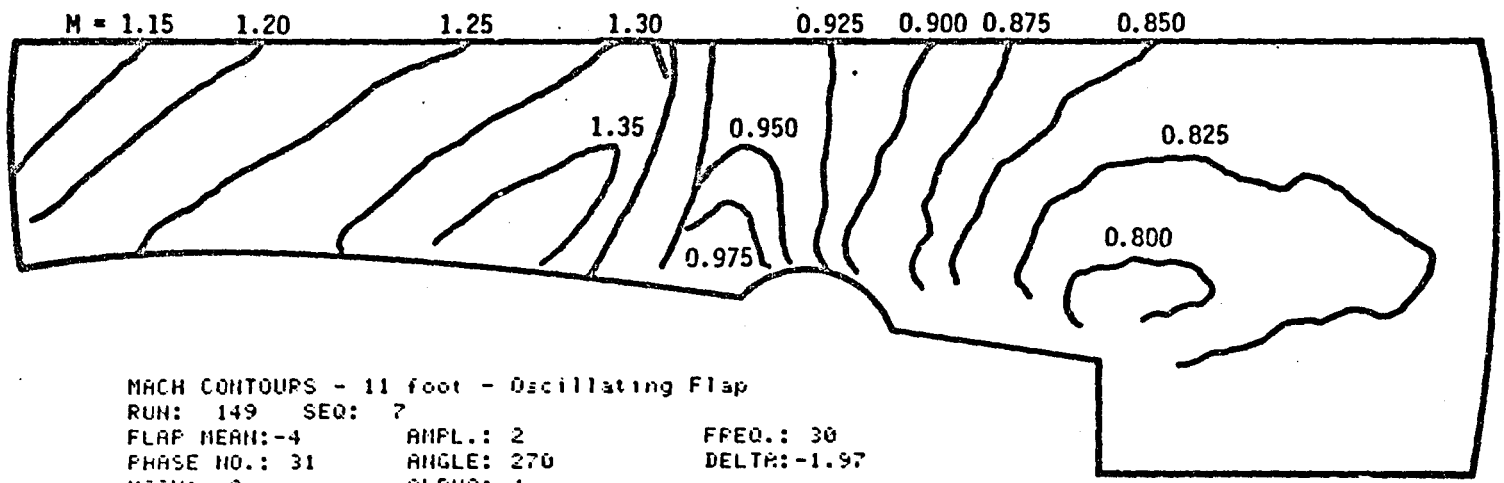

MACH CONTOURS - 11 foot - Oscillating Flap
RUN: 149 SEQ: 7
FLAP MEAN:-4 AMPL.: 2 FREQ.: 30
PHASE NO.: 31 ANGLE: 270 DELTA:-1.97
MACH: .8 ALPHA: 4
Ptot: 2127.5 psf Pinf: 1394.9 psf Ttot: 547.34 Rankine

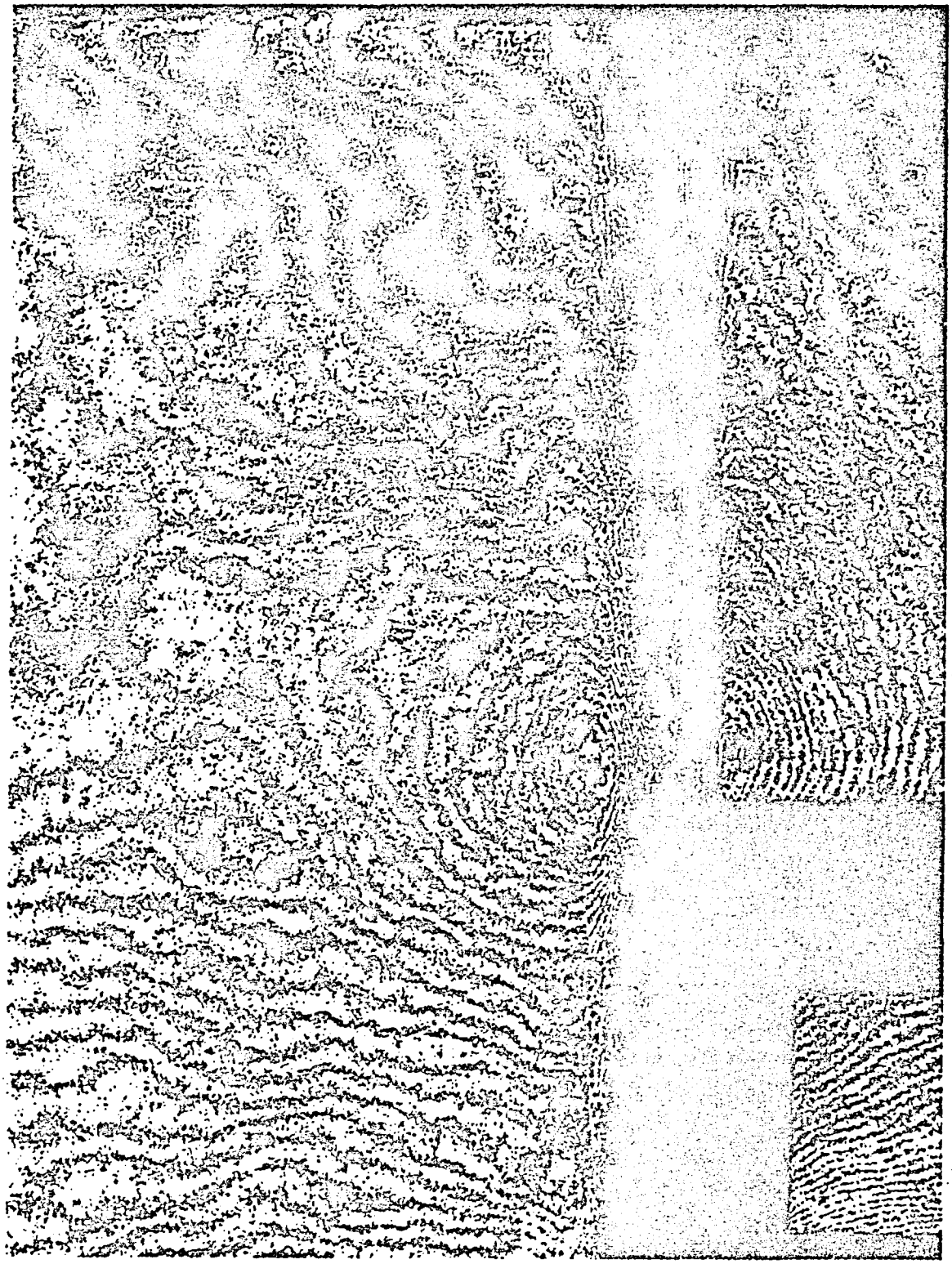

18(a) Phase Angle = 30°

Figure 18 - Polarized Views of the [illegible]

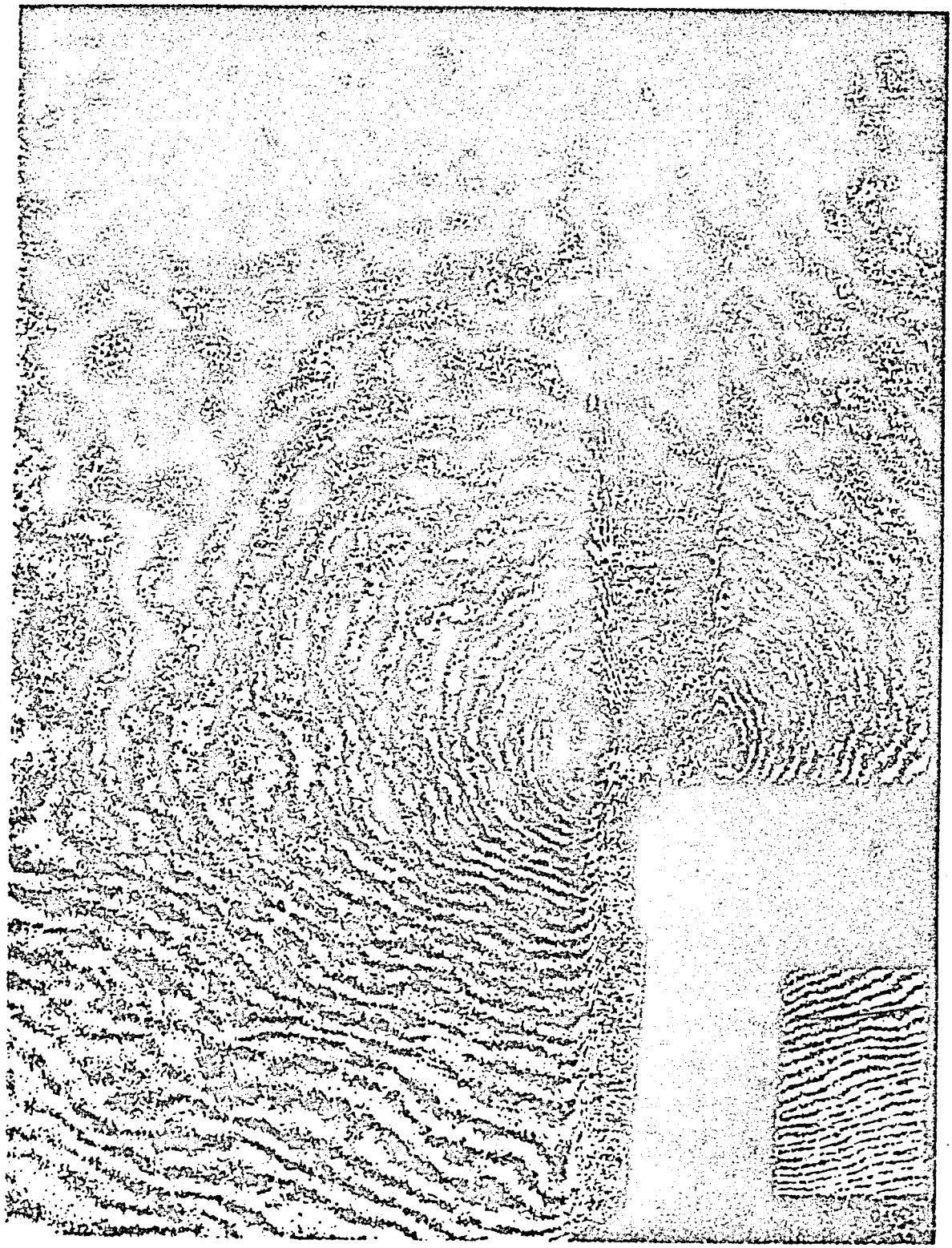

I(μ) Phase Angle = 54°

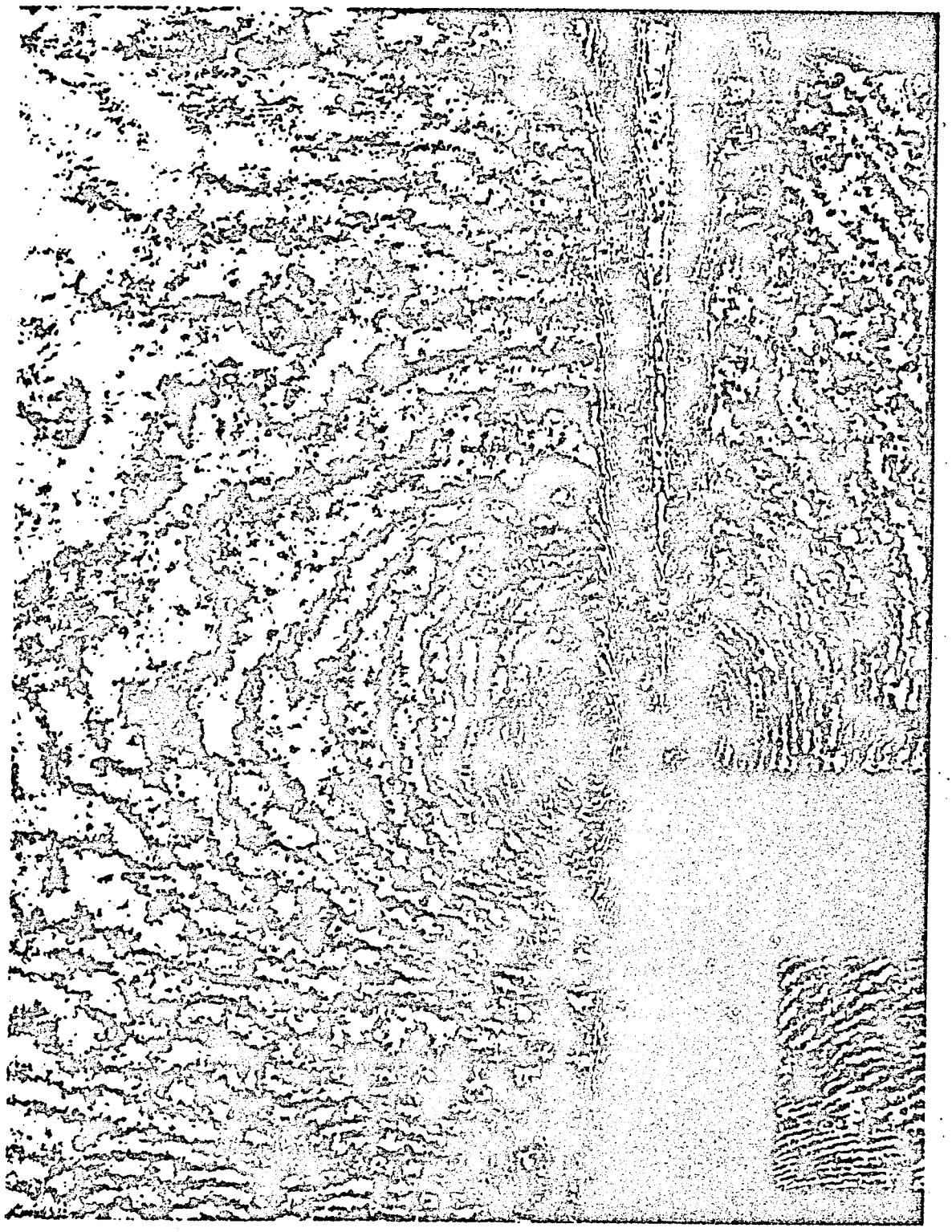

Effective Phase Angle = 7.5°

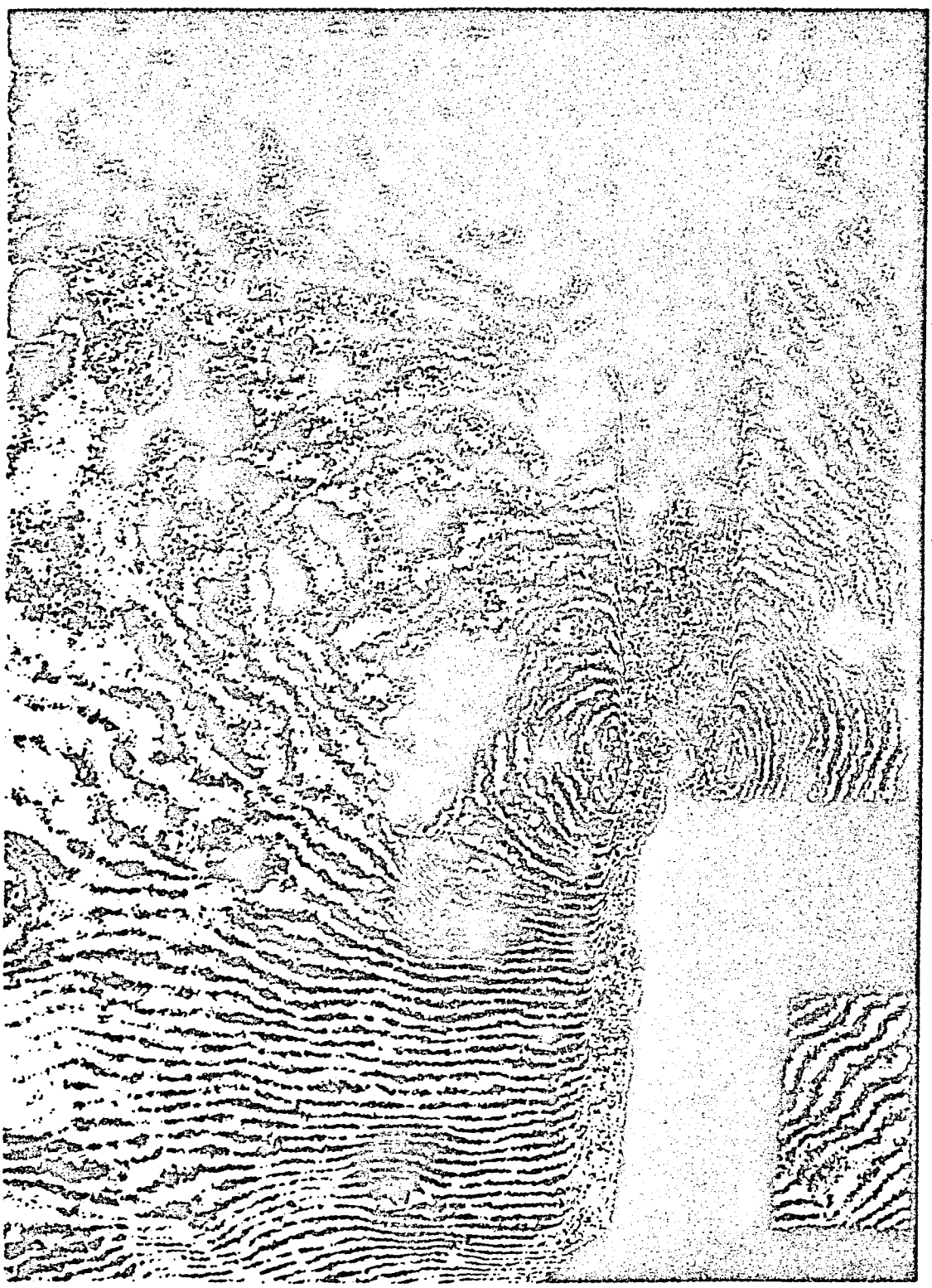

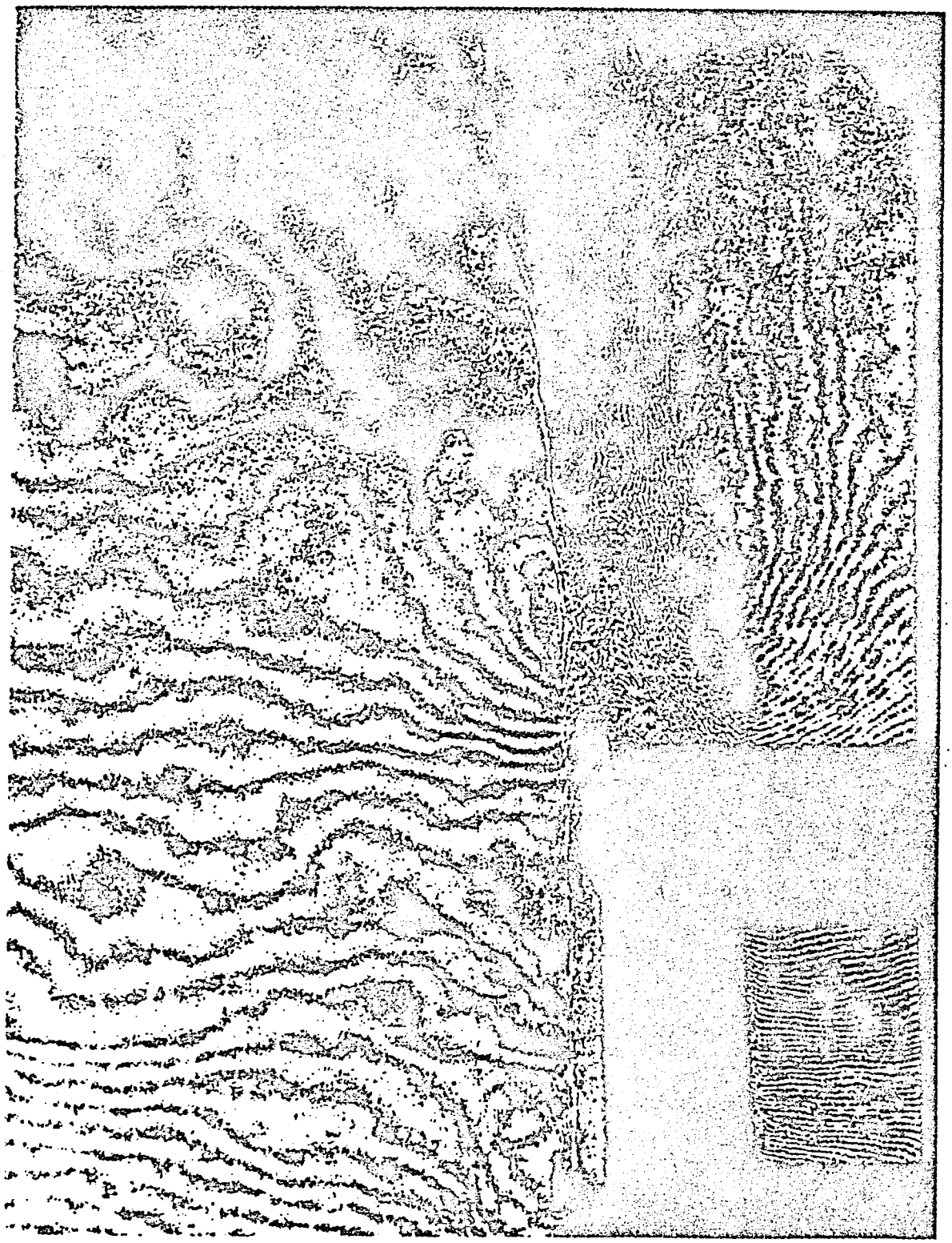

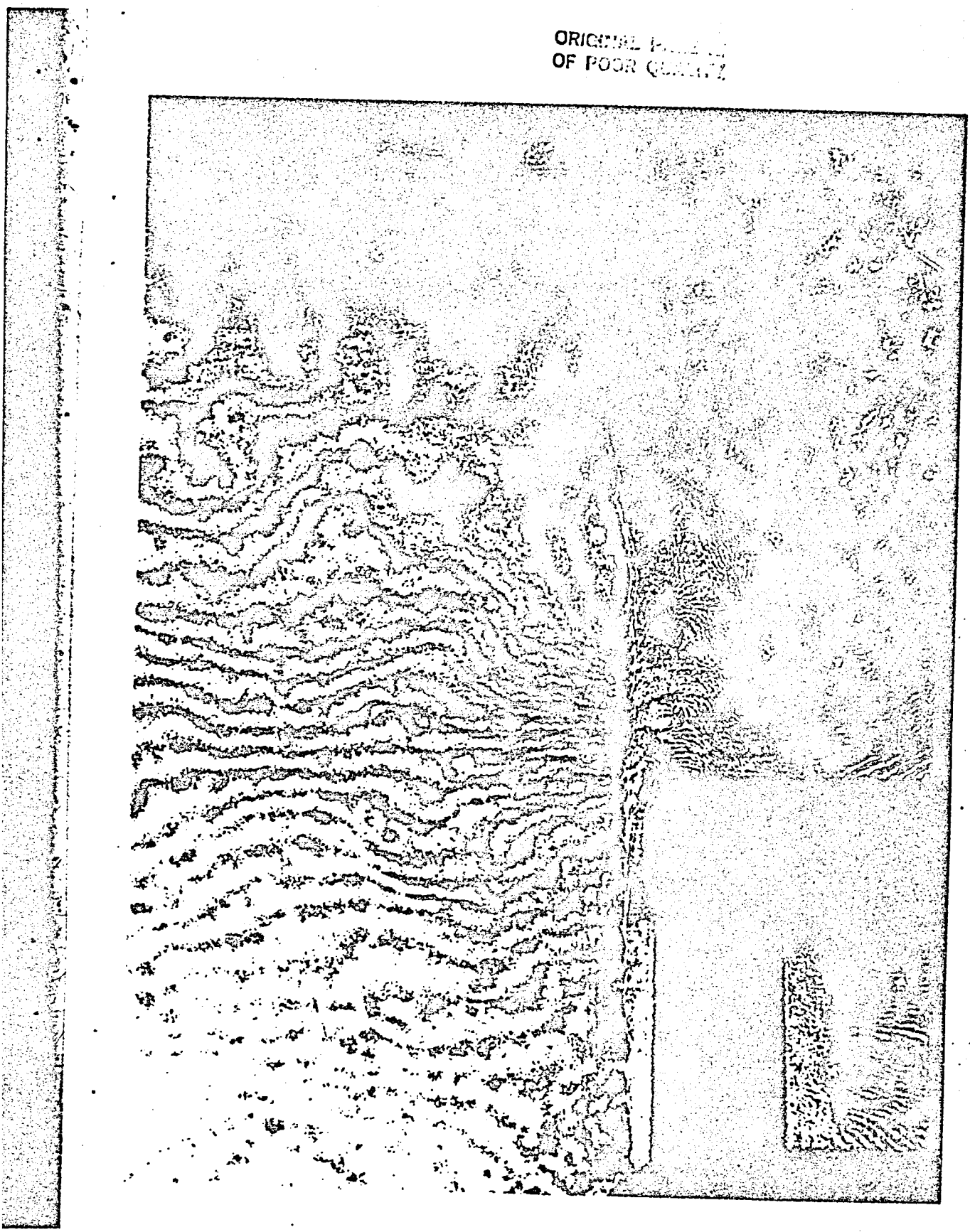

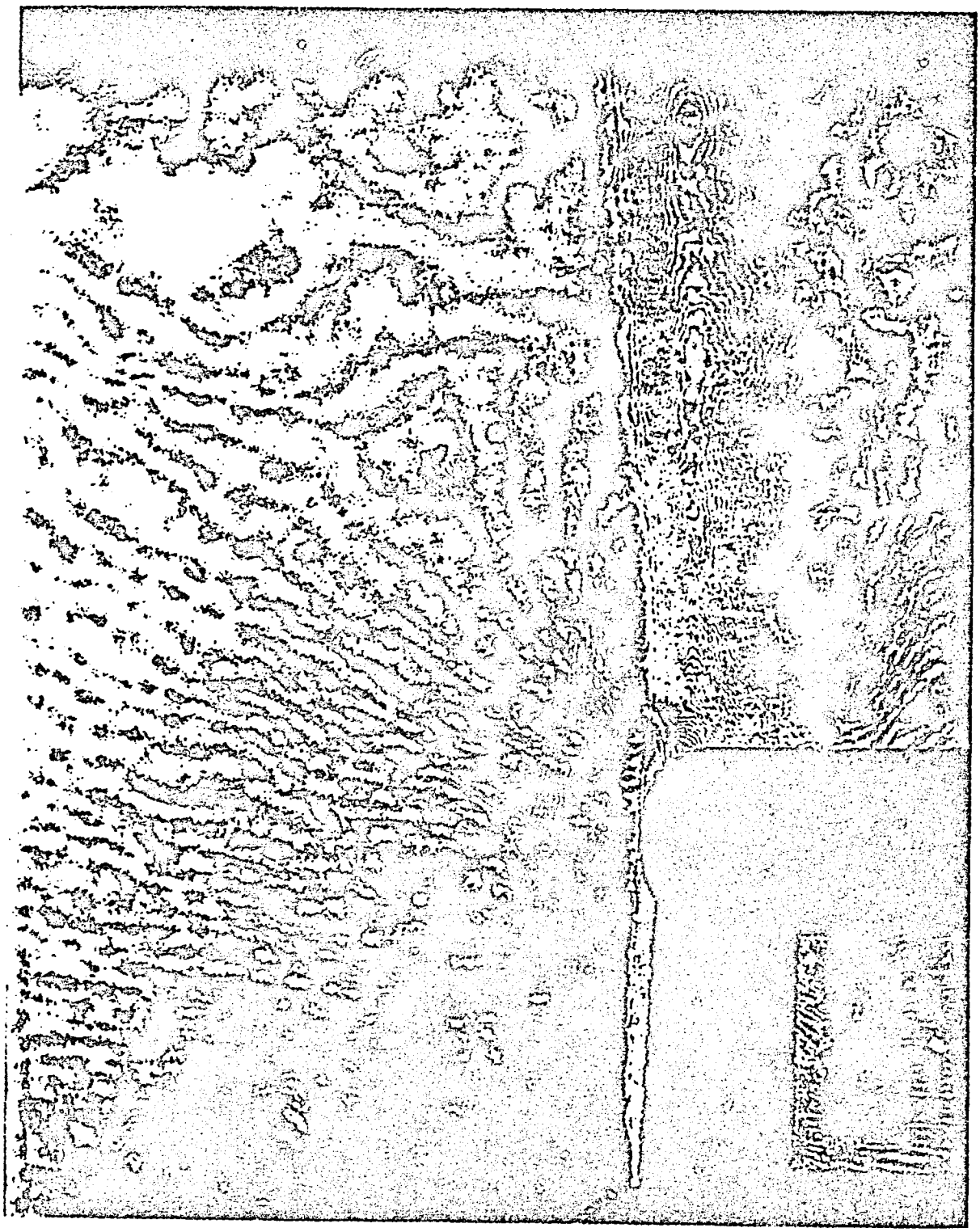

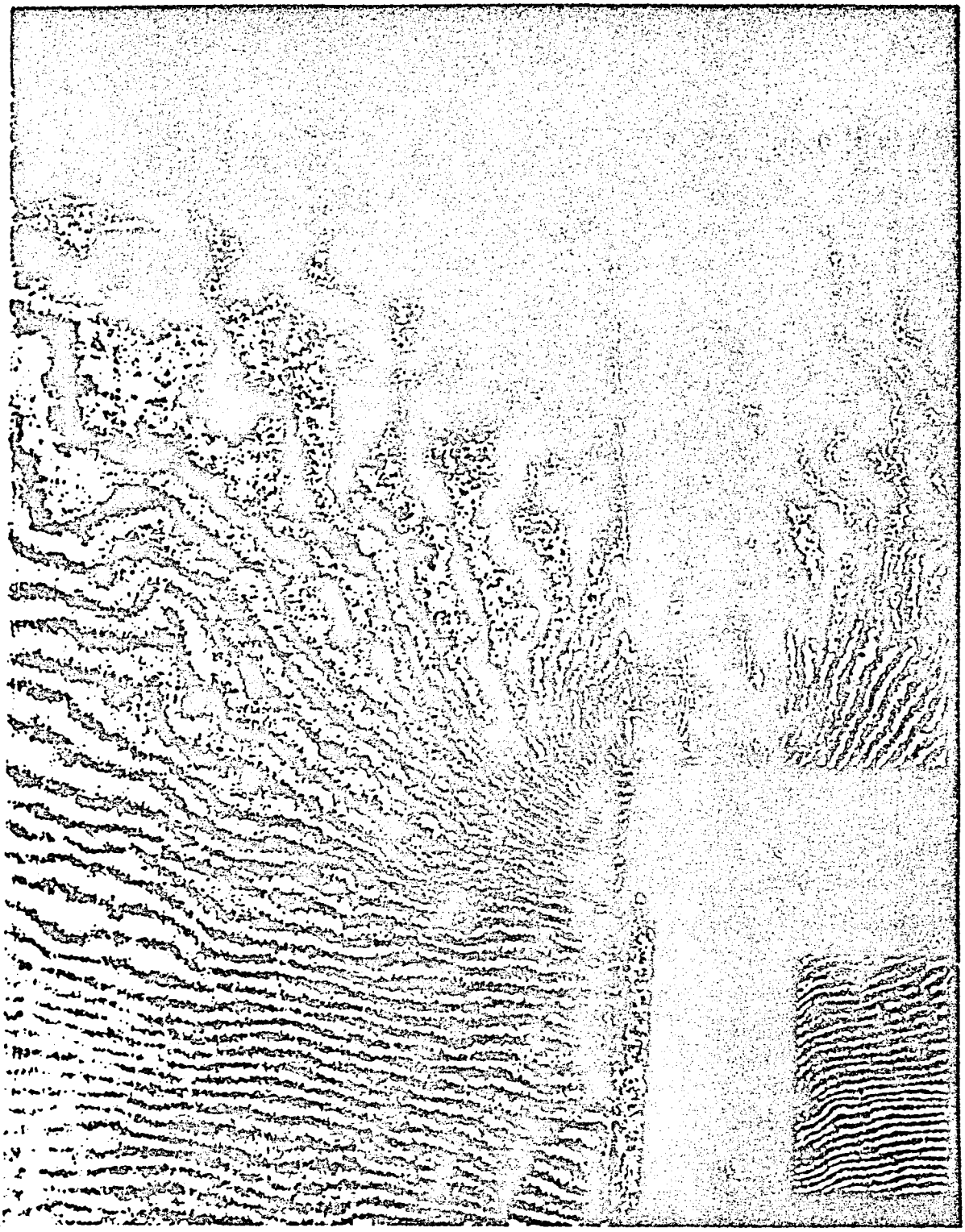

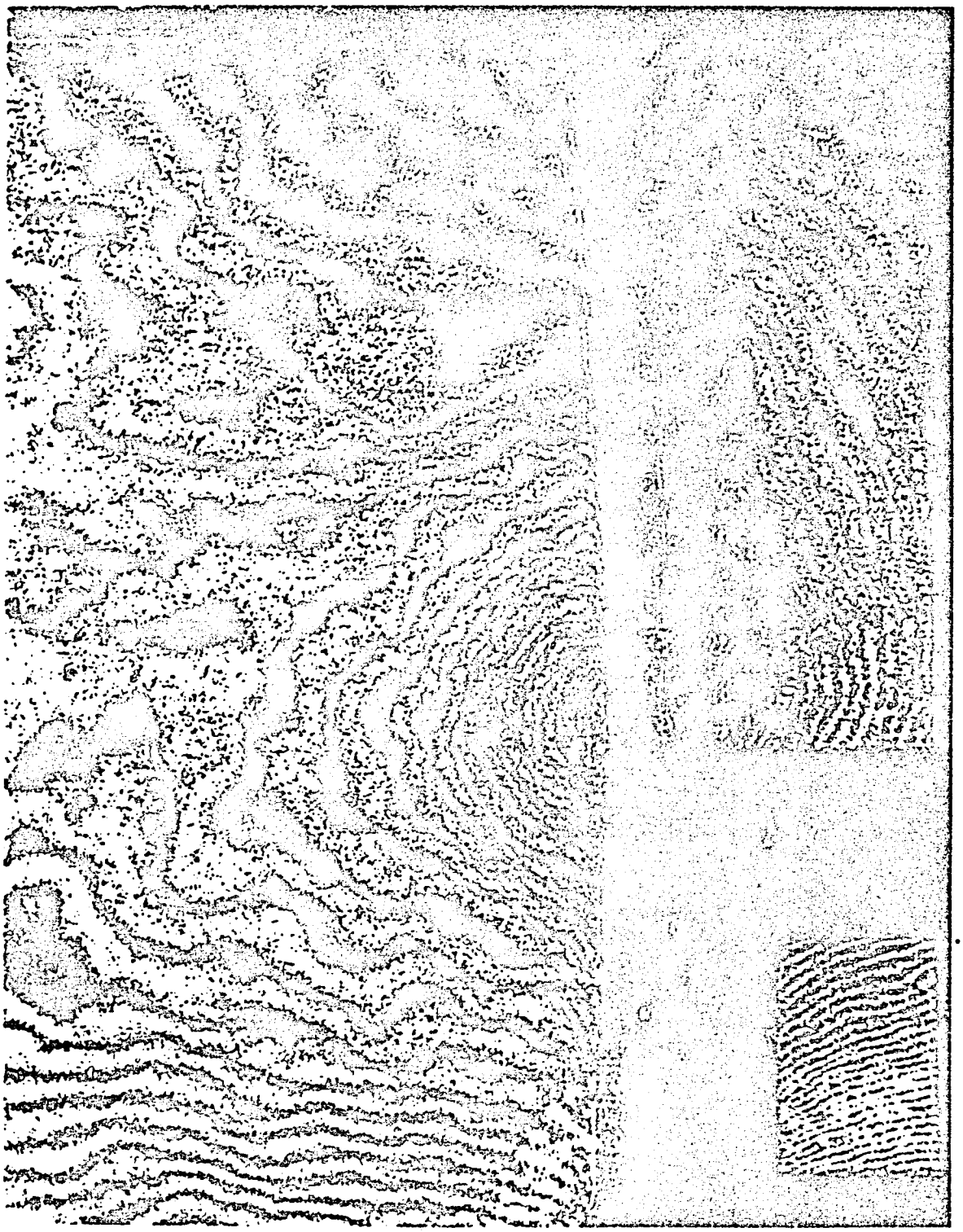

I-(F) Phase Angle = 30.6°

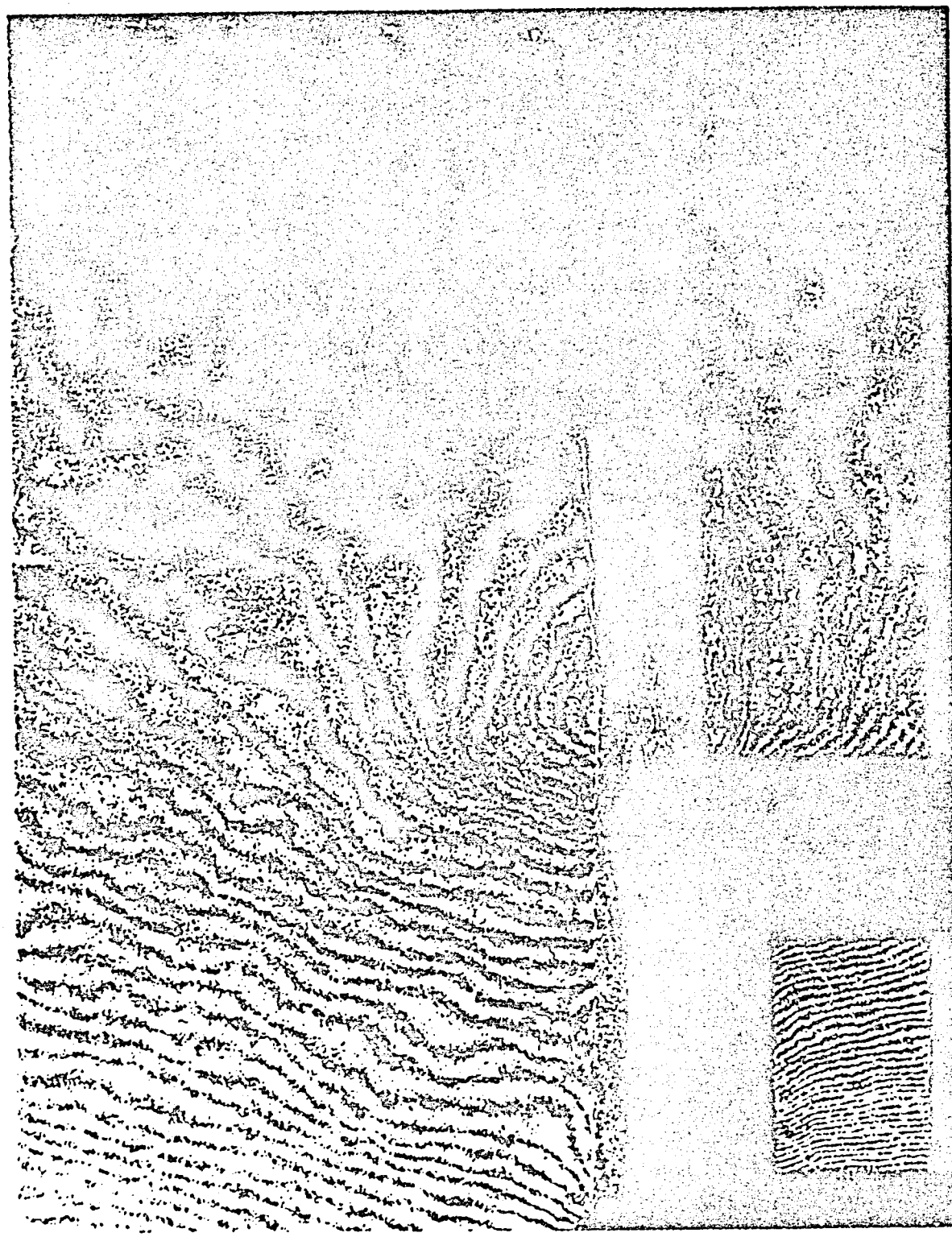

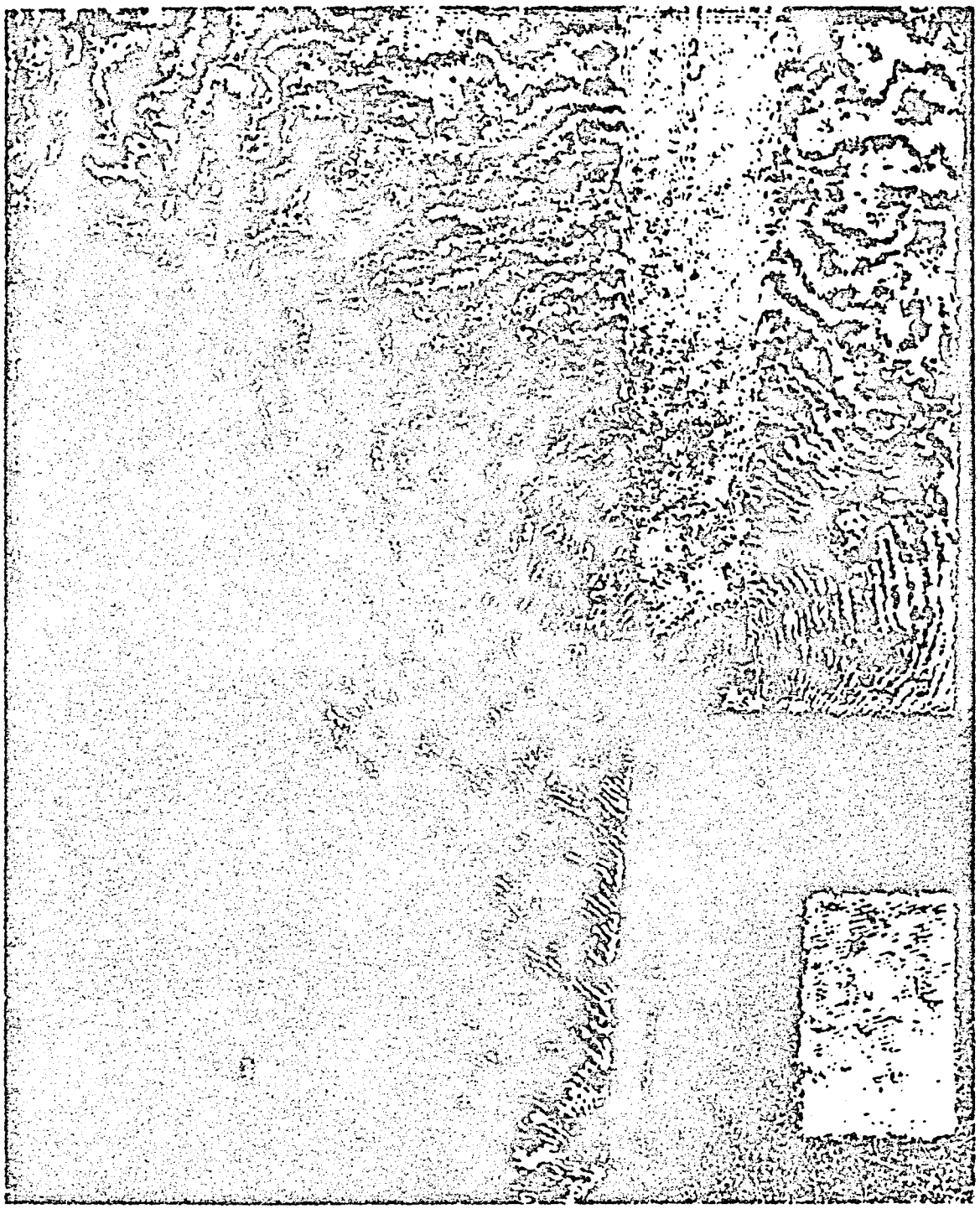

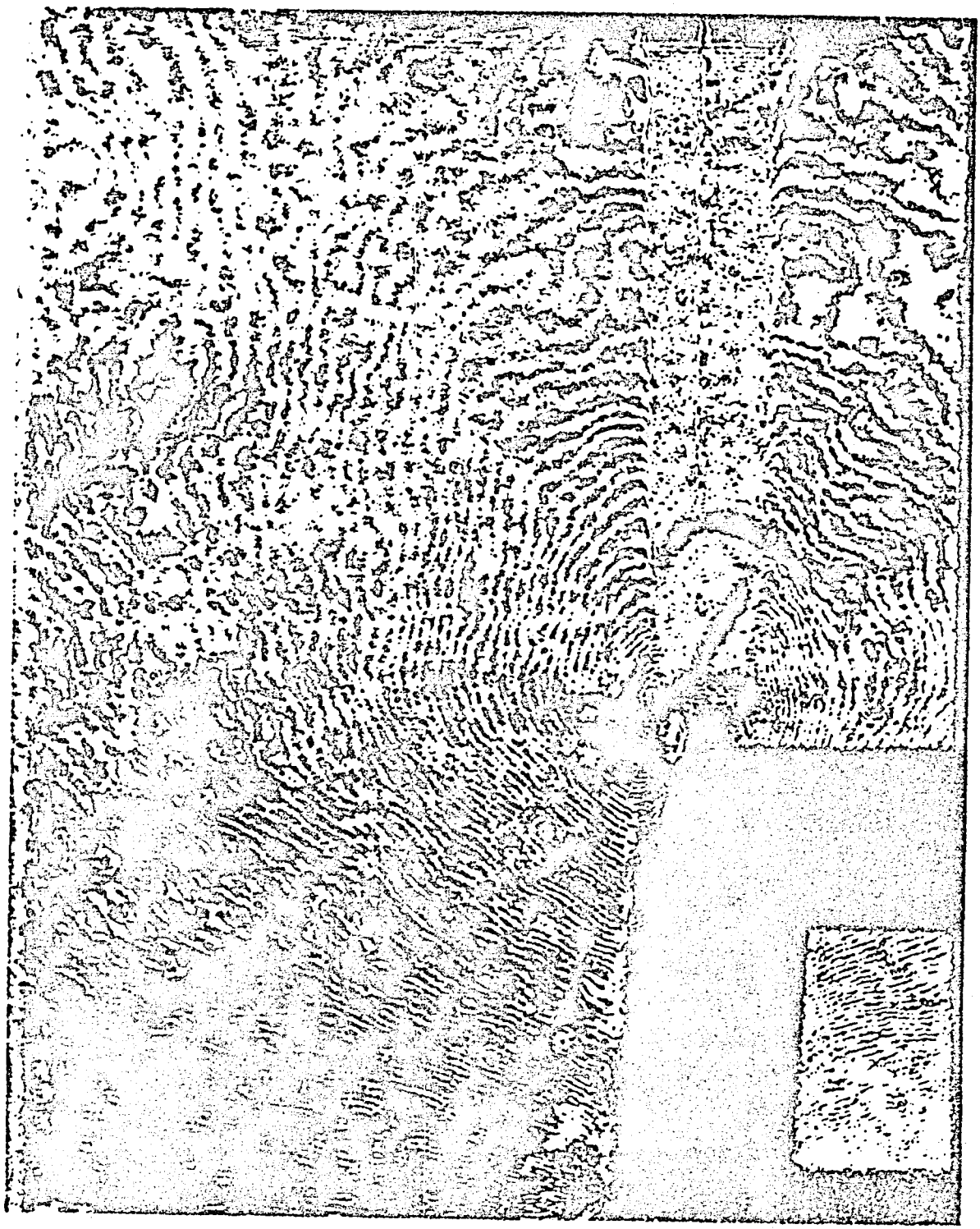

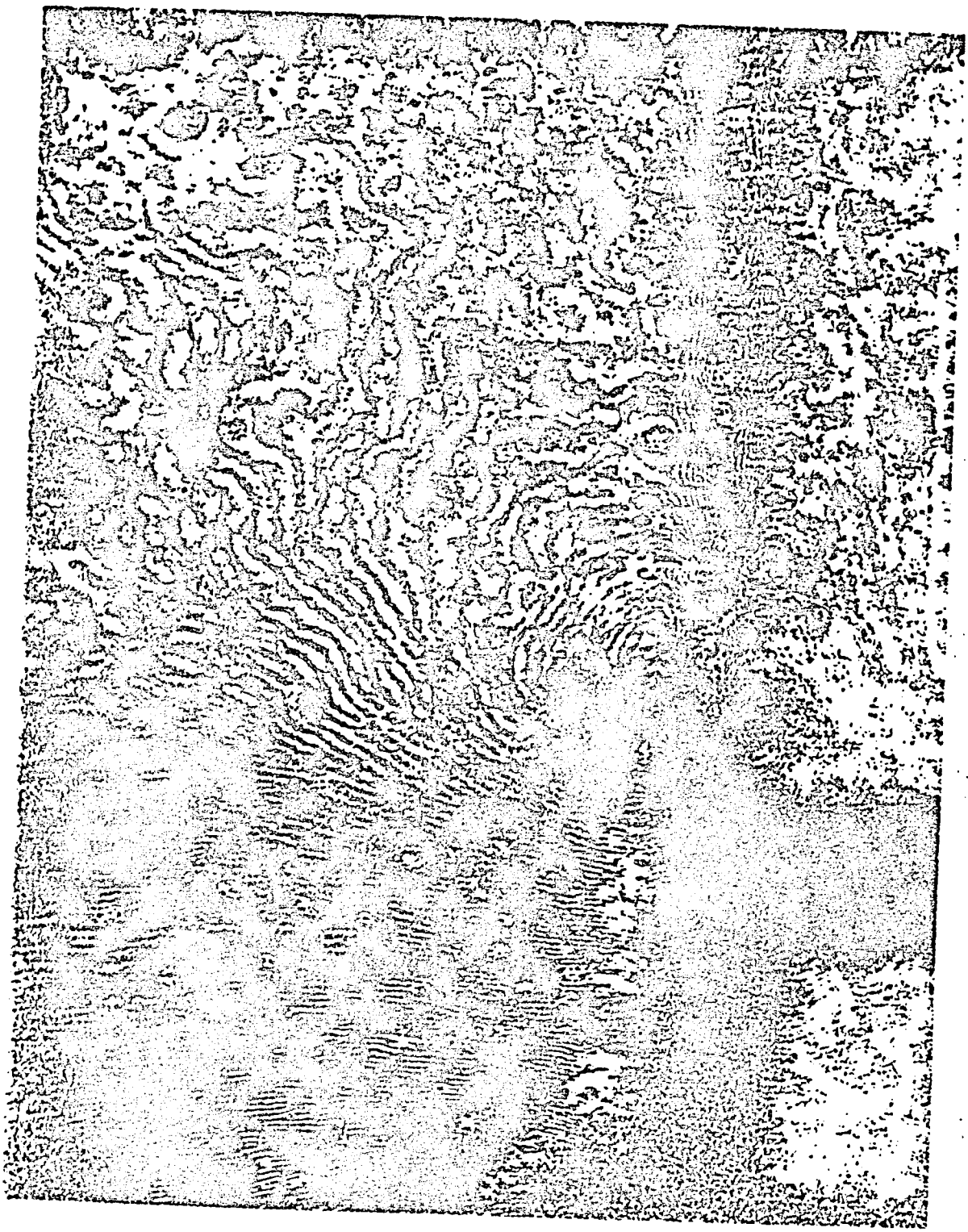

20(c) Phase Angle = 100

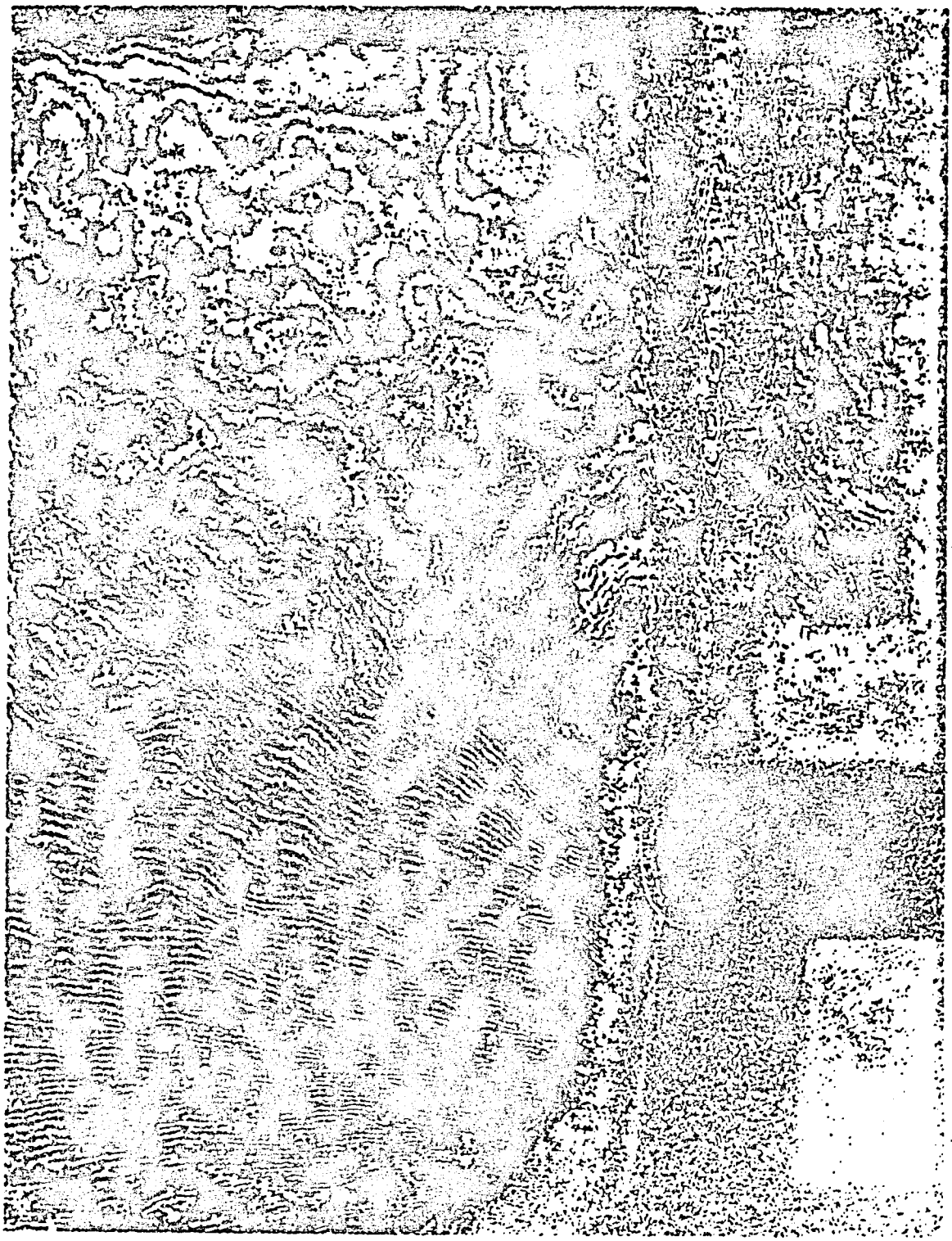

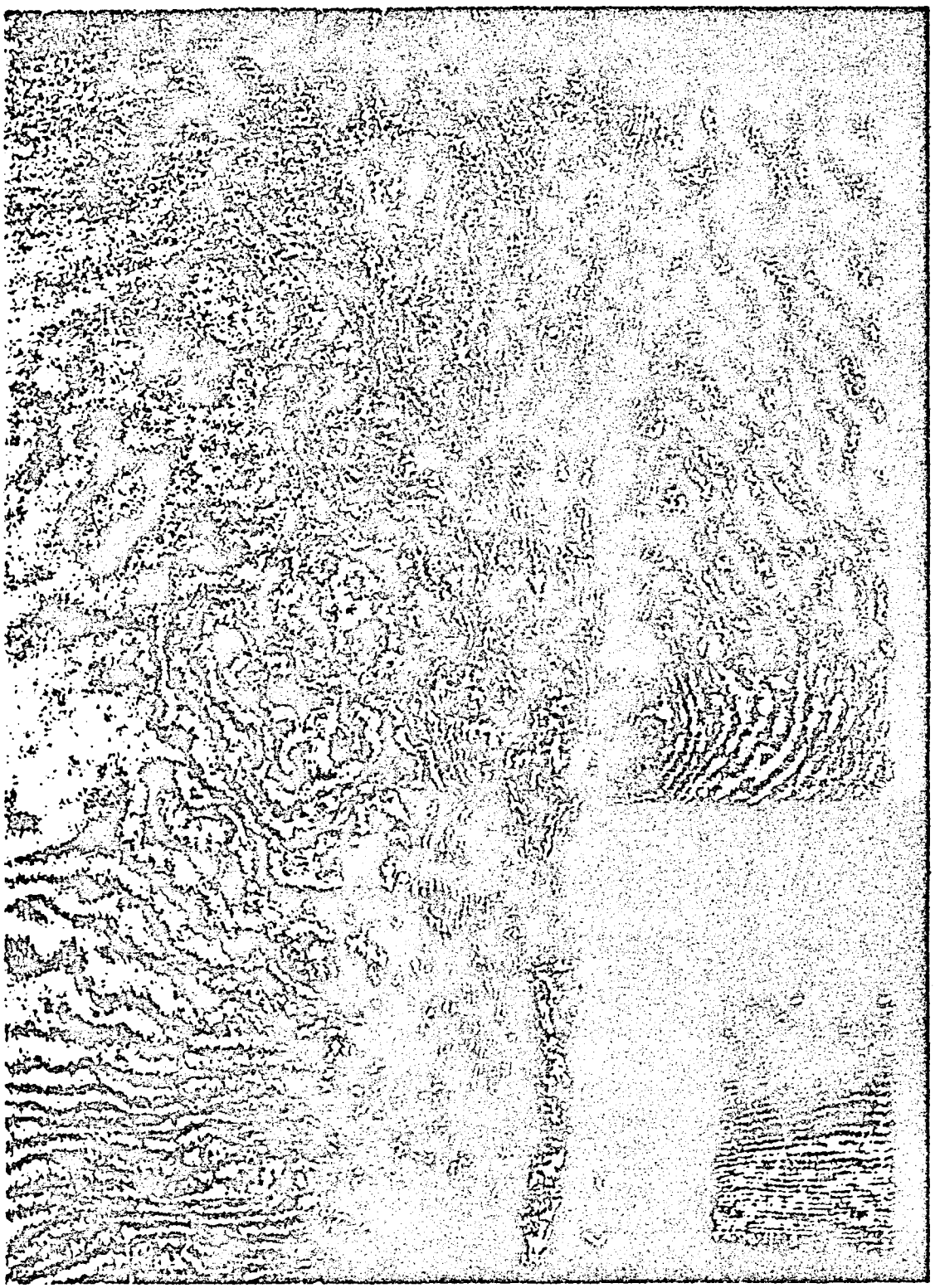

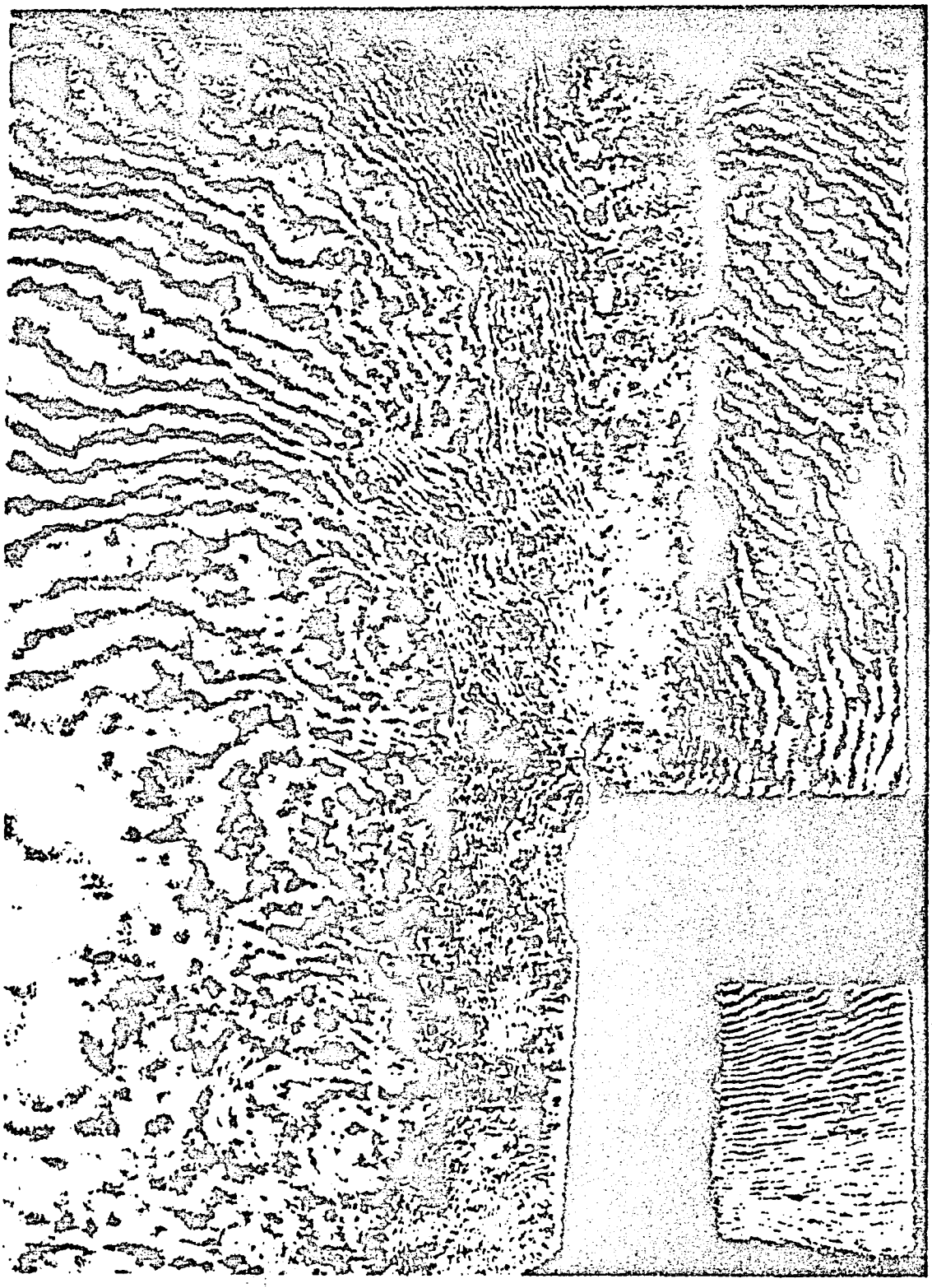

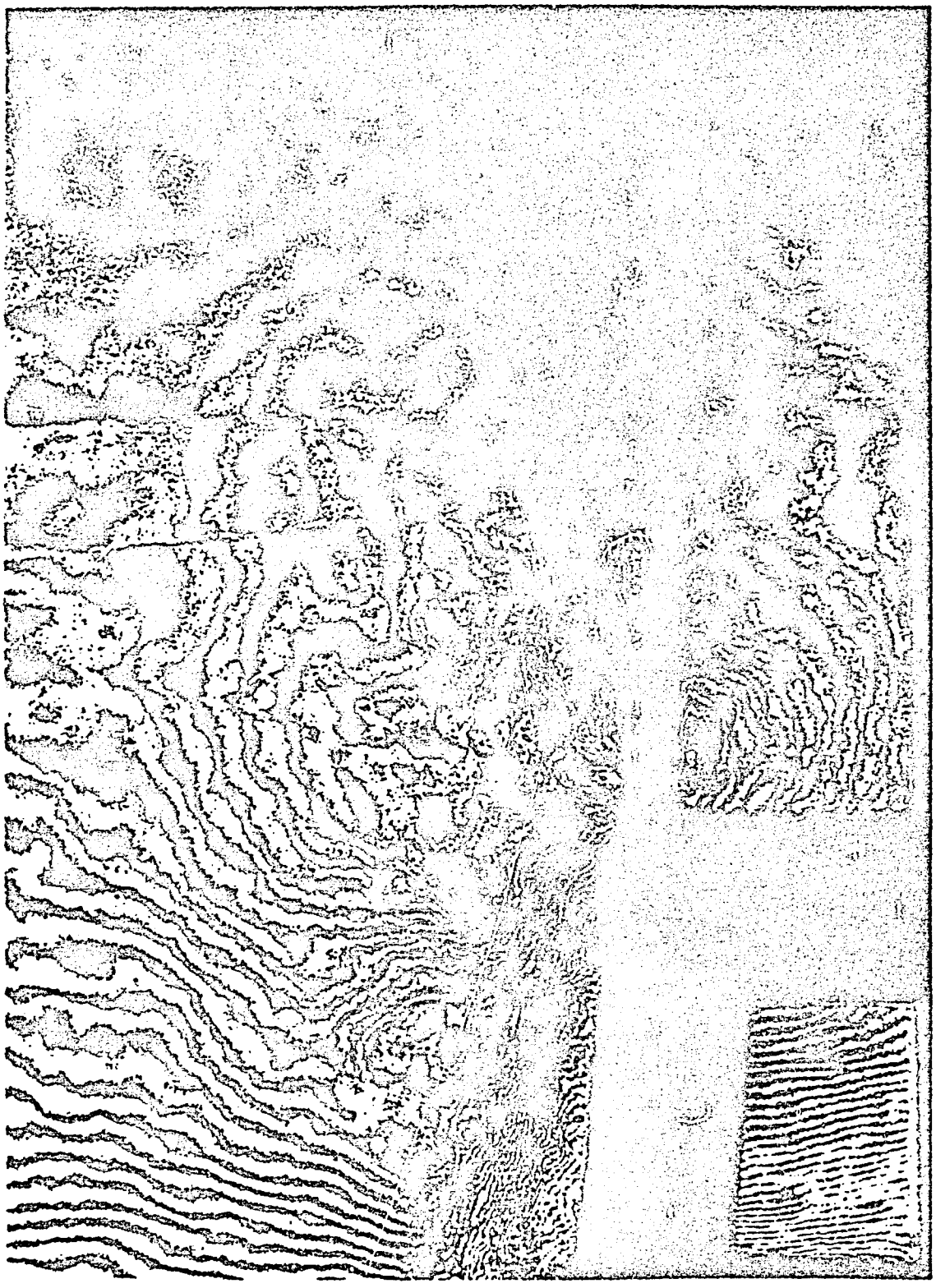

21(a) Phase Angle = 29.0

21(e) Phase Angle = 270°

WAKE PROFILES - 11 foot - Oscillating Flap

RUN: 117 SEQ: 3
FLAP MEAN: 0 AMPL.: 2 FREQ.: 30
PHASE NO.: 1 ANGLE: 0 DELTA:-.04
MACH: .8 ALPHA: 0
Ptot: 2089.3 psf Pinf: 1373 psf Ttot: 549.3 Rankine

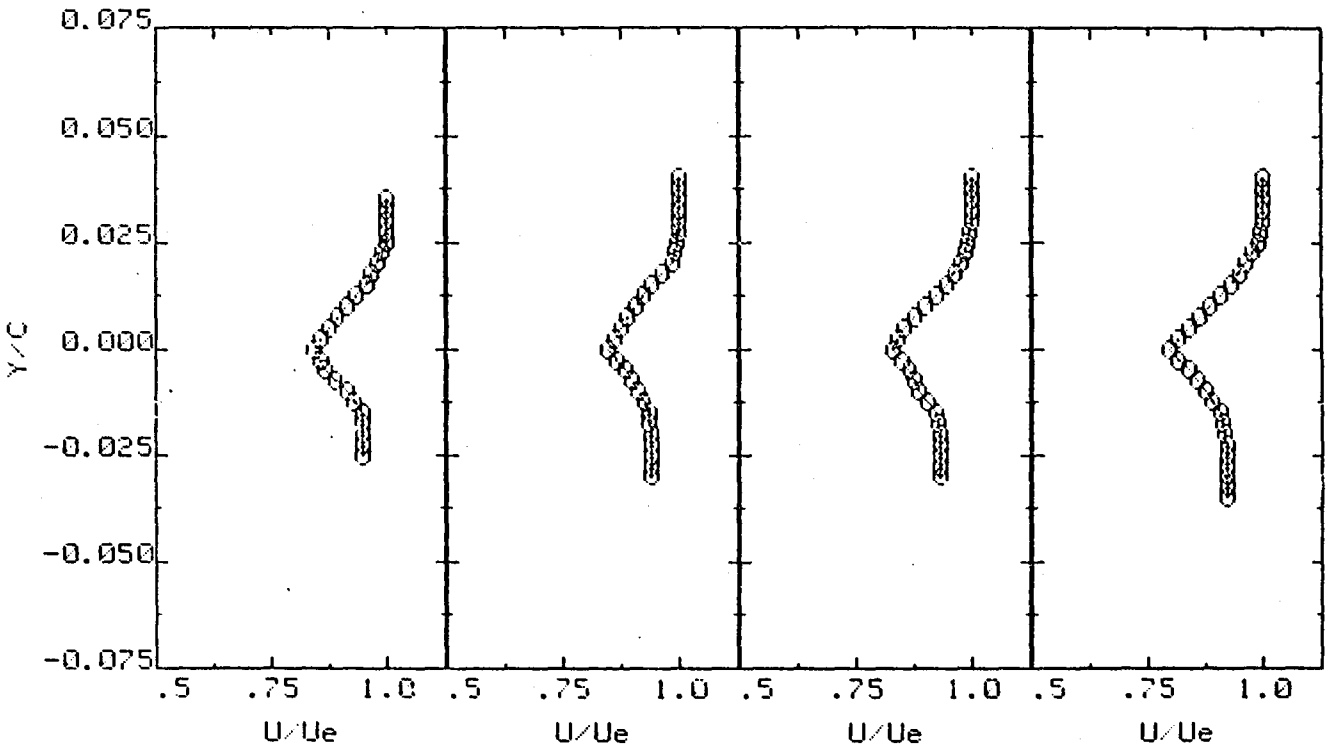

X/C= 1.05 Me = 0.748
X/C= 1.10 Me = 0.769
X/C= 1.15 Me = 0.777
X/C= 1.20 Me = 0.792

WAKE PROFILES - 11 foot - Oscillating Flap

RUN: 128 SEQ: 11
FLAP MEAN: 0 AMPL.: 2 FREQ.: 30
PHASE NO.: 7 ANGLE: 54 DELTA:-1.54
MACH: .8 ALPHA: 0
Ptot: 2087.9 psf Pinf: 1370 psf Ttot: 550.15 Rankine

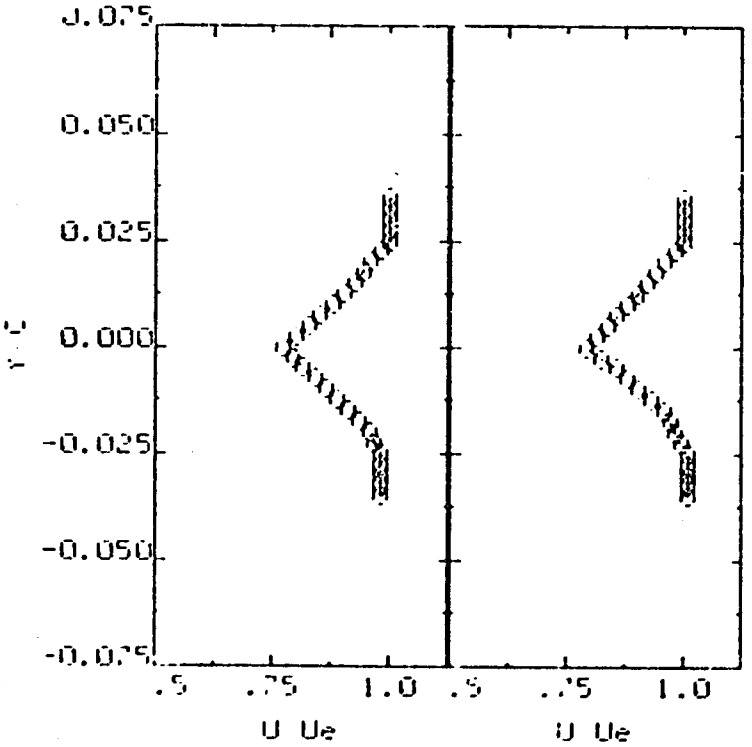

X C= 1.15 X C= 1.20
Me = 0.746 Me = 0.752

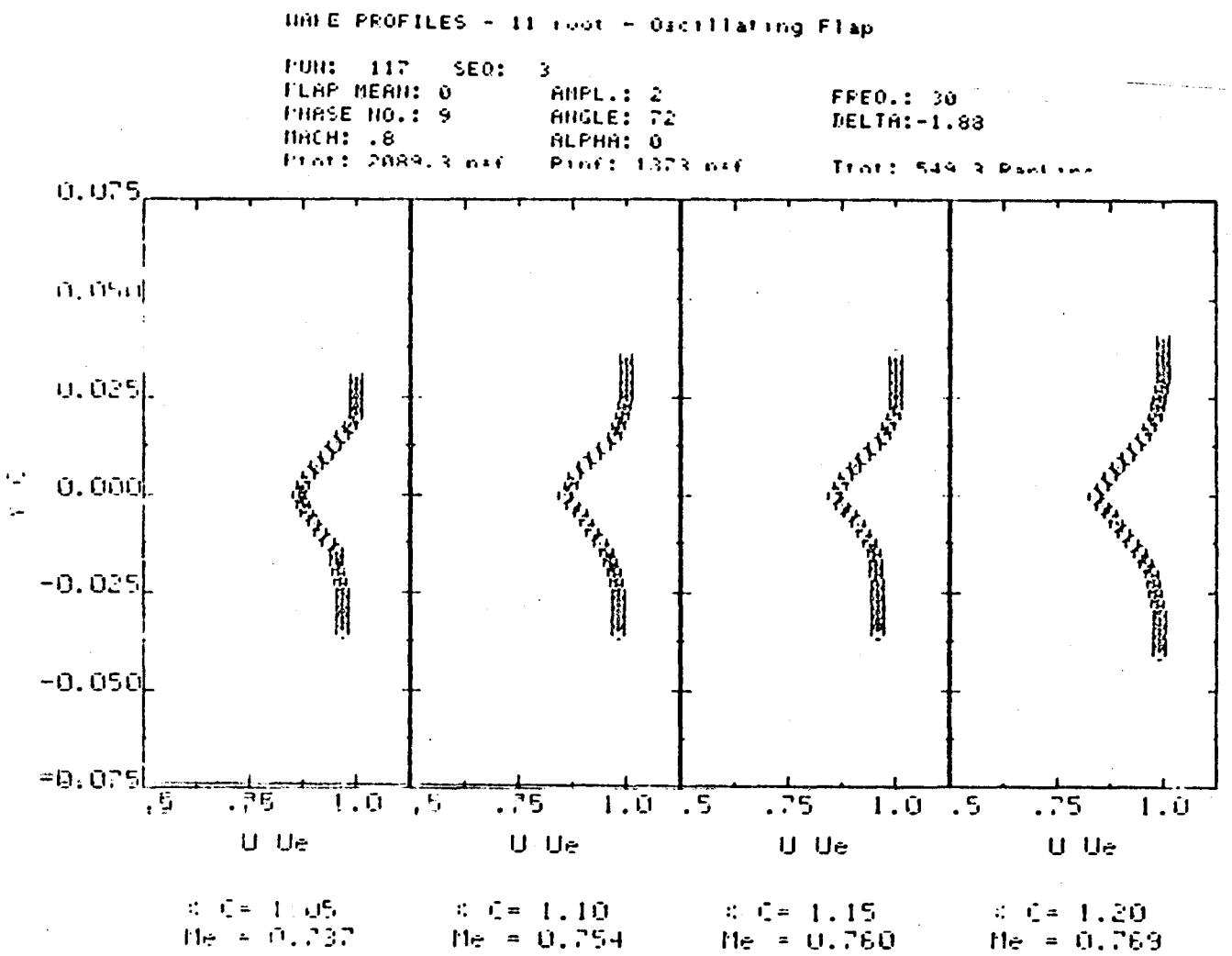

BOUNDARY LAYER PROFILES - 11 foot - Oscillating Flap

RUN: 117 SEQ: 3
FLAP MEAN: 0 AMPL.: 2 FREQ.: 30
PHASE NO.: 13 ANGLE: 108 DELTA: -1.9
MACH: .8 ALPHA: 0
Ptot: 2089.3 psf Pinf: 1373 psf Ttot: 549.3 Rankine

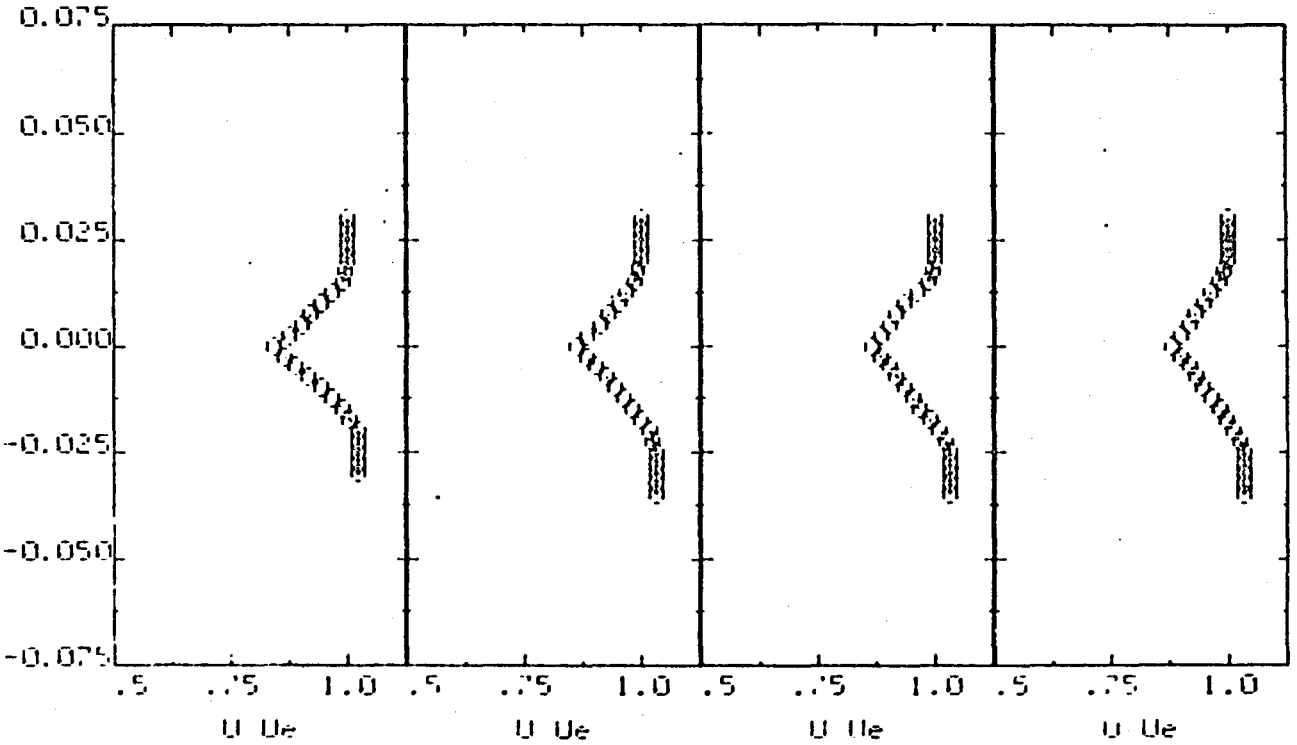

X C= 1.05	X C= 1.10	X C= 1.15	X C= 1.20
Me = 0.716	Me = 0.728	Me = 0.740	Me = 0.748

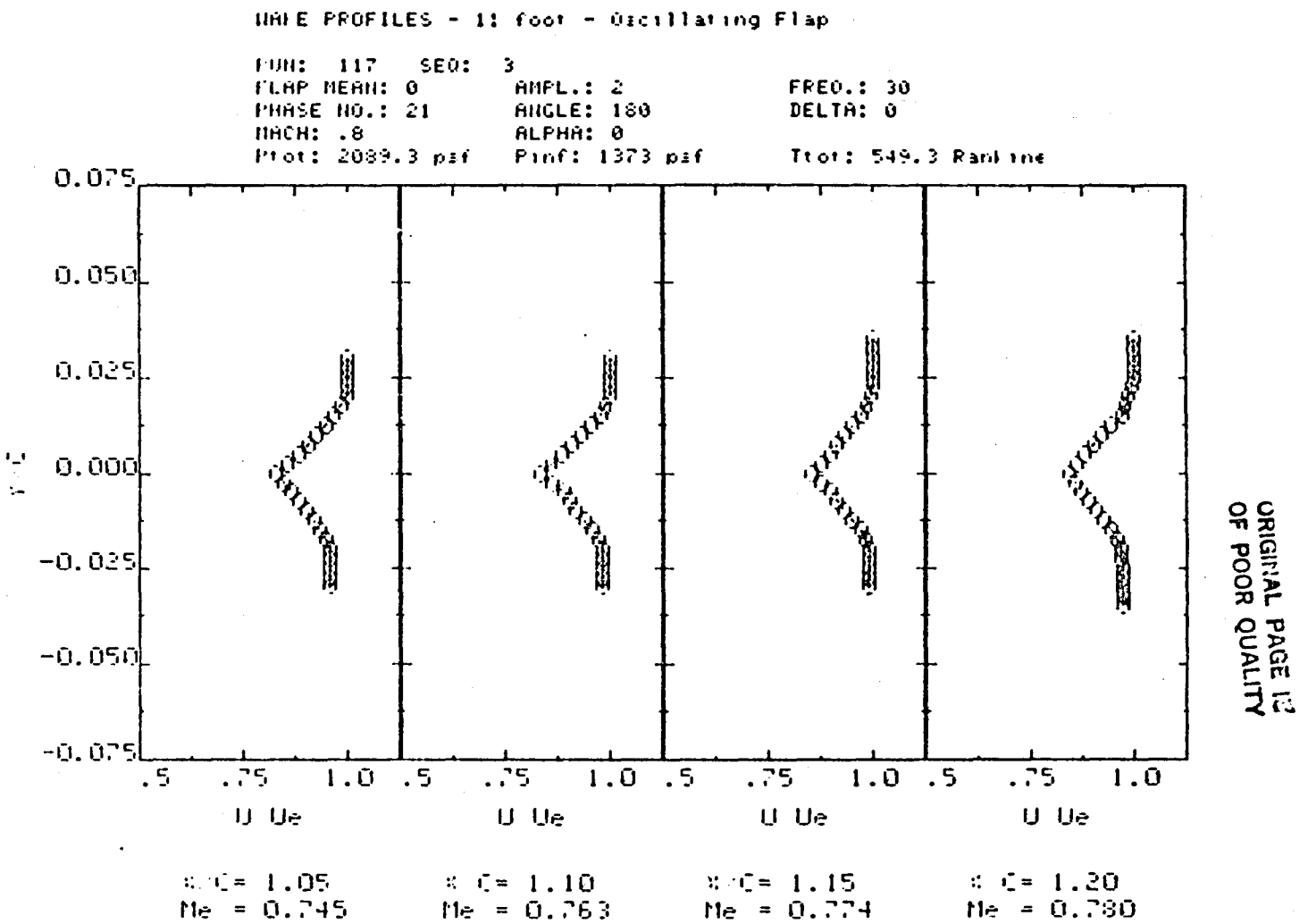

WAKE PROFILES - 11 foot - Oscillating Flap

RUN: 117 SEQ: 3
FLAP MEAN: 0 AMPL.: 2 FREQ.: 30
PHASE NO.: 25 ANGLE: 216 DELTA: 1.15
MACH: .8 ALPHA: 0
Ptot: 2089.3 psf Pinf: 1373 psf Ttot: 549.3 Pantine

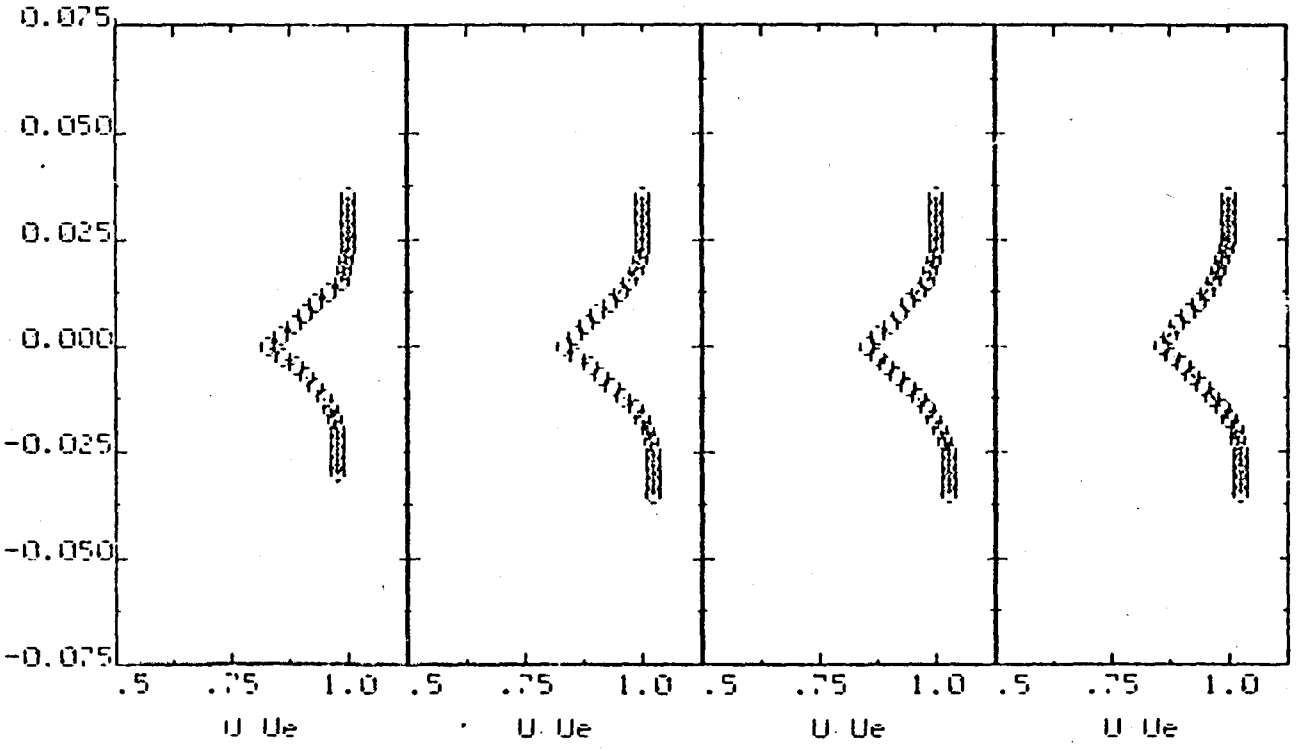

X/C= 1.05	X/C= 1.10	X/C= 1.15	X/C= 1.20
Me = 0.714	Me = 0.719	Me = 0.738	Me = 0.747

WAKE PROFILES - 11 foot - Oscillating Flap

RUN: 128 SEQ: 11
FLAP MEAN: 0 AMPL.: 2 FREQ.: 30
PHASE NO.: 31 ANGLE: 270 DELTA: 2.04
MACH: .8 ALPHA: 0
Ptot: 2087.9 psf Pinf: 1370 psf Ttot: 550.15 Rankine

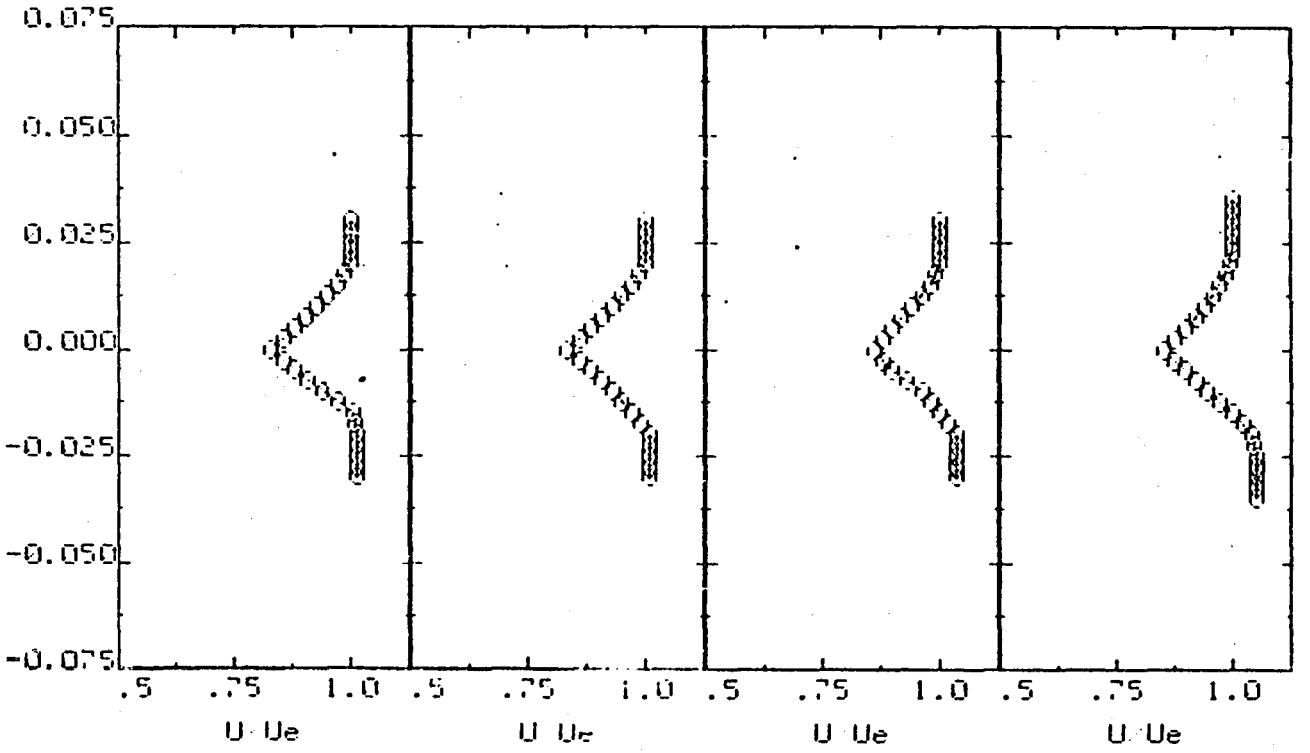

x/C= 1.05 Me = 0.751
x/C= 1.10 Me = 0.766
x/C= 1.15 Me = 0.775
x/C= 1.20 Me = 0.784

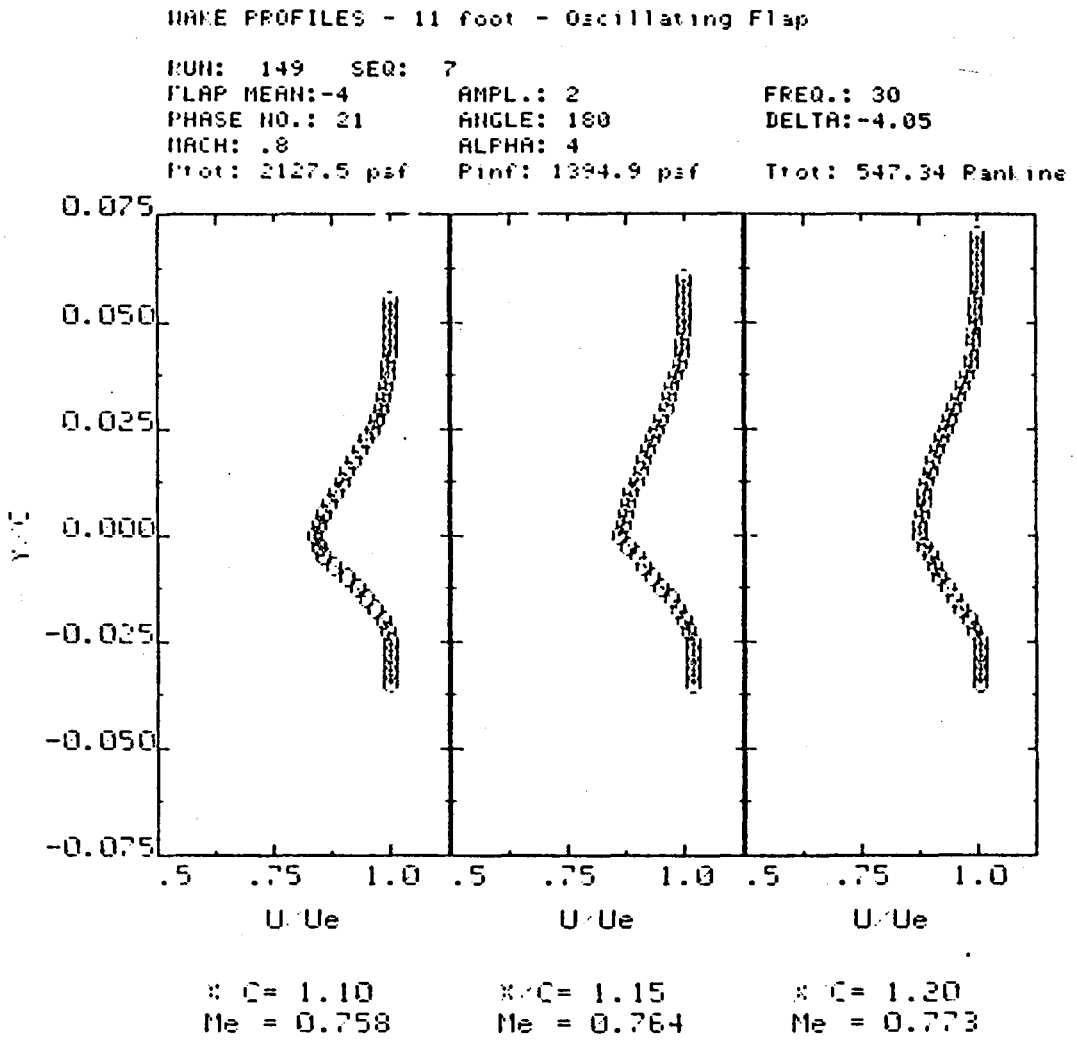

Figure 23.- Wake profiles; $\alpha = 4^{\circ}$, $\delta = -4^{\circ}$

WAKE PROFILES - 11 foot - Oscillating Flap

RUN: 149 SEQ: 7
FLAP MEAN:-4 AMPL.: 2 FREQ.: 30
PHASE NO.: 31 ANGLE: 270 DELTA:-1.97
MACH: .8 ALPHA: 4
Ptot: 2127.5 psf Pinf: 1394.9 psf Ttot: 547.34 Rankine

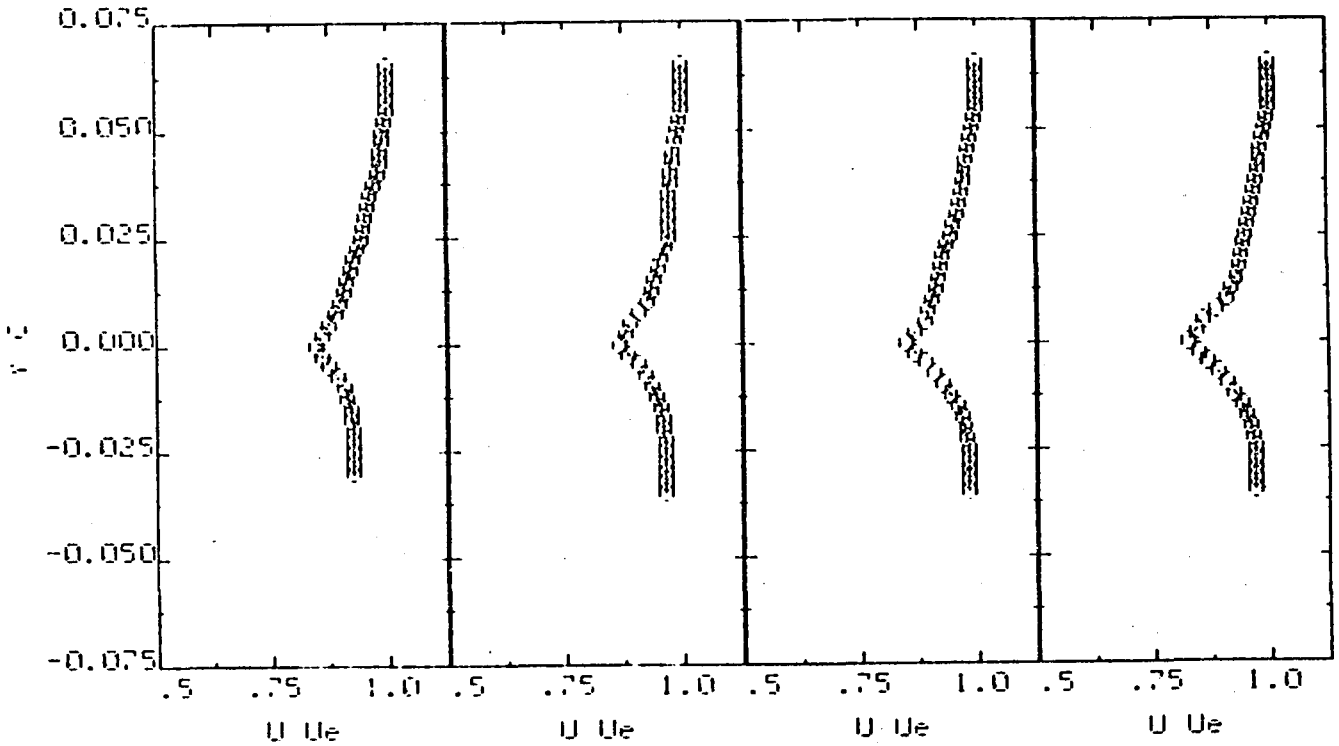

x C= 1.05 Me = 0.797

x C= 1.10 Me = 0.811

x C= 1.15 Me = 0.822

x C= 1.20 Me = 0.825

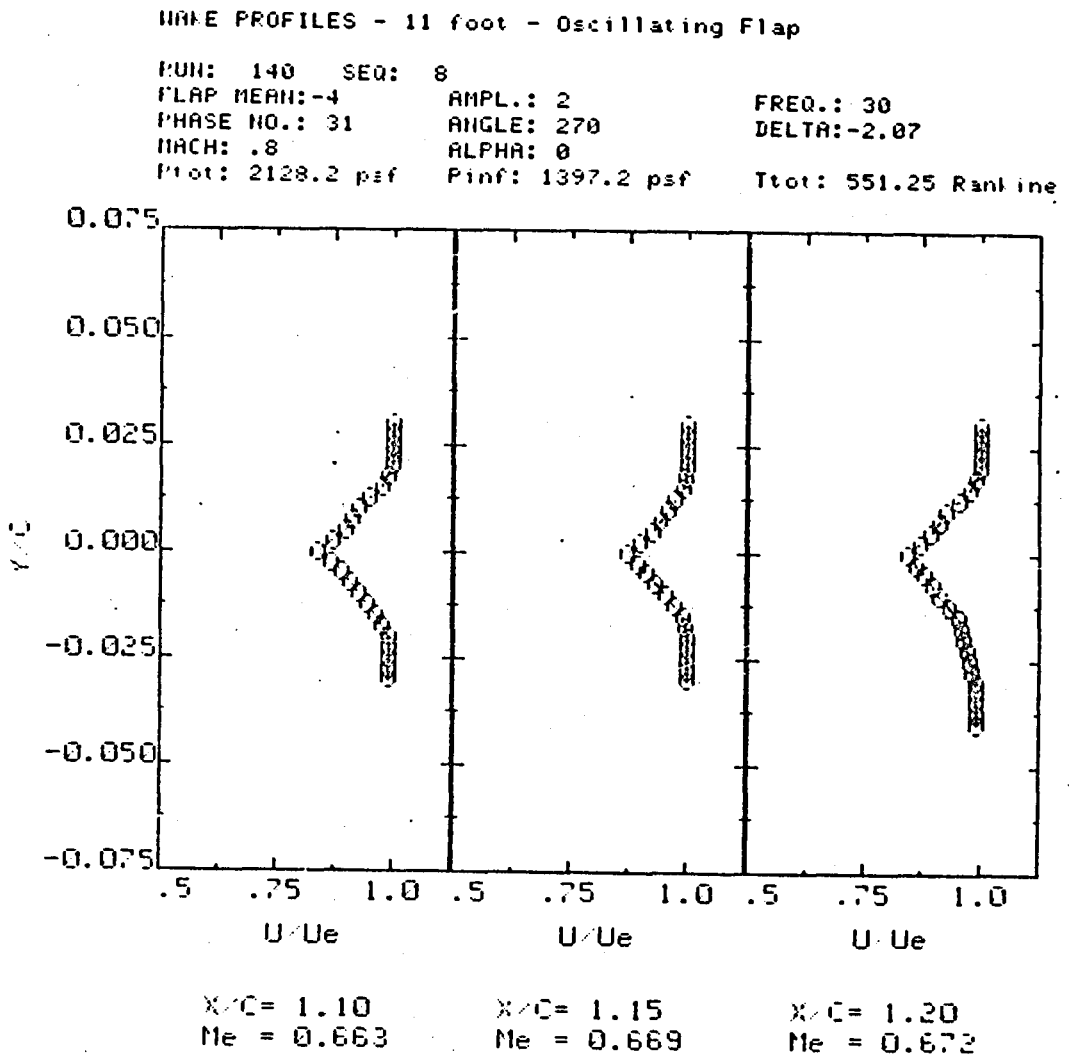

Figure 24.- Wake profiles; $\alpha = 0°$; $\delta = -4°$

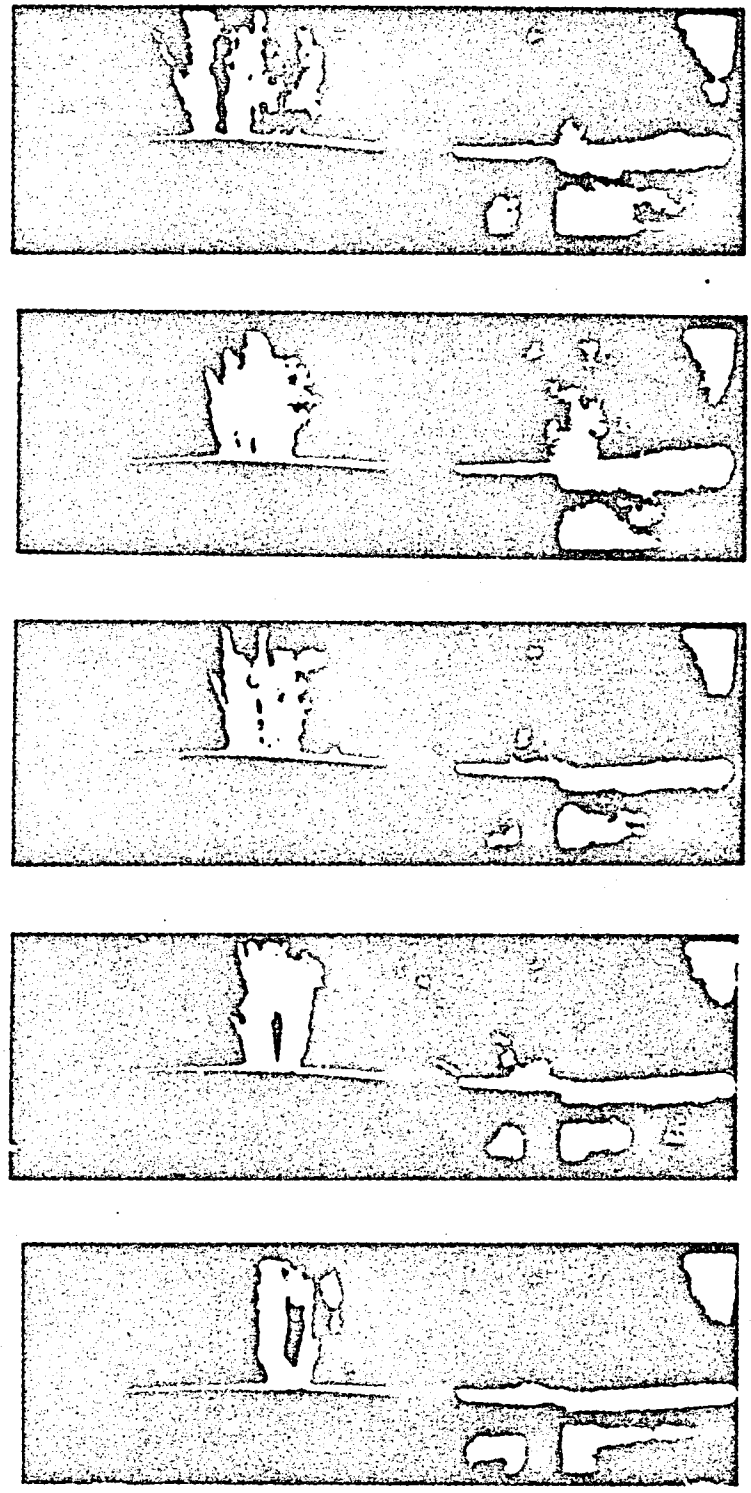

$\alpha = 0°$, $\dot{\alpha} = -4°$, $f = 30$ Hz

Figure 25.- Schlieren Flow Visualization Movie Strip.

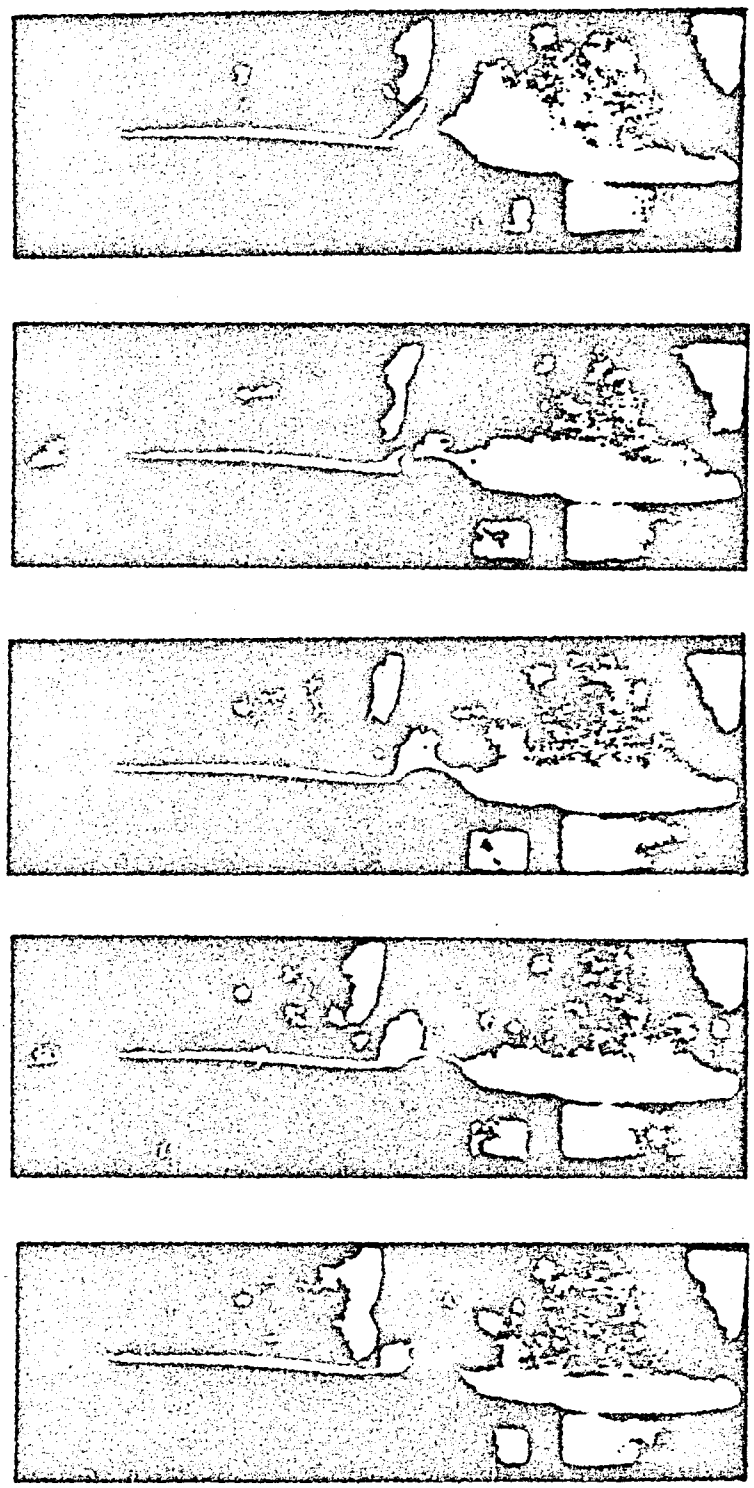

$\alpha = 2°, \quad \delta = 0°, \quad f = 30$ Hz

Figure 26.- Schlieren Flow Visualization Movie Strip

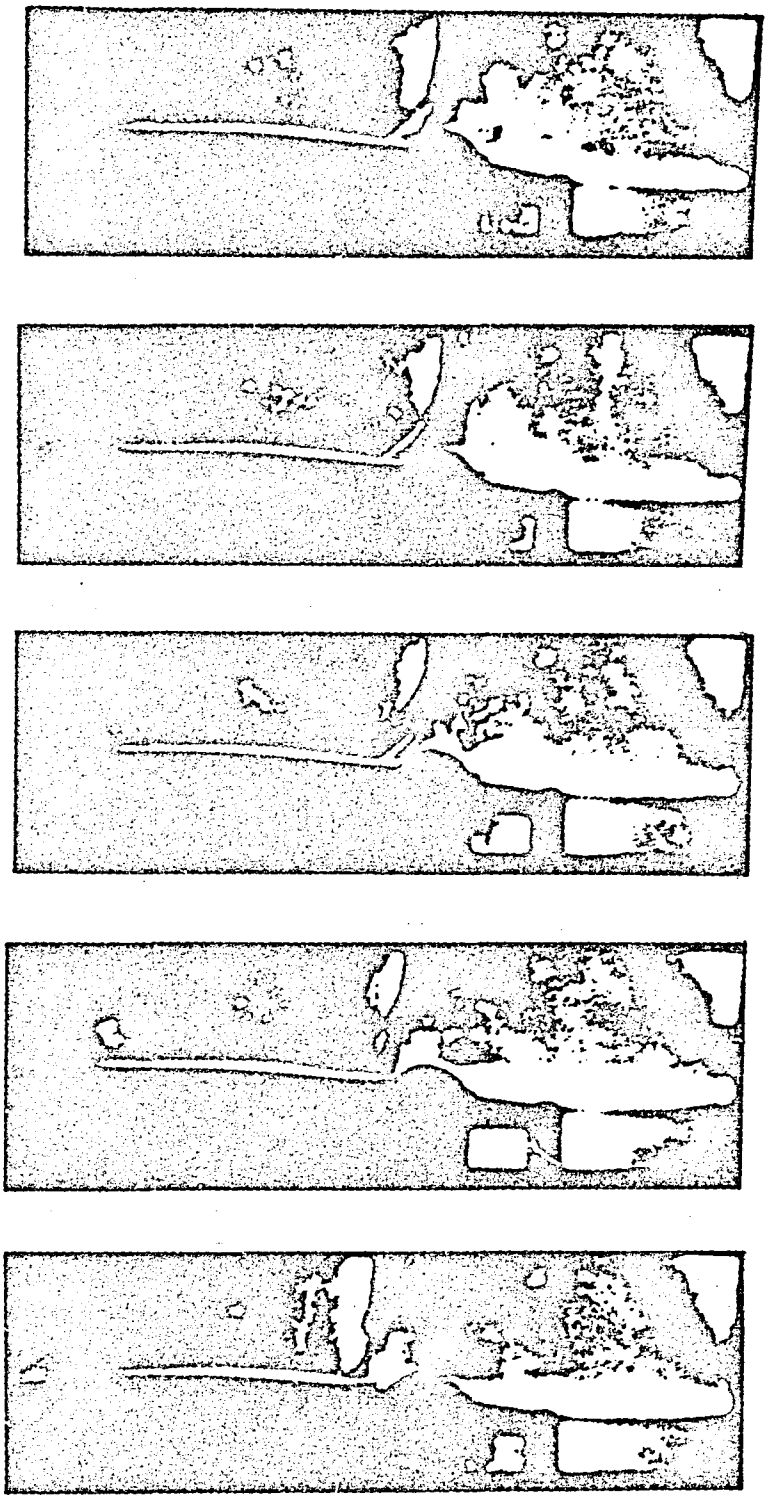

$\alpha = 2°, \quad \delta = 0°, \quad f = 30$ Hz

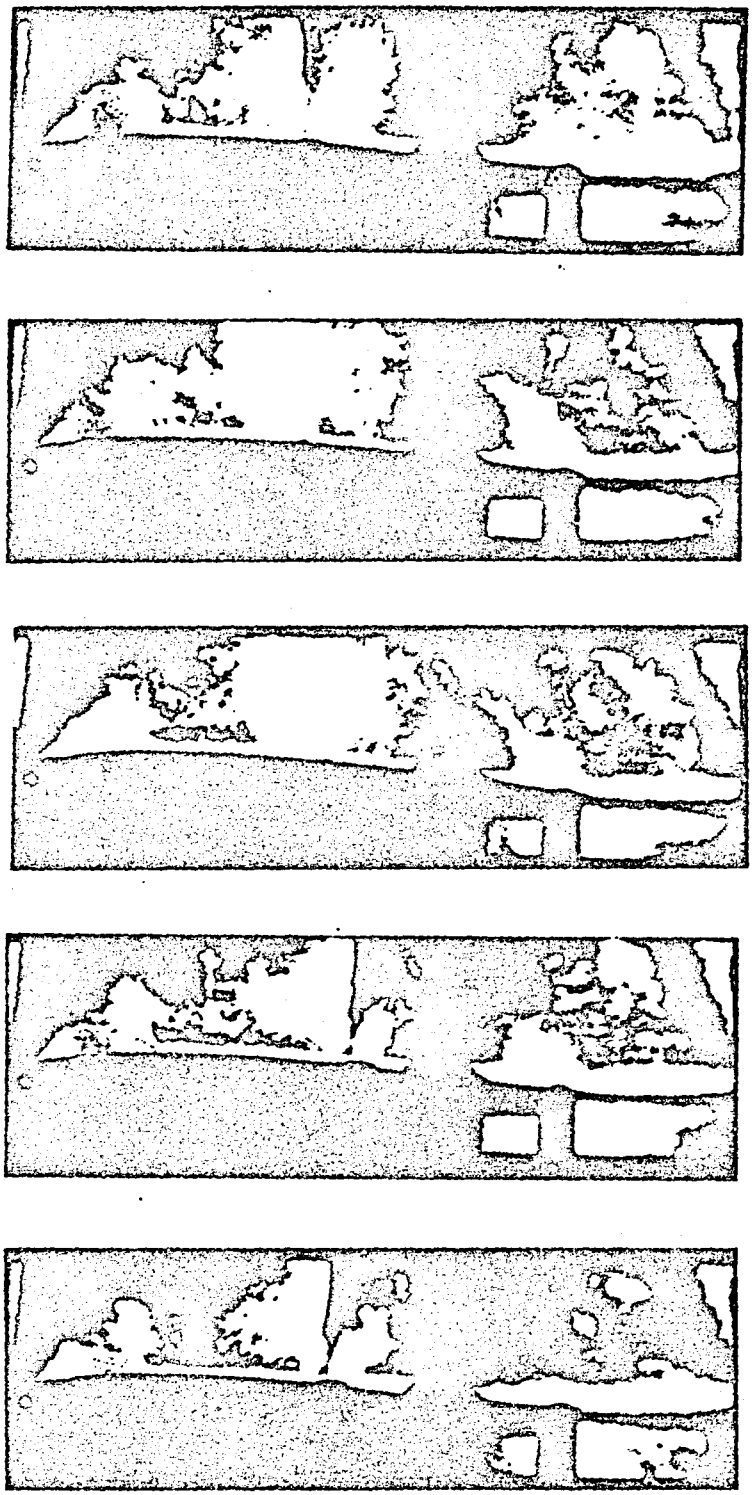

$\alpha = 2°$, $\beta = -4°$, $f = 30$ Hz

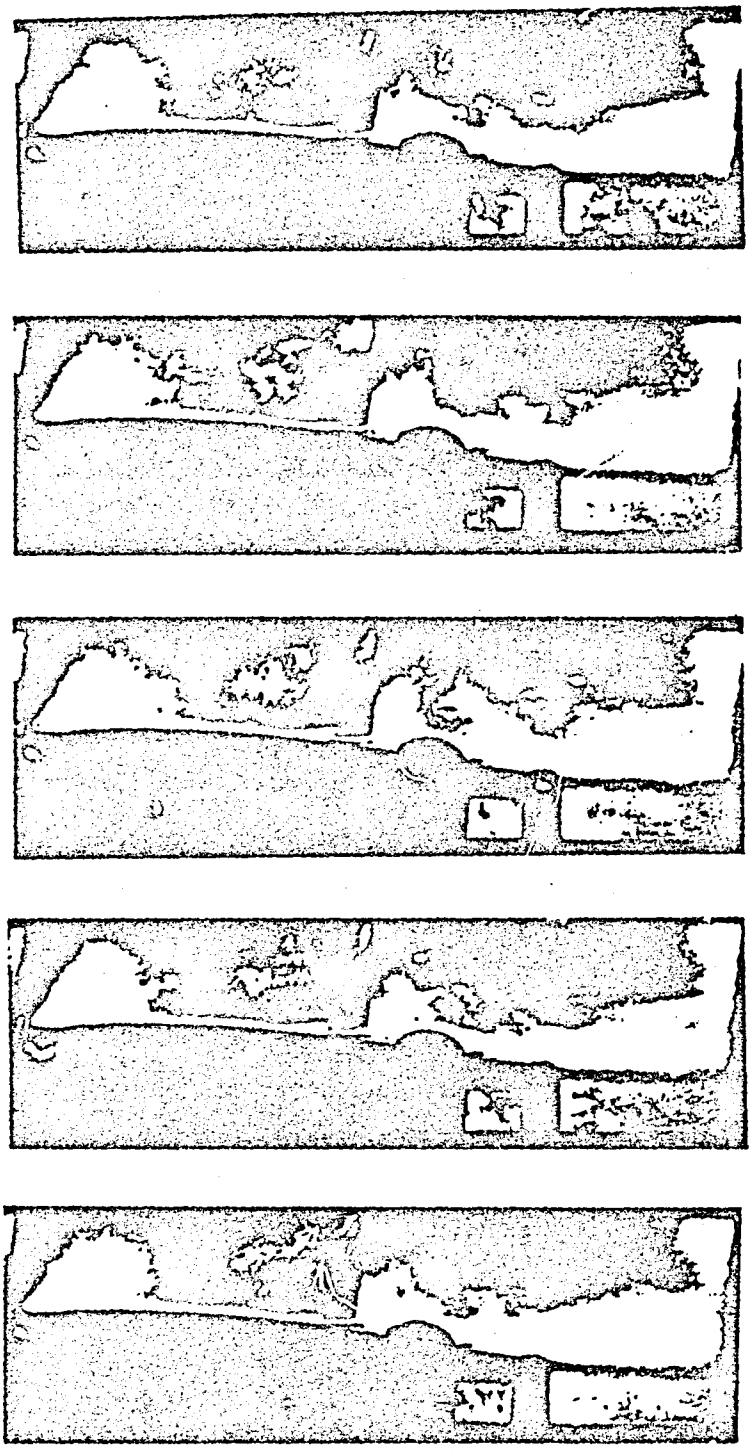

$\alpha = 4°, \quad \dot{\alpha} = -4°, \quad f = 0$ Hz

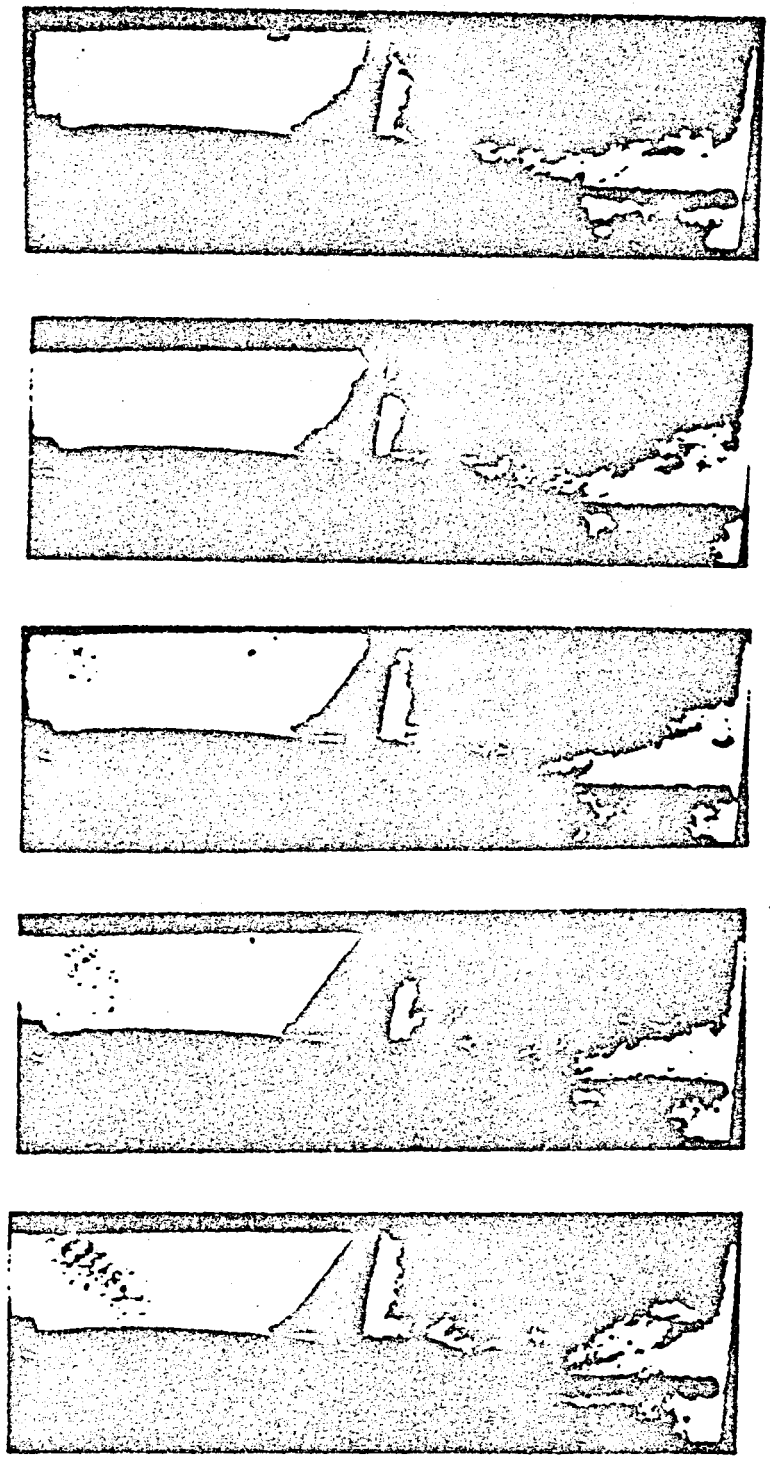

$\alpha = 4°$, $\delta = -4°$, $f = 30$ Hz

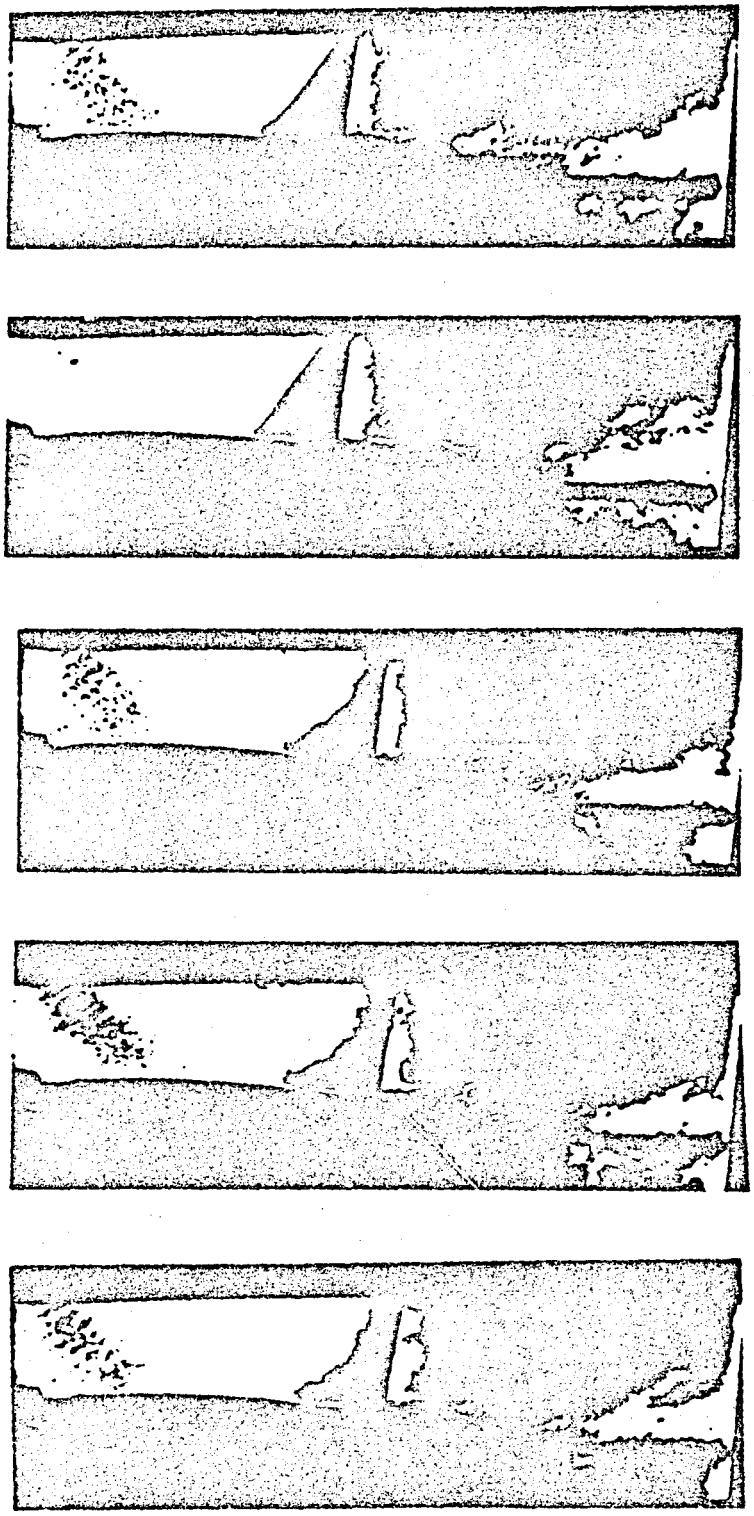

$\alpha = 4°$, $\beta = -4°$, $f = 30$ Hz

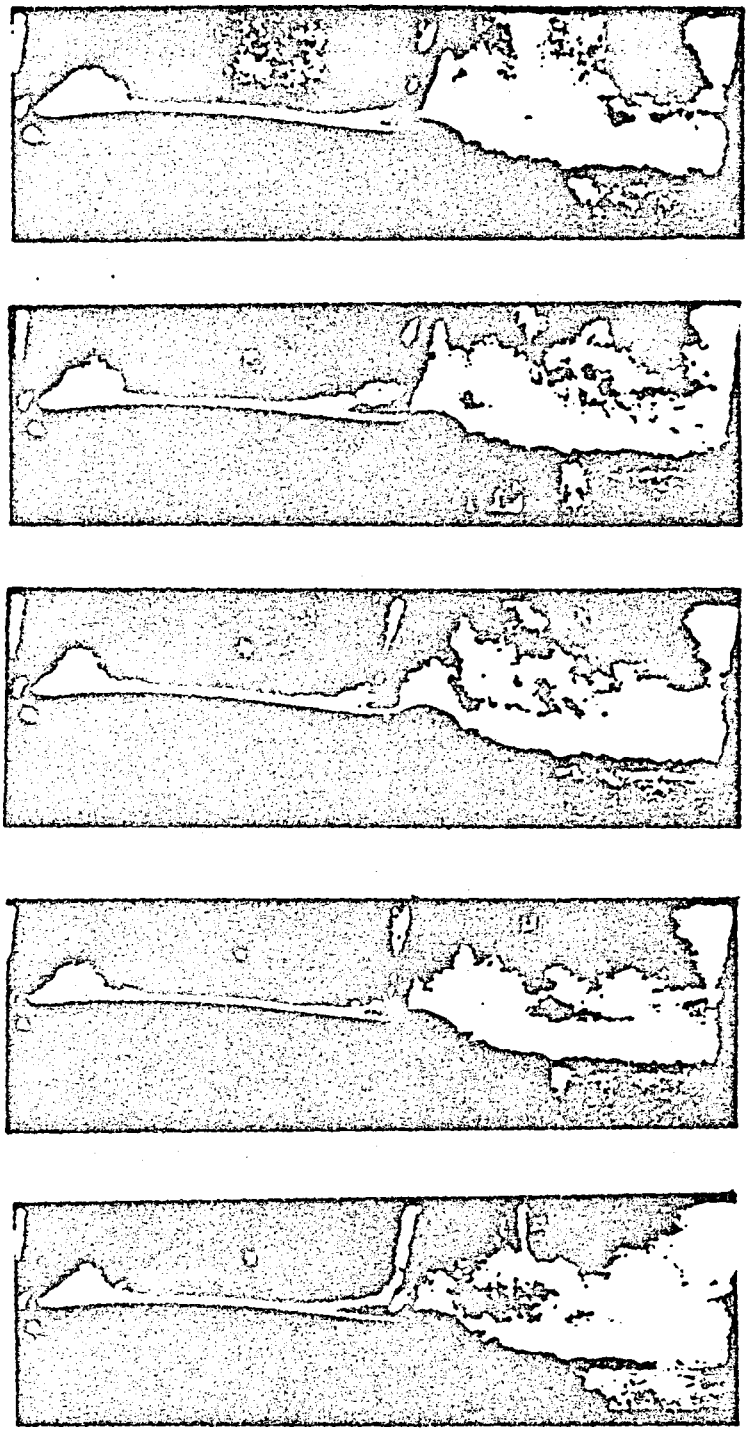

$\alpha = 4°$, $\delta = 0°$, $f = 30$ Hz

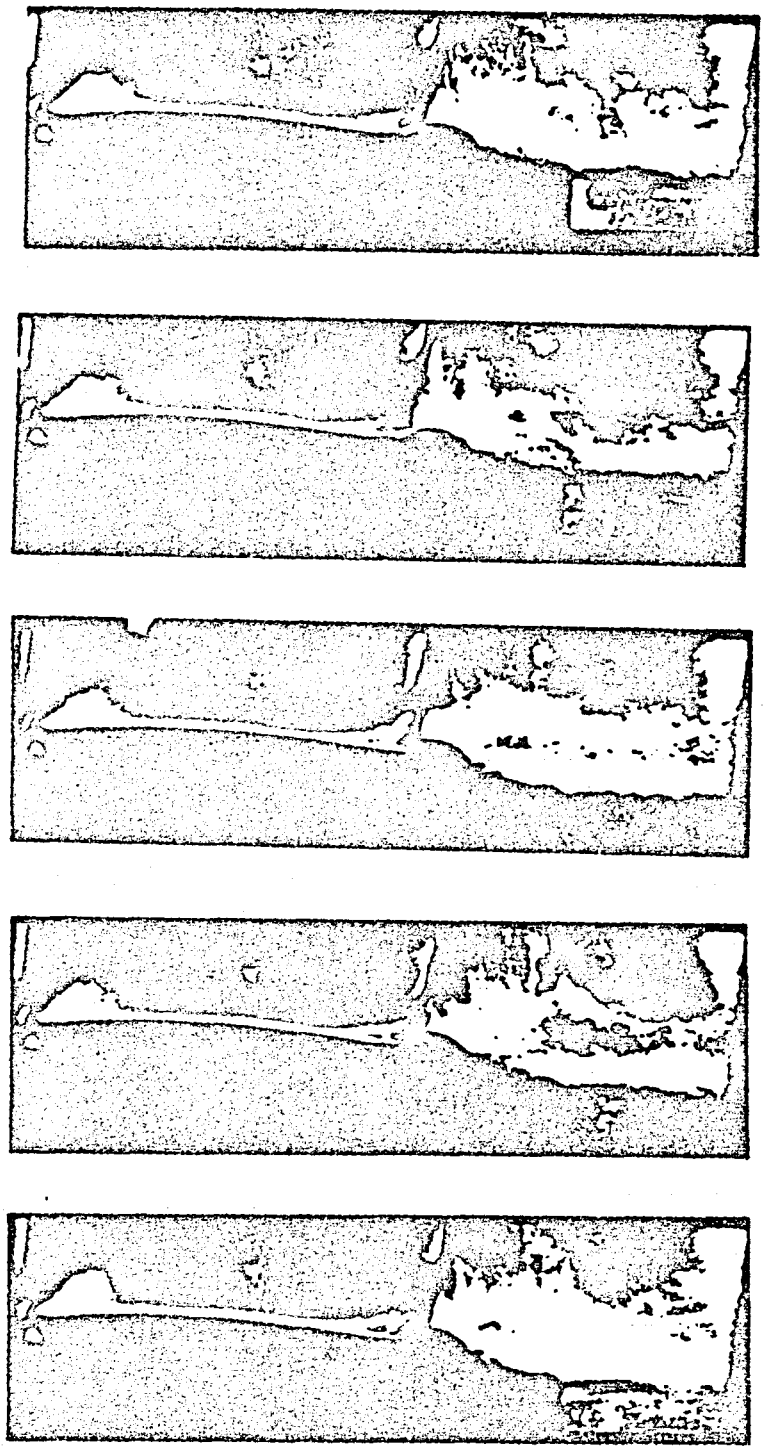

$\alpha = 4°, \quad \delta = 0°, \quad f = 30$ Hz

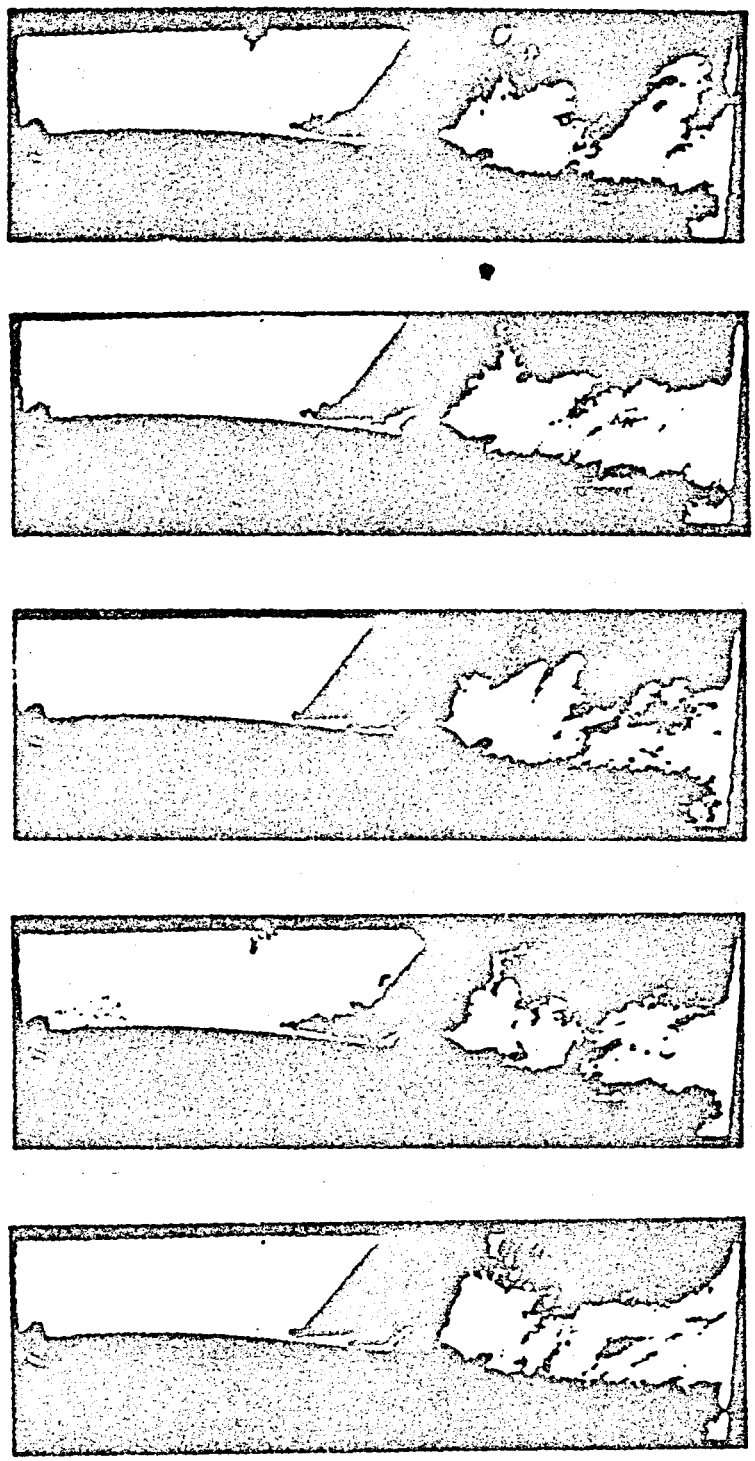

$\alpha = 4°, \quad \delta = +4°, \quad f = 0$ Hz

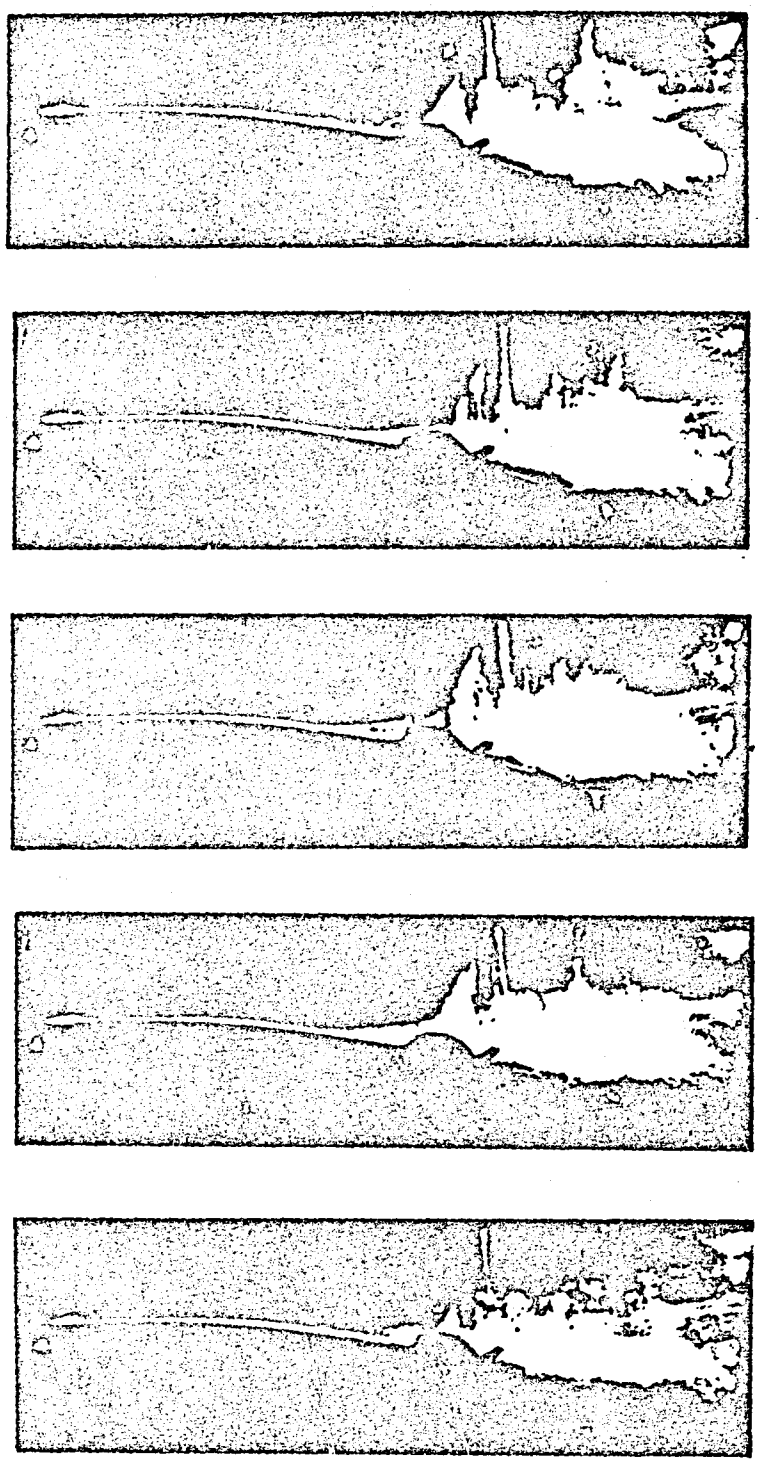

$\alpha = 4°, \quad \xi = 4°, \quad f = 30$ Hz

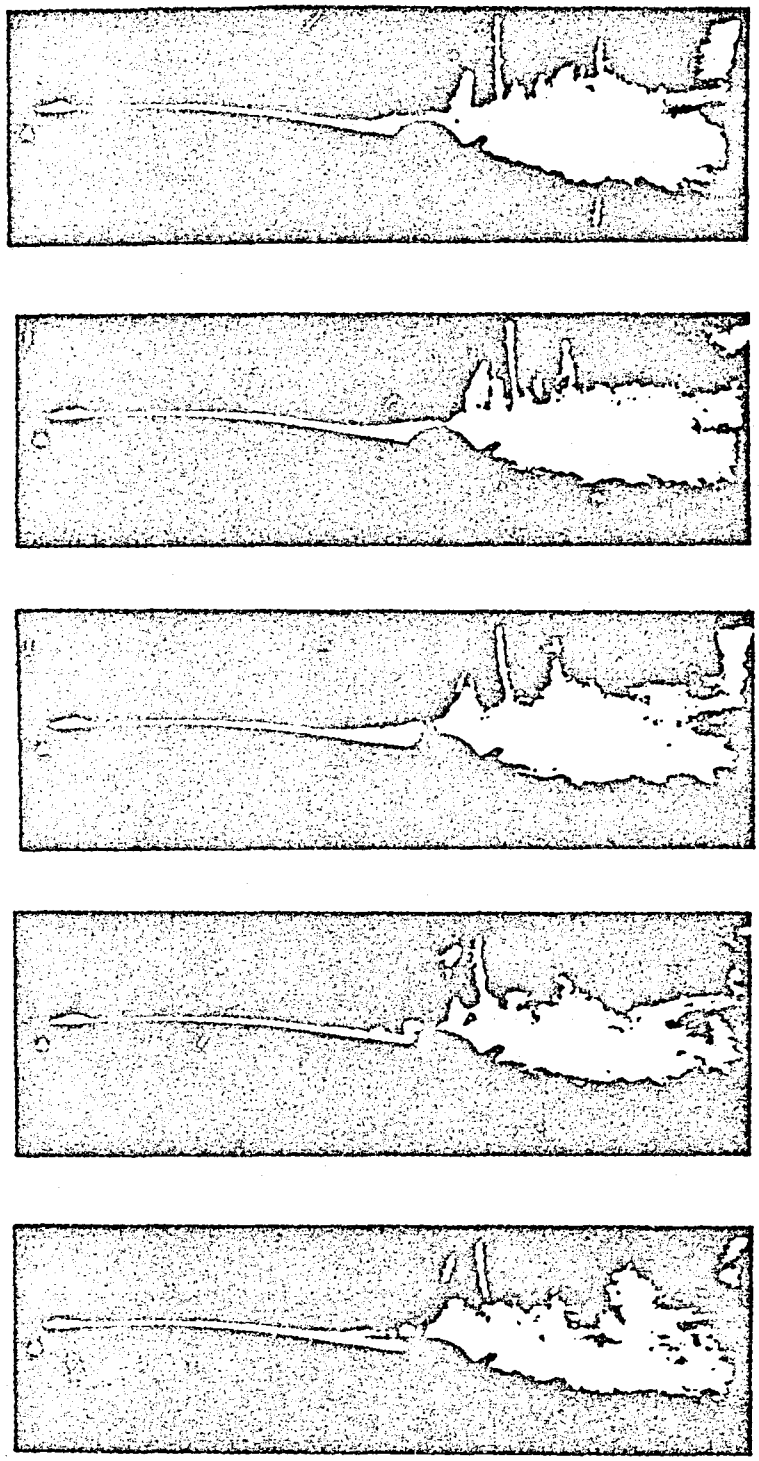

$\alpha = 4°$, $\delta = 4°$, $f = 30$ Hz

END

DATE

FILMED

DEC 13 1984

End of Document